

University of Windsor

Scholarship at UWindor

Electronic Theses and Dissertations

Theses, Dissertations, and Major Papers

1-1-2005

Multivariate knock detection for development and production applications

Todd Tousignant
University of Windsor

Follow this and additional works at: <https://scholar.uwindsor.ca/etd>

Recommended Citation

Tousignant, Todd, "Multivariate knock detection for development and production applications" (2005). *Electronic Theses and Dissertations*. 7794.
<https://scholar.uwindsor.ca/etd/7794>

This online database contains the full-text of PhD dissertations and Masters' theses of University of Windsor students from 1954 forward. These documents are made available for personal study and research purposes only, in accordance with the Canadian Copyright Act and the Creative Commons license—CC BY-NC-ND (Attribution, Non-Commercial, No Derivative Works). Under this license, works must always be attributed to the copyright holder (original author), cannot be used for any commercial purposes, and may not be altered. Any other use would require the permission of the copyright holder. Students may inquire about withdrawing their dissertation and/or thesis from this database. For additional inquiries, please contact the repository administrator via email (scholarship@uwindsor.ca) or by telephone at 519-253-3000ext. 3208.

**Multivariate Knock Detection for Development and
Production Applications**

by

Todd Tousignant

A Dissertation

**Submitted to the Faculty of Graduate Studies and Research
through the Department of Mechanical, Automotive and Materials Engineering
in Partial Fulfillment of the Requirements for
the Degree of Doctor of Philosophy at the
University of Windsor**

**Windsor, Ontario, Canada
2005**



Library and Archives
Canada

Bibliothèque et
Archives Canada

Published Heritage
Branch

Direction du
Patrimoine de l'édition

395 Wellington Street
Ottawa ON K1A 0N4
Canada

395, rue Wellington
Ottawa ON K1A 0N4
Canada

Your file *Votre référence*
ISBN: 978-0-494-70575-9
Our file *Notre référence*
ISBN: 978-0-494-70575-9

NOTICE:

The author has granted a non-exclusive license allowing Library and Archives Canada to reproduce, publish, archive, preserve, conserve, communicate to the public by telecommunication or on the Internet, loan, distribute and sell theses worldwide, for commercial or non-commercial purposes, in microform, paper, electronic and/or any other formats.

The author retains copyright ownership and moral rights in this thesis. Neither the thesis nor substantial extracts from it may be printed or otherwise reproduced without the author's permission.

AVIS:

L'auteur a accordé une licence non exclusive permettant à la Bibliothèque et Archives Canada de reproduire, publier, archiver, sauvegarder, conserver, transmettre au public par télécommunication ou par l'Internet, prêter, distribuer et vendre des thèses partout dans le monde, à des fins commerciales ou autres, sur support microforme, papier, électronique et/ou autres formats.

L'auteur conserve la propriété du droit d'auteur et des droits moraux qui protègent cette thèse. Ni la thèse ni des extraits substantiels de celle-ci ne doivent être imprimés ou autrement reproduits sans son autorisation.

In compliance with the Canadian Privacy Act some supporting forms may have been removed from this thesis.

Conformément à la loi canadienne sur la protection de la vie privée, quelques formulaires secondaires ont été enlevés de cette thèse.

While these forms may be included in the document page count, their removal does not represent any loss of content from the thesis.

Bien que ces formulaires aient inclus dans la pagination, il n'y aura aucun contenu manquant.


Canada

© Todd Tousignant, 2005

ABSTRACT

Combustion knock is a limiting factor in the efficiency of spark ignition internal combustion engines. Therefore, optimization of design and control dictates that an engine must operate as close to the knock limits as possible without allowing knock to occur. This is the challenge presented for knock detection systems.

In-cylinder pressure techniques are considered the most reliable method for knock detection; however, installation of pressure transducers in the combustion chamber is both difficult and expensive. This leads to the requirement of a low cost, non-intrusive alternative. Although the current vibration-based methods meet these requirements, their susceptibility to background noise greatly reduces their effectiveness. Thus, the goal of consistently achieving the optimal operating conditions cannot be achieved.

This research involves the use of multivariate analysis of vibration-based knock signals to improve the detection system reliability through enhanced signal to noise ratio. The techniques proposed apply a relatively new philosophy developed by Genichi Taguchi for pattern recognition based on the statistical parameter Mahalanobis Distance. Application of these methods results in the development of a new knock detection strategy which shows a significant improvement in determining the presence of knock.

The development and validation of this vibration-based system required the use of in-cylinder pressure data for initial classification of knocking and non-knocking operation. This necessitated an independent study to validate pressure transducer type and mounting location. Results of this study are detailed herein.

DEDICATION

This work is dedicated to my parents whose emotional and financial support have given me the opportunity to reach this point in my life. This work is also dedicated to my wife Cynthia who has encouraged me and inspired me every step of the way and to my daughter Autumn who has motivated me to become a better person.

ACKNOWLEDGEMENTS

The author would like to express his appreciation to Dr. J. Tjong and Dr. G.T. Reader whose guidance and encouragement contributed to the completion of this work. Thanks also to Dr. R. Gaspar, Dr. D. Ting and Dr. W. Miller for their assistance and comments.

Special thanks to Dr. Jimi Tjong in his role as Program Chair of the Powertrain Engineering Research and Development Group for supplying the tools and facilities which made this research possible. Thanks also to the dynamometer technicians at both Windsor Engine and Ford Essex Engine plants for their hard work and knowledgeable insight.

Financial Support for this research has been provided by Ford Motor Company, the University of Windsor and the Natural Sciences and Engineering Research Council.

TABLE OF CONTENTS

ABSTRACT	iv
DEDICATION	v
ACKNOWLEDGEMENTS	vi
LIST OF TABLES	xi
LIST OF FIGURES	xii
NOMENCLATURE	xv
CHAPTER 1 – INTRODUCTION	1
CHAPTER 2 – SURVEY OF RELEVANT RESEARCH	5
2.1 Introduction	5
2.2 The Knock Phenomenon	5
2.2.1 Knock Modeling	6
2.2.2 Photographic Studies	8
2.2.3 Flame Propagation Studies	8
2.2.4 Parametric Studies	10
2.2.5 Fuel Factors	11
2.2.6 Knock Damage	11
2.3 Pressure Measurement Accuracy	12
2.3.1 Pressure Pegging	13
2.3.2 Thermal Effects	13
2.3.3 Piezoelectric Pressure Transducers	17
2.3.4 Fiberoptic Pressure Transducers	17
2.4 Knock Detection	18
2.4.1 Pressure Measurement for Knock Detection	18
2.4.1.1 Resonance Issues	19
2.4.1.2 Processing of Pressure Data for Knock	20
2.4.2 Vibration-Based Knock Detection	21
2.4.2.1 Accelerometer Location Issues	22

2.4.2.2	Processing of Knock Vibration Signals	23
2.4.3	Knock Detection by Force Transducers	25
2.4.4	Knock Detection Using the Spark Plug	26
2.5	Conclusions	27
CHAPTER 3	– THEORY	28
3.1	Combustion Knock in SI Engines	28
3.1.1	Detonation Theory	28
3.1.2	Autoignition Theory	29
3.1.3	Pre-Ignition	30
3.1.4	Parameters Affecting Knock	31
3.1.4.1	Design Considerations	31
3.1.4.1.1	Limits on Efficiency	32
3.1.4.2	Operating Parameters	34
3.1.4.2.1	Cyclic Variation	36
3.1.4.3	Maintenance Issues	37
3.1.5	Octane Rating	37
3.1.5.1	Definition and Determination of Octane Number	38
3.1.5.2	Trends in Fuels	39
3.1.5.3	Ignition Delay	39
3.1.5.3.1	Multistage Ignition	40
3.1.5.3.2	Effect of Ignition Delay on ON	41
3.1.6	Characteristic Knock Frequencies	42
3.2	Transducer Theory	44
3.2.1	Piezoelectric Transducers	44
3.2.1.1	Piezoelectric Phenomonon	44
3.2.1.2	High Impedance Piezoelectric Transducers	46
3.2.1.3	Low Impedance Piezoelectric Transducers	47
3.2.1.4	Frequency Response	48
3.2.2	Pressure Transducer Mounting Techniques	49
3.2.2.1	Flush Mounting Technique	49

3.2.2.2 Remote Mounting Technique	50
3.3 Conclusions	52
CHAPTER 4 – TRANSDUCER VALIDATION	53
4.1 Introduction and Objectives	53
4.2 Stage One Comparison	55
4.2.1 Experimental Details	56
4.2.2 Analysis of Data	60
4.2.3 Results and Discussion	61
4.3 Stage Two Comparison	63
4.3.1 Performance Data Comparison	64
4.3.1.1 Experimental Details	64
4.3.1.2 Analysis of Data	67
4.3.1.3 Results and Discussion	67
4.3.2 Knock Data Measurement Comparison	74
4.3.2.1 Experimental Details	75
4.3.2.2 Analysis of Data	76
4.3.2.2.1 Data Resampling	76
4.3.2.2.2 Knock Intensity Calculation	77
4.3.2.3 Results and Discussion	78
4.4 Conclusions	83
CHAPTER 5 – KNOCK DETECTION STRATEGY	85
5.1 Introduction and Objectives	85
5.2 Experimental Details	86
5.3 Analysis of Data	89
5.3.1 Intensity Calculation	89
5.3.2 Statistical Distance	93
5.3.3 Mahalanobis-Taguchi System	97
5.4 Results and Discussion	103
5.5 Conclusions	120

CHAPTER 6 – CONCLUSIONS	122
REFERENCES	125
BIBLIOGRAPHY	133
LITERATURE SUMMARY CHART	135
APPENDIX A – PROCESSING SOURCE CODE	137
APPENDIX B – SUPPLEMENTAL DATA – TRANSDUCER VALIDATION	158
APPENDIX C – SUPPLEMENTAL DATA – KNOCK VALIDATION	197
VITA AUCTORIS	267

LIST OF TABLES

3.1	Knock Frequency Mode Constants	43
4.1	Pressure Transducer Characteristics	56
4.2	Stage 1 Test Matrix	58
4.3	Stage 2a Test Matrix	66
4.4	Stage 2b Test Matrix	75
5.1	L-12 Orthogonal Array	98
5.2	Test Array Based on L-12 Array	99
5.3	SN Calculation – 100 RPM, Cyl. #1	100
5.4	ME Analysis – 1000 RPM, Cyl. #1	101
5.5	SN Calculation – 1000 RPM	101
5.6	ME Analysis – 1000 RPM	102
5.7	ME Summary – 1000 RPM	102
C.1	Signal to Noise Ratio Results	203
C.2	Main Effects Results	204
C.3	Accelerometer Usage Table	205

LIST OF FIGURES

3.1	Illustration of Autoignition Phenomenon	29
3.2	The Otto Cycle	32
3.3	Piezoelectric Effect	45
3.4	Piezoelectric Crystal Stacking	46
3.5	Typical Transducer Frequency Response Curve	48
4.1	Kister 6123 Flush Mount Piezoelectric	56
4.2	Kister 6117 Spark Plug Piezoelectric	56
4.3	Optrand AutoPSI Fiberoptic	56
4.4	Absolute Pressure Measurement	57
4.5	Crank Angle Optical Encoder	58
4.6	Stage 1 Transducer Location	59
4.7	Stage 1 Response Data – Peak Pressure	62
4.8	Stage 1 Response Data – Peak Pressure Crank Angle	62
4.9	Stage 1 Response Data – Indicated Mean Effective Pressure	63
4.10	Stage 2 Transducer Location	65
4.11	Instrumented Cylinder Head	66
4.12	6117 / 6123 Average Pressure Traces	68
4.13	AutoPSI / 6123 Average Pressure Traces	69
4.14	6117 / AutoPSI / 6123 IMEP Comparison	70
4.15	6123 (Offset) / 6125 (Central) Average Pressure Traces	71
4.16	6123 (Central) / 6125 (Offset) Average Pressure Traces	71
4.17	6117 / 6125 Average Pressure Traces (Cylinder #2 and #3)	72
4.18	6117 / 6125 Average Pressure Traces (Cylinder #6 and #7)	72
4.19	6213 (Offset) / 6117 / 6125 (Central) IMEP Comparison	73
4.20	6123 (Central) / 6117 / 6125 (Offset) IMEP Comparison	74
4.21	Knock Intensity Processing	78
4.22	6117 / 6123 Intensity Data Comparison	79
4.23	AutoPSI / 6123 Intensity Data Comparison	80

4.24	Combustion Chamber Location Intensity Data Comparison	80
4.25	45 ° Front (Cylinder #2) / 45 ° Rear (Cylinder #3) Offset Frequency Data Comparison	81
4.26	90 ° Front (Cylinder #8) / 90 ° Rear (Cylinder #4) Offset Frequency Data Comparison	81
4.27	Dominant Acoustic Mode Shape	82
5.1	Pressure Transducer Locations	87
5.2	Accelerometer Locations	87
5.3	Pressure and Vibration Transducer Locations	88
5.4	Euclidean Distance	93
5.5	Standard Distance	94
5.6	Mahalanobis Distance	95
5.7	MD Baseline Selection Sensitivity	97
5.8	MTS Optimization Results	103
5.9	Raw Data – No Knock	104
5.10	Raw Data – Knock Present	105
5.11	Variance Data – No Knock	106
5.12	Variance Data – Knock Present	107
5.13	Mahalanobis Distance Based on Three Intensity Methods	108
5.14	Comparison of Raw Intensity Calculations	109
5.15	MD / IntS Sweep (Linear)	111
5.16	MD / IntS Sweep (Logarithmic)	111
5.17	MD / IntD Sweep (Logarithmic)	112
5.18	MD / IntV Sweep (Logarithmic)	112
5.19	MD / IntS Sweep (Normalized – Logarithmic)	113
5.20	Normalized Intensity – 1000 RPM, IntS	115
5.21	Normalized Intensity – 1000 RPM, IntS, Cyl. #1	115
5.22	Normalized Intensity – 1000 RPM, IntD	116
5.23	Normalized Intensity – 1000 RPM, IntV	117
5.24	Normalized Intensity – 1500 RPM, IntS	118
5.25	Normalized Intensity – 2500 RPM, IntS	118
5.26	Normalized Intensity – 3500 RPM, IntS	119

5.27	Normalized Intensity – 4500 RPM, IntS	119
A.1	Raw Data Processing Front End	138
A.2	Intensity Processing Front End	145
A.3	Data Plotting Front End	150
B.1	Pressure Traces 1000 RPM / PT	161
B.2	Pressure Traces 1000 RPM / WOT	167
B.3	Pressure Traces 2500 RPM / PT	173
B.4	Pressure Traces 2500 RPM / WOT	179
B.5	Pressure Traces 4500 RPM / PT	185
B.6	Pressure Traces 4500 RPM / WOT	191
C.1	MD / IntS Sweeps – 1000 RPM, Cyl. #1 (Heads #2 - #14)	206
C.2	MD / Int Sweeps – 1000 RPM, Head #2 (IntS, IntD, IntV, Cyl. #1 - #8)	210
C.3	MD / IntS Sweeps – Head #2 (Cyl. #1 - #8, 1500 RPM – 4500 RPM)	218
C.4	MD / IntS Normalized Sweeps – 1000 RPM, Cyl. #1 (Heads #2 - #14)	234
C.5	MD / Int Normalized Sweeps – 1000 RPM, Head #2 (IntS, IntD, IntV, Cyl. #1 - #8)	238
C.6	MD / IntS Normalized Sweeps - Head #2 (Cyl. #1 - #8, 1500 RPM – 4500 RPM)	246
C.7	Normalized Intensity (IntS, IntD, IntV, 1000 RPM – 4500 RPM)	262

NOMENCLATURE

a	acceleration [m/s^2]
A_p	Pressure conduit cross-sectional area [mm^2]
ATDC	After Top Dead Center
BTDC	Before Top Dead Center
B	Cylinder Bore Diameter [mm]
BDC	Bottom Dead Center
c	Speed of Sound [m/s]
CA	Crank Angle [degrees]
CI	Compression Ignition
CID	Cylinder Identification
DC	Direct Current
D_{ik}	Euclidean Distance between sample i and k
Δp	pressure drop across conduit [kPa]
DSP	Digital Signal Processing
EEC	Electronic Engine Control
EMI	Electromagnetic Interference
f	frequency [Hz]
f_n	undamped natural frequency [Hz]
f_{mn}	acoustic frequency [Hz]
ϕ	equivalence ratio
γ	ratio of specific heat capacities
i	index
IC	Internal Combustion
ICP	Integrated Circuit Piezoelectric
imep	indicated mean effective pressure [kPa]
IntD	Double Window Intensity
IntS	Single Window Intensity [m^2/s^3]
IntV	Variance-Based Double Window Intensity
j	index

k	index
l_p	pressure conduit passage length [mm]
LED	Light Emitting Diode
MBT	Minimum Advance for Best Torque
MD	Mahalanobis Distance
MON	Motor Octane Number
MTS	Mahalanobis-Taguchi System
μ	viscosity [$N \cdot s/m^2$]
n	number of cycles
n_{mep}	net mean effective pressure [kPa]
η_{otto}	Otto-cycle efficiency
ON	Octane Number
ORI	Octane Requirement Increase
PL/PT	Part Load / Part Thottle
PP	Peak Pressure [kPa]
p_{mep}	pumping mean effective pressure [kPa]
q	specific heat transfer [J/kg]
Q	factor of amplitude increase at resonance
θ	angle [degrees]
ρ	density [kg/m^3]
ρ_{mn}	acoustic mode shape constant
r_v	compression ratio
res	individual cycle resolution of raw time-based data
RES	lowest cycle resolution of raw time-based data
rpm	rotations per minute
RON	Research Octane Number
RTP	Real Time Processor
RTV	Room Temperatures Vulcanizing Rubber
S	covariance matrix
SD_{ik}	Standard Distance between sample i and k
SI	Spark Ignition

SN	Signal to Noise Ratio
σ	standard deviation
σ^2	ensemble variance
T	Temperature [$^{\circ}$ C]
TDC	Top Dead Center
ν	specific volume [m^3/kg]
V_c	Cavity volume (adjacent to transducer diaphragm in remote mounting) [mm^3]
w	specific work [J/kg]
WOT	Wide Open Throttle
ω_s	Standing wave resonant frequency [Hz]
ω_H	Helmholtz resonant frequency [Hz]
x	data sample
X	array of data samples

CHAPTER 1 – INTRODUCTION

Combustion knock in a spark ignition internal combustion engine represents a significant problem in noise and vibration as well as engine durability. High intensity knock can result in erosion or fracture of the piston crown, piston rings or cylinder head gasket [Nates, R., Yates, A., 1994]. Although lower intensity knock is generally not considered detrimental to the structural integrity of the engine components, the noise associated can cause consumer annoyance. Noise and vibration issues such as these are becoming more critical as consumer standards have increased along with advances in engine development. To remain competitive, automotive companies must manufacture engines which satisfy government regulations for fuel economy and emissions, produce sufficient power for the given application and do so while ensuring no excessive noise or vibration is noticed in the passenger compartment.

Conservative design for the avoidance of knock is not an option. This would involve the use of high-cost, premium fuels, low compression ratios, and conservative engine control strategies. Unfortunately, significant manipulation of the compression ratio and spark advance to accommodate knock would result in diminished engine performance. An aggressive strategy for performance improvement involves effective production control systems which allow operation on the borderline of knock operating conditions. This presents the requirement for an accurate knock detection system.

The following chapter reviews several knock detection systems. These range from high accuracy, high cost in-cylinder pressure solutions to less intrusive, production feasible, vibration-based systems. In-cylinder pressure methods are the generally accepted method for laboratory studies aimed at characterizing and modeling knock as well as for engine mapping and diagnosis

work. With the exception of remote mounted pressure transducers (often integrated into the spark plug), most in-cylinder pressure monitoring requires custom machining of the cylinder head. Although the spark plug mounted transducers represent a less intrusive alternative, they require the use of non-production spark plugs (which may alter engine operation) and often present issues related to data integrity.

Vibration-based detection systems represent a significant improvement in terms of cost, convenience and lack of influence on engine operation. However, for current production knock control systems, these improvements are offset by a drastic reduction in accuracy and reliability. As the reliability of the knock detection system is reduced, the automotive calibration engineer is faced with two options: a conservative control strategy which allows less than optimal engine performance must be weighed against an aggressive strategy which could result in the possibility of annoyance and damage due to knock.

The objective of this research is the development of a knock control system which rivals the accuracy of in-cylinder pressure measurement systems without sacrificing the low cost and convenience of non-intrusive vibration-based detection. Failure of current production systems is caused by the degradation in signal to noise ratio inherent with indirect measurement techniques. While pressure is a direct indication of the acoustic events occurring in the combustion chamber, vibration detection involves the measurement of a secondary response to these excitations. Unfortunately, while vibration is a secondary measurement for combustion analysis, it is a direct measurement of structure-born excitations which occur during normal engine operation. The end result is a reduction in signal to noise ratio due to the 'background noise' generated by the transducer's primary response to mechanical vibration.

While oversimplified, the problem can be reduced to the improvement of signal to noise ratio. The thesis presented here proposes the accomplishment of this task by using multivariate analysis of the vibration signals. The increasing emphasis on the importance of knock control has motivated the introduction of multiple accelerometer knock control systems. However, signals from these transducers are processed individually, selecting for each cylinder the vibration transducer which best correlates to the respective in-cylinder pressure data. This research concentrates on combining the information from all responsive sensors to create a single knock metric in an attempt to elevate signal to noise ratio and thus improve overall reliability of the vibration based knock detection system.

The statistical methods presented herein involve comparison to baseline data generated from engines undergoing normal operation. Furthermore, validation of the proposed methods require data from certified knocking conditions. This initial classification is accomplished using in-cylinder pressure data. Though in-cylinder pressure is the generally accepted knock indication method, there are several factors which can affect the accuracy of pressure data. Therefore, a thorough, independent validation study is conducted which investigates the pressure measurement practices employed here.

In view of the above considerations, the following objectives were set for this dissertation:

1. To conduct a comprehensive literature review, with an emphasis on the acquisition and data processing methods used for both laboratory and production knock detection.
2. To independently validate the pressure transducers being used for the development and validation of a vibration based knock detection method.

3. To determine the optimal locations of vibration transducers which exhibit maximum response to knock events.
4. To develop the appropriate experimental design, data acquisition techniques and data reduction techniques to provide a sample set providing sufficient data for the development and validation of a knock detection method.
5. To determine single variable knock intensities based on each vibration transducer based on both new and existing processing methods.
6. To apply relatively new multivariate statistical methods in a novel way to create a single multivariate knock metric.
7. To demonstrate the effectiveness of this multivariate method in increasing knock detection capability through improved response to knock events.
8. To recommend areas for future research and development.

CHAPTER 2 – SURVEY OF RELEVANT RESEARCH

2.1 Introduction

"The phenomenon of knocking in spark ignition engines has been a subject of research since the advent of the internal combustion engine" [Spicher, U., Kollmeier, H.P., 1986]. "During these first years, this phenomenon has not only been hard to predict, but also difficult to detect by means other than the ear of the experienced" [Burgdorf, K., Denbratt, I., 1998]. This poses a significant problem since knock is a limiting factor in compression ratio and thus in the thermal efficiency of the internal combustion engine (as illustrated in chapter 3). Much work has been done in the past 60 years to advance the automotive industry's ability to understand, detect and control knock.

2.2 The Knock Phenomenon

Autoignition is a process which is a matter of necessity in diesel (compression ignition) engines, but its occurrence in the unburned gases of a spark ignition engine is highly undesirable. Combustion knock in the case of both spark ignition and compression ignition engines refers to the rapid pressure rise associated with autoignition. If this rise is severe enough, acoustical cavity resonances of the combustion chamber may be excited, resulting in pressure fluctuations which impart a forced vibration on the engine structure, resulting in a high frequency noise component. "Knock in spark ignition engines is far more severe than that occurring in the worst-case diesel engines (pressure rise rates of 20 bar/degree as compared to 8-10 bar/degree)" [Schaberg, P. et al., 1990]. Schaberg et al. observe that the contribution of pressure oscillation noise is predominant in a spark ignition engine, while not significant in diesel.

The development of effective knock detection and control strategies requires knowledge of the phenomenon itself. This section highlights some work that has been done to model, predict, observe and characterize knocking combustion as well as discussing the mechanisms which cause damage to the components of the internal combustion engine.

2.2.1 Knock Modeling

An important development in the understanding of autoignition is the concept of multistage ignition. Levendahl [1956] discusses and attempts to observe the presence of two precursor stages to the highly exothermic and intense set of reactions which characterize knocking combustion. A peroxide stage (believed to produce alkyl hydroperoxides) represents reactions which are not measurably exothermic, but produce sufficient active radicals to promote the exothermic cool flame reaction. The second (cool flame) stage is slightly exothermic and heats the mixture to the hot flame autoignition limit. The final hot flame stage is highly exothermic. This stage produces intense radiation and is responsible for the pressure rise leading to the audible knock vibrations. Levendahl's work compares the knock sensitivity of different fuels and relates this to the first two stages of autoignition. The presence and speed of these peroxide and cool flame reactions and the lower limits at which they occur determine the autoignition resistance of the mixture.

Empirical models have been developed [Livengood, J.C., Wu, P.C., 1956] which employ global equations and characteristics to predict the onset of knock. Livengood and Wu create an empirical function based on the time history of ignition delay (the time required for the reaction mechanism to result in a hot flame reaction). This study provides insight into the dependence of knock on ignition delay, but fails to capture the multi-stage mechanism.

"While (ignition delay models) result in successful prediction of whether or not autoignition would occur, it gives no indication of the knock intensity. Neither, over a full range of generically different fuels, does the delay time correlate with ON (octane number)" [Bradley, D. et al., 1996]. Bradley et al. attempt to separate the volumetric heat release rate due to autoignition from that due to normal flame propagation and correlate this to knock intensity. Studies which deal with knock damage [Arrigoni, V. et al., 1978, Nates, R., Yates, A., 1994, Renault, R., 1982] illustrate the significance of knowing not only of the existence of knock, but also the severity. Bradley's work addresses this need by predicting the onset and intensity of knock Using the heat release rate criterion for the comparison of fuels, a 2 to 3 fold increase in heat release rates is observed for paraffinic fuels as compared to aromatics (consistent with trends in octane number).

These simple empirical relations are too simple to give any information about the reaction process and fit the data over a limited range [Chun, K. et al., 1988]. A fully comprehensive model would include all elementary reactions which might occur, involving several hundred equations. The popular solution is the use of a simplified chemical kinetic model which includes only the rate-limiting reactions [Chun, K. et al., 1988]. Chun et al. use such a mechanism along with end gas temperature calculations to simulate autoignition. Experimental validation studies show some success in predicting the onset angle of knock with increasing error during slower combustion cycles.

Lee et al. [1999] used the reduced chemical kinetic model together with a premixed turbulent combustion model for the prediction of cycle pressure, flame arrival angle, knock occurrence and the identification of autoignition site. This model proved to provide accurate predictions with the intended end-use of a combustion chamber design tool. Of the observations

made in this study, it was concluded that only autoignition occurring prior to the burning of 80 % of the fuel results in the sharp pressure rise associated with knock.

An important phenomenon which directly relates to the measurement of knock is combustion chamber resonance. Draper [1933] derives the solution to the 3D wave equation for a right cylinder, equating this roughly to a hypothetical combustion chamber. Experimentation shows that the pressure waves follow the laws of simple sound theory, and that the resonance phenomena within the cylinder charge determine the pressure wave frequencies.

2.2.2 Photographic Studies

Observation of the propagation of knock in the combustion chamber has been accomplished using high-speed photography in an optically accessible engine [Ball, G.A., 1956, Konig, G., Sheppard, C.G.W., 1990]. Ball, with the use of Schlieren photography demonstrates the existence of cool flame reactions and the subsequent autoignition. Time of transit for autoignition reaction is determined to be $\frac{1}{4}$ that of a normal spark-ignited flame. Konig and Sheppard use both Schlieren and color photography to observe autoignition. They conclude that autoignition is generally multi-centered and that knock severity correlates well with the angle of onset (early autoignition results in increased intensity).

2.2.3 Flame Propagation Studies

Unfortunately, photographic studies are generally limited to laboratory engines which are well suited for optic accessibility. As an alternative, much work has been done in which engine combustion chambers have been instrumented with multiple transducers, measuring pressure, temperature, radiation or luminosity.

Chun et al. obtain information about autoignition location and cyclic variation through the instrumentation of the combustion chamber with 17 optical probes and in-cylinder pressure transducers [Chun, K. et al., 1993]. Cyclic variation is one of the great difficulties in the detection and control of knock. In fact, although some researchers [Richardson, S., et al., 2004] have used as few as 200 cycles of data for knock detection, it has been determined [Burgdorf, K., Denbratt, L., 1998] that up to 1300 cycles are required for statistical knock values to converge. A reduction of cyclic variation would represent a reduced octane requirement [Leppard, W.R., 1982]. Chun et al. observed large variations in both pressure and propagation patterns. They were able to identify the start of autoignition and determine end gas combustion time of less than 1 degree CA (crank angle).

Similar studies [Chun, L. et al., 1993, Geiser, F. et al., 1998, Spicher, U., Kollmeier, H.P., 1986] use multiple fiberoptic probes to investigate flame propagation. Spicher and Kollmeier were able to measure propagation velocity of up to 1300 m/s. They found that most knock events could be classified by 5 propagation regimes.

Alternatively, attempts have been made to investigate knock origin and propagation using pressure transducers. One approach has been to use a small number of transducers, together with an algorithm for determination of knock origin [Liiva, P. et al., 1992]. Castagne, Mazoyer et al. attempted to improve upon the measurement grid resolution by instrumenting a head gasket with 11 piezoceramic elements for pressure measurement [Castagne, M. et al., 2003, Mazoyer, Th. et al., 2003]. This would allow for more information without the need for cylinder head machining. However, the elements proved to be generally unreliable. An algorithm was then used to determine the knock location, which was determined to be sensitive to swirl, plug position and geometry, but not engine tuning parameters.

Burgdorf and Chomiak discuss an anomaly which they observe in pressure data [Burgdorf, K., Chomiak, J., 1998]. It is generally understood that the occurrence of autoignition creates a spike in pressure accompanied by a decaying fluctuation. Burgdorf and Chomiak note an increase in fluctuation amplitude and relate this to additional pressure waves created by late autoignition in combustion chamber crevices (i.e. around piston crown).

2.2.4 Parametric Studies

Other experimental studies attempt to explain trends in knock behavior through observation of in-cylinder data. Correlation studies provide invaluable insight into the behavior of knock. Chun and Heywood [1989] use pressure data from a single cylinder engine to correlate combustion speed with knock intensity. It is observed that faster burning cycles result in earlier knock resulting in a larger combustible mass and higher knock intensity. They also observe that cyclic variability in knock is caused by variation in the quantity of end gas, temperature and chemical species present, geometry and location of the end gas region and non-uniformity in temperature and mixture composition of the end gas.

Dues [1990] observes a fluctuation of +/- 400 Hz in the characteristic knock frequency (combustion chamber resonance) which is controlled primarily by combustion chamber temperature and cylinder bore geometry (engine speed affects frequency only indirectly through temperature change). Also observed is the load dependence of knock. During part throttle (moderate load) operating conditions, scavenging is less efficient, leaving more exhaust gas residuals in the combustion chamber. This results in slower combustion and less tendency to knock. Conversely, during WOT (wide open throttle) operation, there are less residuals and

faster combustion, leading to what is referred to as 'tip-in' knock (which occurs during acceleration).

Lee and Schaefer [1983] through the use of 4 pressure transducers and 9 film thermocouples study the effect of knock on engine performance and endurance. A slight increase in imep is noted with moderate knock; however, moderate to high losses accompany heavy knock. A threefold increase is observed in wall heat loss. Lee and Schaefer found primary damage zones coincided with end gas regions (far from spark plug at border of cylinder). Knock in this study was induced by both increased spark advance and reduced octane number. It was determined that the nature of knock was independent of the induction method. This is an important observation for those testing with limited fuel resources or engine control capabilities.

2.2.5 Fuel Factors

An important factor in the prevention of knock is the octane rating of the fuels employed. Unfortunately, the automotive engineer has limited control over this development aspect. However, for insight into the knock resistance of various fuels the reader is referred to Walsh, A.D., [1962]. Also, Leveque et al. [1994] discuss the effectiveness of different types of fuels and additives and McNally et al. [1989] investigate the effect of octane number on performance, fuel economy and drivability.

2.2.6 Knock Damage

For effective engine control (knock control via performance parameter monitoring and variation), it is necessary to understand the difference between low intensity knock which can

present the automotive consumer with a minor annoyance for limited operating conditions and high intensity knock which could result in severe engine damage. There are several studies [Arrigoni, V. et al., 1978, Nates, R., Yates, A., 1994, Renault, R., 1982] which not only aid in this distinction, but also investigate the mechanisms which lead to knock.

Renault discusses the phenomenon of runaway knock. This generally occurs at high engine speeds where a high temperature knock condition is sustained. Runaway knock can result in engine damage in less than 1 minute. This is not to be confused with acceleration ("tip-in") knock which can result in annoyance, but minimal serious damage.

Nates and Yates go into detail regarding the mechanisms by which knock can result in damage over longer periods of time. This includes piston land fracture due to plastic yielding of the rings, piston seizure due to increased heat flux (caused by disturbed boundary layer during knock) and ring fracture caused by a lack of support due to blow-by erosion.

2.3 Pressure Measurement Accuracy

In-cylinder pressure has long been considered the standard measurement technique for accurate knock detection. Therefore, in addition to their use for laboratory investigations and calibration, in-cylinder pressure is generally used to validate novel detection methods. Furthermore, it has been shown [He et al., 1993, Muller, R. et al., 2000, Powell, J.D., 1993] that pressure has the potential to improve engine performance if used for closed loop engine control.

Unfortunately, as pressure cannot be measured directly, care must be taken to ensure the pressure data deduced from the pressure's effect on some transducer characteristic is an accurate representation of that pressure. Therefore, knowledge of pressure transduction principles is a prerequisite for any knock detection work.

2.3.1 Pressure Pegging

Most in-cylinder pressure transducers are purely dynamic and are thus incapable of providing an absolute pressure signal without some form of referencing procedure. Randolph [1990b] discusses the attributes of various pegging (referencing) procedures. The most common procedure for pegging [DSP Technology, 1996] involves instrumenting the intake manifold with an absolute pressure transducer and using the pressure value obtained from this as a reference during the intake stroke. This assumes equilibrium exists between the cylinder and intake at approximately bottom dead center of the intake stroke.

Randolph conducts an experimental investigation into the accuracy of the intake referencing method as compared to exhaust referencing and forced polytropic methods. The results in this study indicated optimal results using the intake referencing technique. However, the engine used was not equipped with a tuned intake manifold. The author warns that care should be taken with tuned intakes as the pressure fluctuations inherent in these could degrade accuracy. In cases where the intake reference method fails due to these fluctuations or under operating conditions not explored in this study, the forced polytropic method is recommended. Discretionary caution should be used, however, in the estimation of the polytropic coefficient. Further, non-ideal operation such as blow-by (gas flow past the engine rings) will prevent true polytropic compression which will affect validity of this approach.

2.3.2 Thermal Effects

In addition to the difficulties in deducing pressure information from indirect measurement, complications arise when the transducer is used in a high temperature combustion environment. The effects of this exposure are manifested in two ways. Thermal drift represents

a long term (intercycle) gradual deviation of data due to prolonged exposure of the transducer to high temperature gases. Thermal shock refers to the short term (intracycle) variation due to thermal transients within a cycle. Several causes have been cited. Combustion flames can differentially heat the sensor diaphragm compared to its housing. The resulting different thermal expansions may cause a gain error [He, G. et al., 1994, Higuma, A. et al., 1999, Kuratle, R., Marki, B., 1992]. In the case of piezoelectric transducers, further variation can result from modification of the Young's Modulus and resonant frequency of the crystal [Randolph, A., 1990a].

The application of an appropriate pegging procedure [Randolph, A., 1990b] during each cycle can effectively minimize any adverse affects of long term thermal drift. Thermal shock, however, presents a much larger problem. Although peak pressure can be evaluated within 1 bar using a standard piezoelectric transducer, errors are compounded and become much more significant when evaluating cyclic parameters such as indicated mean effective pressure [Tousignant, T.E. et al., 2002, Tousignant, T.E., et al., 2004]. Rai et al. have mapped thermal shock over a wide range of operating conditions and indicate that error in the estimation of indicated mean effective pressure is highest during high load conditions and moderate to low engine speeds due to increased exposure time [Rai, H.S. et al., 1999].

Much investigation has been dedicated to the minimization of short term thermal error. Strategies can be broadly classified as experimental treatment and processing methods. Experimental methods are somewhat controversial. Past efforts have included the use of water cooling, front sealing, or the use of heat shields or RTV coatings. However, the effectiveness of these solutions is influenced by limited durability or space considerations. For example, although the use of RTV can reduce the effect of thermal shock by up to 75 % [Rai, H.S. et al.,

1999], this coating must be reapplied scrupulously to ensure effectiveness. Similarly, high end thermally compensated transducers incorporate a self-contained cooling system to moderate temperature of the measuring element. However, these transducers are invariably larger and present an installation problem in many production applications [Randolph, A., 1994].

Another experimental approach to alleviate the effects of exposure is to limit such exposure. This is accomplished through remote mounting of the transducer with the use of small cavities which convey pressure information from the combustion chamber to the transducer. Unfortunately, remote mounting further complicates the measurement process by increasing cylinder compression volume and crevice volume, and adding a phase shift and resonant component to the signal [Randolph, A., 1990a]. Randolph addresses this issue with the development of multiple slot adapters which increase the effective cross section of the connecting passages (thus increasing the cavity resonance and reducing pressure drop) while maintaining individually small passageways which can effectively quench the combustion flame prior to contact with the transducer. Rosseel et al. evaluate several transducers and mounting strategies based on both short and long term thermal effects [Rosseel, R. et al., 1999]. Results show transducers which are highly susceptible to thermal error when flush mounted become comparable to high-end thermodynamic transducers with the use of a multi-slot adapter.

Conversely, many studies maintain that a pressure transducer should be mounted as close to the combustion chamber as possible to avoid falsification of data by resonance issues and combustion volume modification [Kuratle, R., Marki, B., 1992]. Sun and Anderton [1990] developed a heat shield for low frequency measurement applications (below 5 kHz) and determined that although noise analysis was unaffected, problems were introduced during heat release rate analysis. Vianna et al. [1999] conducted experimental studies to evaluate various

pressure adapters (for remote mounting) and discovered phase shifts (signal delay) ranging from 12 – 34 ms for 8 - 16 mm adapters. Longer spark plug adapters exhibited delays of up to 165 ms accompanied by pressure drops of up to 2 bar.

To better understand the issues related to remote mounting, mathematical [Benedetti, G.A., Benson, J.Z., 1995] and finite element [Hountalas, D.T., Anestis, A., 1998] models of the transducer / cavity system have been created to independently evaluate the errors associated. These works revealed error dependence on cavity configuration, frequency response of the measurement system, engine speed, pipe length and transducer diameter. Rosenberger et al. conducted a theoretical and experimental study of single and double diameter connecting ports for use in ballistic applications [Rosenberger, T.E. et al., 1995]. In addition, this study investigated the effect of filling materials in the connecting ports for further thermal protection; however, this introduced the possibility of reducing dynamic response and changing the acoustic characteristics due to speed of sound (which would change over time as material leaves the passage).

As mentioned earlier, the inconclusive argument regarding experiment thermal error reduction methods has led some researchers to investigate post-processing alternatives [Higuma, A. et al., 1999, Rai, H.S. et al., 1999]. Algorithms developed by Rai et al. resulted in a reduction of thermal error from 7 – 20 % to approximately 1.5 % for the Kistler 6123 piezoelectric transducer. Higuma et al. deal with simultaneous reduction of thermal shock and time constant error (a problem specific to piezoelectric transducers which will be discussed shortly).

2.3.3 Piezoelectric Pressure Transducers

Many of the principles and challenges associated with this transducer type are highlighted in Chapter 3. Most problems specific to this type of measurement are related to the high impedance output of the piezoelectric crystals. Insulation breakdown can occur with improper care of the high impedance connections and cables [Randolph, A., 1994, Kuratle, R., Marki, B., 1992]. The measurement system must be grounded (and preferably shielded) to reduce electric noise.

Time constant error may result if charge amplification is not executed properly. A short time constant setting can act as a high-pass filter if the amplifier capacitor is allowed to partially discharge through the resistor before completion of measurement. Conversely, a long time constant setting is equivalent to operating in DC mode, allowing low frequency (long term) drift caused by thermal effects or leakage current.

2.3.4 Fiberoptic Pressure Transducers

Pressure measurement by the use of fiberoptics has been explored to accomplish two objectives: The development of a pressure transducer with equal or superior accuracy to the piezoelectric transducer and at a cost which would make individual cylinder pressure monitoring feasible for production applications. This problem has been approached mainly by application of intensity modulation [McCoy, J.J., Taylor, H.F., 1993, Oprand¹] and phase modulation [Fitzpatrick, M. et al., 2000].

The Oprand transducer utilizes an LED light source which contacts a reflective diaphragm. The light power returned to the fiber varies based on the diaphragm deflection and

¹ Oprand is a transducer manufacturer looking to produce a low-cost transducer for individual cylinder production. References include [He, G. et al., 1993, He, G. et al., 1994, Poorman, T. et al., 1995, Poorman T. et al., 1997, Włodarczyk, M. et al., 1998a, Włodarczyk, M. et al., 1998b].

numerical aperture of the fiber. Optrand boasts not only significantly lower costs (as compared to the piezoelectric transducer), but also durability of over 1 billion cycles. This combination of low cost and high durability presents an ideal scenario for production application. Studies conducted by Optrand suggest that this technology is preferred over piezoelectrics due to a higher tolerance to temperature effects and lack of EMI and capacitance loading effects. However, independent studies [Roth, K.J. et al., 2002, Tousignant et al., 2002, Tousignant et al., 2004] indicate a lack of reproducibility in Optrand's commercially available transducers.

The phase modulated technology proposed by Fitzpatrick et al. employs two reflective surfaces. A deflection of the diaphragm (representing one of the reflective surfaces) results in a phase change between the two returning beams. The authors claim a higher accuracy than intensity modulation since there is no error due to intensity decay with age or bending.

2.4 Knock Detection

Several methods exist for the detection of knock. These vary depending on application from simple vibration measurement to the machining of cylinder heads for in-cylinder pressure detection. Continuous efforts are applied to the improvement of data acquisition and processing methods for extraction of signals specific to knock for accurate and reliable detection.

2.4.1 Pressure Measurement for Knock Detection

The most reliable method of knock detection continues to be in-cylinder pressure measurement. Several methods exist for acquiring and manipulating pressure data to indicate the presence of knock [Burgdorf, K., Denbratt, L., 1997].

2.4.1.1 Resonance Issues

The problems discussed previously relating to general pressure data integrity must be dealt with. Particularly relevant for knock detection are resonance issues which are greatly influenced by transducer location. Some have proposed tuning the resonant frequency of pressure conduits (for remote mounted transducers) to characteristic knock frequencies to enhance signal to noise ratios [Morris, J., 1987]. However, the general consensus is that alias frequencies in these passages are a deterrent to effective knock detection. In some cases, analysis of high frequency pressure fluctuation has indicated the majority of energy at the resonant frequency of the transducer rather than a characteristic knock frequency [Brunt, M.F.J. et al., 1998].

In addition to difficulties associated with remote mounting strategies, the acoustic resonance which accompanies knock presents additional complications relating to transducer location. Depending on the transducer placement relative to nodal positions, transducers can show very little sensitivity to the frequency modes of interest [Checkel, M., Dale, J., 1989]. Analytical studies [Draper, C.S., 1933, Scholl, D. et al., 1998] have been conducted to better understand this acoustic behavior and make decisions a priori regarding the placement of transducers.

As an aside, it should be noted that although nodal transducer placement degrades the absolute measured knock intensity, data from such a transducer would require less filtering when being applied to heat release analysis [Syrimis, M., Assanis, D.N., 1997].

2.4.1.2 Processing of Pressure Data for Knock

As inferred throughout this chapter, a common knock detection strategy involves analysis of the high frequency pressure fluctuations resulting from acoustic resonance (excited by the abnormally large pressure rise rates which accompany autoignition) in the cylinder. This involves extracting data using time and frequency domain filtering.

Since knock occurs only for a small portion of the cycle, data is extracted over the relevant crank angle window. Most knock occurs between 8 and 33 degrees ATDC [Brunt, M.F.J. et al., 1998]; therefore, Brunt et al. recommend a knock window from TDC to 40 degrees ATDC. Conversely, Burgdorf and Denbratt [1997] suggest that knock energy analysis is adversely affected even when truncating data at 50 degrees ATDC.

When the relevant data is extracted, it is necessary to remove the low frequency pressure information. This is commonly accomplished using a high-pass filter, although some researchers suggest that moving average smoothing techniques tolerate lower sampling rates and capture all knock modes [Brunt, M.F.J. et al., 1998]. Frequencies of interest range between 5 and 20 kHz. This reveals an additional concern: To capture all knock frequency modes, minimum sampling rates of 40 – 50 kHz are required.

The two most common metrics which are derived from this filtered window of data are knocking peak pressure and integral-based knock intensity. The knocking peak pressure is simply the maximum amplitude of pressure fluctuation. This metric has the advantage of being physically meaningful, with a theoretical value of zero for non-knocking cases. Similarly, the knock intensity metric is derived from the integral of the rectified or squared fluctuating component. Although more computationally complex, this metric is less sensitive to sampling rate [Brunt, M.F.J. et al., 1998].

Though more popular for the processing of vibration signals, some approaches delve more into the specific frequency domain information in this high frequency component. However, simple frequency analysis often fails due to variation in the characteristic frequencies caused by variations in cylinder geometry and the speed of sound within the combustion chamber [Burgdorf, K., Denbratt, L., 1997].

Checkel and Dale have proposed methods of processing which attempt to circumvent all difficulties associated with cavity resonance, transducer placement and sampling rate requirements [Checkel, M., Dale, J., 1986]. Recommended in this work is the detection of knock through the observation of trends in the gross pressure signal rather than concentrating on the high frequency component.

Autoignition results in both higher peak cylinder pressures as well as high pressure rise rates. However, due to normal cyclic variation, it becomes difficult to establish reliable thresholds based on these quantities. Checkel and Dale observe that the onset of knock is accompanied by a rapid pressure rise (large positive curvature) followed by an abnormally narrow peak due to rapid heat loss (large negative curvature). Therefore, it is suggested that the 3rd Derivative of the gross pressure curve (which represents the rate of change of curvature) is an ideal knock metric. Independent studies [Burgdorf, K., Denbratt, L., 1997, Puzinauskas, P., 1992] corroborate the effectiveness of this metric due to its lack of sensitivity to noise, sampling rate and cylinder and mounting cavity acoustics.

2.4.2 Vibration-Based Knock Detection

Pressure-based knock detection, although considered most accurate, is a very intrusive and expensive measurement strategy. This fact has resulted in the development and application

of several non-intrusive methods, the most common of which is vibration measurement. Vibration-based knock detection is based on the principle that the acoustic modes of vibration result in mechanical excitation of the structural components of the engine. Combustion noise is primarily transferred through the piston and connecting rod. This is dominant only below 1000 Hz [Patro, T.N., 1997]. A secondary combustion noise path which proves more useful for knock detection is through the cylinder block and cylinder head.

2.4.2.1 Accelerometer Location Issues

Accelerometer (vibration transducer) location issues are analogous to those involved with pressure transducer applications. Where the pressure transducer location must accommodate acoustic resonance in the cylinder, the accelerometer placement must be done with consideration of structural mode shapes. "While analytical methods exist to identify knock sensor locations and the frequency at which knock will occur, these methods are approximations and do not account for all factors that contribute to engine knock vibration" [Forbes, J. et al., 1995]. Therefore it is usually necessary to conduct experimental investigations to determine optimal accelerometer locations.

Trial and error experimentation [Soylu., S., Gerpen, J., 1997] can prove inefficient, particularly in light of the fact that any structural modifications to the engine necessitate repetition of these efforts [Collings, N. et al., 1986]. Therefore, it is useful to employ advanced methods such as laser scanning velocimetry [Beidl, C. et al., 1999] or Holography [Forbes, J. et al., 1995, Nakamura, N. et al., 1987] for the determination of locations with both high signal to noise ratio and a broad frequency range of detection.

Generally, mechanically stiff locations more readily allow transmission of knock-induced vibrations [Dues, S. et al., 1990]. Dues also warns that locations which react to combustion vibrations with significant motion are also prone to vibration sources other than knock. One such location is the cylinder head bolts, which show high response to both knock vibration and valve train excitation [Arrigoni, V. et al., 1978]. It is particularly important to consider vibration sources [Hirako, O. et al., 1988, Witer, A.J., Lim, T.C., 1999] which occur at similar frequencies or share the same transfer path as those generated by knock.

2.4.2.2 Processing of Knock Vibration Signals

The indirect nature of vibration data makes it prone to increased background noise as the signal must propagate through the engine structure [Lee, J. et al., 1998]. This background noise increases with engine speed, often making high-speed knock detection almost impossible [Daniels, C.F. et al., 2003]. The issue of background noise is accommodated with the use of a modified version of the intensity analysis used for pressure data.

Often a noise reference window is used [Ford Internal Report, 2002] to indicate the background noise level. This can be subtracted from the knock signal, or processed independently and used to normalize the intensity calculated in the knock window. Care must be taken in the selection of these windows. If placed in a region where excessive background vibration occurs, the sensitivity of the normalized knock signal can be drastically reduced. Schmillan and Rechs conducted an investigation to locate the crank angles at which vibrations due to valve closure and piston slap occur to ensure proper placement of the knock window [Schmillan, K.P., Rechs, M., 1991].

Another method which improves signal to noise ratio is frequency discrimination. Traditionally a band pass filter of 5-20 kHz is applied to the windowed knock data to remove vibration outside the frequency range of knock. Further noise reduction can be accomplished by isolating only the fundamental knock frequency with a tighter pass-band of 7-9 kHz [Arrigoni, V. et al., 1978]. Lee et al. [1998] took this one step further by applying multiple filters to isolate the first three harmonics. Other researchers [Nakamura, N. et al., 1987, Kaneyasu, M. et al., 1992] have discovered improved knock controllability by using only the harmonic(s) which exhibited high signal to noise ratios.

Although many prefer the flexibility of wider response accelerometers [Boccardo, Y., Kizer, T., 1984], transducers can be manufactured such that their resonant frequency corresponds with the characteristic frequency being measured [Iwata, T. et al., 1989]. This has the effect of mechanically amplifying the desired frequency, and effectively acting as a narrow band filter. However, this requires extensive development [Kaji, K., 1986] to ensure a sound design.

Although not commonly used for production applications, investigations have been made into the benefits of time-frequency analysis [Samimy, B., et al., 1995, Scholl, D. et al., 1997a, Scholl, D. et al., 1997b]. Knowledge of the evolution of resonant frequencies can be used to evaluate accelerometer locations and develop time-varying filters to improve signal to noise ratio. Zhang and Tomita have developed a wavelet analysis technique (using real knocking vibrations signals as the mother wavelet) which shows less reduction in signal to noise ratio at high engine speeds [Zhang, Z., Tomita, E., 2001].

The use of statistical analysis of knock data has also been reported [Lee, J. et al., 1998, Iwata, T. et al., 1989, Ford Internal Report, 1997]. These investigations take into account the differences in cyclic intensity distribution to identify knock. Iwata et al. have demonstrated the

ability to create an automatic adjustment to knock limit based on this information. However, the nature of these methods requires the analysis of several cycles of data which could provide insufficient response time for engine management applications as reported in [Boccardo, Y., Kizer, T., 1984].

Applications of multivariate statistical analysis have been limited to reconstruction of the cylinder pressure trace based on structural vibration signals [Urlaub, M., Bohme, J., 2004, Zurita, G. V. et al., 1999] and development of interrelationships between noise and vibration indicators and engine operating conditions [Zurita, G.V. et al., 1997]. Although successful implementation of these concepts presents possibilities for improved closed loop engine control, no viable knock detection strategy has been presented. It should also be noted that the works presented by Zurita et al. applied to compression ignition engines only.

2.4.3 Knock Detection by Force Transducers

The distinction between pressure transducers and force transducers is small since pressure transducers are generally based on a force applied to their measurement surface. Piezoelectric force transducers are essentially piezoelectric elements which provide an electric output proportion to a directly applied force. Applications include instrumented cylinder head gaskets [Moble, C., 1999, Mobly, C., 2000], piezoelectric washers [Gonzalez, C., 1995, Morris, J., 1987, Sawamoto, K. et al., 1987] and custom built piezoelectric sensors [Sellnau, M.C., et al., 2000, Shimasaki, Y., et al., 2004].

Moble uses a cylinder head gasket instrumented with 20 force transducers along with advanced digital signal processing methods to construct cylinder pressure traces using non-

intrusive means. In the 2000 work, Mobley reports the ability to detect start of combustion in a multi-cylinder engine.

The application of piezoelectric washers (installed under the spark plug) reveals mixed results. The most encouraging results for knock detection come from Sawamoto et al. This work reports power improvements with the use of individual cylinder knock control as compared to global vibration-based knock control.

Sellnau et al. discuss the use of a custom-built spark plug boss with an integrated piezoelectric element. This transducer is developed primarily for closed loop engine control, but improvements in background noise over the production knock sensor are cited. Similarly, Shimasaki et al. integrate a piezoelectric element directly into the spark plug. Again, improvements are seen over the (resonant type) production knock sensor.

2.4.4 Knock Detection Using the Spark Plug

An alternative approach to knock detection uses the electrodes of the spark plug to provide information about the state of the combustion chamber gases. The most common application is through measurement of the ionization current across the electrodes when an electric bias is introduced [Collings, N. et al., 1986, Daniels, D.F. et al., 2003, Zhu, G.G. et al., 2004].

Ion current depends on the concentration of charged particles (ions). Daniels sites the presence of two distinct peaks: The first peak occurs after the spark due to the initial flame kernel development. The second peak is a result of ionization of the combusted mixture around the spark plug due to higher temperature from combustion. This second peak correlates well to

in-cylinder pressure. Daniels indicates an improvement in the detection of low intensity knock and the detection of knock at high engine speeds.

Martychenko et al. [1999] propose the use of breakdown voltage instead of ionization current. Since the dependency of breakdown voltage is on gas density rather than ion concentration, pressure measurement capability is not dependent on the presence of combustion. Although a correlation is seen with pressure, no reference is made to a knock detection application.

2.5 Conclusions

The work summarized in this chapter reveals that there are many ways to measure the knock phenomenon. A common theme in this work indicates that the amount of information on the occurrence and severity of knock depends on the number of transducers used and the processing method applied. Based on this information, a knock detection system is proposed which collects data from multiple transducers, and fully utilizes this data with the application of a multivariate analysis system.

CHAPTER 3 - THEORY

3.1 Combustion Knock In SI Engines

The term 'Combustion Knock' in the context of this thesis refers to the rapid combustion of the homogeneous air-fuel mixture present in a spark ignition (SI) engine. This condition is generally recognizable from the in-cylinder pressure trace as it is associated with an unusually high peak pressure, followed by high frequency pressure fluctuations.

There are two common theories which attempt to explain combustion knock. These are the detonation theory and the autoignition theory. The phenomenon described by these theories should not be confused with a different event known as pre-ignition. The above will be explained and contrasted in the following sections.

3.1.1 Detonation Theory

The detonation theory suggests that the normal spark-ignition flame front undergoes a transition from a subsonic deflagration to a supersonic detonation coupled with shock waves [Spicher, U. et al., 1992]. Simply put, the normal flame front associated with pre-mixed combustion accelerates to sonic velocity and consumes the end gas (unburned air-fuel mixture) at a rate much faster than would occur with normal flame speeds, thus creating the large pressure gradients associated with shock waves. Although this situation is easily repeated in long combustion tubes, there is little evidence confirming its occurrence in an IC engine combustion chamber.

3.1.2 Autoignition Theory

The more widely accepted theory is the autoignition theory. This theory being that knock in a spark ignition engine is caused by virtually instantaneous combustion of the unburned end gases ahead of the normal flame front. This rapid, constant volume combustion process produces a local pressure excess in the end gas region which results in pressure waves rushing across the diameter of the chamber at a characteristic frequency (typically 4-10 kHz [Checkel, M., Dale, J., 1986]) determined by the cylinder geometry and gas properties.

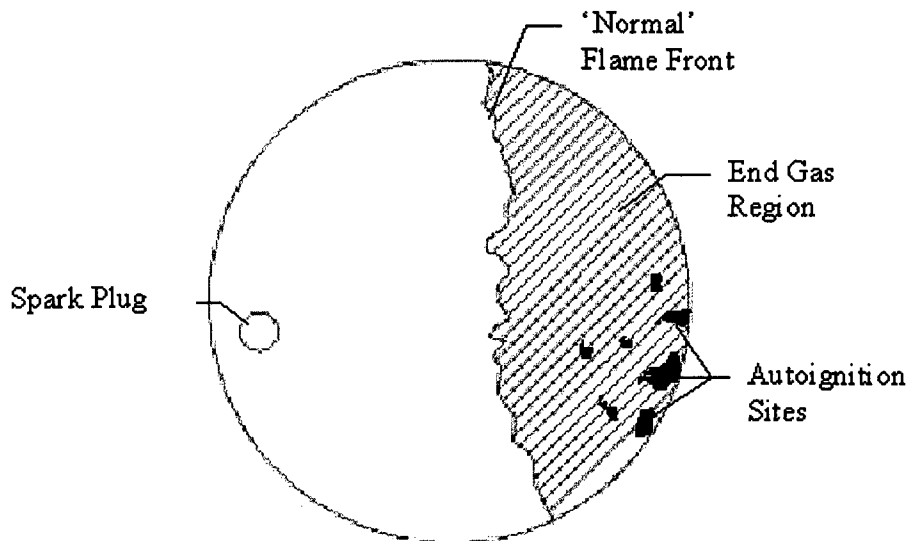


Figure 3.1 – Illustration of Autoignition Phenomenon

Ignition of the end gas occurs when the self-ignition point is reached and sustained for a finite time interval known as ignition delay. Both the ignition point and ignition delay are functions of pressure, temperature and fuel characteristics.

Combustion Knock in an SI engine is similar to that which occurs normally in a compression ignition (CI) engine with a few major differences. First (and perhaps most significant) of which is the fact that in a CI engine, the piston compresses air only. Ignition does

not occur until the fuel is injected directly into the cylinder resulting in a limited amount of fuel undergoing spontaneous combustion. The term 'Diesel Knock' refers to when ignition delay becomes large (in this case dependent on fuel and mixing), and too much fuel enters the cylinder before ignition takes place. This results in excessive pressure rise rates in the CI engine. In the SI engine, the combustion chamber is filled with a homogeneous charge of air and fuel. If this were all to ignite instantaneously, the engine would fail structurally.

Another difference between autoignition in SI and CI engines is the fact that in compression ignition engines, the ignition state is reached by piston compression alone. In an SI engine, the end gas is compressed first by the piston compression stroke, then by the expansion of the charge due to the combustion process [Heywood, J., 1988].

3.1.3 Pre-Ignition

The term 'pre-ignition' is often used interchangeably with combustion or spark knock. This tends to be misleading, since although there is an important relationship between autoignition and pre-ignition, these terms refer to two different phenomena. Pre-ignition refers to the ignition of the charge (air-fuel mixture) prior to spark plug ignition by 'hot spots' in the cylinder. A common ignition source is the exhaust valve, which undergoes constant exposure to the high temperature gases during the expulsion of burned combustion products.

As will be discussed in a later section, early ignition results in higher peak combustion pressures. These high pressure/temperature conditions can increase susceptibility to autoignition. Conversely, autoignition can result in the creation of hot spots, leading to pre-ignition. This is mainly attributed to excessive heat transfer to mechanical components due to the breakdown of their thermal boundary layers by the high pressure waves resulting from

autoignition. Therefore, pre-ignition and autoignition can potentially create a spiraling chain reaction, resulting in serious implications regarding engine durability and performance.

3.1.4 Parameters Affecting Knock

The difficulty arising in knock control is related not only to the complexity of the phenomenon itself, but to the number of inter-related parameters influencing its occurrence. Consideration of these parameters must take place everywhere, from initial design stages, to control strategies, to maintenance practices.

3.1.4.1 Design Considerations

In the design stages, knock must be considered in the development of the combustion chamber geometry. The use of a squish area (area of low clearance between piston and cylinder head) tends to promote increased heat transfer (cooling) due to a local increase in surface-to-volume ratio. Therefore, a squish area located in the end gas region can reduce temperature and thus susceptibility to autoignition [Stone, R., 1998]. Using the same principles, it is advisable to locate the exhaust valve near the spark plug. By placing this heat source near the start of combustion, excessive heating of the end gas can be avoided. Furthermore, as flame propagation speeds increase, less time is allowed for heat transfer from the end gas to the engine cooling system. Therefore, combustion chambers designed for faster combustion (ie. the use of high swirl numbers) run the risk of encountering knock problems.

One of the most important design considerations related to knock is the determination of an ideal compression ratio. Increased compression ratios result in higher peak pressures. Although this provides benefits in efficiency, power and specific fuel consumption, it creates an

unfavorable condition from the knock perspective. Therefore, as will be illustrated presently, knock is a limiting factor on engine efficiency.

3.1.4.1.1 Limits on Efficiency

The thermodynamic cycle used to model the spark ignition engine is the Otto cycle. This is illustrated below in both pressure vs. volume, and temperature vs. entropy diagrams.

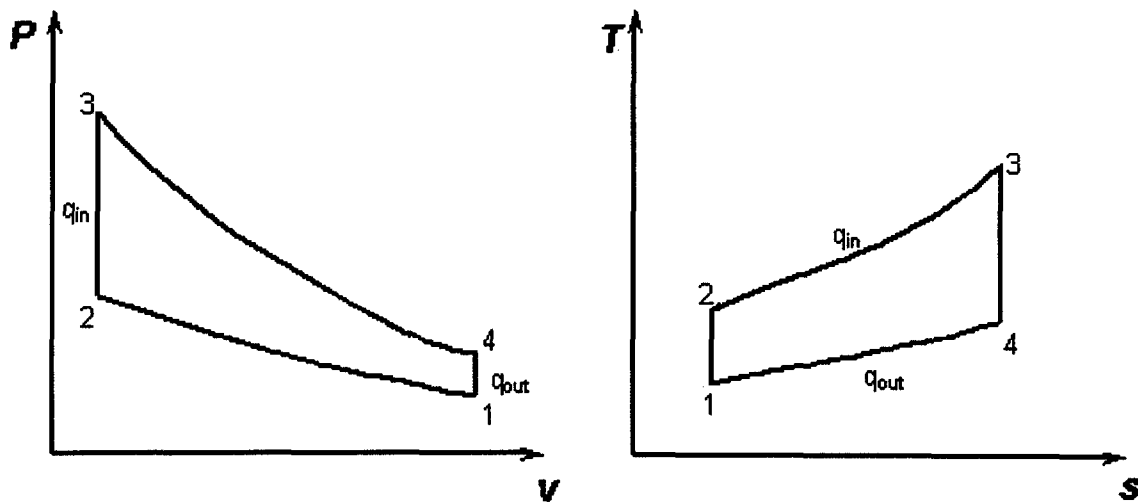


Figure 3.2 – Otto Cycle Thermodynamic Cycle

Thermodynamic Efficiency is derived as follows:

$$\eta_{otto} = \frac{w_{net}}{q_{in}} = \frac{q_{23} - q_{41}}{q_{23}} = 1 - \frac{q_{41}}{q_{23}} \quad (3.1)$$

where, for closed systems:

$$q - w = \Delta u \quad (3.2)$$

For the constant volume heat transfer processes (2-3 and 4-1), no work is involved. Using the cold air-standard assumptions*, we get:

$$\begin{aligned} q_{23} &= u_3 - u_2 = c_v(T_3 - T_2) \\ q_{41} &= u_4 - u_1 = c_v(T_4 - T_1) \end{aligned} \quad (3.3)$$

Therefore, the expression for efficiency becomes:

$$\eta_{otto} = 1 - \frac{q_{41}}{q_{23}} = 1 - \frac{T_4 - T_1}{T_3 - T_2} \quad (3.4)$$

Assuming processes 1-2 and 3-4 are isentropic:

$$\frac{T_1}{T_2} = \left(\frac{v_2}{v_1}\right)^{\gamma-1} = \left(\frac{v_3}{v_4}\right)^{\gamma-1} = \frac{T_4}{T_3} = \left(\frac{1}{r_v}\right)^{\gamma-1} \quad (3.5)$$

where r_v = compression ratio.

Using the above relationship:

$$\eta_{otto} = 1 - \frac{T_4 - T_1}{T_3 - T_2} = 1 - \frac{T_1(T_4/T_1 - 1)}{T_2(T_3/T_2 - 1)} = 1 - \frac{T_1}{T_2} \quad (3.6)$$

$$\eta_{otto} = 1 - \frac{1}{r_v^{\gamma-1}}$$

Therefore, it can be seen that since efficiency is proportional to compression ratio, and since combustion knock represents the upper limit on compression ratio, it follows that combustion knock is a limiting factor in efficiency.

* Cold Air-Standard Assumptions:

1. The working fluid is air which continuously circulates in a closed loop and always behaves as an ideal gas with constant specific heat.
2. All the processes which make up the cycle are internally reversible.
3. The combustion process is replaced by a heat addition process from an external source.
4. The exhaust process is replaced by a heat rejection process which restores the working fluid to its initial state.

3.1.4.2 Operating Parameters

During operation, several factors affect the occurrence of knock. These factors include (but are not limited to) engine load, throttle position (intake manifold vacuum), engine speed, coolant temperature, intake air temperature and pressure, spark advance, equivalence ratio and exhaust gas recirculation (EGR). Note that the majority of the above parameters are not controllable by the engine designer, and depend on driving conditions alone.

Engine load is generally measured by throttle position (max load corresponding to wide open throttle – WOT). At WOT the manifold pressure is increased, resulting in more effective scavenging of combustion products from the cylinder. A reduction of burned combustion products increases the speed of combustion. As stated in the design considerations, faster combustion promotes a high temperature knock condition.

Conversely, engine speed has a positive effect on knock by limiting the time available for the autoignition reaction to occur. This will be discussed further in the 'ignition delay' subsection. Therefore, the worst case scenario exists at high load and low rpm.

It is quite apparent that increased pressures and temperatures of air entering the cylinder will create a knock prone condition through a higher combustion temperature history. Therefore, in applications involving forced air induction (turbocharger / supercharger), inter-cooling allows a wider range of knock-free operation. Another parameter affecting temperature history directly is coolant temperature. Since heat transfer from the cylinder to coolant is proportional to the temperature gradient, high coolant temperature results in lower heat transfer from the cylinder and thus a higher combustion temperature history.

Spark advance is a common factor used to control knock; however, this presents serious implications affecting performance. If the spark is late, the peak pressure will occur too far after

top dead center (TDC), resulting in a reduction of torque. Torque then increases with spark advance until the combustion pressure begins creating too much resistance for the piston on the compression stroke, resulting in negative work. The minimum advance for best torque (MBT) is the spark advance required to reach peak torque operation. The problem that arises is that as spark is advanced, peak combustion pressure occurs at a smaller volume. This creates higher torque, but with it the risk of autoignition. Therefore, the strategy of the spark timing is to operate as close as possible to MBT without allowing knock.

Another method of reducing peak combustion temperature involves altering the equivalence ratio. The equivalence ratio (ϕ) is defined as the ratio of the actual fuel/air ratio to the stoichiometric fuel/air ratio. Therefore, at $\phi=1$, combustion is occurring at stoichiometric. Values greater than unity indicate rich (fuel rich) operation, and values less than unity indicate lean operation.

The nature of hydrocarbon combustion indicates that peak adiabatic flame temperature occurs at $\phi=1.1$, with a steep gradient on the lean side and a more gradual drop on the rich side (as the reaction is leaned out, the Nitrogen in the air (non-reacting species) acts as a dilutant). Therefore, to remove the engine from a knock condition, the equivalence ratio can be brought to a level away from that which causes peak flame temperature.

A relatively new application in IC engines is exhaust gas recirculation. Although the purpose of this system is generally aimed at emissions reductions, it benefits knock performance as well. By diluting the charge with exhaust gases, the combustion temperatures are lowered. Watanabe and Fukutani suggest that EGR is an effective replacement for spark control, as the performance loss associated with retarded spark is not present with EGR control [Watanabe, E., Fukutani, I., 1986]

3.1.4.2.1 Cyclic Variation

One characteristic of IC engines that provides an additional source of complication to many issues, including knock, is cyclic variation. Due to the nature of its operation, the internal combustion engine does not behave in a precisely repeatable fashion. This applies particularly to the combustion process.

Sources of cyclic variation in the autoignition process include [Heywood, J., Chun, K., 1989]:

- The temperatures of the residual gas, piston crown, cylinder head, cylinder liner and exhaust valve are all hotter than the intake charge (this causes a variable temperature distribution in the unburned mixture due to imperfect mixing)
- Autoignition will occur first at one or several locations where the local end gas has passed through the highest temperatures
- Flame thickness can be comparable to thickness of the end gas region, therefore wrinkles in the flame can divide the end gas into separate regions

In the case of knock, complications present themselves when trying to design a control system to accurately determine when knock conditions are present, and provide an effective strategy to eliminate such conditions. Since knock is not consistent, even during steady state [Iwata, T. et al., 1989], one approach to solving this problem is treating knock statistically.

Cyclic variability does present one advantage in the field of knock control. If knock were to occur consistently, a slight knock could easily lead to a runaway knock condition. Since the problem begins intermittently, it can be corrected before a substantial amount of damage is caused. However, although this principle applies to temporal variation, cylinder-to-cylinder variation creates only problems. Without individual cylinder control, the detection of knock

caused in only one cylinder could lead to a spark retard strategy, adversely affecting performance in all cylinders.

3.1.4.3 Maintenance Issues

Octane Number is a concept that will be discussed thoroughly in the next section. For now, it will be simply defined as the rating of a fuel's resistance to knock (the higher the rating, the more resistance to knock). An important factor in the maintenance of an IC engine is the use of fuels with the correct octane number.

Octane requirement is initially determined in the design stage and can change throughout the life of the vehicle. Combustion (carbon) deposits lead to a phenomenon known as octane requirement increase (ORI) which can increase several octane numbers over 18 000 miles [Liiva, P. et al., 1992]. However, although high correlations have been established between combustion deposits and octane requirement, it is not known whether these contributions are dominated by thermal, volumetric or chemical effects.

3.1.5 Octane Rating

Although there is a degree of validity to the statement “high octane fuels are performance fuels”, it is somewhat misleading. Higher octane fuel does not create performance, it merely allows it. Octane rating is a number which indicates a fuel's resistance to knock; therefore, when an engine is designed for higher octane fuel, a more aggressive strategy (high compression ratio, more spark advance, ...) can be used to enhance performance and efficiency.

3.1.5.1 Definition and Determination of Octane Number

The octane number of a fuel is simply a practical measure of its resistance to knock. The scale is established by defining n-heptane as zero octane fuel (low knock resistance) and iso-octane (2,2,4-trimethylpentane) as 100 octane fuel (high knock resistance).

The antiknock index (value indicated as octane number at the pump) is an average of two values. The research octane number (RON) and motor octane number (MON) are both determined using a single cylinder, variable compression research engine. In both methods, the air/fuel ratio is adjusted to obtain maximum knock conditions for the given test fuel. The compression ratio is then increased until a standard knock intensity is reached. This test fuel is then compared to reference fuels to determine its knock resistance.

When testing fuels with octane number between 0 and 100, the reference fuel is a blend of n-heptane and iso-octane, and the ON is defined as the percent by volume of iso-octane. For fuels with ON greater than 100, iso-octane is used with knock additives (trace compounds which increase ON). The knock resistance is then determined by the amount of additive used to match test fuel performance.

The RON and MON use different operating conditions such as intake air temperature, engine speed and spark advance. Since the conditions used for MON are more severe, the knock resistance values tend to be lower. The arithmetic mean of these two values is defined as the antiknock index and is that which is used commercially.

3.1.5.2 Trends in Fuels

Several trends have been identified which predict the knock performance of various hydrocarbon structures:

- Knock resistance is higher with more compact structures (shorter or branching chains).
 - Ex.1 – Straight Chains: $ON(\text{n-heptane}) < ON(\text{n-butane}) < ON(\text{methane})$
 - Ex.2 – Isomers: $ON(\text{n-heptane}) < ON(\text{2-methylhexane}) < ON(\text{2,3-dimethylpentane})$ (all have 7 carbon atoms)
- Double and triple bonds generally increase knock resistance (with the common exceptions of acetylene and ethylene).
 - Ex. 1 – General Rule: $ON(\text{butane}) < ON(\text{2-butene})$
 - Ex. 2 – Exceptions: $ON(\text{ethane}) < ON(\text{ethylene}) < ON(\text{acetylene})$ (all have 2 carbon atoms – latter two species have double and triple bonds respectively)
- Knock resistance of cyclic hydrocarbons is greater than straight chain hydrocarbons, but significantly lower than that of corresponding aromatics.
 - Ex: $ON(\text{n-hexane}) < ON(\text{cyclo-hexane}) \ll ON(\text{benzene})$
- Knock resistance of aromatics is reduced considerably with increasing size of chain attached to the basic carbon ring.
 - Ex: $ON(\text{toluene}) < ON(\text{benzene})$

3.1.5.3 Ignition Delay

Although self-ignition results in a rapid combustion process, the initiation reactions involved require a finite time to occur. This time interval is termed 'ignition delay'. In fact, the end gas in all spark ignition engines running at compression ratios near their critical values

reaches the fuel's ignition point before flame arrival. It is therefore ignition delay that prevents knock from occurring. Since ignition delay is a characteristic of the fuel, this offers an explanation for the differences in octane rating from one fuel to the next.

3.1.5.3.1 Multistage Ignition

Autoignition generally occurs in three stages which are named by their distinguishing characteristics [Levendahl, W.J., 1956]:

1. Peroxide Stage:

- Believed to produce alkyl hydroperoxides
- Not measurably exothermic
- Function: Responsible for producing sufficient active particles to promote the exothermic cool flame reaction

2. Cool Flame Stage:

- Slightly exothermic
- Produces a blue radiation, believed to be from excited formaldehyde
- Reaches a maximum rate @ moderate temperatures
- Function: Promotes autoignition by heating the mixture (end gas) to the characteristic temperature region (hot flame limit)

3. Hot Flame Stage:

- Highly Exothermic
- Generally rapid
- Produces intense radiation
- Function: Responsible for the audible “knock”

Ignition delay consists of the time required to complete stages 1 and 2 of the multistage ignition process. The time required to produce the reactive species in the peroxide stage is sometimes termed the 'primary delay'; correspondingly, the time taken for the cool flame reactions to heat the mixture to the hot flame limit is termed the 'secondary delay'. The sum of these is known as 'total delay' or simply 'ignition delay'.

3.1.5.3.2 Effect of Ignition Delay on ON

Determination of the correlation of ignition delay to knock rating has been accomplished [Livengood, J.C., Wu, P.C., 1956] using a rapid compression machine. Various air-fuel mixtures (different knock ratings) are compressed to a constant volume, and the time for the reaction to initiate (ignition delay) is determined. This provides evidence of a high correlation between ignition delay and octane rating.

Further studies [Levendahl, W.J., 1956] have strived to determine the relationship between knock resistance and the preliminary peroxide and cool flame reactions. It has been determined that although the hot flame limits (autoignition points) of various hydrocarbons are similar, their peroxide stage and cool flame limits differ considerably. Therefore, it is postulated that a fuel's knock resistance is heavily dependant on the low temperature initiating reactions.

Therefore, for fuels which readily undergo cool flame reactions at low temperatures, once the cool flame limit is reached it is only a matter of time (ignition delay) before these reactions raise the temperature to a point where autoignition (hot flame reaction) occurs. This explains the relatively high knock rating of methane. Upon observing the full reaction mechanism of methane, one cannot identify the reactions or species commonly associated with the low temperature reactions. Therefore, for knock to occur in a methane-fueled engine, the end gas

must be compressed up to the high temperature hot flame limit without the aid of the low temperature exothermic cool flame reactions; thus decreasing the likelihood of knock or increasing the octane rating.

3.1.6 Characteristic Knock Frequencies

When autoignition occurs, a local high pressure exists initially in the end gas region (autoignition sites). This creates a high pressure wave which propagates from the outer edge of the end gas towards the spark plug, while an expansion wave propagates into the high pressure region toward the near wall. As these waves reflect within the cylinder a resonance may occur, causing the audible 'knock' associated with autoignition.

The resonance frequencies associated with knock can be determined by Draper's equation [Draper, C.S., 1933]:

$$f_{mn} = \frac{\rho_{mn}}{\pi} \cdot \frac{c}{B} \quad (3.7)$$

where,

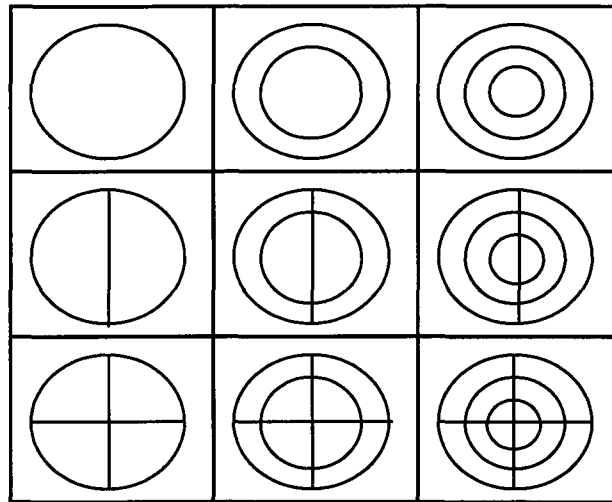
c = speed of sound

b = cylinder bore diameter

ρ_{mn} = mode constant

Table 3.1 illustrates the lines of projections of nodal surfaces for some examples of possible mode shapes present during combustion knock.

Table 3.1 – Knock Frequency Mode Shapes



It should be noted that the modes shown in the first column are consistent with the generalization made suggesting that the characteristic knock frequencies lie between 3 and 10 kHz; however, higher frequency radial modes have also been observed [Schaberg, P. et al., 1990] although they are not dominant. Also note that this frequency is controlled primarily by temperature and bore diameter. It can also be seen that this dependence on temperature has the potential of causing control problems due to variation of the resonance frequency with operating conditions.

3.2 Transducer Theory

Transducers are devices which convert an input energy into an output which can be read by a data acquisition device. Some of the fundamentals associated with piezoelectric transducers and techniques for mounting pressure transducers will be discussed here.

3.2.1 Piezoelectric Transducers

Piezo is a Greek term which means “to squeeze”. When piezoelectric elements are strained by an external force (squeezed), displaced electrical charge accumulates on opposing surfaces. Therefore, strained crystal elements create electrical output (hence the origin of the term piezoelectric).

3.2.1.1 Piezoelectric Phenomenon

Consider that a crystalline solid is made up of positively and negatively charged atoms (ie. silicon atoms and oxygen atoms respectively). If the distribution of these atoms (charges) is non-symmetrical, stressing the crystal may displace positive charges relative to the negative charges. Resulting are two opposing sides which were previously electrically neutral becoming positively and negatively charged. Figure 3.3 illustrates the effect of an applied compressive force on the crystal.

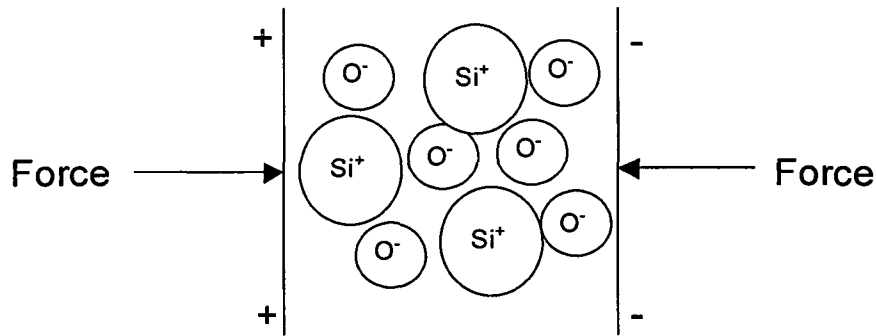


Figure 3.3 – Piezoelectric Effect

The above figure illustrates the longitudinal effect. This implies merely that charges on the x-planes of the crystal are created from force acting upon the x-plane. It is also apparent from this figure that the same deflection could be caused by creating tension in the perpendicular direction. This is known as the transversal effect.

Note that substances such as table salt (NaCl) have symmetrical distribution of charges and therefore do not lead to piezoelectricity. In the case of a piezoelectric material, the crystal should be cut along a crystalline axis such that the relative charge displacement is a maximum.

The crystal elements in transducers actually serve a dual function. They act as a precision spring to oppose the applied pressure and force as well as supplying the electrical signal proportional to their deflection. With stiffness values on the order of 15E6 psi (104E9 N/m²), which is similar to that of many metals, piezoelectric materials produce a high output with very little strain (elements have essentially no deflection and are often referred to as solid-state devices). This is the reason that piezoelectric sensors are so rugged and feature excellent linearity over a wide amplitude range. In fact, a single accelerometer can measure from 0.0001 g's to 100 g's. To vary sensitivities, piezoelectric crystals can be connected electrically in parallel and mechanically in series or parallel.

ie.

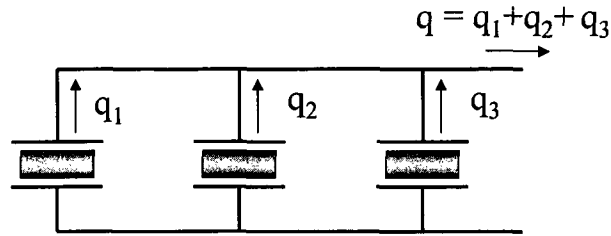


Figure 3.4 – Piezoelectric Crystal Stacking

3.2.1.2 High Impedance Piezoelectric Transducers

High impedance, or charge mode transducers represent the original configuration of piezoelectric transducer. As the name implies, these transducers represent directly output the high impedance electrical charge signal that is generated by the piezoelectric sensing element.

To conduct accurate measurements, it is necessary to condition this high impedance charge signal into a low impedance voltage which can be read into a readout or recording device. This is usually accomplished via an external charge amplifier or an in-line charge converter. As the signal is passed from the transducer to the charge amplifier, it is extremely sensitive to corruption from environmental influences such as triboelectric effect (motion induced), electromagnetic signals and radio frequency interference. Therefore, special low noise, coaxial cable is required between the transducer and amplifier. It is also necessary to maintain a high insulation resistance of the transducer, cabling and connectors (must be kept dry and clean).

Despite the problems associated with this transducer type, they have two significant advantages. Since there are no internal electronics (in contrast to the Low Impedance transducers which will be discussed shortly), certain models are capable of operating at temperatures up to 1000°F (540°C). Furthermore, these transducers represent much more versatility. Characteristics such as time constant, gain, normalization and reset can all be

controlled via the external components, whereas some of these are fixed in the case of internal circuit transducers.

3.2.1.3 Low Impedance Piezoelectric Transducers

As alluded to above, the other major classification of piezoelectric transducer is known as the voltage mode or low impedance type transducer. Also mentioned above is the main difference associated with these transducers – internal conditioning. These are also commonly known by PCB's registered trademark name – Internal Circuit Piezoelectric or ICP transducers.

The built-in electronics in the low impedance transducers serve to convert the high impedance charge signal generated by the piezoelectric sensing element into a usable low impedance voltage signal which can be readily transmitted over ordinary two-wire or coaxial cable to any voltage readout or recording device. This has the obvious advantage of ease of use. All that is required externally is an excitation power from a constant current, DC voltage source. For further convenience these sources are often built in to analyzers and data collectors (ie. Hewlett Packard 35670A Dynamic Signal Analyzer).

Another advantage is the capability of being transmitted over long cables through harsh environments with negligible signal degradation. As mentioned in the discussion of high impedance transducers, the main disadvantages associated with this type are the limited operational temperature range (< 121 °C) and the fixed functional characteristics.

3.2.1.4 Frequency Response

All piezoelectric transducers for measuring pressure, force and acceleration may be regarded as underdamped, spring mass systems with a single degree of freedom. They are modeled by the classical second order differential equation whose solution is given as:

$$\frac{a_o}{a_b} \cong \frac{1}{\sqrt{\left[1 - \left(\frac{f}{f_n}\right)^2\right]^2 + \left(\frac{1}{Q^2}\right)\left(\frac{f}{f_n}\right)^2}} \quad (3.8)$$

where,

f_n = undamped natural (resonant) frequency (Hz)

f = frequency at any given point of the curve (Hz)

a_o / a_b = output and mounting base acceleration

Q = factor of amplitude increase at resonance (approx. 10-40 for quartz transducers)

A typical frequency response curve is shown below in Figure 3.5. As can be seen in this figure, approximately 5% amplitude rise can be expected at about 9/40 of the resonant frequency.

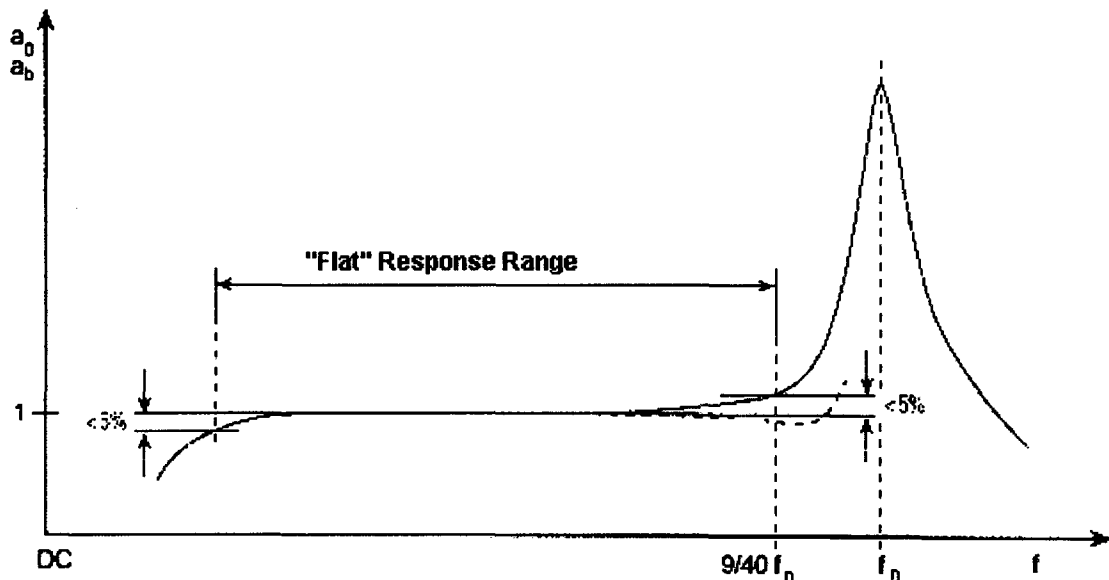


Figure 3.5 – Typical Transducer Frequency Response Curve

The "Flat Response Range" in the above figure applies to flat response type transducers. The defining characteristic of this group is the high resonant frequency leading to a relatively flat response throughout the operating range. Filtering is done externally which allows for more versatility.

In contrast, the other broad category of transducers is known as resonant type transducers. These utilize the built-in mechanical amplification and filtering characteristics associated with resonance. Since resonant transducers must be tuned to the frequency of interest, these are application specific products. Two sub-classifications include the spike resonant and broadband resonant transducers. Spike resonant transducers have a narrow bandwidth of approximately 100 Hz, requiring careful design and/or selection. Broadband resonant transducers are a little more forgiving with a bandwidth of approximately 1000 Hz.

3.2.2 Pressure Transducer Mounting Techniques

There are generally two categories of methods used when mounting a pressure transducer in a combustion environment. These include the flush mount technique as well as several techniques that use various strategies for mounting the transducer at a location remote from the combustion environment.

3.2.2.1 Flush Mount Technique

Mounting a transducer flush within the measurement environment is the most common mounting technique. The popularity of this method stems from its ability to respond quickly to transient pressures and avoid the introduction of false resonances as seen in remote mounting

techniques. However, by mounting the transducer in the high temperature combustion environment, the transducer is exceedingly susceptible to thermal shock.

Thermal shock is described as high temperature transients resulting in transducer drift error. This error is due to changes in Young's Modulus of the sensing element (in the case of piezoelectric transducers) and distortion of the diaphragm or base. The diaphragm will tend to deform toward the base since it is generally pinned at the ends and preloaded.

3.2.2.2 Remote Mounting Strategies

Methods involving mounting of the transducer at a location removed from the combustion environment represent a step taken to eliminate or reduce error due to thermal shock. This is an alternative to methods such as heat shields or silicon coatings protecting sensor housings from direct exposure to combustion products. It should be noted that for applications in which there is high cyclic variability (ie. IC engines), there are currently no effective methods of post-processing the data to remove the resulting signal distortion.

When mounting the pressure transducer in a remote location, a small passage is used to relay pressure information from the measurement region to the transducer diaphragm. If designed properly, this passage can quench the combustion flame before contact with the transducer. Randolph [1990a] refers to a study conducted by Shi and Shang which claims significant improvements in accuracy when adding this passage. This is particularly impressive since the transducer used in their study was a Kistler 6121 which is equipped with a head shield and is supposed to be relatively resistant to thermal shock effects.

As also pointed out by Randolph [1990a, 1990b], the implementation of this passage must be done with several factors in mind. These include not only flame quenching criteria, but signal degradation and erroneous pressure signals.

The following equations describe the conditions for standing waves and Helmholtz Resonances respectively:

$$\omega_s = \frac{c}{2l_p} \quad (3.9)$$

$$\omega_H = \frac{c}{2\pi} \sqrt{\frac{A_p}{l_p V_c}} \quad (3.10)$$

where,

ω_s = standing wave resonant frequency

c = speed of sound

l_p = passage length

ω_H = Helmholtz resonant frequency

A_p = cross-sectional area of passage

V_c = volume of cavity adjacent to transducer diaphragm

As seen from above, both resonances are dependant on passage length, and the Helmholtz resonance also depends on the passage cross-sectional area and cavity volume. Therefore, to raise the resonant frequencies above values which would interfere with pressure measurement, a short passage with a large cross-sectional area is favored.

The following equation governs the rate of pressure drop through the passage:

$$\frac{d\Delta p}{dt} = \left[\frac{2l_p V_c}{R_h^2 A_p} \right] \mu(t) \frac{d \ln(\rho_c)}{dt} \quad (3.11)$$

where,

Δp = pressure drop across passage

R_H = hydraulic radius = A_p/L_p

μ = viscosity

ρ = density

As seen above, the same criterion (short passage with large cross-sectional area) is favored for minimizing pressure drop. Therefore, the ideal passage has a diameter equal to that of the pressure diaphragm and a length of zero, which reverts back to the flush mount strategy, allowing the combustion flame to contact the transducer diaphragm directly. In fact, to effectively quench the combustion flames, the passage must have a finite length, with a diameter of under 0.2 mm for a circular passage or a minor distance of 0.15 mm for a rectangular passage [Randolph, A., 1990a].

3.3 Conclusions

The compilation of information in this chapter serves two main objectives. First, a detailed knowledge of the knock phenomenon allows greater understanding of methods required for inducing and detecting knock. Second, information about transducer theory of operation ensures an educated application of these transducers in the development of an effective measurement system.

CHAPTER 4 – TRANSDUCER VALIDATION

4.1 Introduction And Objectives

Several algorithms and techniques have been developed to gain insight into the combustion process based on in-cylinder pressure-time or pressure-volume history. Information such as peak pressure, peak pressure location, mean effective pressures, or pressure fluctuations caused by abnormal combustion can be derived directly from pressure-time or pressure-volume information. Still more work has been done [DSP Technology (1996), Heywood (1988)] which derives from the pressure information insight into heat transfer and mass burn processes.

However, pressure is not measured directly, but is deduced generally from the effects of the pressure on some other parameter or the effects of the prevailing pressure on some characteristic of the sensor being employed in the measurement system. Therefore, the validation of transducers used for quantification of the in-cylinder pressure becomes a very important and complex endeavor.

The studies presented in this work involved the use of pressure transducers for general performance evaluation as well as detection of abnormal combustion. In the evaluation of performance parameters such as cycle peak pressure, the crank angle at which this peak pressure occurs and indicated mean effective pressure, accuracy of the absolute pressure signal throughout the engine cycle is essential. In contrast, in-cylinder knock detection relies only on the amplitude of fluctuation of the pressure signal during the knock event. Reliability here is paramount, as in-cylinder knock detection provides the standard of comparison in the development of a vibration-based knock detection system. Details of the in-cylinder and vibration-based knock detection strategies are provided in Chapter 5.

The transducer technologies investigated include piezoelectricity and fiberoptics. Furthermore, transducer mounting techniques were also studied. The study of these techniques comprises the effects of flush mounting vs. remote mounting as well as the location dependence on measurement accuracy and signal-to-noise ratio.

A flush mounted transducer (measurement surface installed flush with the combustion chamber wall) is in direct contact with the high temperature combustion environment. Consequently, the transducer is vulnerable to short term and long term thermally induced transient signals known respectively as thermal shock and thermal drift. This vulnerability can be partially alleviated by the removal of the transducer from the high temperature environment by means of remote mounting. However, this requires the utilization of a connecting passage which communicates the in-cylinder pressure to the remote location. It has been shown [Randolph (1990a)] that this can present new difficulties relating to pressure attenuation and resonance within these passages.

Transducer location within the cylinder becomes particularly important in cases where abnormal combustion occurs. The audible nature of combustion knock is a result of acoustic resonance within the cylinder. The mode shape of this resonance will result in nodes and antinodes within the measurement environment. It becomes readily apparent that location near a node (region of limited response) is undesirable for the detection of the pressure fluctuation associated with knock.

Specifically, the four models tested are the Kistler 6123 flush mounted piezoelectric transducer, the Kistler 6125 flush mounted piezoelectric transducer, the Kistler 6117 spark plug mounted piezoelectric transducer and the Optrand AutoPSI flush mounted fiberoptic transducer.

Mounting strategies were evaluated based on the remotely mounted spark plug integrated transducer as well as five flush mount locations oriented along the combustion chamber wall.

Validation was conducted via comparison studies. The various transducers were used to measure the same events and the results compared to evaluate consistency.

It should be noted that ideally comparison would include an industrial standard for accuracy such as the Kistler water-cooled 7071 ThermoCOMP Quartz Pressure Sensor. This transducer quotes a much lower thermal shift and thermal shock sensitivity than the non-cooled 6123 and 6125. However, this class of transducers is not only much more costly, but the size poses constraints when installed in a production internal combustion engine. One of these constraints relates to severe limitation or elimination of coolant flow when installed through the cylinder head water jacket (passage through which glycol flows to provide cooling of the engine components). The results of this could range from significantly modified combustion chamber temperatures to engine failure.

4.2 Stage One Comparison

In the first stage of comparison, the flush mount transducers were mounted in the same position on the combustion chamber wall. This quite obviously poses the limitation of measurement by one transducer at a time. For the purpose of obtaining a low bias in the comparison of the three transducer types, a full factorial experiment was conducted.

4.2.1 Experimental Details

A design of experiment was conducted for transducer comparison. To this end, the transducer type was treated as a three-level factor (those levels include the flush mount piezoelectric (6123), flush mount optical (AutoPSI) and spark plug mount piezoelectric (6117)).

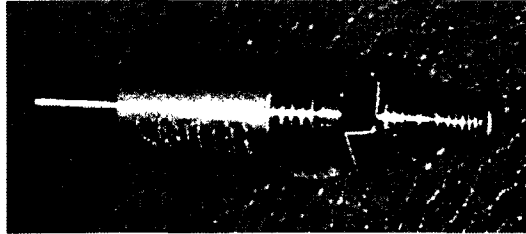


Figure 4. 1 - Kistler 6123 Flush Mount Piezoelectric



Figure 4. 2 - Kistler 6117 Spark Plug Piezoelectric

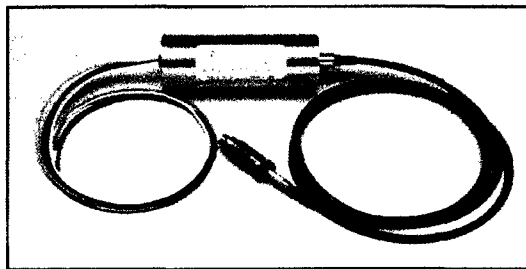


Figure 4. 3 - Optrand AutoPSI Fiberoptic

Table 4. 1 - Pressure Transducer Characteristics

Model	Range	Sensitivity	Natural Frequency	Linearity	Sensitivity Shift	Thermal Shock	Linearity, Hysteresis & Thermal Shock
6123	250 bar	-16 pC/bar	100 kHz	± 0.5 % FSO	± 3 % @ 200±150 °C	ΔP < -1.5 bar	
6125	250 bar	-16 pC/bar	75 kHz	± 0.5 % FSO	± 2 % @ 200±150 °C	ΔP < -0.5 bar	
6117	200 bar	-16 pC/bar	130 kHz	± 0.6 % FSO	± 1.5 % @ 200±50 °C	ΔP < -0.8 bar	
AutoPSI	200 bar	40 mV/bar	120 kHz		± 0.03 % / °C		± 1 % FSO

The in-cylinder pressure transducers used are purely dynamic transducers. That is, they measure only changes in pressure and are incapable of measuring absolute pressures. Several methods have been proposed [Randolph (1990b)] for providing an adequate reference for these dynamic signals. A commonly accepted pegging (referencing) method is the measurement of intake port pressure when the piston reaches bottom dead center (BDC) of the intake stroke. An assumption is made here that at this point in the cycle, the intake port pressure equalizes with that in the cylinder. This therefore provides an estimate of in-cylinder pressure. The dynamic transducers then measure pressure throughout the remainder of the cycle.

A Kistler 4045 piezoresistive absolute pressure transducer was used for pressure pegging. It was mounted in the cylinder #1 intake runner as shown in Figure 4.4.

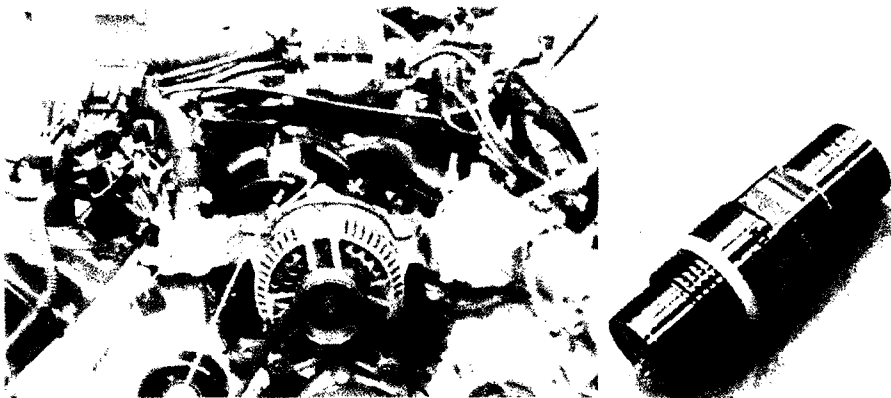


Figure 4. 4 - Absolute Pressure Measurement

Data were acquired in the position (crank angle) domain using a Kistler Model 2612 optical encoder installed on the crankshaft damper pulley. This encoder produces two signals. A 360 pulse/revolution signal provides an encoder signal with a resolution of 1 degree. A second signal consisting of a single pulse/revolution allows synchronization of the measurement signals with engine crank angle.

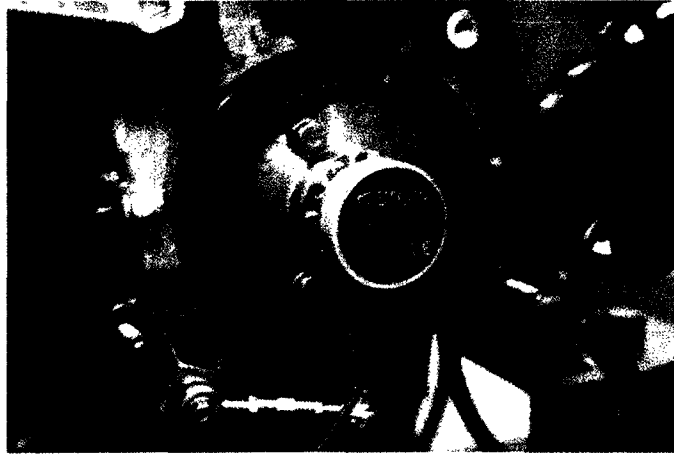


Figure 4. 5 - Crank Angle Optical Encoder

Transducers were installed in each cylinder of a V8 engine. The cylinder head was used as an additional two level factor, these levels consisting simply of right and left cylinder heads. Four transducers were used to obtain the average response for each cylinder head. A full factorial study based one two-level factor and one three-level factor requires a total of six test conditions. Table 4.2 lists these conditions.

Table 4. 2 - Stage 1 Test Matrix

Condition	Right Bank	Left Bank
1	Fiberoptic (flush)	Piezoelectric (flush)
2	Spark Plug (piezoelectric)	Piezoelectric (flush)
3	Fiberoptic (flush)	Spark Plug (piezoelectric)
4	Piezoelectric (flush)	Fiberoptic (flush)
5	Spark Plug (piezoelectric)	Fiberoptic (flush)
6	Piezoelectric (flush)	Spark Plug (piezoelectric)

One advantage of this test plan is the fact that both banks are tested simultaneously. This not only increases the amount of data collected from each transducer, but also allows multiple transducer types to be tested at identical operating conditions. Also indicated is the fact that each set of transducers was tested on both cylinder banks an equal number of times, reducing the

effect of bank-to-bank variation. Furthermore, the above set of conditions was run three times in a quasi-random order (testing efficiency issues prohibited full randomization) to further reduce bias and noise caused from variation in engine operating conditions.

The location of the transducers is indicated in Figure 4.6. Positions p1-p4 and p5-p8 indicate the external mounting location of the flush mount transducers when tested in the right and left banks respectively. Also illustrated using a combustion chamber schematic is the difference in position of the flush mount and spark plug mounted transducers.

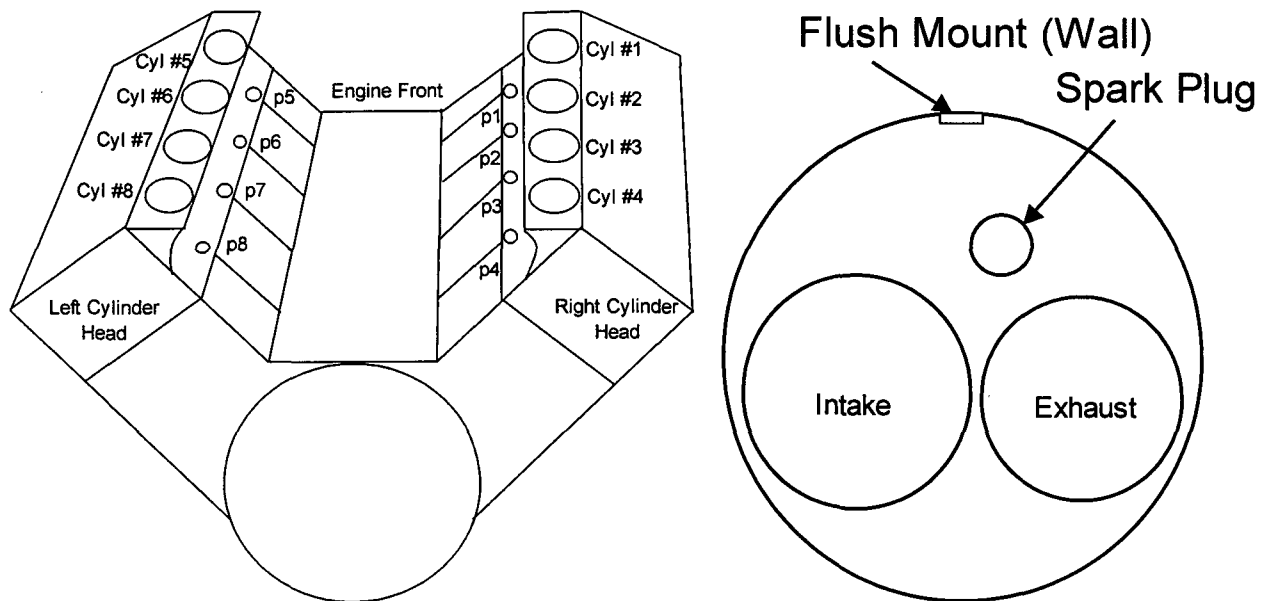


Figure 4. 6 - Stage 1 Transducer Location

Operating conditions such as rpm, spark advance, coolant temperature and engine load were controlled using a dynamometer control system and a programmable EEC (Electronic Engine Control) System. Still more parameters were acquired along with the response data to assess reproducibility.

The engine operating conditions tested include:

- 1000 rpm, Part Load (10 inHg intake manifold vacuum)
- 1000 rpm, WOT (Wide Open Throttle – full load)
- 3000 rpm, Part Load
- 3000 rpm, WOT
- 5000 rpm, Part Load
- 5000 rpm, WOT

Data were acquired using DSP Technology combustion data acquisition equipment in conjunction with RedLine ACAP software. This modular system is equipped with a Model 2812 ADC card which provides 12 bit resolution with a maximum 100 ksample/channel analog to digital conversion rate.

4.2.2 Analysis of Data

The Response data used for the purpose of transducer comparison includes the imep (indicated mean effective pressure), cycle peak pressure and crank angle at which peak pressure occurs.

All data analysis for this stage of testing was conducted in real time using the DSP Model 4325 Real Time Processor (RTP) and the RedLine ACAP Software. This processor uses a Texas Instrument TMS320C25 digital signal processing chip. Digital data from the signal input channels (Model 2812) were simultaneously processed by the RTPs and stored in raw data format. Data output files were created for both processed and raw data. In this case, processed

data files were produced for imep, cycle peak pressure and cycle peak pressure location (crank angle).

These processed data files were then exported to MS Excel for further data reduction, analysis and display. For each test/operating condition, the results were averaged over 3 runs, 300 samples/run and 4 cylinders.

4.2.3 Results and Discussion

It can be observed from Table 4.2 that after three replications, 18 runs will produce 6 sets of response data from each transducer in each cylinder bank. The average response data of these 12 runs are combined and averaged to obtain the baseline transducer data for the purpose of comparison.

The following steps were taken to increase precision and reduce bias in the results:

- Three hundred engine cycles were averaged to reduce the effect of cyclic variability
- A total of 6 sets of data were acquired from each cylinder bank to reduce the effect of bank-to-bank variation
- Data were acquired simultaneously from each bank, and three replications were completed to randomize any contribution from engine operating conditions

A summary of average response data and data comparison is presented in Figures 4.7–4.9. For the purpose of normalized comparison, the piezoelectric flush mounted transducer was taken to be the standard, and the fiberoptic and spark plug mount piezoelectric transducers were compared to it using the standard equation:

$$\%Diff = \frac{(\text{result from spark plug / fiberoptic}) - (\text{result from piezoelectric})}{(\text{result from piezoelectric})} \times 100 \quad (4.1)$$

The response data represented in Figure 4.7 indicates that the peak pressure measurements from all transducers agree within approximately 1 bar. Again, treating the 6123 transducer as the standard, a variation of less than 3 percent is seen in the AutoPSI and 6117 transducer results. Although no consistent trend can be seen with respect to engine speed, peak pressure measurement variation tended to increase with load.

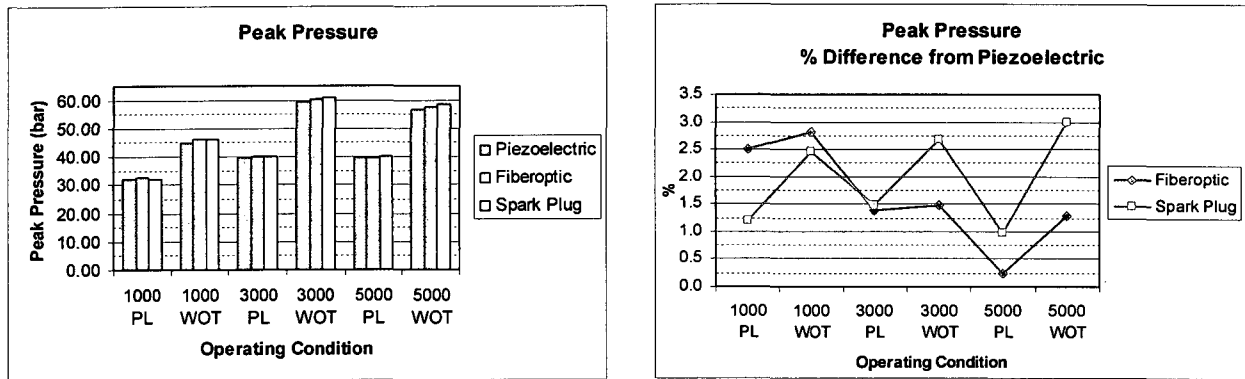


Figure 4. 7 - Stage 1 Response Data - Peak Pressure

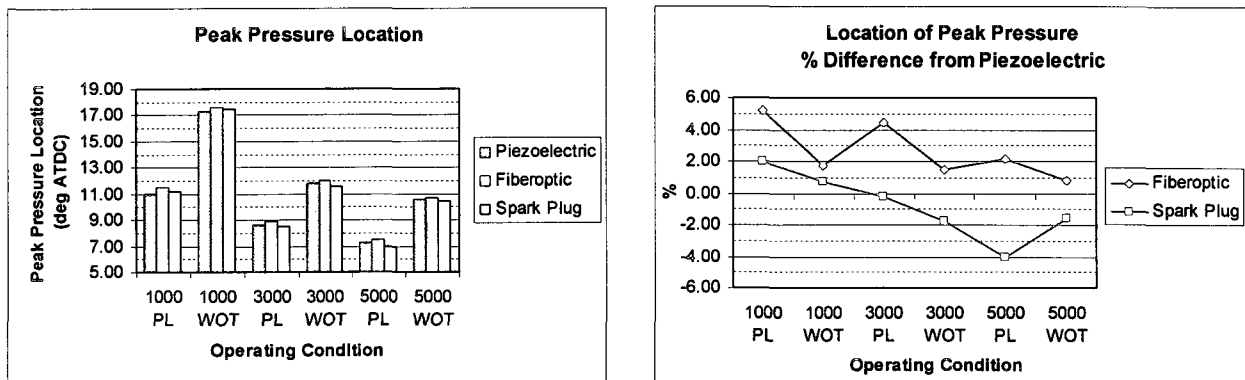


Figure 4. 8 - Stage 1 Response Data - Peak Pressure Crank Angle

Figure 4.8 indicates a variation of up to 6 percent when measuring the crank angle at which peak pressure occurs. However, this translates to agreement of less than 0.5 degrees. Since the encoder signal had a crank angle resolution of 1 degree, the transducers were not a limiting factor in the accurate determination of peak pressure location.

Indicated mean effective pressure is calculated through integration of the pressure-volume curve throughout the engine cycle. Therefore, any errors in the measurement of pressure magnitude and location are compounded. This large compounded error manifests itself in the excessive imep variation shown in Figure 4.9. Insight into these variations is difficult to obtain without simultaneous pressure traces from each transducer. For this reason, further interpretation of this variation is reserved for the stage 2 validation testing.

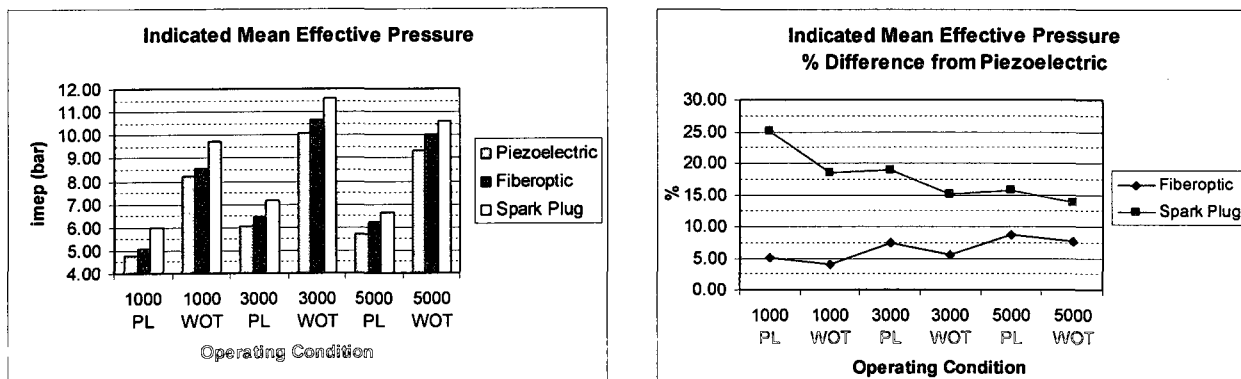


Figure 4. 9 - Stage 1 Response Data - Indicated Mean Effective Pressure

4.3 Stage Two Comparison

For the stage two comparison, additional cylinder head machining facilitated the installation of pressure transducers in multiple locations within the combustion chamber. The purpose of this modified testing format was twofold. First, simultaneous acquisition allowed a more direct comparison of transducer technologies. Second, an optimal transducer location can

be investigated through the use of a consistent transducer technology in multiple combustion chamber locations.

Another aspect to this stage of testing is the assessment of the knock detection capabilities of the transducers technologies and locations. Accurate engine performance evaluation relies on a transducer's ability to effectively determine the absolute pressure history during a complete engine cycle. Knock detection requires the measurement system to capture the high frequency pressure fluctuations which occur over a brief period of time within the cycle as a result of acoustic resonance created by the abnormal combustion event.

4.3.1 Performance Data Measurement Comparison

This subsection of stage two validation is concerned with revisiting the investigation of performance measurements such as imep, peak pressure and peak pressure location. Through simultaneous measurement with multiple transducers, more insight can be gained into the source of variation between transduction technologies.

4.3.1.1 Experimental Details

Included in this stage of evaluation was the Kistler 6125 flush mount piezoelectric transducer as well as the Kistler 6123, Kistler 6117 and the Optrand AutoPSI transducers tested in the first stage. The 6125 is structurally similar to the 6123, but the materials used are modified to reduce sensitivity to thermal effects. Pressure pegging was conducted as described in section 4.2.1 using the Kistler 4045 piezoresistive transducer.

Following is a list of the transducer locations studied. It should be noted that forward (front) offset refers to an offset toward the intake side of the cylinder (which is toward the front

of the engine on the right cylinder head and rear of the engine on left cylinder head). These locations are illustrated in Figures 4.10 and 4.11 and include:

- Spark plug mount
- Central flush mount (all cylinders)
- 45 degree forward offset (cylinders #2 and #7)
- 45 degree rearward offset (cylinders #3 and #6)
- 90 degree forward offset (cylinder #8)
- 90 degree rearward offset (cylinder #4)

Space constraints prohibited the mounting of more than two flush mount transducers per cylinder. Therefore, to complete all comparisons, multiple runs were needed as indicated in Table 4.3.

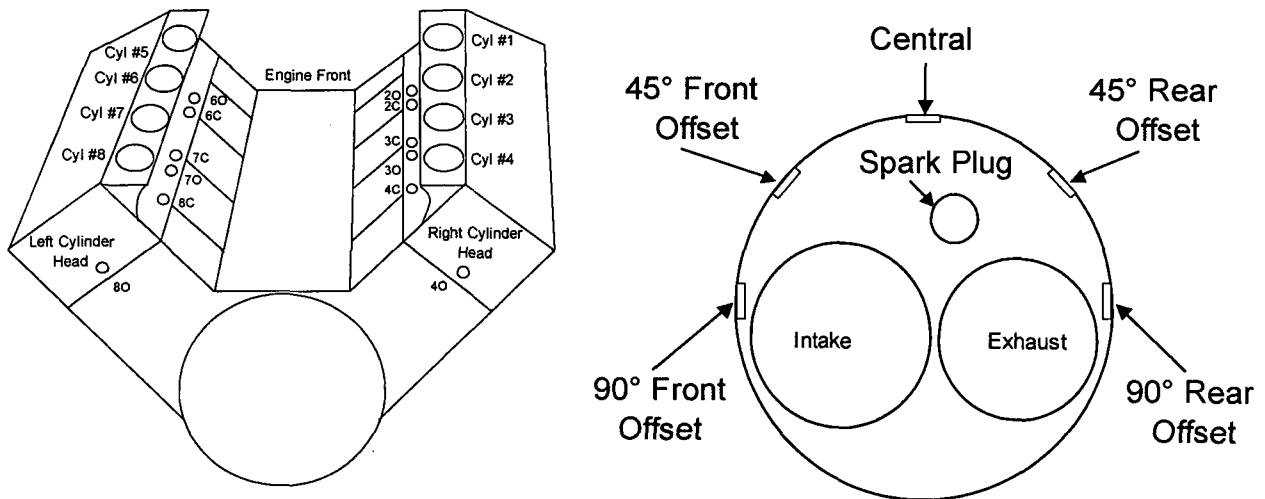


Figure 4. 10 - Stage 2 Transducer Location



Figure 4.11 – Instrumented Cylinder Head

Table 4.3 - Stage 2a Test Matrix

Run	Cylinder	Transducer	Location
1	6	6123	45° Rear Offset
		AutoPSI	Central Flush Mount
		6127	Spark Plug
2	7	6123	45° Front Offset
		AutoPSI	Central Flush Mount
		6117	Spark Plug
3	2	6125	Central Flush Mount
		6123	45° Front Offset
		6117	Spark Plug
4	3	6125	Central Flush Mount
		6123	45° Rear Offset
		6117	Spark Plug
5	6	6125	45° Rear Offset
		6123	Central Flush Mount
		6117	Spark Plug
6	7	6125	45° Front Offset
		6123	Central Flush Mount
		6117	Spark Plug

Engine operating conditions varied slightly from stage 1 to include engine speeds at which peak torque and peak horsepower occur:

- 1000 rpm, Part Load (10 inHg intake manifold vacuum)
- 1000 rpm, WOT (Wide Open Throttle – full load)
- 2500 rpm, Part Load
- 2500 rpm, WOT
- 4500 rpm, Part Load
- 4500 rpm, WOT

Data were again acquired using DSP Technology combustion data acquisition equipment in conjunction with RedLine ACAP software.

4.3.1.2 Analysis of Data

Performance data were analyzed real time using the DSP Model 4325 Real Time Processor (RTP) and the RedLine ACAP Software.

Raw pressure data were imported to MATLAB and average pressure traces were created. Processed data files containing cycle imep, peak pressure and peak pressure location as well as the MATLAB-generated pressure traces were then exported to MS Excel for further data reduction, analysis and display.

4.3.1.3 Results and Discussion

Figures 4.12 – 4.14 illustrate the results for 1000 rpm. Data for higher engine speeds can be found in Appendix B. Average pressure traces (300 cycles) for the Kistler 6117 (spark plug

mount) and the Kistler 6123 (flush mount) are shown in Figure 4.12. These figures reveal that the pressure measured by the 6117 transducers experiences a dip relative to that measured by the 6123 flush mount transducers. This dip occurs roughly at the beginning of combustion (corresponds to the point of inflection on the overall pressure trace). This dip is followed by a large positive spike which does not fully recover until the end of the cycle. This slow recovery time results in a net overestimate in relative pressure as shown in the imep calculation results of Figure 4.14. This figure shows an increase of between ten and twenty percent in indicated mean effective pressure based on pressure measured from the 6117 relative to that measured by the 6123. Variation is dependent on engine operating conditions. Although absolute imep difference increased with load as expected, the percentage difference was reduced due to higher magnitudes. Also, trends in engine speed show an inverse relation with percent difference. This could be explained by the thermal shock in the 6123 transducer. Thermal shock in this transducer results in an underestimate of imep. This error would decrease at higher engine speeds due to reduced exposure of the transducer diaphragm to the hot combustion gases.

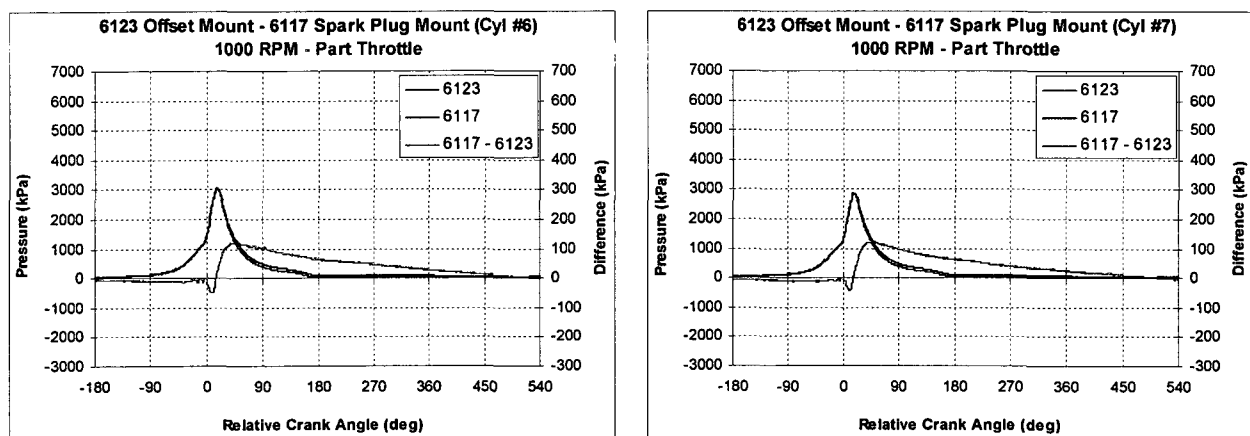


Figure 4. 12 - 6117 / 6123 Average Pressure Traces

The Optrand AutoPSI average pressure trace is compared to that of the 6123 in Figure 4.13. As can be seen in the comparison of the results in Cylinders #6 and #7, the only observation that can be made regarding the AutoPSI is that of inconsistency. Cylinder #6 results indicate a large overestimate of pressure by the AutoPSI while a slight underestimate exists in cylinder #7.

As a result of the large variation in pressures, the AutoPSI produces unpredictable values of indicated mean effective pressure as can be observed in Figure 4.14. Differences shown here range anywhere from a relative increase of 20 percent to a decrease of almost 5 percent.

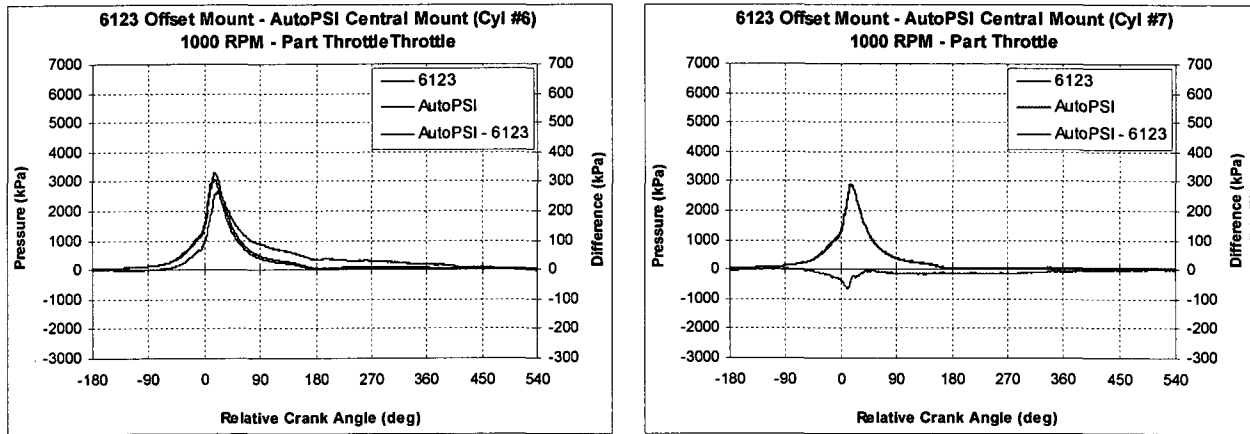


Figure 4. 13 - AutoPSI / 6123 Average Pressure Traces

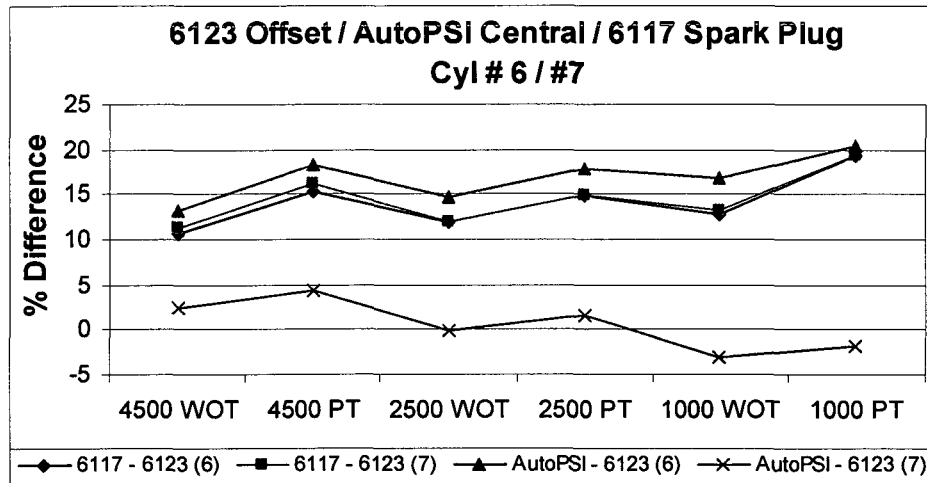


Figure 4. 14 - 6117 / AutoPSI / 6123 IMEP Comparison

In the remaining figures, comparisons are made relative to the Kistler 6125 flush mount transducer. Again, this transducer is structurally similar to the 6123, but with improvements in response to thermal effects. Furthermore, the transducer location is studied indirectly by means of changing the placement of the reference 6125 transducer. Figures 4.15, 4.17 and 4.19 illustrate data collected with the 6125 mounted in the central flush mount position, while Figures 4.16, 4.18 and 4.20 correspond to data collected with the 6125 offset 45 degrees in each direction.

In Figures 4.15 and 4.16, a comparison is made between the 6123 and 6125 transducers (as well as the central and offset locations). Figure 4.15 is indicative of the thermal shock behavior of the 6123 in comparison to the thermally resistant 6125 transducer. A drop in relative pressure occurs at the start of combustion, followed by a gradual recovery. This same trend is exhibited in 4.16. However, comparison of these figures provides insight into the effects of transducer location. In both cases, it can be observed that pre-combustion pressure is measured higher in the central location relative to both the 45 degree front offset (cylinders #2 and #7) and 45 degree rear offset (cylinders #3 and #6) locations. This phenomenon manifests itself as a

decrease in pre-combustion pressure as measured by the 6123 in the offset locations (Figure 4.15) and an increase as measured by the 6123 in the central location (Figure 4.16).

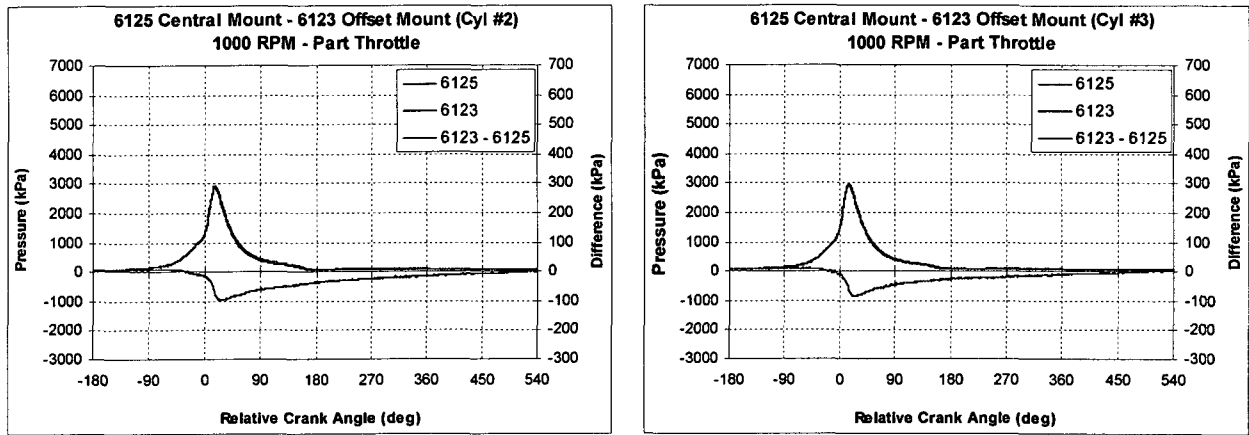


Figure 4. 15 - 6123 (Offset) / 6125 (Central) Average Pressure Traces

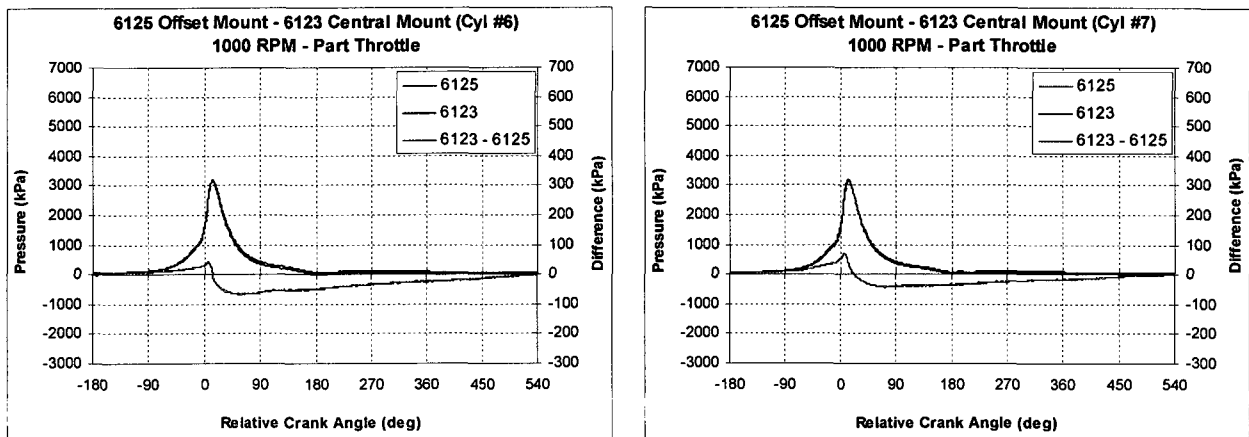


Figure 4. 16 - 6123 (Central) / 6125 (Offset) Average Pressure Traces

Figures 4.17 and 4.18 show the results of the comparison between the 6117 and the 6125 transducers. These results indicate a similar trend to that exhibited in the comparison of the 6117 to the 6123 transducer, with the exception of the cylinder #2 results (here the pressure drop at combustion is larger than the relative positive spike which follows).

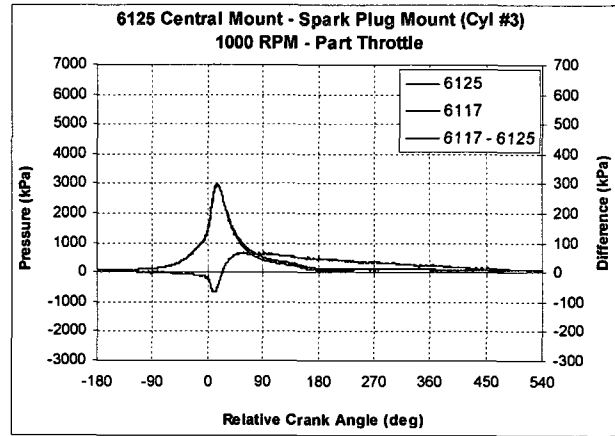
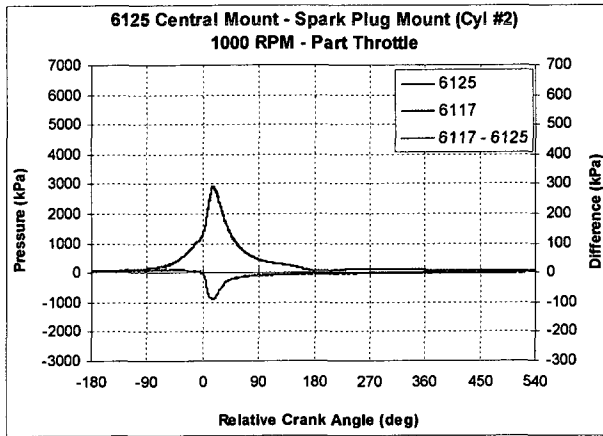


Figure 4. 17 - 6117 / 6125 Average Pressure Traces (Cylinder #2 and #3)

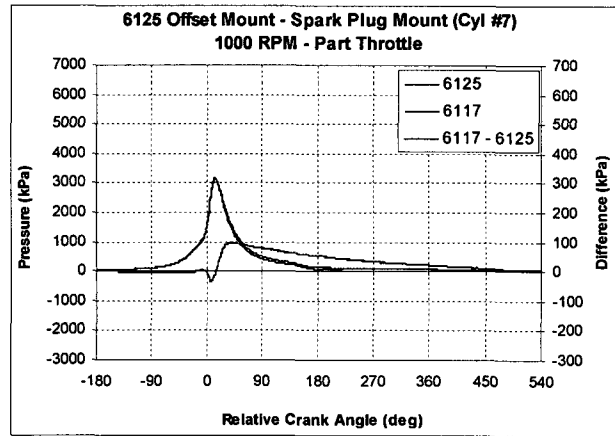
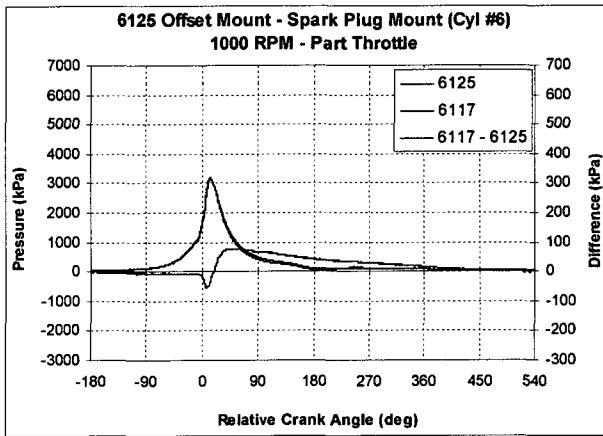


Figure 4. 18 - 6117 / 6125 Average Pressure Traces (Cylinder #6 and #7)

The effects of pressure variation on imep are illustrated in Figure 4.19 and 4.20. In observing the 6123 / 6125 comparisons, it can again be observed that percent differences are generally higher with decreased load and increased engine speed. Comparison of figures indicates that imep is higher when calculated based on the pressure measured by a centrally mounted transducer. This is likely a result of transducer sensitivity variation due to differences temperatures at each of the mounting locations.

The results from the 6117 / 6125 comparison indicate similar trends with respect to engine operating conditions. The imep calculated based on the spark plug transducers (with the exception of cylinder #2 results) is between 2 and 15 percent higher than that calculated based on the 6125 transducers. It can be noted that this is significantly lower than the differences found in the 6117 / 6123 comparison, indicated that those differences were compounded by the thermal shock exhibited by the 6123 transducers. Again, since this positive offset is seen to be less when the 6125 is centrally mounted (Figure 4.19), it can be insinuated that the centrally mounted transducer provides a higher estimate of indicated mean effective pressure.

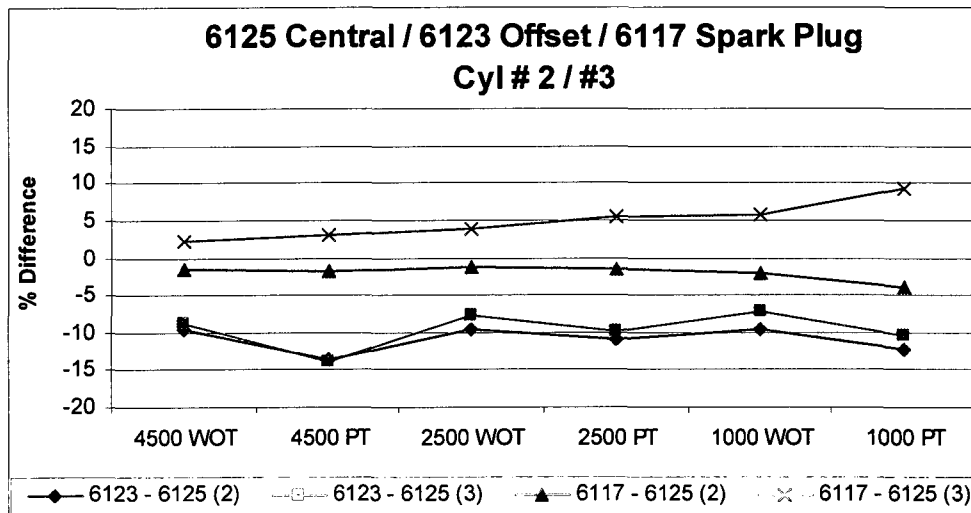


Figure 4. 19 - 6123 (Offset) / 6117 / 6125 (Central) IMEP Comparison

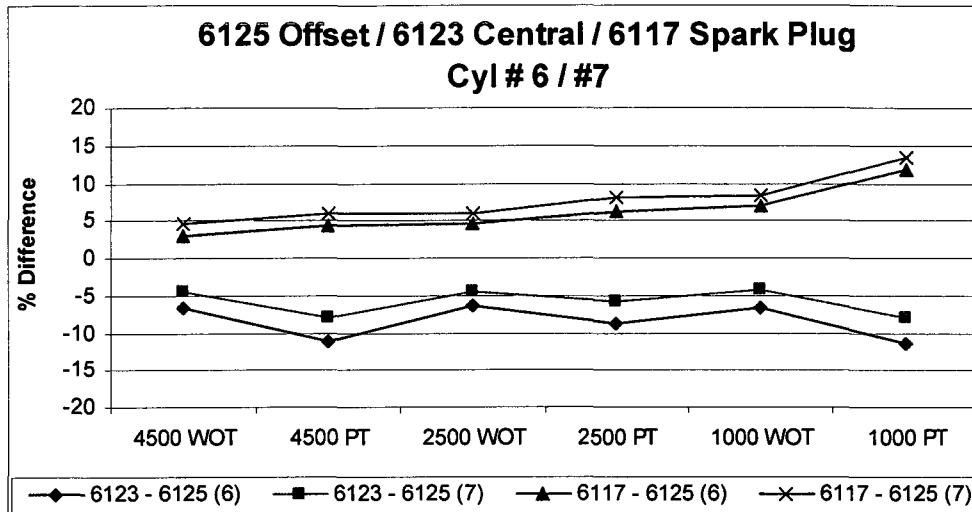


Figure 4. 20 - 6123 (Central) / 6117 / 6125 (Offset) IMEP Comparison

4.3.2 Knock Data Measurement Comparison

Development and validation of new knock detection methods requires a reliable determination of borderline knock. That is, to judge whether a measurement system is distinguishing knock signals from non-knock signals, an independent evaluation of this state is necessary. In this work, a vibration-based knock detection system has been developed. The standard (independent) method used to determine whether knock is present involves pressure-based knock detection.

This validation stage is involved with the comparison of both transducer technology and transducer location in their ability to correctly identify knock. Simultaneous pressure measurement allows assessment of the same knock event by multiple transducers and from multiple locations.

4.3.2.1 Experimental Details

The transducers used in this study included the Kistler 6123, the Kistler 6117 and the Optrand AutoPSI. Although the Kistler 6125 has improved thermal characteristics, it is structurally similar to the 6123. Thermal effects are relatively unimportant over the short duration knock measurement; therefore, the improvements in the 6125 transducer design could not justify exposure of these more expensive transducers to the knock operating conditions. For this reason, the 6125 transducer was excluded from consideration for knock detection.

Summarized in Table 4.4 is the test plan for transducer and location comparison. The flush mounted 6123 was used as the standard of comparison for transducer type due to higher confidence in results. This transducer is the only one of those tested that is purely flush mounted and invulnerable to acoustic distortion (although the external casing of the AutoPSI is mounted flush to the combustion chamber wall, a small cavity exists between this outer casing and the actual sensing element). The central flush mount location was used as a reference for transducer location. This was done merely for practical purposes since it was the only location feasible for all cylinders.

Table 4. 4 - Stage 2b Test Matrix

Run	Cylinder	Transducer	Location
1	2	6123	Central Flush Mount
		6123	45° Front Offset
2	3	6123	Central Flush Mount
		6123	45° Rear Offset
3	4	6123	Central Flush Mount
		6123	90° Rear Offset
4	8	6123	Central Flush Mount
		6123	90° Front Offset
5	3	6123	Central Flush Mount
		6117	Spark Plug
6	7	6123	45° Front Offset
		AutoPSI	Central Flush Mount

All knock data comparison data was acquired at full load, with engine speeds ranging from 1000-4500 rpm at 500 rpm increments. At each speed, ignition was advanced in the individual cylinder being tested until knock was heard. Data were then acquired at knocking conditions.

Data acquisition was accomplished using a 32 channel 12 bit time-based data acquisition system designed and built by members of the Powertrain Engineering Research and Development Group and CHECKSUM Incorporated. Data was sampled at 250 ksamples/second for 10 seconds for each run.

4.3.2.2 Analysis of Data

The CHECKSUM system stores data in signed integer binary format which can be readily imported into most data analysis packages. All processing of raw knock data is completed using Mathworks MATLAB. Using this software, data are imported, resampled and processed to determine knock intensity. This section will provide an executive summary of the processing methods used. For more detail, the reader is encouraged to refer to Appendix A.

4.3.2.2.1 Data Resampling

A novel method was used to convert the time based data (sampled at 250 kHz) into the position domain which in this case implies synchronization with crank angle. The CID (cylinder identification) signal was used to provide a reference for this synchronization. This CID sensor is linked with the camshaft to produce a single pulse per engine cycle. This is used by the Electronic Engine Controller to determine when cylinder #1 will reach top dead center. In the

same manner, when acquired simultaneously with data this signal provides a crank angle marker for each engine cycle.

Ideally, if an engine were running perfectly at steady state and a constant sampling rate was used, a linear conversion factor could be used to determine the position-time relationship (ie. 2 samples per crank angle). However, during a sampling period, the engine speed will fluctuate. This results in a variable relationship between position and time domain.

A brief outline of the resampling procedure used here is given (for more detailed information, refer to Appendix A):

1. Calculate resolution for each channel:

$$res(j) = \frac{720 \text{ degrees}}{\text{minimum number of points}} \Big| j = 1 \text{ to Number of Cycles}$$

2. Determine optimum resolution:

$$RES = \max[res(j)]$$

3. Create reference cycle based on calculated resolution (this is an array of crank angle values at which data will be used):

$$x_{reference}(i) = RES \times i \Big| i = 1 \text{ to } \frac{720}{res}$$

4. Reduce data points in higher resolution cycles, fitting remaining data to reference crank angle values

4.3.2.2.2 Knock Intensity Calculation

Figure 4.21 illustrates the steps for extracting knock related information from the pressure signals. A high-pass 8 Pole Butterworth filter [Mathworks, 2005] is used to extract the high frequency pressure fluctuations from the overall pressure signal. This signal can then be

squared and integrated (over a specified crank angle window) to determine a form of knock intensity. To determine the frequencies present in the combustion chamber acoustic resonance, a Fast Fourier Transform (algorithm for the calculation of the Discrete Fourier Transform [Mathworks, 2005]) can be used. Or for this stage of study, the transducers can be compared in their ability to pick up amplitudes throughout the frequency range.

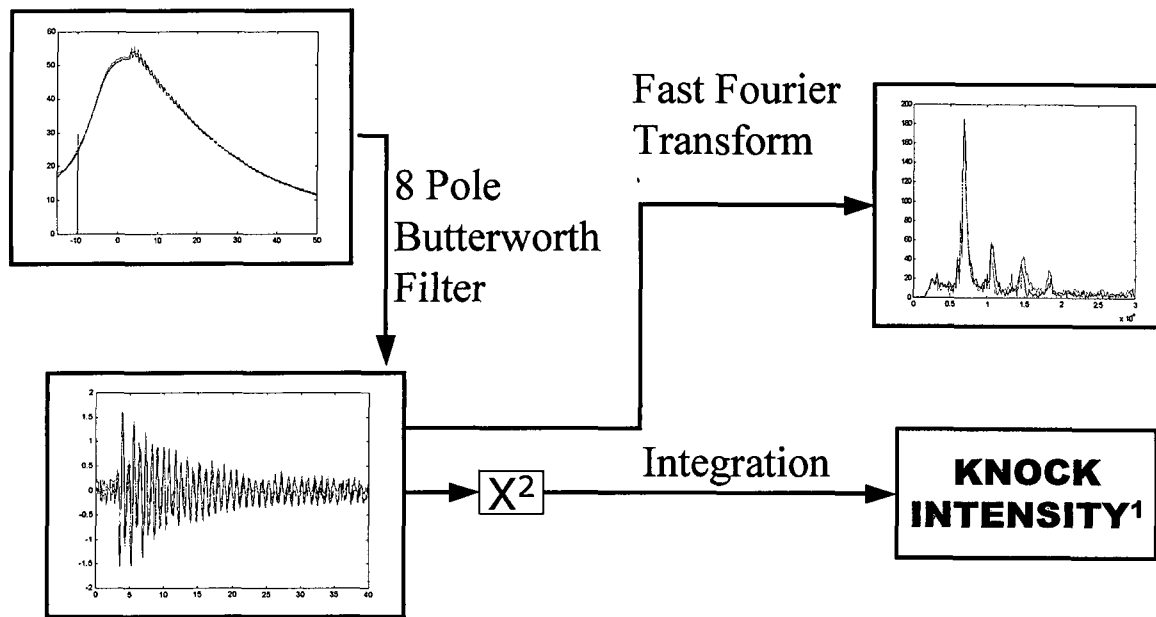


Figure 4. 21 - Knock Intensity Processing²

4.3.2.3 Results and Discussion

In Figures 4.22 – 4.26, transducer comparisons are illustrated by means of both overall knock intensity and frequency content of the measured knock signal. Figure 4.22 compares the 6117 spark plug mounted transducer to the 6123 flush mounted transducer. It is obvious based on overall intensity values that the 6117 shows a limited response to the knock phenomenon. This is expounded by observation of the frequency information. Here it can be seen that the

² Refer to Chapter 5, Page 91

spark plug transducer shows less than half of the response to the fundamental knock frequency, with little to no response in the higher harmonic frequencies. This lack of response can be attributed to the remote mounting of the transducer on the spark plug.

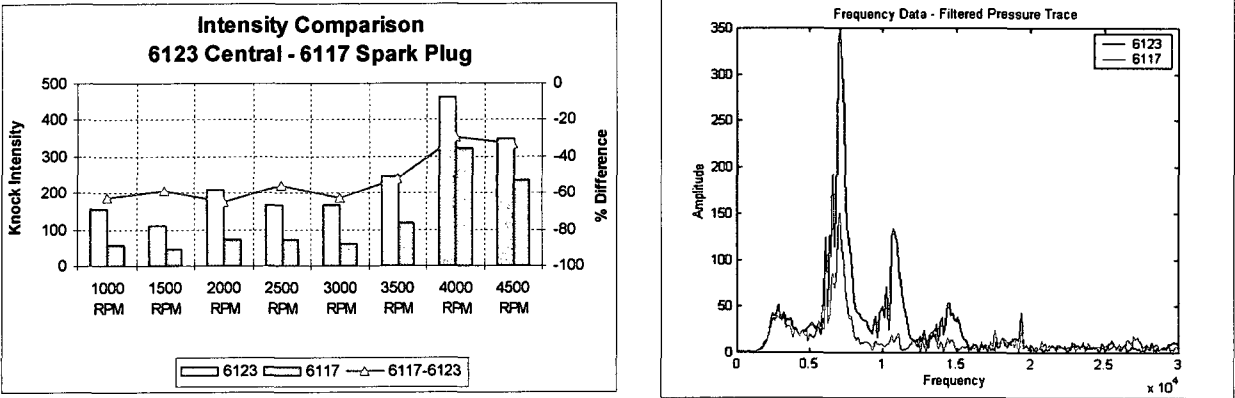


Figure 4. 22 - 6117 / 6123 Intensity Data Comparison

Figure 4.23 shows the results of comparison between the Oprand AutoPSI and the Kistler 6123 transducers. The overall intensity calculations indicate a 40 – 60 percent higher response with the AutoPSI transducers. This is also apparent in the frequency spectrum, where it can be seen that the optical transducer shows higher response throughout the frequency range. Although this suggests a great potential for the optical transducer in knock detection, the previous section discussed the lack of repeatability inherent with these transducers.

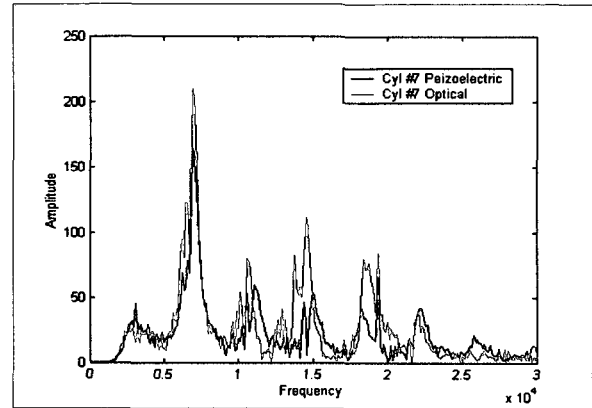
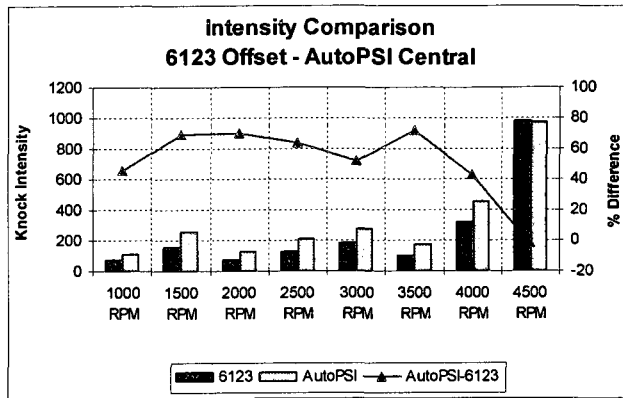


Figure 4. 23 - AutoPSI / 6123 Intensity Data Comparison

Figures 4.24 – 4.26 illustrate the effect of mounting location within the combustion chamber. The four offset locations are compared to the standard central mount in its ability to detect the pressure fluctuations inherent with knock. It can be seen from Figure 4.24 that although the intensity measured at the 45 degree offset locations is comparable, the 90 degree offset shows much lower values.

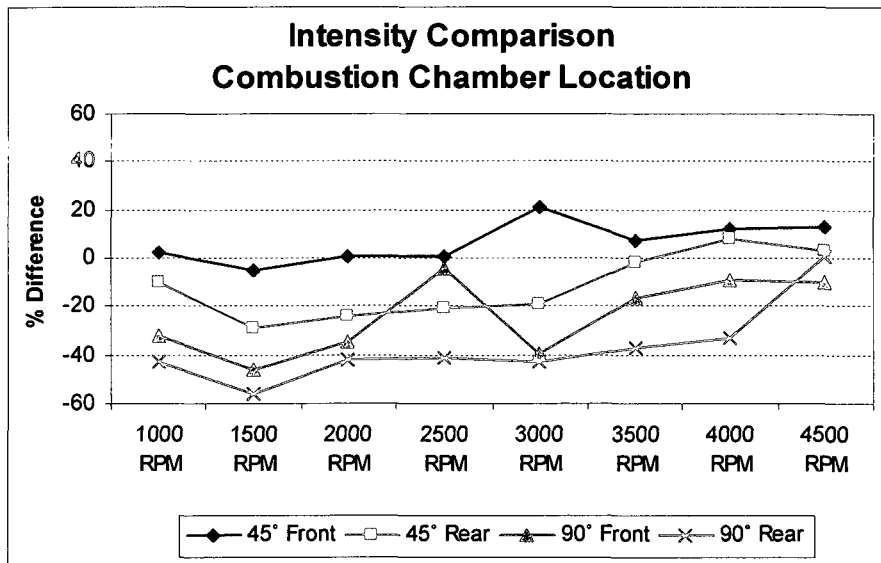


Figure 4. 24 - Combustion Chamber Location Intensity Data Comparison

Observations of the frequency content of these signals (Figures 4.25 and 4.26) are consistent with the overall intensity results. Figure 4.25 shows that in both cases, the 45 degree offset results follow the central mount data quite closely with slightly lower response to the fundamental knock frequency. From Figure 4.26, it can be seen that the 90 degree locations not only show lower response throughout the studied frequency range, but also a shift in the frequencies measured.

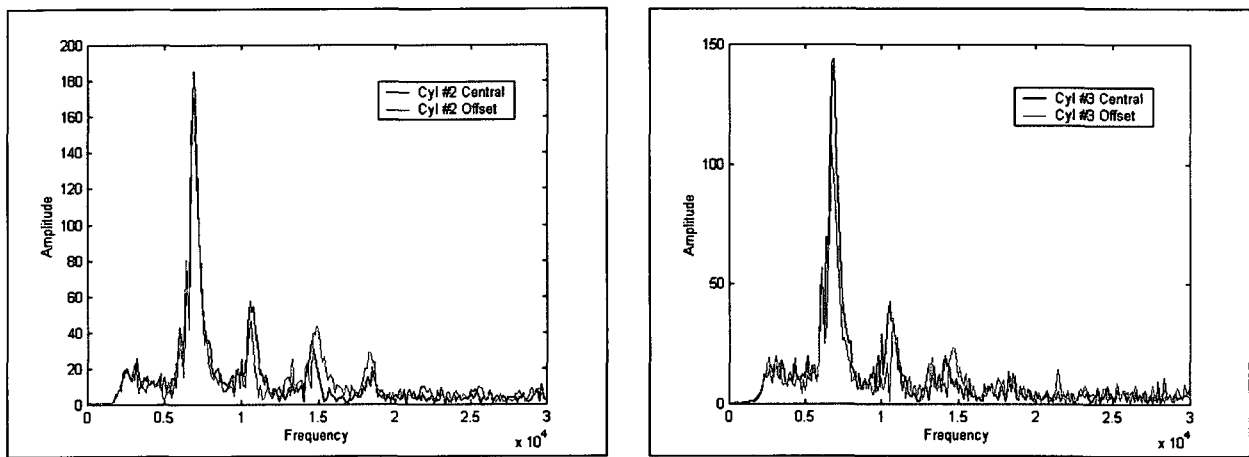


Figure 4. 25 - 45 ° Front (Cylinder #2) / 45 ° Rear (Cylinder #3) Offset Frequency Data Comparison

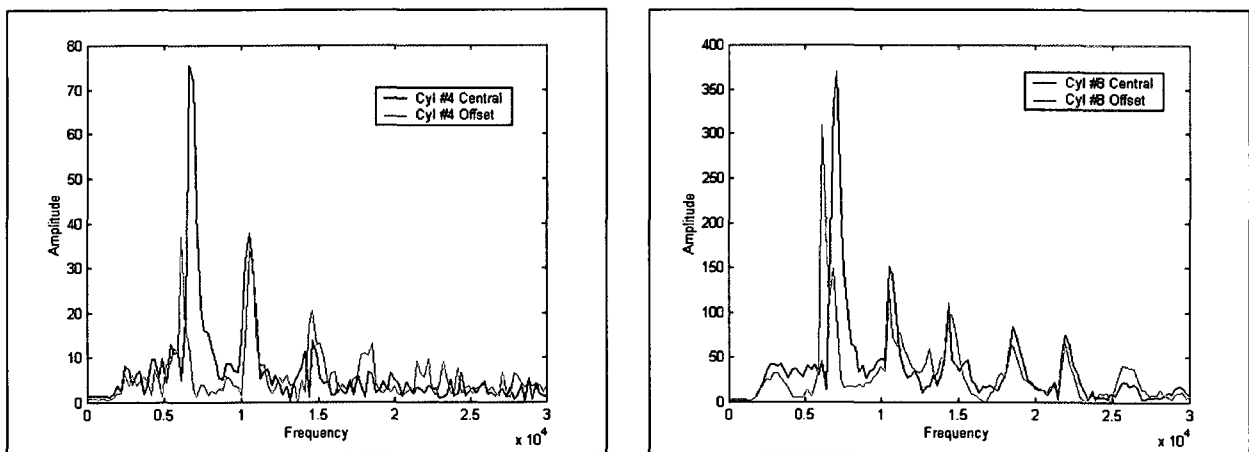


Figure 4. 26 - 90 ° Front (Cylinder #8) / 90 ° Rear (Cylinder #4) Offset Frequency Data Comparison

These results suggest a dominant standing wave pattern as shown in Figure 4.27. Note the nodal axis illustrated lies closest to the 90 degree offset points which would explain the limited response at these points. Furthermore, the antinode is centered between the central and 45 degree front offset, explaining slightly higher response in the front portion of the combustion chamber. Based on the results obtained, and the cylinder head machining feasibility the standard central location continues to be the optimum for the detection of knock (no other location can be machined into all cylinders).

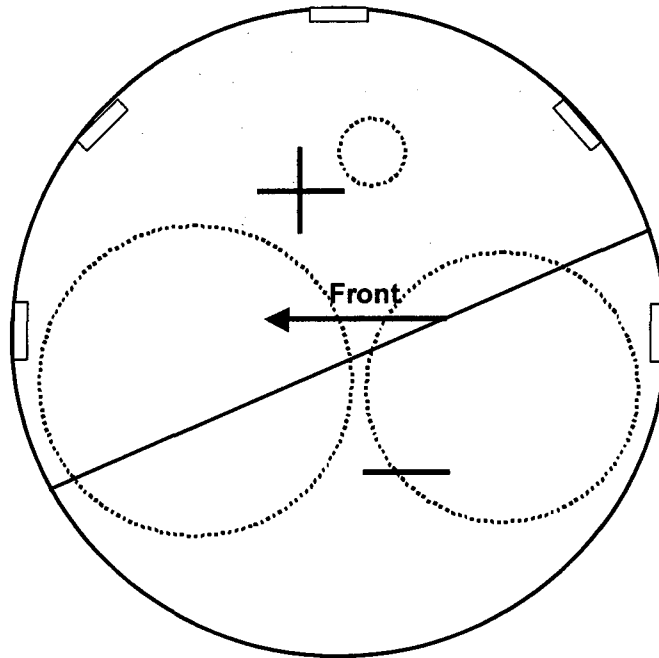


Figure 4. 27- Dominant Acoustic Mode Shape

4.4 Conclusions

1. For measurement of peak pressure, the Kistler 6123 flush mount transducer, the Kistler 6117 spark plug mount transducer and the Optrand AutoPSI agree within 1 bar. However, based on the stage two comparison testing, the Kistler 6125 is recommended for increased accuracy.
2. All transducers were capable of determining the crank angle at which peak pressure occurred within the limits of the 1 degree resolution encoder used. For finer resolution, this testing must be repeated with a higher resolution encoder.
3. For accurate calculation of indicated mean effective pressure, it is recommended that pressure be acquired using the Kistler 6125 transducer. This testing indicated that the Kistler 6123 showed significant error in absolute pressure measurement due to thermal shock and the AutoPSI did not produce repeatable results. However, for a more convenient approach, the Kistler 6117 spark plug mounted transducer has been proven to be an adequate substitute if marginal error is acceptable.
4. Transducer location has been shown to have a moderate effect on measurements for the calculation of indicated mean effective pressure. This is likely due to compounding error resulting from a small phase shift throughout the cycle.
5. The recommended transducer for knock detection continues to be the Kistler flush mounted transducers (6123 / 6125). Not surprisingly, the remote mounted 6117 spark plug transducer was shown to be unsuitable for this purpose as its response was lower throughout the studied frequency range. Although preliminary results suggest that the AutoPSI transducer is potentially superior for knock detection, further testing is required to assess the reproducibility of this trait.

6. The standard central flush mount continues to be the optimum location for knock detection. Although the 45 degree front offset shows slightly higher response, machining of this location becomes difficult for cylinders #1 and #8.

CHAPTER 5 – KNOCK DETECTION STRATEGY

5.1 Introduction And Objectives

Due to the impact of knock on the performance of internal combustion engines, effective knock detection methods are required for engine mapping and control. Generally, mapping and control are distinct applications and as such utilize different detection methods. Engine mapping or offline diagnosis take place in a laboratory environment, and are frequently completed with the installation of in-cylinder pressure transducers. With careful selection of transducer type and location [Tousignant et al., 2004], this method is considered most accurate; however, it is also relatively expensive and inefficient, requiring expensive transducers and instrumentation methods. Further, the installation of these transducers often modifies engine components or structure, with potential effects on engine operation (ie. installation of transducer through cylinder head cooling passage).

The cost of in-cylinder knock detection prohibits its widespread use for production engine control applications. Therefore, in-cylinder methods are almost universally replaced by vibration-based knock detection methods. Vibration-based methods are based on the principle that the in-cylinder resonance associated with autoignition creates a structural vibration which propagates through the engine structure. The obvious goal of any knock detection system is the detection of 100% of knock events, with zero false detects. Unfortunately, current production knock detection systems fall considerably short of this goal. This forces one of two different calibration strategies: the use of relaxed knock threshold limits, allowing borderline knock to occur under some operating conditions or the use of conservative limits leading to false positive

detection (misdetection). Misdetection results in changing engine operating conditions unnecessarily, with possible adverse effects on performance, fuel economy and emissions.

Most production systems use either single accelerometer or multiple accelerometer systems with univariate analysis: Each cylinder is mapped to the transducer which shows the closest correlation to the intensity calculated based on in-cylinder methods. A system is proposed here which uses an array of nine accelerometers, conducting multivariate analysis on knock intensity values obtained from all or part of this array. The purpose of this research is to develop a system with the accuracy to replace current laboratory methods, and a simplicity and cost that makes it feasible for production applications.

5.2 Experimental Details

Development and validation of the knock detection system is being conducted on a 2 valve, V-8 automotive engine. During testing, engine operating conditions are controlled via a dynamometer control system and a proprietary programmable electronic engine control system.

Vibrational response of the engine structure is highly dependent on the cylinder in which autoignition is occurring. Therefore, knock has been induced in each cylinder individually by independent control of spark advance. Ten-point spark sweeps were conducted for each of eight cylinders at five engine speeds. This test was repeated with thirteen sets of cylinder heads.

The cylinder heads were machined and instrumented with Kistler 6125 piezoelectric pressure transducers. These were mounted flush to the combustion chamber wall as shown in Figure 5.1. The 6125 transducers were pegged (as discussed in Chapter 4) using a Kistler 4045 piezoresistive absolute pressure transducer.

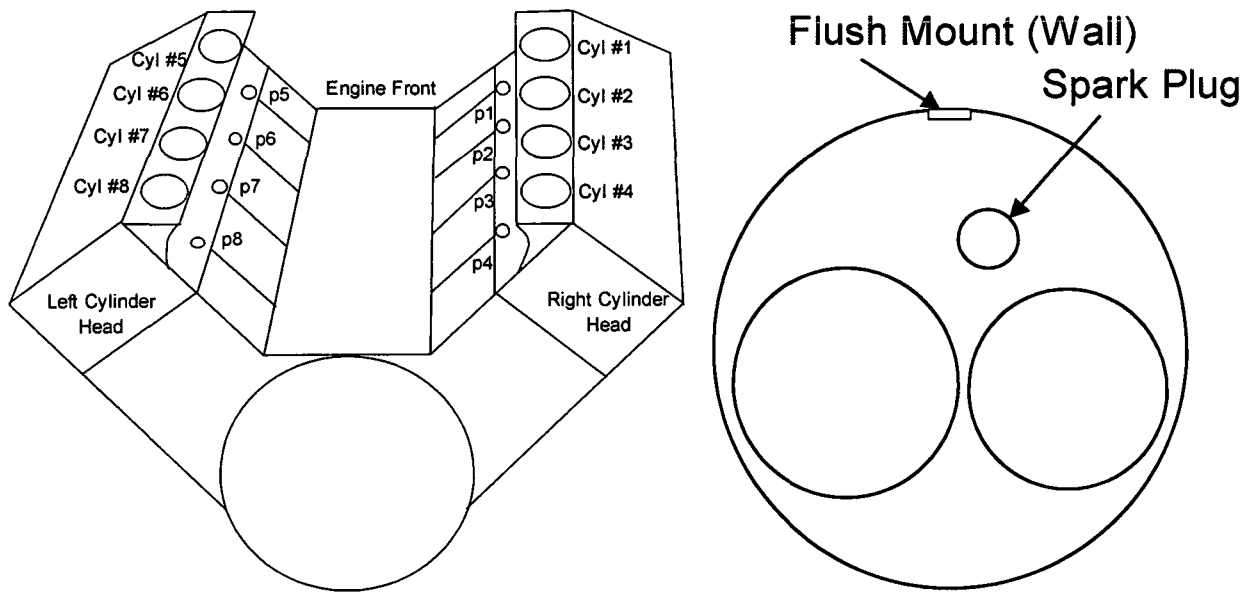


Figure 5. 1 - Pressure Transducer Locations

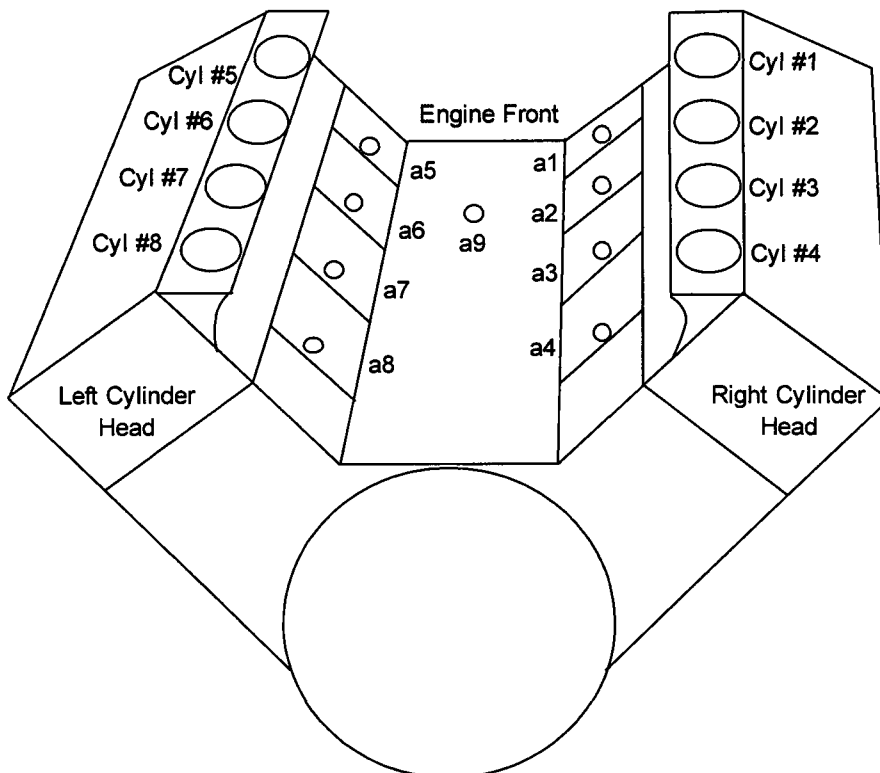


Figure 5. 2 - Accelerometer Locations

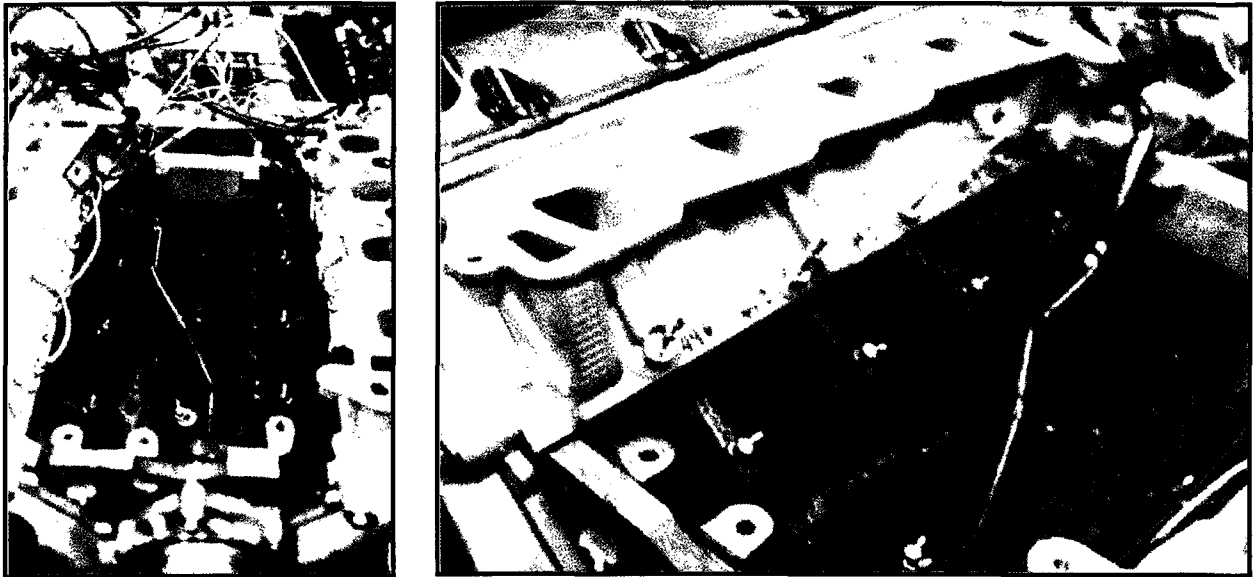


Figure 5. 3 - Pressure and Vibration Transducer Locations

The engine block was instrumented with nine charge mode PCB micro-accelerometers for the measurement of knock vibration response. The original production knock sensor location in the front-center of the tappet valley (refer to location a9 in Figure 5.2) was used. In addition, eight other accelerometer locations were chosen with the aid of scanning laser velocimetry. These were located on the longitudinal center and slightly offset from the transverse center of each cylinder (directly behind a cast longitudinal support – refer to positions a1 – a8, Figure 5.2).

Additional data acquired included a microphone which was placed approximately 1.5 m in front of the engine which was used strictly for the creation of audio files and an analog Cylinder Identification Sensor (CID) signal which was used for data re-sampling into the angle (position) domain.

All data were acquired with a 12 bit data acquisition system. Data were sampled for 10 s at 250 kHz per channel.

5.3 Analysis of Data

Analysis of pressure and vibration data took place in three stages. An energy calculation known as knock intensity was calculated based on three methods. A statistical distance was used to create a multivariate knock parameter based on the nine accelerometer signals. Finally, the principles of the Mahalanobis-Taguchi System were used to optimize the multivariate knock parameter calculation.

All data processing was completed using MATLAB software. Initially, a novel data resampling algorithm (as discussed briefly in Chapter 4) was used to translate all time domain data into the angle (position) domain while retaining the ability to conduct time and frequency domain analysis with negligible error.

5.3.1 Intensity Calculation

Knock intensity was calculated using three methods. These are referred to as a Single Window Intensity (IntS), Double Window Intensity (IntD) and Variance-Based Double Window Intensity (IntV). The analytical equations for each of these metrics is as follows:

$$IntS = \int_{\theta_{knock}} x^2 d\theta \quad (5.1)$$

$$IntD = \frac{\int_{\theta_{knock}} x^2 d\theta}{\int_{\theta_{reference}} x^2 d\theta} \quad (5.2)$$

$$IntV = \frac{\int_{\theta_{knock}} \frac{\sum_{i=1}^n (x_{i,\theta} - \bar{x}_{\theta})^2}{n} d\theta}{\int_{\theta_{reference}} \frac{\sum_{i=1}^n (x_{i,\theta} - \bar{x}_{\theta})^2}{n} d\theta} \quad (5.3)$$

where,

x = vibration data point

θ = crank angle

θ_{knock} = the crank angle region during which knock occurs

$\theta_{reference}$ = the crank angle region used to determine background vibration

n = number of cycles acquired (for variance calculation)

Calculation of these intensity metrics based on experimental data is accomplished using the procedure below:

1. Single Window Intensity (IntS):

- Vibration and pressure data are extracted during the knock event for each cylinder - 5 ° BTDC (before top dead center) to 40 ° ATDC (after top dead center).
- An eighth order butterworth high pass filter with a cutoff frequency of 5 kHz is used to extract the high frequency knock information from this data.
- This high frequency content is squared and then integrated using a simple trapezoidal numerical algorithm resolved at each point.

2. Double Window Intensity (IntD):

- Vibration and pressure data are extracted during the knock event – this time estimated between 5 ° BTDC and 35 ° ATDC.
- A second set of data is extracted before the knock event – between 20 ° and 10 ° BTDC – which act as a noise reference window.
- Filtering and integration calculations are completed for data sets from each window.
- Double window intensity is defined as the ratio between intensities calculated from the knock and noise reference data.

3. Variance-Based Double Window Intensity (IntV):

- An ensemble variance was calculated using:

$$\sigma^2(\theta) = \frac{\sum_{i=1}^n (x_{i,\theta} - \bar{x}_\theta)^2}{n}$$

where,

$\sigma^2(\theta)$ = variance at crank angle θ

i = cycle number

n = number of cycles acquired

- A double window intensity was calculated using this manipulated data series with a knock window of 5 ° BTDC to 45 ° ATDC, and a noise reference window of 90 ° to 5 ° BTDC.

The advantages and disadvantages of this method will become more apparent upon observation of results. Single window variance is procedurally and computationally much more simple than the latter two methods. The obvious disadvantage of this method is the lack of

consideration for background noise. This can be significant when calculating intensity based on vibration signals, as there are many excitation sources which can contribute to the overall vibration response in the measurement region.

The double window approach attempts to accommodate background noise by comparing the intensity to a baseline value calculated when no knock is present. Generally, the noise reference window is sized to no more than one quarter of the size of the knock window to avoid excessive reduction of the intensity ratio. The main difficulty with this method is selection of the noise reference window. For example, if an accelerometer is placed nearby an intake or exhaust valve, care must be taken to avoid setting the noise reference window around the crank angle which corresponds to the valve closing event. This would result in an increase in noise reference intensity and subsequently a reduced intensity ratio which could lead to the missed diagnosis of a knock event. Although a constant window was used in this study for the sake of consistency, production application of this method relies on a complex mapping of this window based on engine operating conditions. This procedure becomes considerably more complex when dealing with advanced engine technologies such as variable valve timing.

The variance method is a novel approach developed to take advantage of the double window intensity concept, with less sensitivity to background noise issues. The main advantages of variance analysis is its ability to pick up semi-periodic signals [Tjong, J., 1993]. Signals which are repeatable (periodic) from cycle to cycle will result in a minute variance intensity. Therefore, background noises caused by cyclic events such as valve train movements will be minimized. Conversely, knock events do not occur every cycle, and each occurrence varies significantly in terms of timing and magnitude. Therefore when abnormal combustion takes place a large knock variance intensity results. Combined with the reduction of background

noise, this method should yield an improved signal-to-noise ratio with less concern regarding noise reference window definition. To illustrate this lack of noise sensitivity, the noise reference window for the variance intensity method was chosen to be significantly larger than that for the standard double window method.

5.3.2 Statistical Distance

Statistical distance is a useful classification tool for multidimensional (or multivariate) comparison of a single sample to a set of acceptable or baseline values. The simplest form of statistical distance is the Euclidean Distance which is simply the root-sum-square of the distances in each dimension. Equation (5.5) shows the p-dimensional Euclidean Distance between observations i and k:

$$D_{ik} = \sqrt{\sum_{j=1}^p (x_{ij} - x_{kj})^2} \quad (5.5)$$

Figure 5.4 shows a hypothetical 2-dimensional example in which the equidistant lines as defined by Euclidean Distance are illustrated as concentric circles about observation k (or in this case the mean).

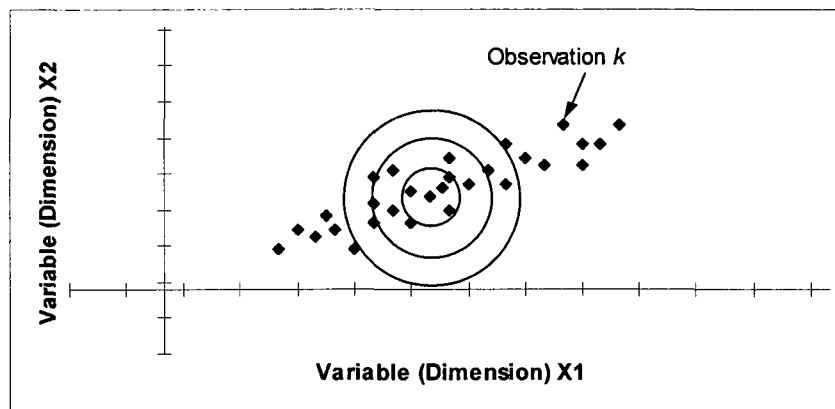


Figure 5. 4 - Euclidean Distance

It should be noted that two problems exist with this distance measure. First of all, it is not scale invariant and thus, distance measure would be affected by the units used in the analysis. Secondly, data dispersion is not taken into account, resulting in applying equal weight to each variable regardless of its associated variability.

The Standard Distance technique can be used to address these issues by dividing each term by the standard deviation in that dimension:

$$SD_{ik} = \sqrt{\sum_{j=1}^p \left(\frac{x_{ij} - x_{kj}}{\sigma_j} \right)^2} \tag{5.6}$$

The result is elliptical equidistant curves as shown in Fig. 5.5. However, although the data are now normalized, another problem becomes apparent. The ellipses (ellipsoids) are shown as perpendicular to the axes and do not follow the data trends (major axis of the ellipse is horizontal, while the data points follow an increasing linear trend).

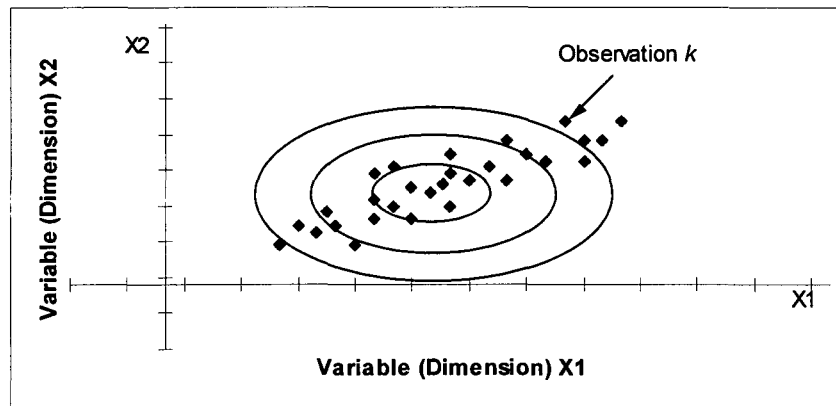


Figure 5. 5 - Standard Distance

Mahalanobis proposed a distance measure which accounts for correlation between variables. The Mahalanobis Distance can be represented in the multi-dimensional form using matrix notation,

$$MD_{ik}^2 = (X_i - X_k)' S^{-1} (X_i - X_k) \quad (5.7)$$

where S is the covariance matrix of observations i and k, or in 2-dimensional form as,

$$MD_{ik}^2 = \frac{1}{1-r^2} \left[\frac{(x_{i1} - x_{k1})^2}{\sigma_1^2} + \frac{(x_{i2} - x_{k2})^2}{\sigma_2^2} - \frac{2r(x_{i1} - x_{k1})(x_{i2} - x_{k2})}{\sigma_1\sigma_2} \right] \quad (5.8)$$

where r represents the correlation coefficient.

Figure 5.6 illustrates the improvement in data representation with the use of this new metric (major axis of ellipses lie on the trend line which would be obtained by regression analysis of the data points). Due to improved representation of data, any distance calculation will better indicate how a given sample deviates from the accepted baseline. Note from Equation 5.8 that in the case of independent variables, MD simplifies to the Standard Distance. This simplifies further to the Euclidean Distance in the event that all standard deviations equal unity. More detailed information on statistical differences is given by Flury and Riedwyl [1988] and Sharma [1996].

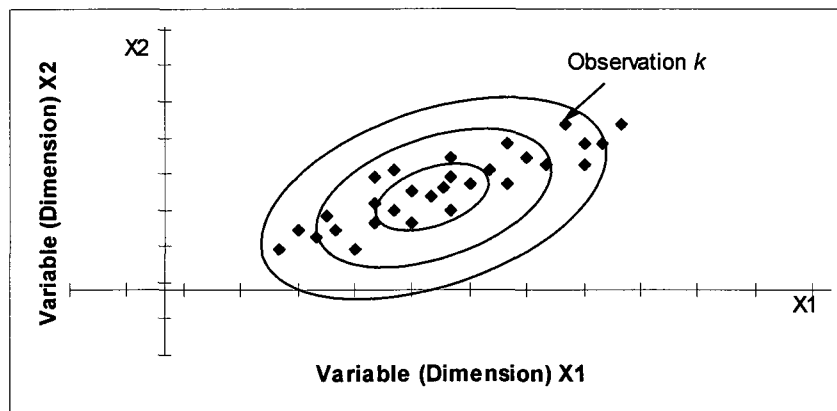


Figure 5. 6 - Mahalanobis Distance

Based on the review of audio reconstructions and in-cylinder pressure data, a pressure intensity threshold can be determined to classify data as non-knocking or knocking. In this manner, a baseline can be established using only samples in which knock is not occurring.

Regarding the intensity calculated from each accelerometer as a variable (dimension), a modified nine-dimensional Mahalanobis Distance can be used to define a new multi-transducer, multivariate knock parameter (the mean and standard deviation of the baseline are used for normalization and comparison):

$$MD = \frac{\left(\frac{X - \bar{X}_{baseline}}{\sigma_{baseline}} \right) \cdot S_{baseline}^{-1} \cdot \left(\frac{X - \bar{X}_{baseline}}{\sigma_{baseline}} \right)^T}{\text{Number of Dimensions (9)}} \quad (5.9)$$

The importance of baseline (pressure intensity threshold) definition is shown in Figure 5.7 below. The Distance was calculated from data points on a single 3500 rpm spark sweep to the baselines defined by varying Single Window Intensity (IntS) thresholds. It can be observed that as the threshold value is increased, the Mahalanobis Distance metric becomes less sensitive to knock events (lower values corresponding to increased spark). This result is intuitive since a higher threshold leads to the inclusion of higher intensity data in the baseline (accepted) values.

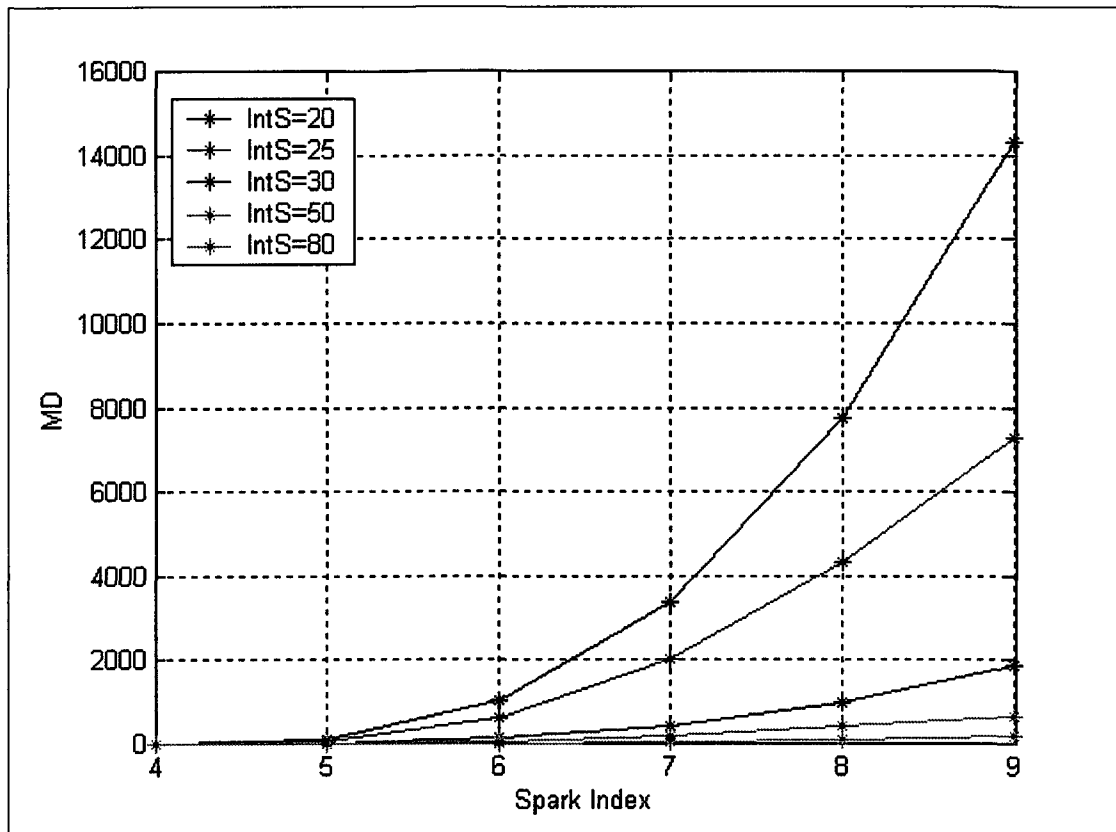


Figure 5. 7 - MD Baseline Selection Sensitivity

5.3.3 Mahalanobis-Taguchi System

The Mahalanobis-Taguchi System (MTS) is a relatively new philosophy that was created by Genichi Taguchi for pattern recognition and it combines the Mahalanobis Distance (MD) with some of Taguchi's Robust Design Methods [Taguchi, G. et al., 2001]. Fundamental to these methods are the concepts of orthogonal arrays and signal-to-noise ratio (SN).

Orthogonal Arrays are tabulated designs that allow for the maximum number of main effects to be estimated in an unbiased (orthogonal) manner with a minimum number of runs in the experiment. An L-12 array is illustrated in Table 5.1 as an example. A full factorial experiment would consist of 2^{11} or 2048 runs. Using the L-12 array, it is possible to test the

effects of up to 11 factors at 2 levels with only 12 experimental runs. The unbiased nature of the array is illustrated by observing that each factor is tested exactly 6 times at each level.

Table 5. 1 - L-12 Orthogonal Array

Run #	F1	F2	F3	F4	F5	F6	F7	F8	F9	F10	F11
1	1	1	1	1	1	1	1	1	1	1	1
2	1	1	1	1	1	2	2	2	2	2	2
3	1	1	2	2	2	1	1	1	2	2	2
4	1	2	1	2	2	1	2	2	1	1	2
5	1	2	2	1	2	2	1	2	1	2	1
6	1	2	2	2	1	2	2	1	2	1	1
7	2	1	2	2	1	1	2	2	1	2	1
8	2	1	2	1	2	2	2	1	1	1	2
9	2	1	1	2	2	2	1	2	2	1	1
10	2	2	2	1	1	1	1	2	2	1	2
11	2	2	1	2	1	2	1	1	1	2	2
12	2	2	1	1	2	1	2	1	2	2	1

Signal-to-Noise Ratio (SN) is a summary statistic proposed by Taguchi and widely adopted. It is based on Taguchi's "Quadratic Loss Function" and expressed in the decibel scale. For 'Larger the Better', Signal-to-Noise Ratio is defined for a random variable y as follows:

$$SN = -10 \log \left(\frac{1}{n} \sum_{i=1}^n \frac{1}{y_i^2} \right) \quad (5.10)$$

For each sample, SN is calculated using the level combinations indicated by the corresponding Orthogonal Array. Main Effects (ME) are then determined for each factor by calculating the difference between SN at each predefined level:

$$Main\ Effect = \sum_{i=1}^6 SN_{Level1}(i) - \sum_{i=1}^6 SN_{Level2}(i) \quad (5.11)$$

Based on the Main Effects analysis, the contribution of each variable can be determined, and a judgment can be made as to the suitability of inclusion. The distance calculation can then

be repeated using positive effects variables, thus increasing the accuracy of the distance representation.

Since the only factors considered here are the intensities calculated from nine accelerometer signals, only nine columns of the L12 orthogonal array are to be used. It can be noted that each accelerometer is treated as a two-level factor. However, levels here indicate whether a transducer is to be used in the Mahalanobis Distance calculation (level 1 indicates the accelerometer intensity is used). For example, in Run #1 a nine-dimensional Mahalanobis Distance is calculated using all signals, whereas in Run #2 a five-dimensional calculation is completed using only accelerometers A1 – A5.

Table 5. 2 - Test Array Based on L12 Array

Run #	Accelerometer Number									SN
	A1	A2	A3	A4	A5	A6	A7	A8	A9	
1	1	1	1	1	1	1	1	1	1	SN1
2	1	1	1	1	1	2	2	2	2	SN2
3	1	1	2	2	2	1	1	1	2	SN3
4	1	2	1	2	2	1	2	2	1	SN4
5	1	2	2	1	2	2	1	2	1	SN5
6	1	2	2	2	1	2	2	1	2	SN6
7	2	1	2	2	1	1	2	2	1	SN7
8	2	1	2	1	2	2	2	1	1	SN8
9	2	1	1	2	2	2	1	2	2	SN9
10	2	2	2	1	1	1	1	2	2	SN10
11	2	2	1	2	1	2	1	1	1	SN11
12	2	2	1	1	2	1	2	1	2	SN12

For each of the twelve accelerometer combinations prescribed by the array, a signal-to-noise ratio was calculated based on the Mahalanobis Distance for n samples of data which are to compared to the baseline (only data classified as knocking are used for this stage of processing):

$$SN = -10 \log \left(\frac{1}{n} \sum_{i=1}^n \frac{1}{MD_i^2} \right) \tag{5.12}$$

Main effects analysis can then be conducted based on equation 5.12 above. As an example, if accelerometer A2 were considered, the main effect would be determined as follows:

$$ME(A2) = SN(R1) + SN(R2) + SN(R3) + SN(R7) + SN(R8) + SN(R9) - SN(R4) - SN(R5) - SN(R6) - SN(R10) - SN(R11) - SN(R12) \tag{5.13}$$

For illustrative purposes, sample calculation results are provided in Tables 5.3 – 5.7. Table 5.3 indicates the signal-to-noise ratio (SN) calculated for knocking data from all cylinder heads at 1000 rpm, with spark advanced in cylinder #1 (based on single window intensity). A summary of the main effects analysis based on these signal-to-noise ratios is summarized in Table 5.4, where positive main effects are indicated with gray shading. These results indicate that at 1000 rpm, and the crank angle range in which cylinder #1 is firing, the MD calculation can be optimized by using only accelerometers A1, A2, A3 and A9.

Table 5. 3 - SN Calculation - 1000 RPM, Cyl. #1

Run #	Accelerometer Number									SN
	A1	A2	A3	A4	A5	A6	A7	A8	A9	
1	1	1	1	1	1	1	1	1	1	26.0
2	1	1	1	1	1	0	0	0	0	29.1
3	1	1	0	0	0	1	1	1	0	26.9
4	1	0	1	0	0	1	0	0	1	29.6
5	1	0	0	1	0	0	1	0	1	26.6
6	1	0	0	0	1	0	0	1	0	25.9
7	0	1	0	0	1	1	0	0	1	27.6
8	0	1	0	1	0	0	0	1	1	27.5
9	0	1	1	0	0	0	1	0	0	30.3
10	0	0	0	1	1	1	1	0	0	1.8
11	0	0	1	0	1	0	1	1	1	18.5
12	0	0	1	1	0	1	0	1	0	16.5

Table 5. 4 - ME Analysis - 1000 RPM, Cyl. #1

Main Effects	
A1	41.9
A2	48.7
A3	13.7
A4	-31.3
A5	-28.5
A6	-29.5
A7	-26.2
A8	-3.8
A9	25.3

Tables 5.5 – 5.7 summarize results from all cylinders at 1000 rpm. Signal-to-noise ratio results are shown in Table 5.5. The outcome of main effects analysis is shown in Table 5.6, while Table 5.7 presents a more concise summary of this analysis. Complete results for all engine speeds and intensity calculation types are included in Appendix C.

Table 5. 5 - SN Calculation - 1000 RPM

SPEED	Cyl Used	INTS							
		C1	C2	C3	C4	C5	C6	C7	C8
1000	111111111	26.0	26.5	29.3	28.5	33.4	30.7	34.1	29.7
	111110000	29.1	30.1	33.9	32.6	36.3	16.2	7.2	-1.4
	110001110	26.9	28.8	20.8	7.4	28.8	27.9	38.6	34.5
	101001001	29.6	28.1	32.0	25.8	29.4	32.5	25.6	17.2
	100100101	26.6	25.6	21.1	34.0	26.3	17.9	36.8	23.2
	100010010	25.9	20.1	7.2	-12.1	40.7	18.8	32.6	35.1
	010011001	27.6	29.9	25.2	-9.1	39.6	33.5	28.5	20.4
	010100011	27.5	29.3	24.5	34.0	29.2	10.4	30.2	33.1
	011000100	30.3	31.9	33.4	30.1	18.0	18.9	38.3	21.7
	000111100	1.8	8.5	17.7	33.4	39.6	33.0	37.8	21.2
	001010111	18.5	24.2	29.4	24.8	37.1	25.9	36.7	33.9
	001101010	16.5	21.2	33.3	33.8	29.4	29.6	30.8	33.2

Table 5. 6 - ME Analysis - 1000 RPM

SPEED	Cyl Accel	INTS							
		C1	C2	C3	C4	C5	C6	C7	C8
1000	A1	41.9	14.4	-19.2	-30.8	2.2	-7.3	-27.4	-25.3
	A2	48.7	48.8	26.3	-16.1	-17.2	-20.2	-23.2	-25.8
	A3	13.7	19.9	74.8	88.0	-20.5	12.3	-31.8	-33.1
	A4	-31.3	-21.7	11.8	129.3	0.6	-19.8	-23.2	-23.9
	A5	-28.5	-25.7	-22.3	-66.9	65.7	20.8	-23.5	-24.0
	A6	-29.5	-18.1	8.8	-23.4	12.7	79.0	13.6	10.6
	A7	-26.2	-13.0	-4.4	53.2	-21.5	13.4	67.4	26.7
	A8	-3.8	-4.1	-18.9	-30.3	9.4	-8.6	28.8	97.4
	A9	25.3	23.0	15.3	12.7	2.1	6.3	6.6	13.1

Table 5. 7 - ME Summary - 1000 RPM

SPEED	INTS							
	C1	C2	C3	C4	C5	C6	C7	C8
1000	1	1	2	3	1	3	6	6
	2	2	3	4	4	5	7	7
	3	3	4	7	5	6	8	8
	9	9	6	9	6	7	9	9
			9		8	9		
					9			

The benefit of the this optimization is illustrated in Figure 5.8, again using data acquired at 1000 rpm, with spark advanced in cylinder #1 and processed based on the single window intensity method. In this figure, the MD values based on Run #1 from the original test array of Table 5.2 (all accelerometers used) were compared to the optimized array of accelerometers indicated in Column C1 of Table 5.7. The advantage of MTS is readily apparent. It can be observed that the Mahalanobis Distance based on the optimized accelerometer array exceeds that calculated using the comprehensive test plan by up to 100 percent.

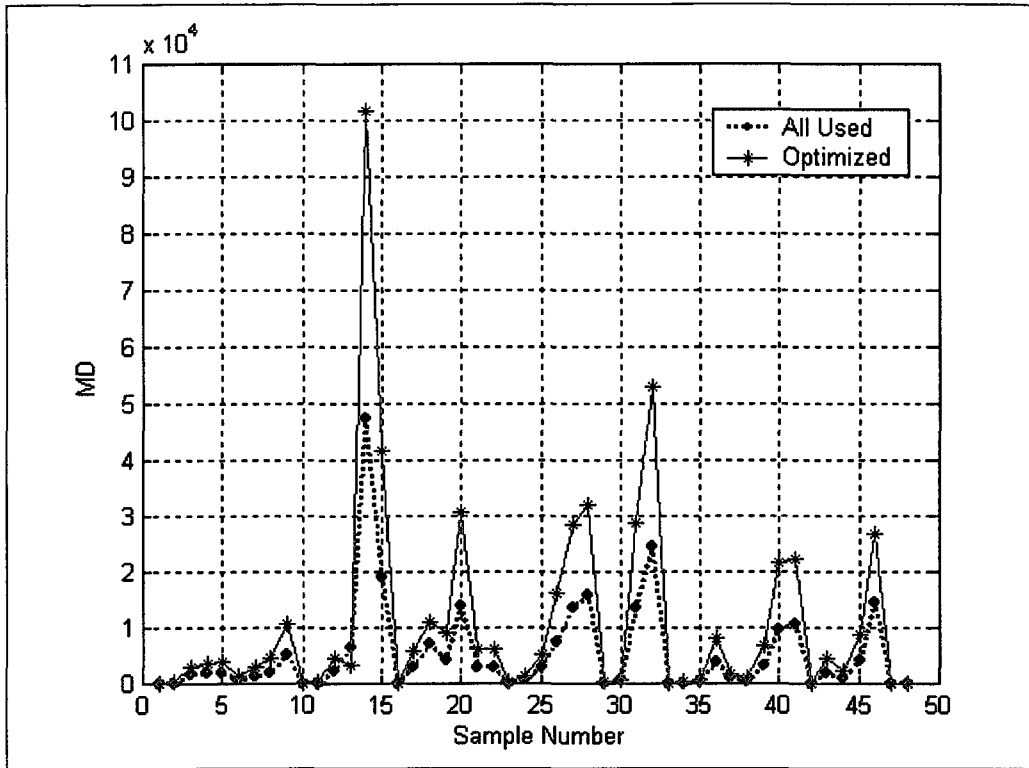


Figure 5. 8 - MTS Optimization Results

For the purpose of development and validation of the proposed knock detection techniques, an algorithm was developed which classifies samples, conducts Main Effects analysis, and calculates MD based on these results.

5.4 Results and Discussion

For the purpose of data verification and observation, two multiple chart figures were created for each operating condition. Samples of these from cylinder #1 data at 3500 rpm are shown in Figures 5.7 and 5.9 for a low spark advance and in Figures 5.8 and 5.10 for high spark advance. Figures 5.7 and 5.9 show raw pressure data as well as filtered pressure and vibration data for each channel. In Figures 5.8 and 5.10, the filtered vibration data is replaced with the ensemble variance data used in the calculation of IntV.

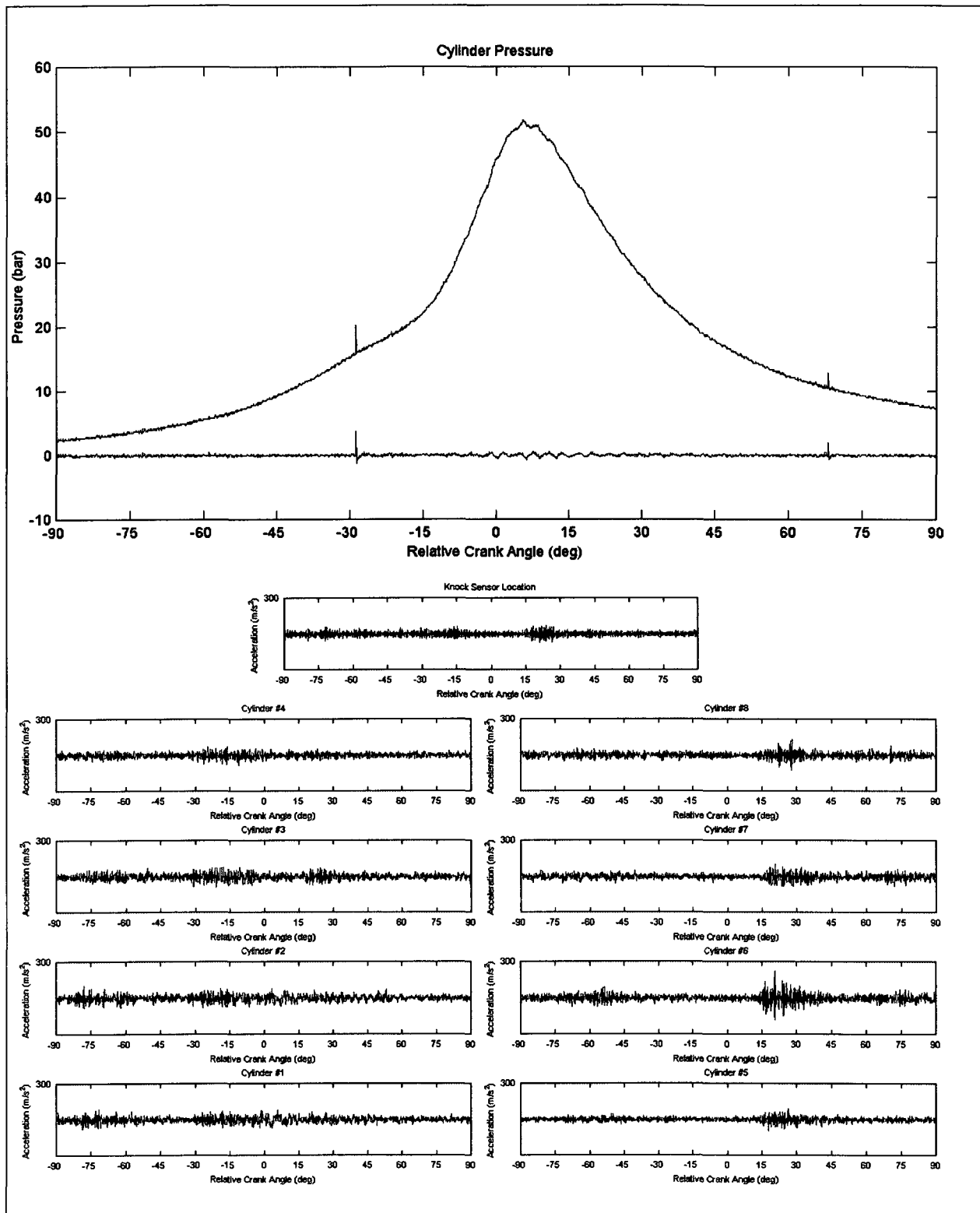


Figure 5.9 - Raw Data – No Knock

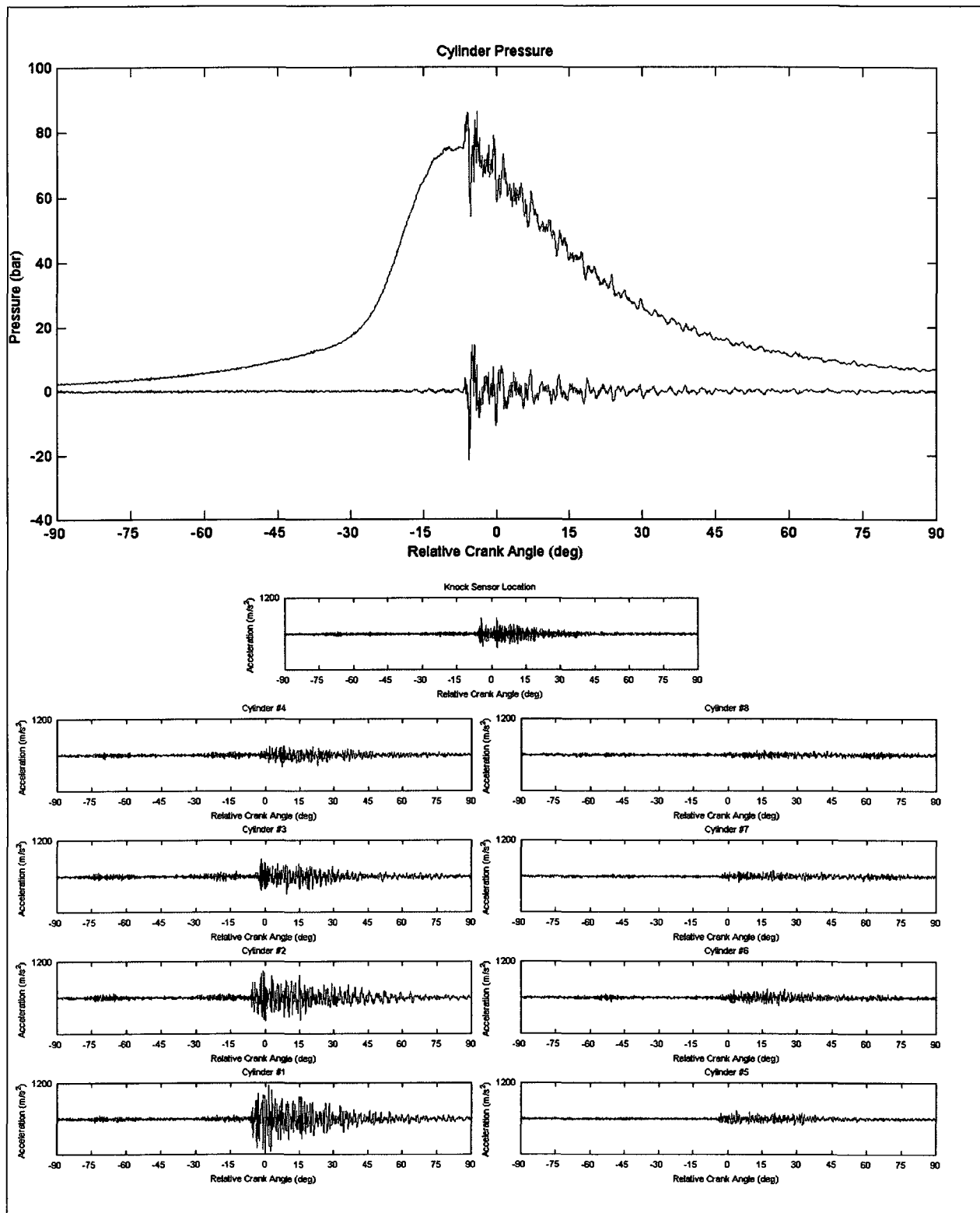


Figure 5. 10 – Raw Data – Knock Present

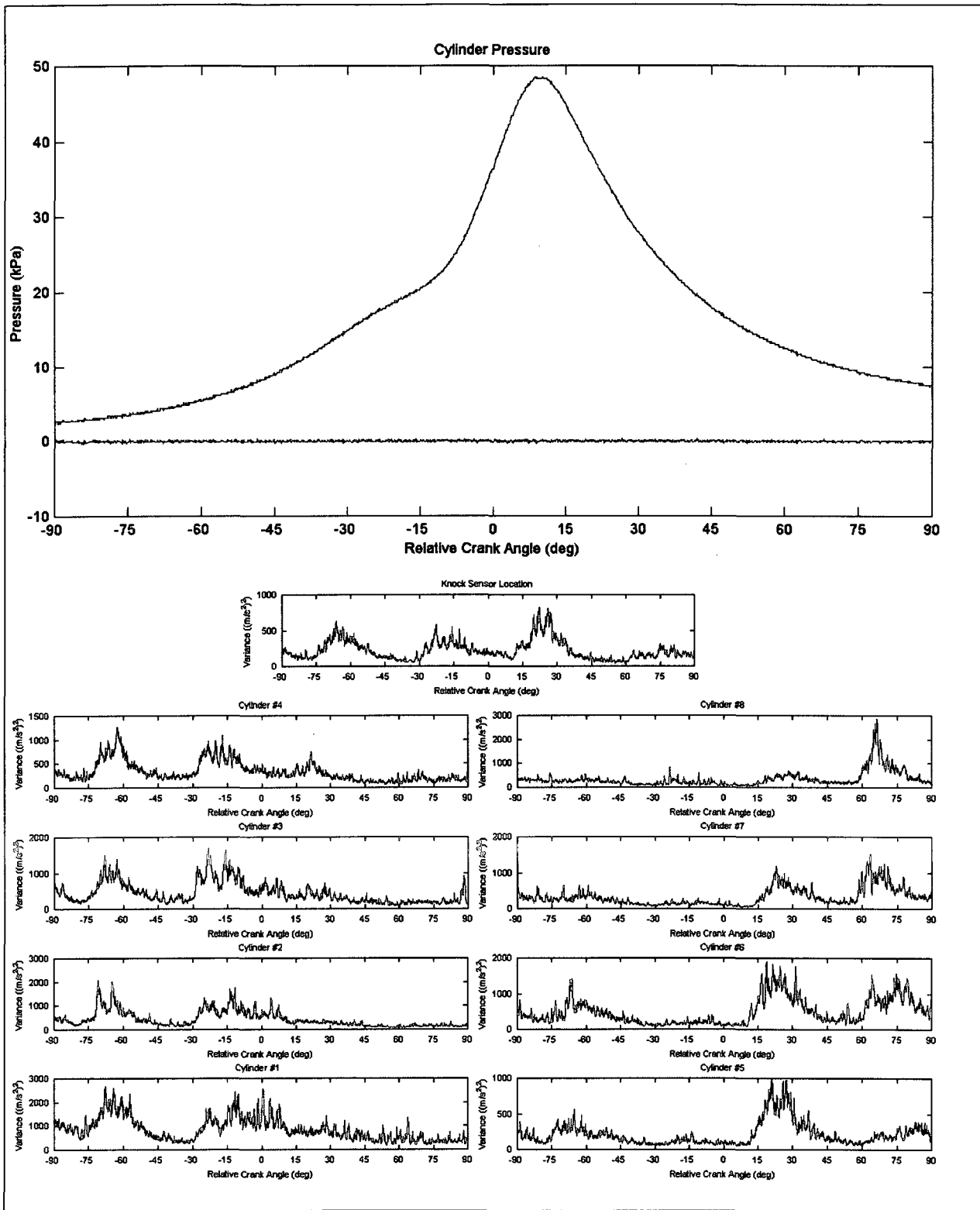


Figure 5. 11 - Variance Data - No Knock

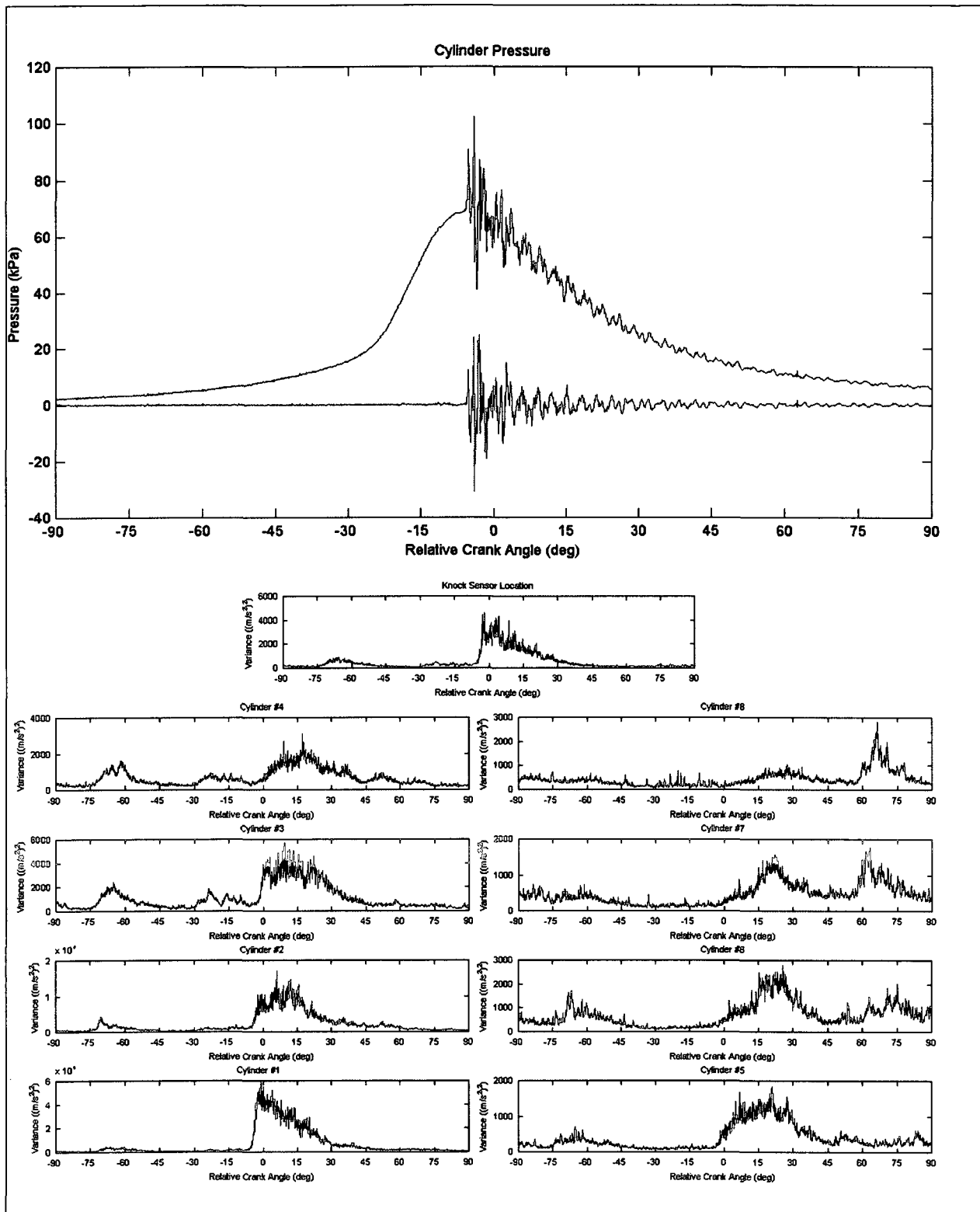


Figure 5. 12 - Variance Data - Knock Present

Upon observation of the knocking versus non-knocking figures, it becomes apparent that the accelerometer locations which best respond to knock events are those located near cylinder numbers 1, 2 and 3 and in the production knock sensor location. This serves as a validation for the results of the MTS analysis of Section 5.3.3 in which locations A1, A2, A3 and A9 are chosen through main effects analysis of the MD-based signal-to-noise ratio calculations.

Knock Intensity was calculated for each accelerometer and pressure channel based on the IntS, IntD and IntV methods described in Section 5.3.1. Mahalanobis Distance was then calculated based on the accelerometer channels which are deemed to have a positive effect on the distance metric. The Mahalanobis Distance for cylinder #1 data at 1000 rpm data, based on each intensity type is shown in Figure 5.13.

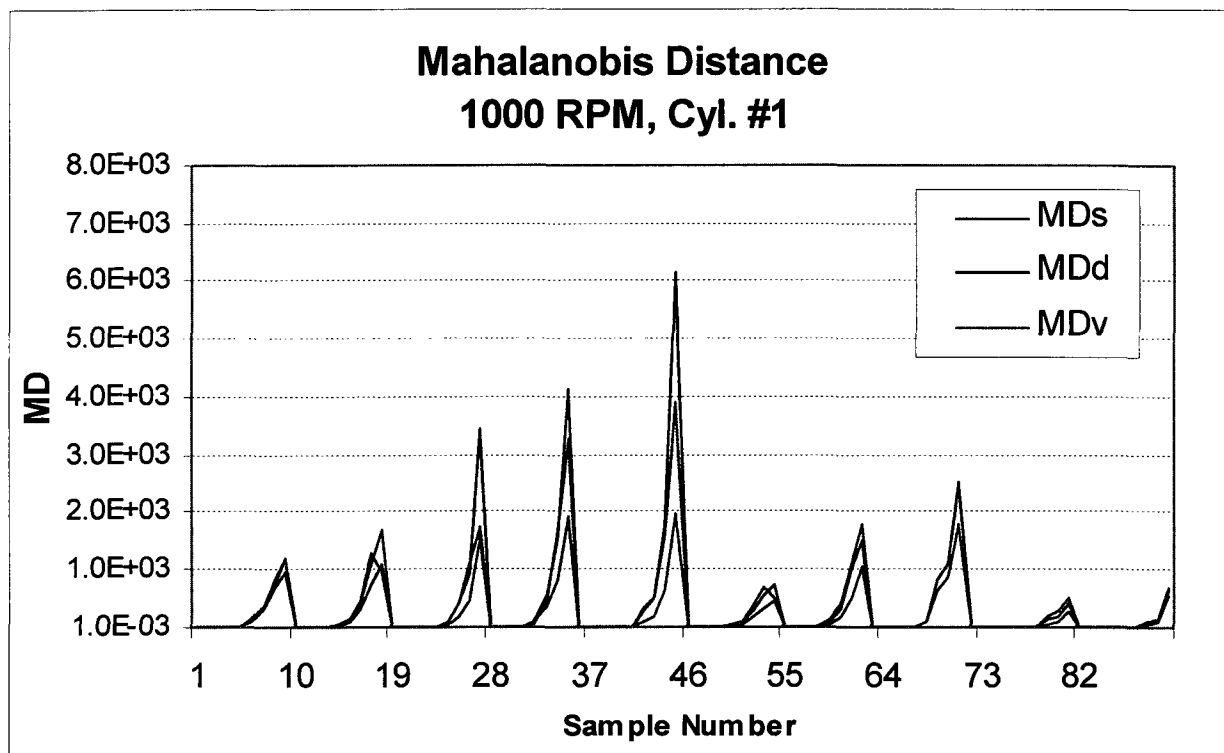


Figure 5. 13 - Mahalanobis Distance Based on Three Intensity Methods

As can be observed from Figure 5.13, Mahalanobis Distance shows little dependence on the type of intensity calculation employed. This is not unexpected, since as stated earlier, the Mahalanobis Distance is scale invariant and since it is normalized by the baseline data, additional normalization based on background noise has little effect.

In contrast, a comparison of the univariate intensity calculation methods was made. Figure 5.14 shows the intensity calculations based on accelerometer A1, for the 1000 rpm, cylinder #1 spark sweeps.

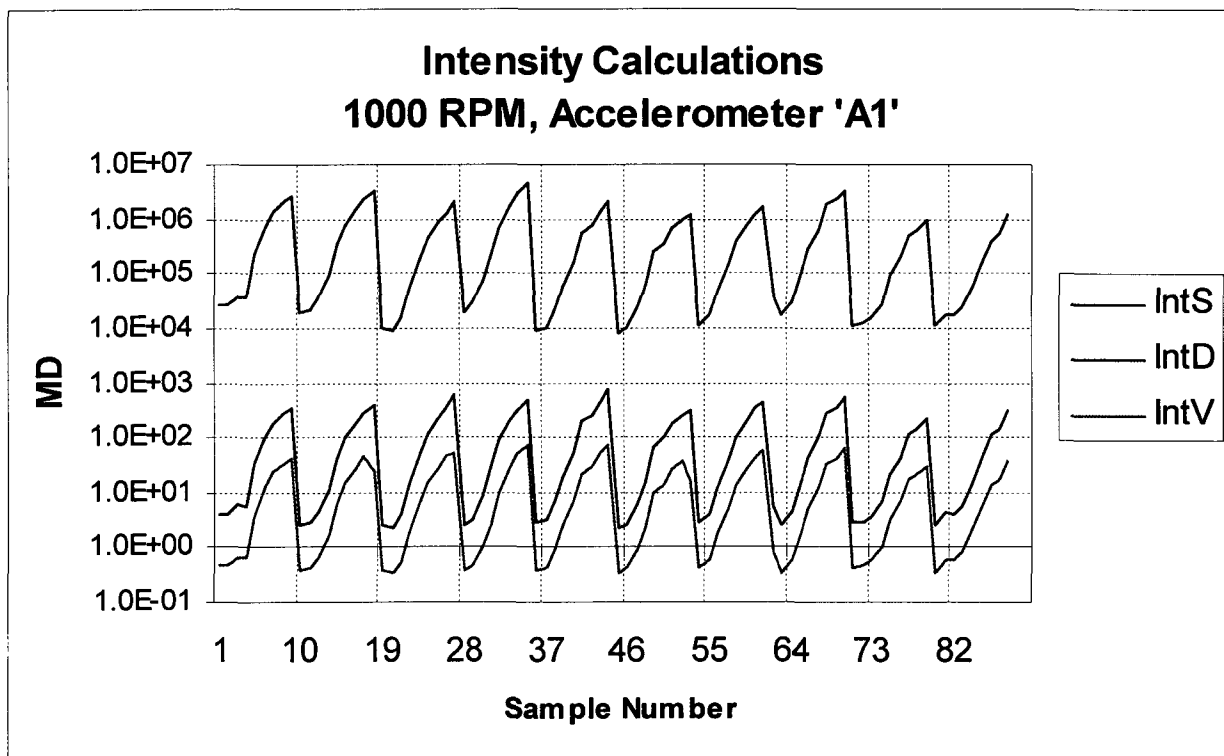


Figure 5. 14 - Comparison of Raw Intensity Calculations

As expected, the intensity calculated based on the single window method (IntS) is significantly higher than those based on a dual window method as the IntD and IntV are both normalized by a noise reference window. It is also unsurprising that the variance based

intensities fall below the standard intensity as the noise reference window is larger by a factor of four.

Closer comparison of the IntD and IntV results reveals that variance analysis reduces bias at non-knocking conditions without any adverse effects on sensitivity. This suggests a potential for the improvement of signal-to-noise ratio in knock detection using variance analysis.

The multivariate distance was then compared to the univariate intensity metric. This comparison is best illustrated by observing a single spark sweep. The following figures compare the single and multivariate knock intensity metrics based on the single window intensity method.

Figure 5.15 illustrates the linear relationship between knock severity and each metric. When viewed on the a linear scale, it appears that the univariate metric, IntS, calculated based on accelerometers A1 (positioned at cylinders #1) shows the best sensitivity to borderline knock (which occurs at spark index 5).

Figure 5.16 shows the same information on a logarithmic scale. Here, it is apparent that, the Mahalanobis Distance shows significant improvement in the ability to distinguish knocking and non-knocking conditions; this is owing to the low zero offset bias associated with the distance metric.

This comparison can also be made based on the alternate intensity calculation methods. Figures 5.17 and 5.18 show this comparison based on the standard and variance dual window methods respectively, using the same data sample as shown in Fig. 5.15.

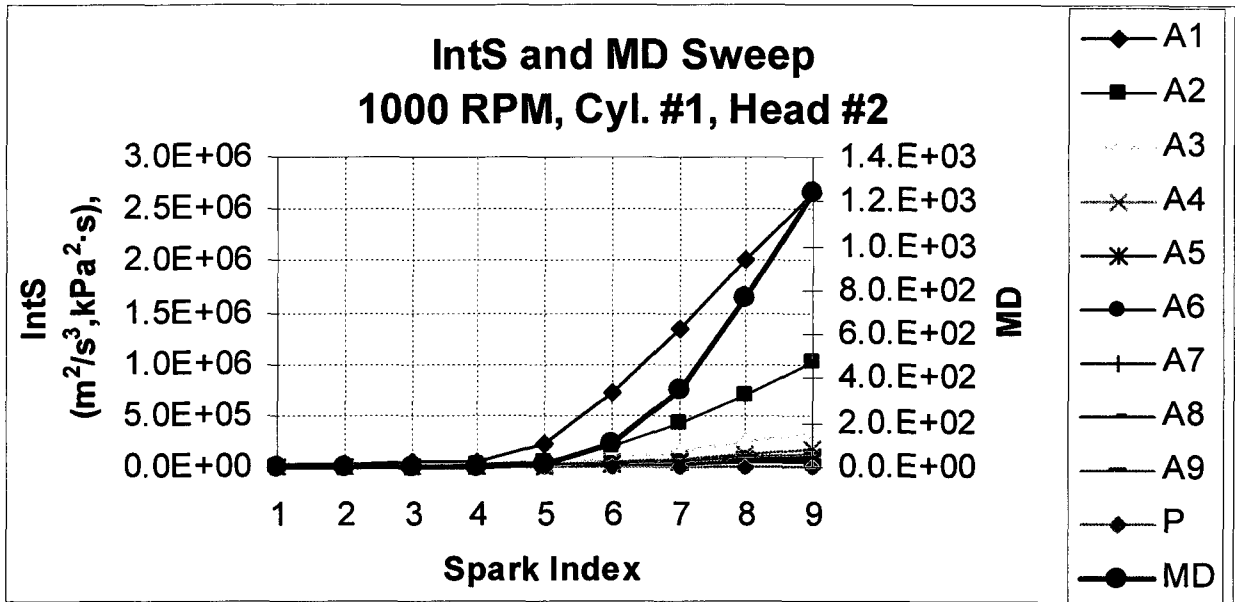


Figure 5. 15 - MD / IntS Sweep (Linear)

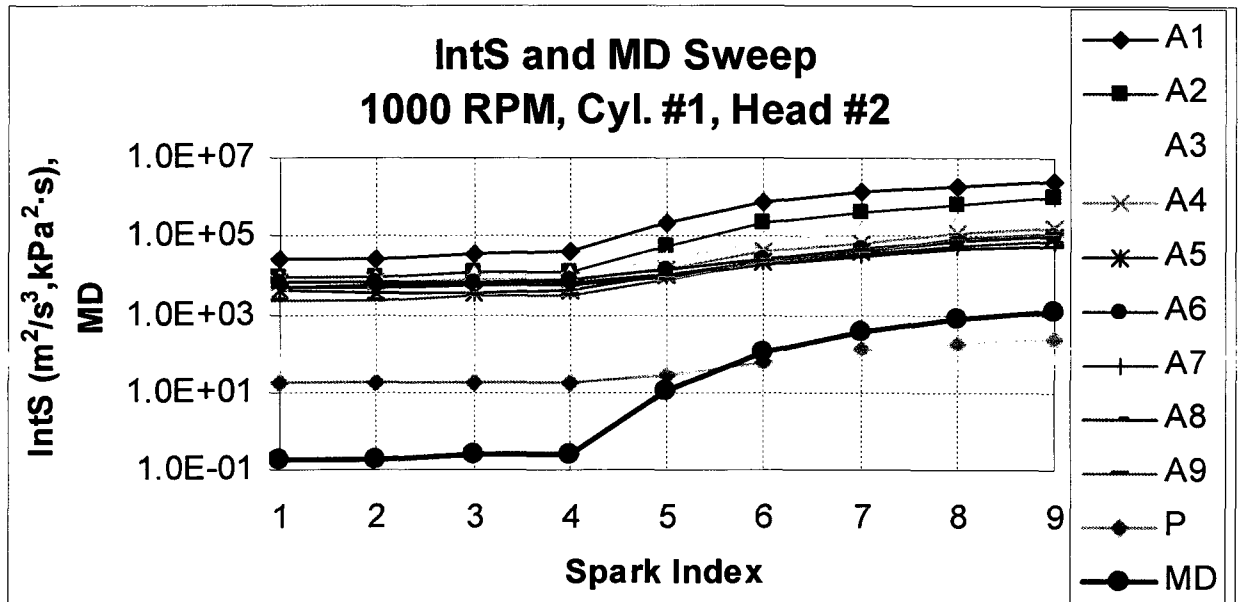


Figure 5. 16 - MD / IntS Sweep (Logarithmic)

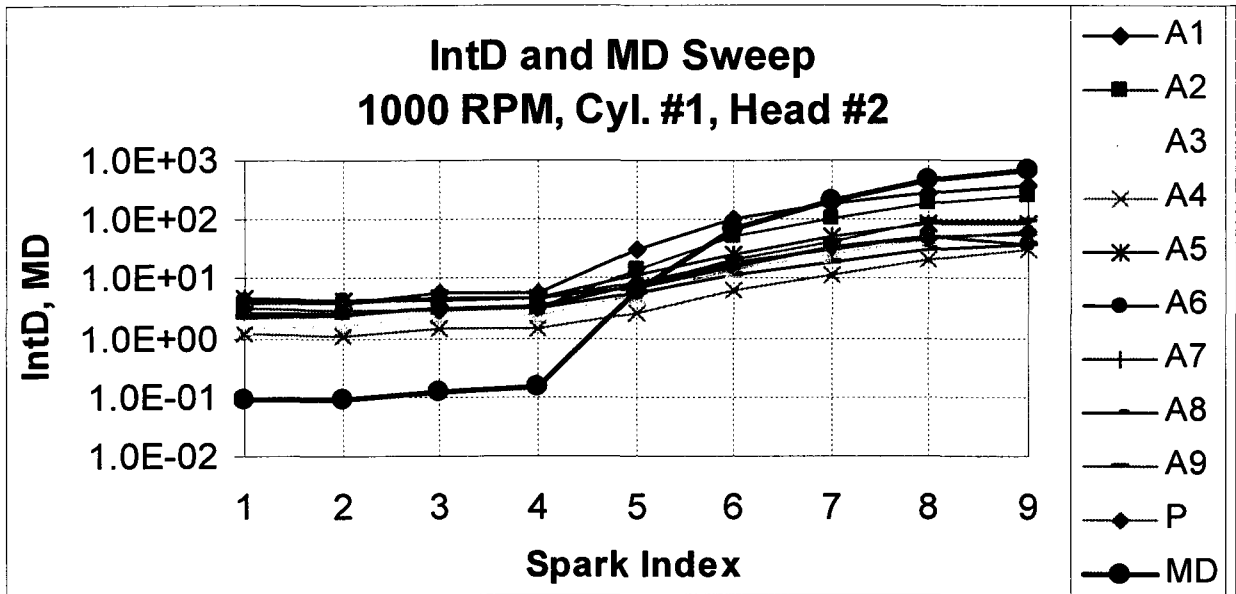


Figure 5. 17 - MD / IntD Sweep (Logarithmic)

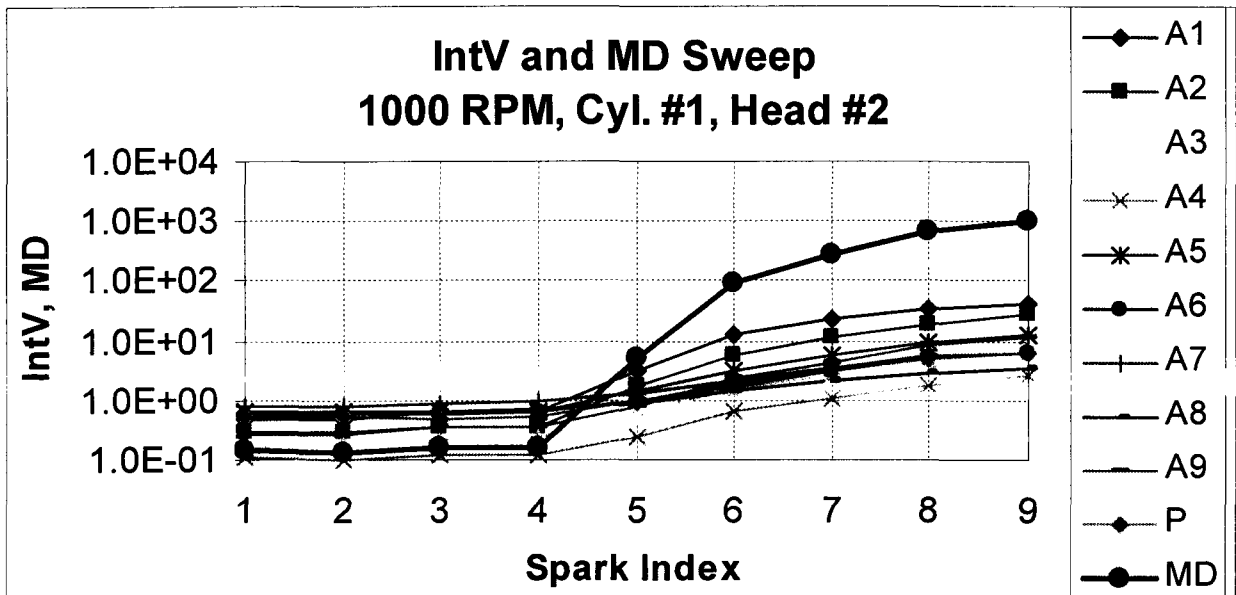


Figure 5. 18 - MD / IntV Sweep (Logarithmic)

As observed in the intensity calculation comparison, although the zero offset is reduced with the dual window methods, their trend varies little. Similarly, we see that due to normalization by a baseline, the MD calculations are influenced little by the intensity calculation technique employed.

Further comparison can be facilitated with an additional normalization procedure. The knock metric values for all knocking samples were divided by the mean value for that metric under non-knocking conditions. In this manner, all metrics can be observed as a non-dimensional ratio, describing their ability to separate knock from normal vibration. Figure 5.19 illustrates this normalized data comparison. Obvious in Figures 5.16 – 5.19 is the significant improvement in knock classification with the use of the multivariate distance metric.

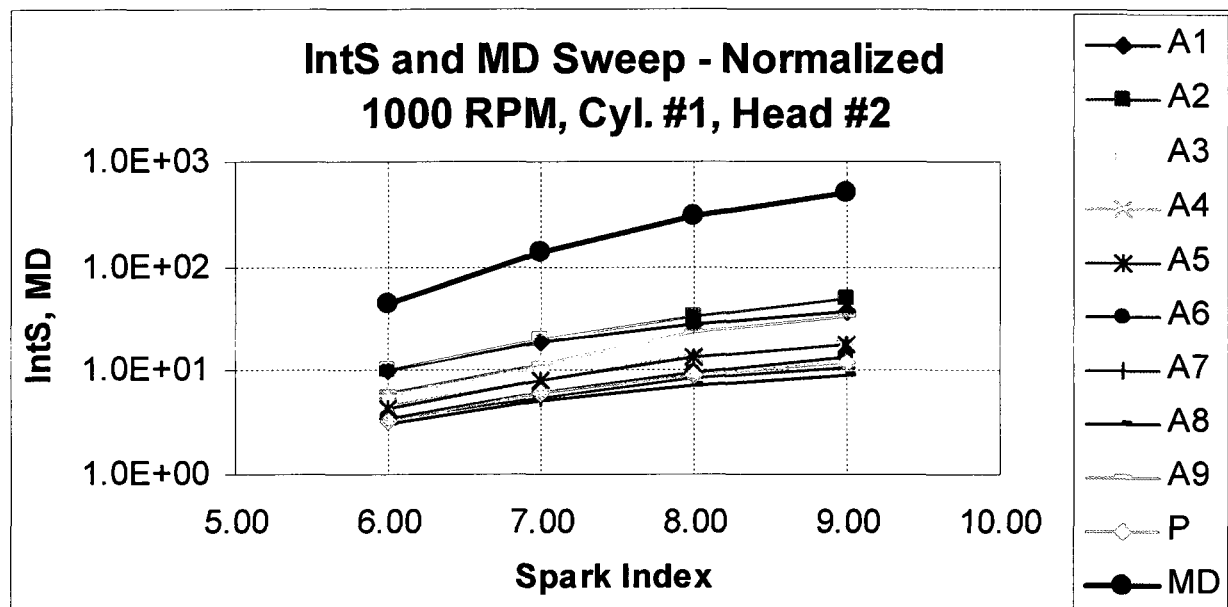


Figure 5. 19 - MD / IntS Sweep (Normalized - Logarithmic)

In both the calculation of MD and the plotting of Figure 5.19 a pressure knock intensity of 50 was used to differentiate knocking data from baseline data. For the sweep being illustrated,

this places borderline knock at a spark index of 6 (spark index of 5 corresponds to a pressure intensity of 30). As evidenced by the Figure 5.7 (sensitivity to baseline selection) and Figures 5.15 – 5.18 above, this intensity approach is conservative. Use of the pressure intensity value of 30 would increase the sensitivity MD, creating an even greater argument for this multivariate approach. This conservative approach was used for all data plotted in Appendix C.

The above figures serve as an illustration of the realizable effectiveness of the proposed multivariate diagnosis techniques; however, they do little to summarize the results from the extensive data sample used for validation. For this purpose, average knocking and non-knocking intensities were calculated for each channel, intensity type and engine speed and cylinder. These averages included all cylinder heads and spark advance values. A ratio was computed between the average knocking and non-knocking intensities and defined as the normalized intensity. This quantity was defined purely for validation (not application) purposes. Figure 5.20 provides an example of this summary value for single window intensity at 1000 rpm.

For closer examination of the results, data from only cylinder #1 is shown in Figure 5.21. A few observations can be made: It is first apparent that the overall results further substantiate the conclusion that multivariate analysis has a higher sensitivity to knock. Second, a comparison between accelerometer signals indicates a higher normalized intensity (signal-to-noise ratio) for accelerometers A1, A2, A3 and A9. This serves to validate both the results from the MTS optimization process and the speculative observations made from the raw data of Figures 5.9 – 5.12. Finally, it can be observed that at this operating condition, the selected accelerometer signals show a greater response to knock than the in-cylinder pressure intensity.

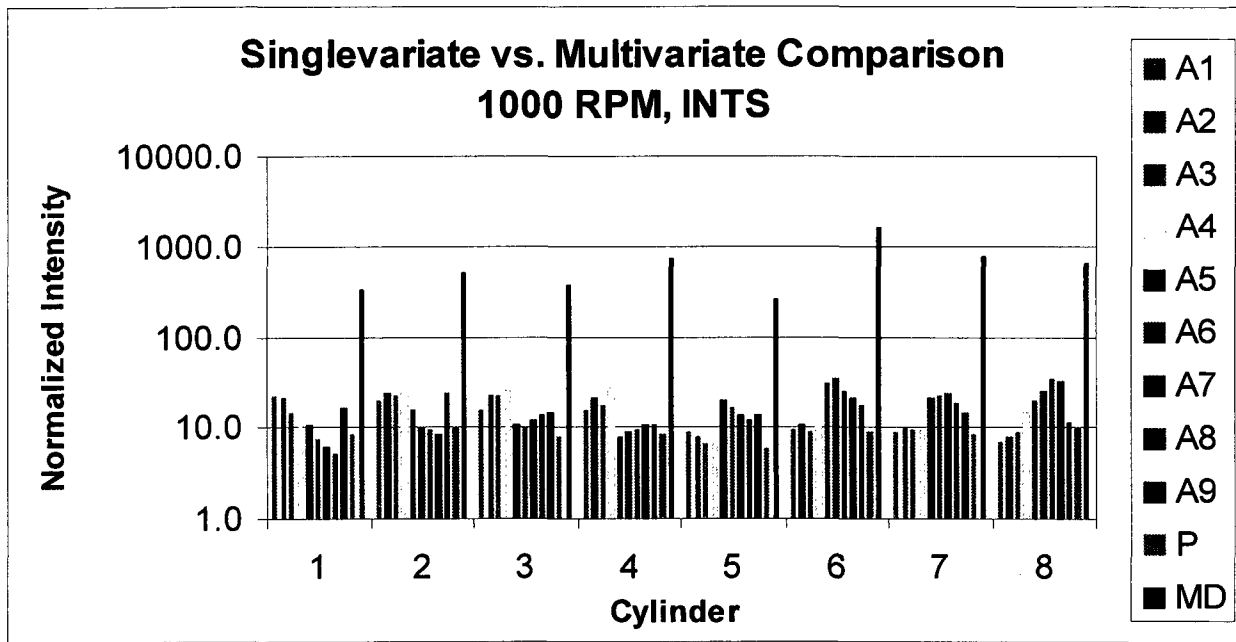


Figure 5. 20 - Normalized Intensity - 1000 RPM, IntS

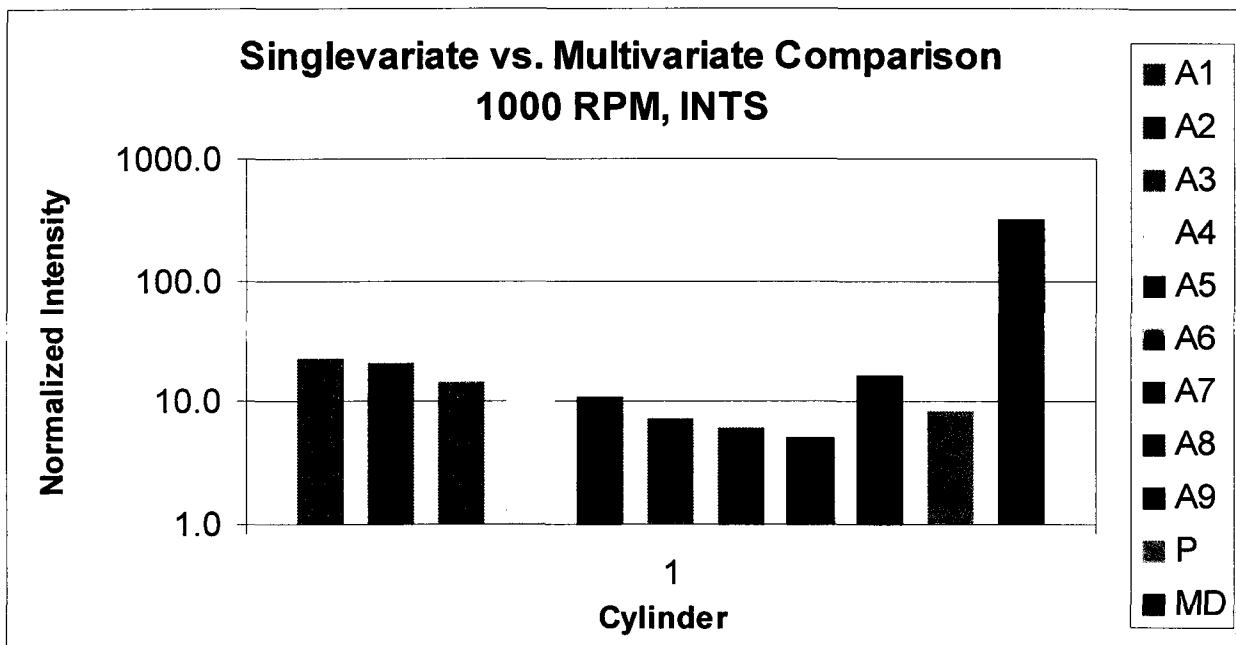


Figure 5. 21 - Normalized Intensity - 1000 RPM, IntS, Cyl. #1

Figures 5.22 – 5.23 use the Normalized Intensity metric to compare the intensity calculation types. The trends exhibited in the dual window intensity data of Figure 5.22 are very similar to the single window data of Figure 5.20. This suggests that the overall knock response of the raw data integration method is affected little when normalized by background noise. Utilizing single-variate knock intensity, the dual window has the advantage of providing a non-dimensional quantity which aids in the selection knock thresholds and is independent of transducer sensitivity.

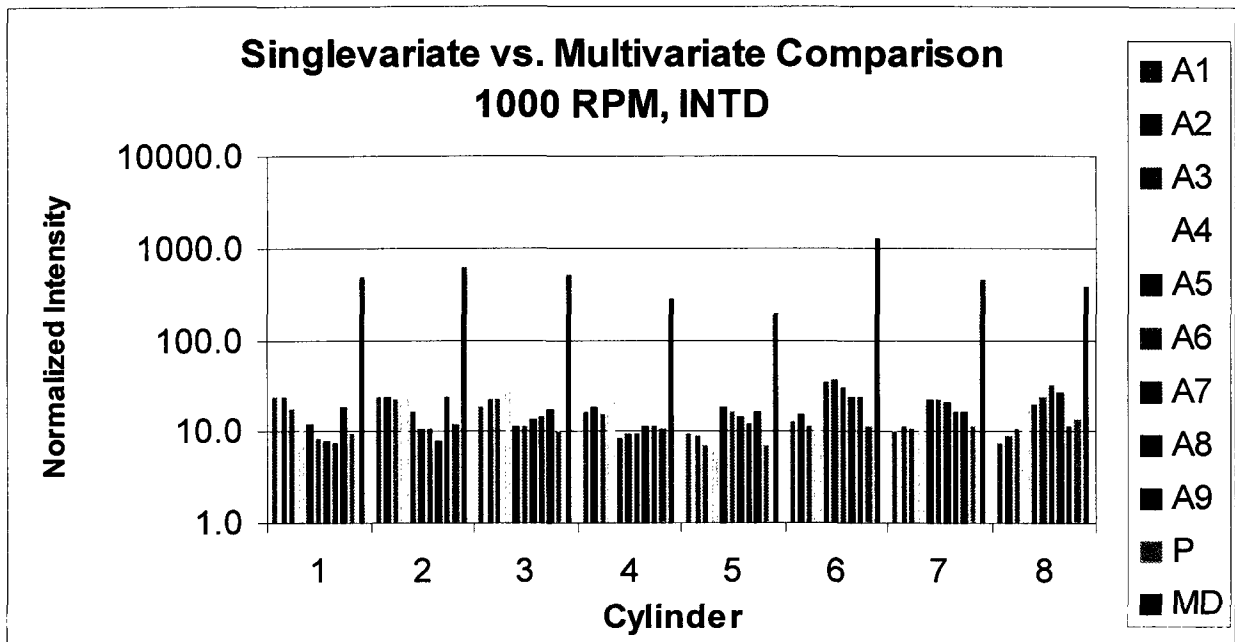


Figure 5. 22 - Normalized Intensity - 1000 RPM, IntD

Contrary to the similar trends observed between the two raw data integration intensity methods, Figure 5.23 illustrates a deviation from these trends with the use of variance data integration intensity. Based on this data set, the variance intensity tends to show a clearer distinction between used and unused channels.

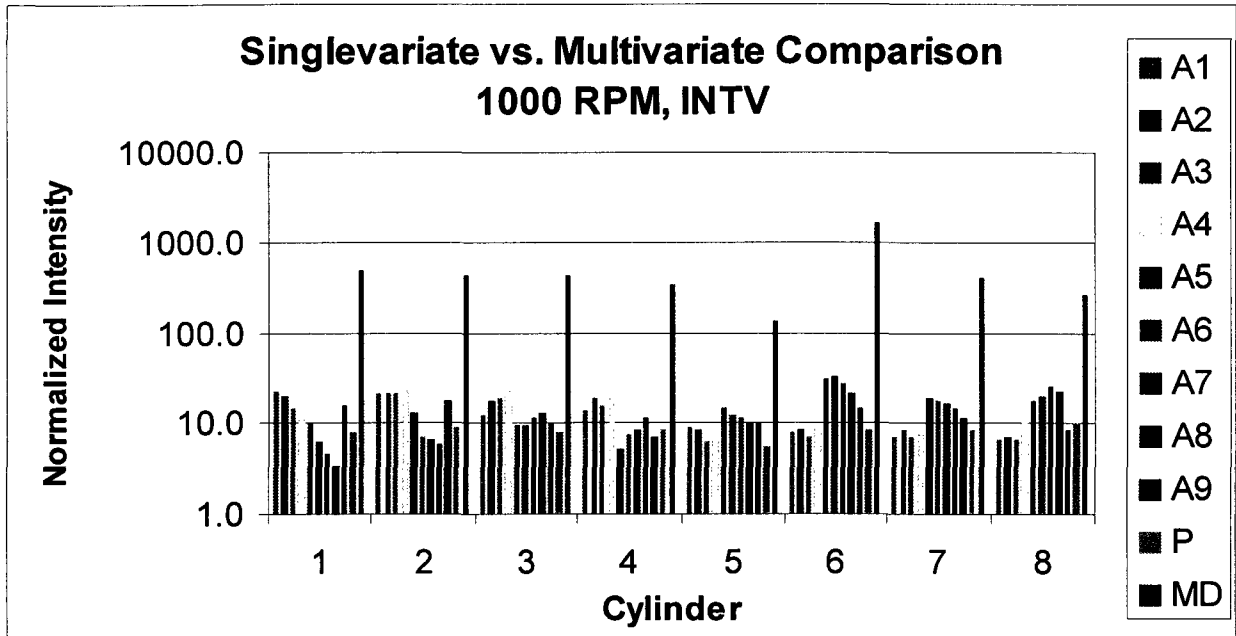


Figure 5. 23 - Normalized Intensity - 1000 RPM, IntV

The comparisons shown in Figures 5.24 – 5.27 include single window intensity data for all remaining engine speeds tested. Increasing engine speed leads to an overall increase in engine vibration. This is manifested as higher background noise levels and a diminished signal-to-noise ratio. The following figures illustrate this trend with a decreasing normalized intensity for the accelerometer signals. Although seen in all accelerometer signals, this is particularly obvious in the accelerometers which were deemed not useful by the MTS system. The advantages of both pressure intensity and multivariate analysis is emphasized by the relatively low impact of engine speed on these quantities.

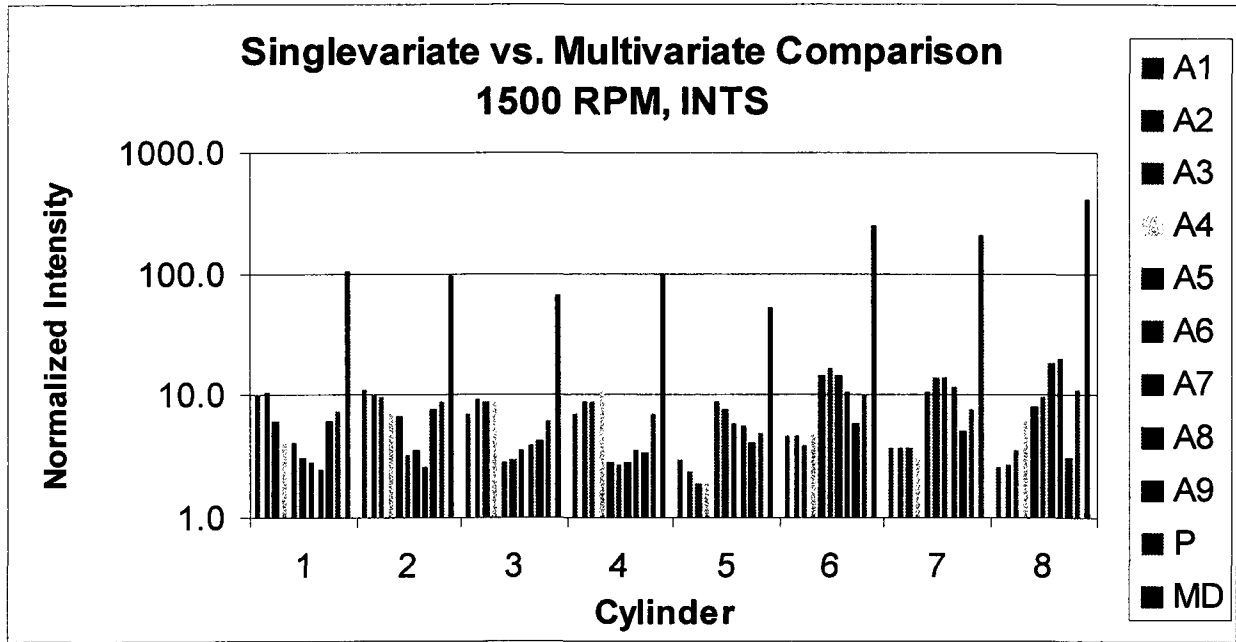


Figure 5. 24 - Normalized Intensity - 1500 RPM, IntS

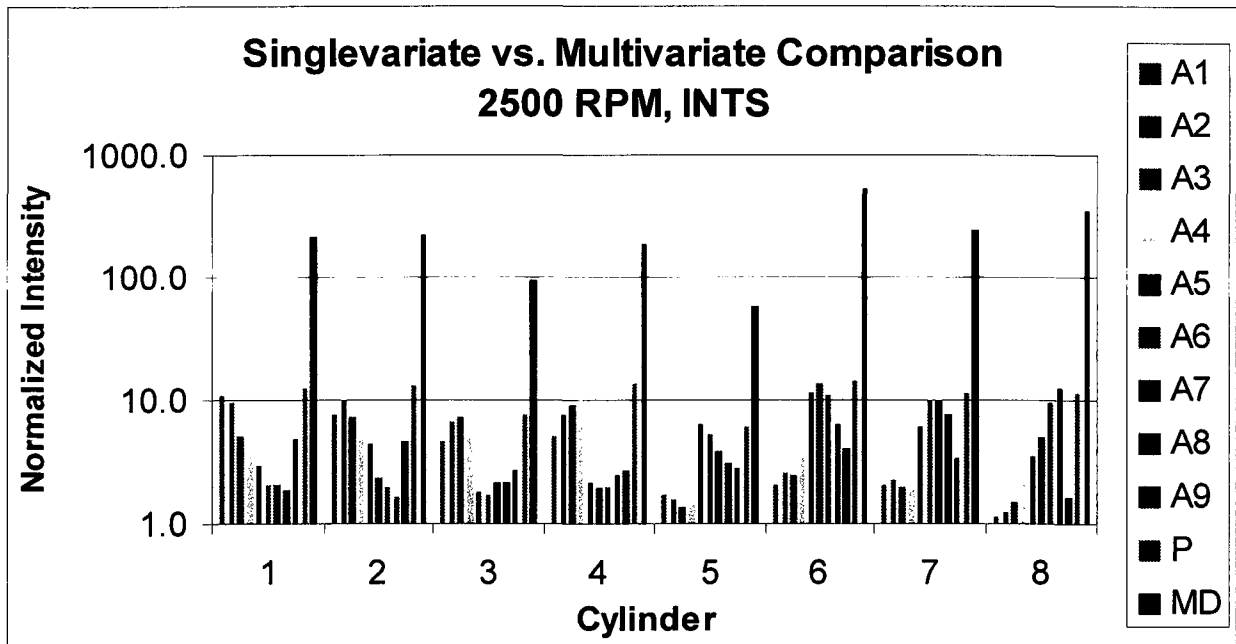


Figure 5. 25 - Normalized Intensity - 2500 RPM, IntS

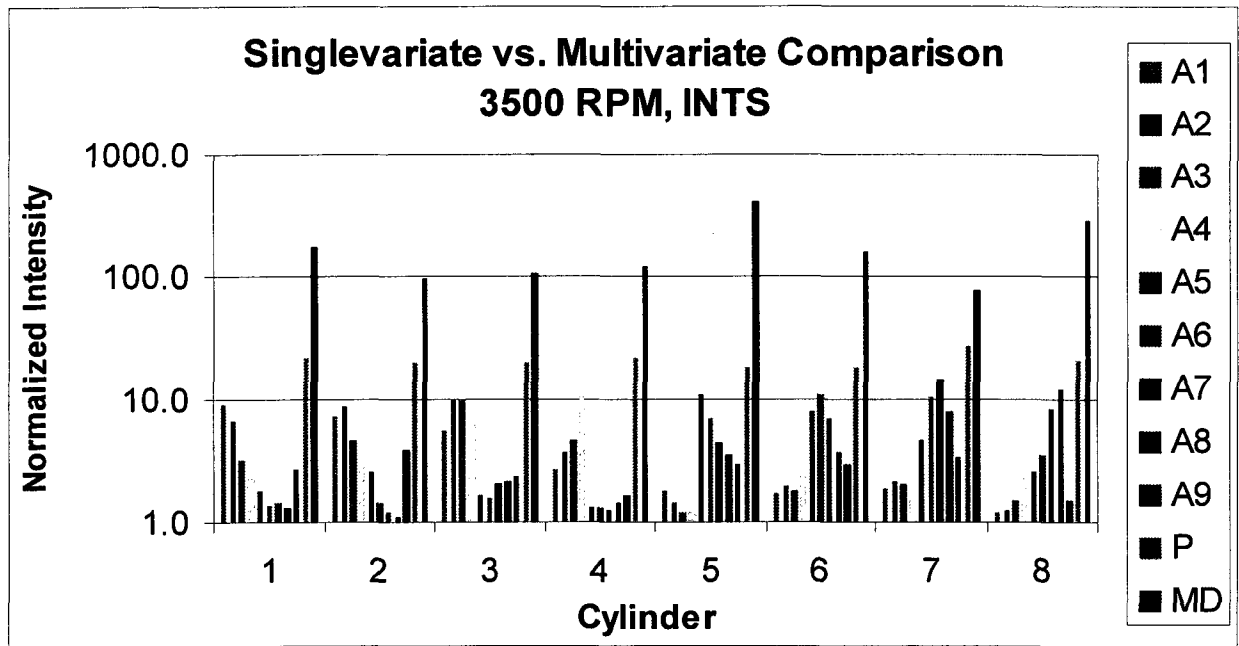


Figure 5. 26 - Normalized Intensity - 3500 RPM, IntS

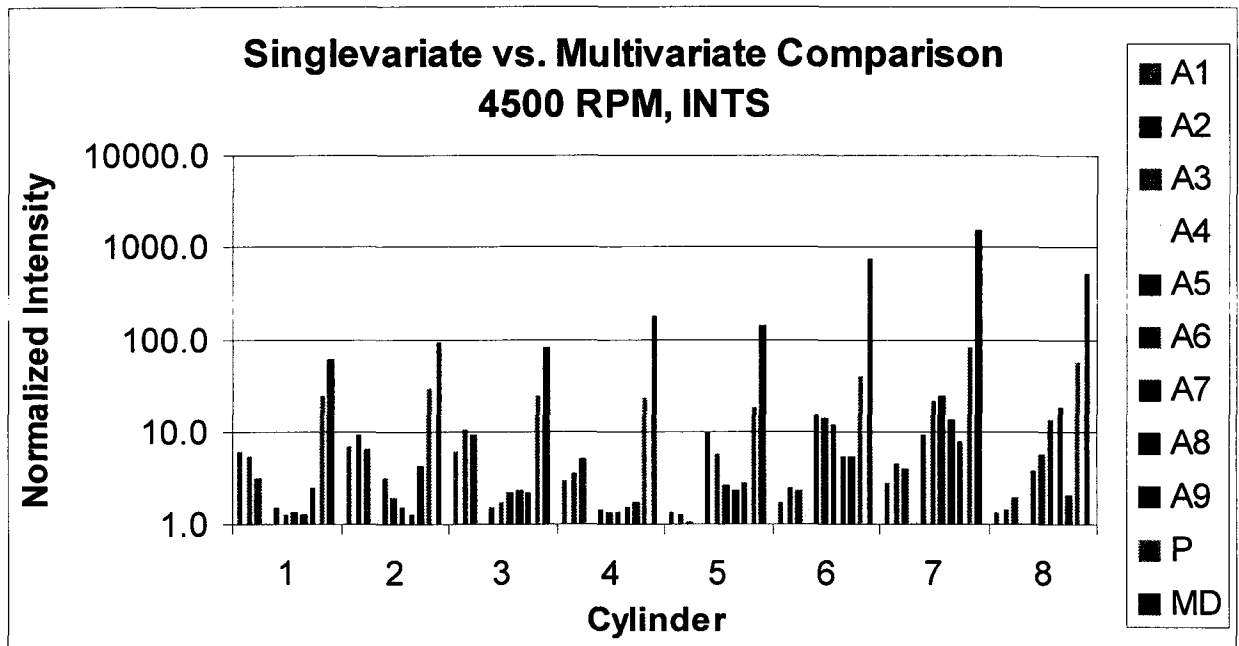


Figure 5. 27 - Normalized Intensity - 4500 RPM, IntS

5.5 Conclusions

1. The standard single window and double window intensity methods as well as the non-standard double window variance intensity method proved to be effective in knock intensity evaluation. The most obvious difference between these methods is the degree of normalization inherent to the method. For single-signal knock evaluation, the variance intensity method is recommended. This recommendation results from improved response to knock and ease of use. An improved response to knock is evidenced by the greater ability to identify the signals useful for knock detection (as seen in the normalized intensity data). The ease of use refers to the non-discriminate manner in which the noise reference window was selected. Variance is useful in extracting semi-periodic signals with little sensitivity to periodic noise. Therefore a larger noise reference window may be used without adversely affecting the intensity value.
2. Section 5.3.2 highlights the utility of multivariate statistical distance and the advantage of Mahalanobis Distance over the more fundamental Euclidean Distance and Standard Distance measurements. The Mahalanobis Distance measurement is scale invariant as (like the Standard Distance) it is normalized by the sample mean and standard deviation. Further, Mahalanobis Distance takes into account correlations between the variables used in the distance calculation. These characteristics result in a more reliable unbiased distance metric.
3. The results of this study have shown an improvement in knock response (normalized intensity improvement greater than an order of magnitude) when applying multivariate analysis. The increased demands for accurate diagnosis of knock is accompanied by an increasing trend towards multiple knock sensors. Results presented here indicate the

advantage of utilizing multiple transducers for each cylinder, rather than mapping single accelerometers to cylinders based on high correlation to in-cylinder intensity.

4. The statistical nature of the Mahalanobis Distance calculation reduces the sensitivity to intensity calculation method. Since Mahalanobis Distance measures the "distance" to a baseline, it is inherently normalized and additional normalization by a noise reference window becomes slightly redundant.
5. Optimization techniques proposed by Taguchi in the Mahalanobis-Taguchi System provide tools for increasing efficiency and quality of the multivariate knock detection strategy. The use of MTS has allowed selection of accelerometer signals which show the best response to knock events. Results of this analysis were validated by both observation of raw data and relative magnitudes of normalized knock intensity.

CHAPTER 6 – CONCLUSIONS AND RECOMMENDATIONS

Corresponding to the objectives presented in Chapter 1 and based on the work presented herein, the following conclusions are drawn:

1. A comprehensive literature review was conducted providing valuable information regarding proper testing methods and the current state of knock detection capabilities. The literature cited indicates that vibration-based knock detection continues to be the standard. Also indicated is the fact that even in multiple transducer systems, the knock detection metric is based on a single transducer (although transducer selection may depend on the cylinder being monitored).
2. Three pressure transducer types and six transducer locations were tested to determine the most reliable technique for obtaining a reference knock signal.
 - Although the Oprand AutoPSI transducer shows some potential for knock detection, its overall lack of reproducibility discounts its use as a reference transducer.
 - Although the spark plug mounted transducer has shown its potential for some applications, its low response to knock signals made it unsuitable for this purpose.
 - The Kistler flush mount transducers were selected for this study based on its overall performance in all validation studies performed.
 - The standard (central) flush mount location was chosen based on a high response to knock signal and the accessibility of this location for each cylinder.
3. A preliminary study was conducted in which laser scanning velocimetry was used to determine the overall structural response of the engine cylinder block to knock excitations. Based on this study, eight vibration transducer locations were determined in addition to the

production knock sensor location. These nine accelerometers provide the signals to be used in the multivariate knock metric calculation.

4. Data were acquired from 13 sets of cylinder heads at 5 engine speeds for up to 10 spark advance settings. This provided a comprehensive set of data for both normal and knocking operations. Data reduction involved a data resampling technique which provided position domain data while sacrificing little information from the original 250 kHz time domain data set.
5. Knock intensity was calculated based on each transducer signal for each cylinder. This was accomplished using the standard integral based intensity calculations as well as a new modified intensity calculation which employs an ensemble variance to take advantage of the cyclic variability associated with knock. This variance intensity method improves the response to knock and reduces the sensitivity to noise referencing methods.
6. The Mahalanobis Distance multivariate statistical calculation was used to create a single knock metric based on the signals from the 9 accelerometers. Again, the novelty in this is the utilization of all transducers in a knock detection system for each cylinder with the goal of improving knock response and improving knock detection reliability. The reliability of statistical distance analysis was further improved with the application of the Mahalanobis-Taguchi System, which incorporates Taguchi's Principles of Robust Engineering.
7. The multivariate knock metric is compared to each of the single variable knock intensities calculated from each transducer. The effectiveness of the knock detection system is measured by its ability to distinguish knocking from non-knocking signals. Therefore, comparisons were made by normalizing the signals obtained during knock conditions by those obtained during normal operation (including only background noise). As shown in

Chapter 5 and throughout Appendix C, the multivariate knock metric shows a significant improvement (normalized intensity improvement greater than an order of magnitude) in response to the knock signal. This represents the potential for a more reliable knock detection system which has applications in both laboratory and production environments.

8. Future work will be related to the development of application-specific techniques. Distinctive algorithms and procedures must be produced for applications in engine mapping, diagnosis and control. It should be noted that the work presented here utilized nine accelerometers. Production control applications including this many sensors is limited to high performance vehicles. Therefore, further validation studies will look at the effects of reducing transducer number. Although some degree of performance reduction is expected, this work illustrates the need to take full advantage of multi-sensor systems.

REFERENCES

1. Arrigoni, V., Calvi, G.F., Gaetani, B., Giavazzi, F., Zanoni, G.F., "Recent Advances in the Detection of Knock in S.I. Engines", SAE Paper 780153, 1978
2. Ball, G.A., "Photographic Studies of Cool Flames and Knock in an Engine", Fifth Symposium on Combustion, pp. 360 – 371, 1956
3. Ball, J., Stone, C.R., Raine, R.R., "A Technique for Estimating Completeness of Combustion and its Use in Modeling Cycle-By-Cycle Variations in Combustion", SAE Paper 2000-01-0953, 2000
4. Beidl, C., Rust, A., Rasser, M., "Key Steps and Methods in the Design and Development of Low Noise Engines", SAE Paper 1999-01-1745, 1999
5. Benedetti, G.A., Benson, J.Z., "Dynamic Response of a Transducer Mounted At One End Of An Acoustic Cavity Which Is Subjected To A Specified Pressure At The Open End Of The Cavity, U.S. Department of Energy Contract DE-AC04-94AL85000, NTIS SAND95-8200, 1995
6. Boccadoro, Y., Kizer, T., "Adaptive Spark Control with Knock Detection", SAE Paper 840447, 1984
7. Bradley, D., Kalghatgi, G.T., Golombok, M., Yeo, J., "Heat Release Rates Due to Autoignition, and Their Relationship to Knock Intensity in Spark Ignition Engines", Twenty-Sixth Symposium on Combustion pp, 2653-2660, 1996
8. Brunt, M.F.J., Pond, C.R., Biundo, J., "Gasoline Engine Knock Analysis using Cylinder Pressure Data", SAE Paper 980896, 1998
9. Burgdorf, K., Chomiak, J., "A New Knock Form – an Experimental Study", SAE Paper 982589, 1998
10. Burgdorf, K., Denbratt, I., "Comparison of Cylinder Pressure Based Knock Detection Methods", SAE Paper 972932, 1997
11. Burgdorf, K., Denbratt, I., "A Contribution to Knock Statistics", SAE Paper 982475, 1998
12. Castagne, M., Dumas, J.P., Henriot S., Lafossas, F.A., Mazoyer, T., "New Knock Localization Methodology for SI Engines", SAE Paper 2003-01-1118, 2003
13. Checkel, M., Dale, J., "Computerized Knock Detection from Engine Pressure Records", SAE Paper 860028, 1986

14. Checkel, M., Dale, J., "Pressure Trace Knock Measurement in a Current S.I. Production Engine", SAE Paper 890243, 1989
15. Chun, K., Heywood, J., "Characterization of Knock in a Spark-Ignition Engine", SAE Paper 890156, 1989
16. Chun, K., Heywood, J., Keck, J.C., "Prediction of Knock Occurrence in a Spark-Ignition Engine", Twenty-Second Symposium on Combustion / The Combustion Institute pp. 455-463, 1988
17. Chun, K., Kim, S., Kim, T., "Flame Propagation and Knock Detection Using an Optical Fiber Technique in a Spark-Ignition Engine", SAE Paper 931906, 1993
18. Collings, N., Dinsdale, S., Eade, D., "Knock Detection by Means of the Spark Plug", SAE Paper 860635, 1986
19. Daniels, C.F., Zhu, G.G., Winkelman, J., "Inaudible Knock and Partial-Burn Detection Using In-Cylinder Ionization Signal", SAE Paper 2003-01-3149, 2003
20. Draper, C.S., "The Physical Effects of Detonation in a Closed Cylindrical Chamber", Report No.493 National Advisory Committee for Aeronautics, 1933
21. DSP Technology, "RedLine ACAP 5.0 User Manual", 1996
22. Dues, S., Adams, J., Shinkle, G., "Combustion Knock Sensing: Sensor Selection and Application Issues", SAE Paper 900488, 1990
23. Fitzpatrick, M., Pechstedt, R., Lu, Y., "A New Design of Optical In-Cylinder Pressure Sensor for Automotive Applications", SAE Paper 2000-01-0539, 2000
24. Flurry, B., Riedwyl, H., "Multivariate Statistics: A Practical Approach", Chapman and Hall, New York, USA, 1988
25. Forbes, J., Carlstrom, K., Graessley, W., "Engine Knock Control Via Optimization of Sensor Location", SAE Paper 951237, 1995
26. Geiser, F., Wytrykus, F., Spicher, U., "Combustion Control with the Optical Fibre Fitted Production Spark Plug", SAE Paper 980139, 1998
27. Gonzalez, C., "On-Board Equipment for the Evaluation of Aviation Gasolines Abnormal Combustion Characteristics", SAE Paper 951156, 1995
28. He, G., Patania, A., Kluzner, M., Vokovich, D., Astrakhan, V., Wall, T., Wlodarczyk, M., "Low-Cost Spark Plug-Integrated Fiber Optic Sensor for Combustion Pressure Monitoring", SAE Paper 930853, 1993

29. He, G., Wlodarczyk, T., Evaluation of a Spark-Plug-Integrated Fiber-Optic Combustion Pressure Sensor”, SAE Paper 940381, 1994
30. Heywood, J., “Internal Combustion Engine Fundamentals”, McGraw-Hill Series in Mechanical Engineering, 1988
31. Higuma, A., Suzuki, T., Yoshida, M., Oguri, Y., Minoyama, T., “Improvement of Error in Piezoelectric Pressure Transducer”, SAE Paper 1999-01-0207, 1999
32. Hirako, O., Murakami, N., Akishino, K., “Influence of Valve Noise on Knock Detection in Spark Ignition Engines”, SAE Paper 880084, 1988
33. Hountalas, D.T., Anestis, A., "Effect of Pressure Transducer Position on Measured Cylinder Pressure Diagram of High Speed Diesel Engines", Energy Conserv. Mgmt. Vol. 39, No. 7, pp.589-607, 1998
34. Iwata, T., Sakakivara, K., Haraguchi, H., “A New Method to Automatically Optimize the Knock Detection Level in the Knock Control System”, SAE Paper 891964, 1989
35. Kaji, K., Matsushige, S., Kanamaru, M., Takahashi, J., Asano, S., “Development of Knock Sensor”, SAE Paper 861375, 1986
36. Kaneyasu, M., Kurihara, N., Katogi, K., Tokuda, H., “Engine Knock Detection Using Multi-Spectrum Method”, SAE Paper 920702, 1992
37. Konig, G., Sheppard, C.G.W., "End Gas Autoignition and Knock in a Spark Ignition Engine", SAE Paper 902135, 1990
38. Kuratle, R., Marki, B., “Influencing Parameters and Error Sources During Indication on Internal Combustion Engines”, SAE Paper 920233, 1992
39. Lee, J., Hwang, S., Lim, J., Jeon, D., Cho, Y., “A New Knock-Detection Method using Cylinder Pressure, Block Vibration and Sound Pressure Signals from a SI Engine”, SAE Paper 981436, 1998
40. Lee, Y., Pae, S., Min, K., Kim, E.S., "Prediction on Knock Onset and the Autoignition Site in Spark-Ignition Engines", Proceedings of the Institution of Mechanical Engineers Vol 214 Part D, 1999
41. Lee, W., Schaefer, H.J., "Analysis of Local Pressures, Surface Temperatures and Engine Damages under Knock Conditions", SAE Paper 830508, 1983
42. Leppard, W.R., "Individual-Cylinder Knock Occurrence and Intensity in Multicylinder Engines", SAE Paper 820074, 1982

43. Levendahl, W.J., "Multistage Autoignition of Engine Fuels", Fifth Symposium on Combustion / The Combustion Institute, pp. 372-385, 1956
44. Leveque, R., Marcusich, M., Patriquin, G., "Unleaded Racing Gasoline Components and Blends in the 110 Octane Range", SAE Paper 942541, 1994
45. Liiva, P., Valentine, J., Cobb, J., Acker, W., "Use of Multiple Pressure Transducers to Find In-Cylinder Knock Location", SAE Paper 922368, 1992
46. Livengood, J.C., Wu, P.C., "Correlation of Autoignition Phenomena in Internal Combustion Engines and Rapid Compression Machines", Fifth Symposium on Combustion / The Combustion Institute, pp. 347-356, 1956
47. Martychenko, A., Park, J., Ko, Y., Balin, A., Hwang, J., Chae, J., "A Study on the Possibility of Estimation of In-Cylinder Pressure by Means of Measurement of Spark Gap Breakdown Voltage", SAE Paper 1999-01-1115, 1999
48. Mathworks, "MATLAB Help Desk", Retrieved from the World Wide Web on September 6, 2005: <http://www.mathworks.com/access/helpdesk/help/techdoc/ref/ref.html>, 2005
49. Mazoyer, Th., Fayet, P., Castagne, M., Dumas, J.P., "Development of a Multi-Sensors Head Gasket for Knock Localization", SAE Paper 2003-01-1117, 2003
50. McCoy, J.J., Taylor, H.F., "The development of a Fiber-Optic In-Cylinder Pressure Transducer", ASME 93-ICE-28, 1993
51. McNally, M.J., Benson, J.D., Callison, J.C., Graham, J.P., Wusz, T., Evans, B., "Quantifying Performance of Knock-Sensor Equipped Vehicles with Varying Octane Level Fuels -A Coordinating Research Council Program-", SAE Paper 892037, 1989
52. Mobley, C., "Non-Intrusive In-Cylinder Pressure Measurement of Internal Combustion Engines", SAE Paper 1999-01-0544, 1999
53. Mobley, C., "Wavelet Analysis of Non-Intrusive Pressure Transducer Traces", SAE Paper 2000-01-0931, 2000
54. Morris, J., "Intra-Cylinder Combustion Pressure Sensing", SAE Paper 870816, 1987
55. Muller, R., Hart, M., Krotz, G., Eickhoff, M., Truscott, A., Noble, A., Cavalloni, C., Gnielka, M., "Combustion Pressure Based Engine Management System", SAE Paper 2000-01-0928, 2000
56. Nakamura, N., Ohno, E., Kanamaru, M., Funayama, T., "Detection of Higher Frequency Vibration to Improve Knock Controllability", SAE Paper 871912, 1987

57. Nates, R., Yates, A., "Knock Damage Mechanisms in Spark-Ignition Engines", SAE Paper 942064, 1994
58. Patro, T.N., "Combustion Induced Powertrain NVH – A Time-Frequency Analysis" SAE Paper 971874, 1997
59. Poorman, T., Kalashnikov, S., Wlodarczyk, M.T., Daire, A., Goeke, W., Kropp, R., Kamat, P., "Multi-Channel and Portable Fiber Optic Combustion Pressure Sensor System", SAE Paper 952084, 1995
60. Poorman, T., Xia, L., Wlodarczyk, M.T., "Ignition System-Embedded Fiber-Optic Combustion Pressure Sensor for Engine Control and Monitoring" SAE Paper 970845, 1997
61. Powell, D., "Engine Control Using Pressure: Past, Present and, Future", Journal of Dynamic Systems, 1993
62. Puzinauskas, P., "Examination of Methods Used to Characterize Engine Knock", SAE Paper 920808, 1992
63. Rai, H., Brunt, M.F.J., Loader, C.P., "Quantification and Reduction of IMEP Errors Resulting from Pressure Transducer Thermal Shock in an S.I. Engine", SAE Paper 1999-01-1329, 1999
64. Randolph, A., "Cylinder-Pressure-Based Combustion Analysis in Race Engines", SAE Paper 942487, 1994
65. Randolph, A., "Cylinder-Pressure-Transducer Mounting Techniques to Maximize Data Accuracy", SAE Paper 900171, 1990
66. Randolph, A., "Methods of Processing Cylinder-Pressure Transducer Signals to Maximize Data Accuracy", SAE Paper 900170, 1990
67. Renault, F., "A New Technique to Detect and Control Knock Damage", SAE Paper 820073, 1982
68. Richardson, S., McMillian, M.H., Woodruff, S.D., McIntyre, D., "Misfire, Knock and Nox Mapping of a Laser Spark Ignited Single Cylinder Lean Burn Natural Gas Engine", SAE Paper 2004-01-1853, 2004
69. Rosenberger, T.E., Colburn, J.W., Ruth, C.R., "Pressure Transducer Performance and Measurement Trade-Offs in a Transient, High Temperature, Combustion Environment", Army Research Laboratory, NTIS ARL-TR-914, 1995
70. Rosseel, E., Sierens, R., Baert, R., "Evaluating Piezo-electric Transducer Response to Thermal Shock from In-cylinder Pressure Data", SAE Paper 1999-01-0935, 1999

71. Roth, K.J., Sobiesiak, A., Robertson, L., Yates, S., "In-Cylinder Pressure Measurements with Optical Fiber and Piezoelectric Pressure Transducers", SAE Paper 2002-01-0745, 2002
72. Samimy, B., Rizzoni, G., Leisenring, K., "Improved Knock Detection by Advanced Signal Processing", SAE Paper 950845, 1995
73. Sawamoto, K., Kawamura, Y., Kita, T., Matsushita, K., "Individual Cylinder Knock Control by Detecting Cylinder Pressure", SAE Paper 871911, 1987
74. Schaberg, P., Priede, T., Dutkiewicz, R., "Effects of a Rapid Pressure Rise on Engine Vibration and Noise", SAE Paper 900013, 1990
75. Schmillen, K.P., Rechs, M., "Different Methods of Knock Detection and Knock Control", SAE Paper 910858, 1991
76. Scholl, D., Davis, C., Russ, S., Barash, T., "The Volume Acoustic Modes of Spark-Ignited Internal Combustion Chambers", SAE Paper 980893, 1998
77. Scholl, D., Davis, C., Russ, S., Stockhausen, W., "Spectrogram Analysis of Accelerometer-Based Spark Knock Detection Waveforms", SAE Paper 972020, 1997
78. Scholl, D., Russ, S., Stockhausen, W., "Detection of Spark Knock Oscillations: Dependence on Combustion Temperature", SAE Paper 970038, 1997
79. Sellnau, M.C., Matekunas, F.A., Battiston, P.A., Chang, C.F., Lancaster, D.R., "Cylinder-Pressure-Based Engine Control Using Pressure-Ratio-Management and Low-Cost Non-Intrusive Cylinder Pressure Sensors", SAE Paper 2000-01-0932, 2000
80. Sharma, S., "Applied Multivariate Techniques", John Wiley & Sons, New York, USA, 1996
81. Shimasaki, Y., Kobayashi, M., Sakamoto, H., Ueno, M., Hasegawa, M., Yamaguchi, S., Suzuki, T., "Study on Engine Management System Using In-Cylinder Pressure Sensor Integrated with Spark Plug", SAE Paper 2004-01-0519, 2004
82. Soyly, S., Gerpen, J., "Determination of Knock Sensor Location on a Heavy-Duty Natural Gas Engine", SAE Paper 971705, 1997
83. Spicher, U., Kollmeier, H., "Detection of Flame Propagation During Knocking Combustion by Optical Fiber Diagnostics", SAE Paper 861532, 1986
84. Spicher, U., Spiegel, L., Reggelin, B., Heuser, G., "Investigation into the Applicability of an Optical Fiber Sensor for Knock Detection and Knock Control System", SAE Paper 922370, 1992
85. Stone, R., "Introduction to Internal Combustion Engines – 2nd Edition", SAE International, 1998

86. Sun, L, Anderton, D., "One Way to Reduce Thermal Effects in a Piezoelectric Pressure Transducer Mounted in the Combustion Chamber of a C.I. Engine", Institute of Sound and Vibration Research Technical Report No. 189, NTIS, 1990
87. Syrimis, M., Assanis, D. N., "Knocking Cylinder Pressure Data Characteristics in a Spark-Ignition Engine", ASME 97-ICE-9, 1997
88. Taguchi, G., Chowdhury, S., Wu, Y., "The Mahalanobis-Taguchi System", McGraw-Hill, New York, USA, 2001
89. Tousignant, T.E., Tjong, J., Reader, G.T., "Experience Using Different In-Cylinder Pressure Measurement Methods in an IC Engine", CI/CS Spring Conference, 2002
90. Tousignant, T.E., Tjong, J., Reader, G.T., "Importance of Transducer Type and Position in the Detection of Abnormal Combustion", CI/CS Spring Conference, 2004
91. Urlaub, M., Bohme, J.F., "Reconstruction of Pressure Signals on Structure-borne Sound for Knock Investigation", SAE Paper 2004-01-0521, 2004
92. Vianna, J., Damion, J., Carvalho, M., "Contribution to the Study of Measurement of Dynamic Pressure in the Interiors of Combustion Engine Cylinders", SAE Paper 942401, 1994
93. Walsh, A.D., "The Knock Ratings of Fuels", Ninth Symposium on Combustion / The Combustion Institute, pp. 1046-1055, 1962
94. Watanabe, E., Fukutani, I., "Knock Reduction of Spark-Ignition Engines by EGR", SAE Paper 860034, 1986
95. Witer, A.J., Lim, T.C., "Crankshaft Rumble Noise Phenomenon: Experimental Characterization of Source Strength and Path Response", SAE Paper 1999-01-1770, 1999
96. Wlodarczyk, M., Poorman, T., Xia, L., Arnold, J., Coleman, T., "Embedded Fiber-Optic Combustion-Pressure Sensors for Automotive Engine Controls", FISITA World Automotive Congress, 1998
97. Wlodarczyk, M., Poorman, T., Xia, L., Arnold, J., Coleman, T., "In-Cylinder Fiber-Optic Pressure Sensor for Monitoring and Control of Diesel Engines", SAE Paper 981913, 1998
98. Zhang, Z., Tomita, E., "Diagnostic of Knocking by Wavelet Transform Method Utilizing Real Signal as Mother Wavelet", SAE Paper 2001-01-3546, 2001
99. Zurita, G.V., Agren, A., Petterson, E., "Multivariate Analysis of Engine Noise and Exhaust Emissions from Ethanol Fueled Diesel Engine", SAE Paper 971871, 1997

100. Zurita, G.V., Agren, A., Petterson, E., "Reconstruction of the Cylinder Pressure from Vibration Measurements for Prediction of Exhaust and Noise Emissions in Ethanol Engines", SAE Paper 1999-01-1658, 1999
101. Zurita, G.V., "Vibration Based Diagnostics for Analysis of Combustion Properties and Noise Emissions of IC Engines", Doctoral Thesis, Lulea University of Technology, Lulea, Sweden, 2001
102. Zhu, G.G., Daniels, C.F., Winkelman, J., "MBT Timing Detection and its Closed-Loop Control Using In-Cylinder Ionization Signal", SAE Paper 2004-01-2976, 2004

BIBLIOGRAPHY

1. Breyfogle, F.W., "Implementing Six Sigma – Smarter Solutions Using Statistical Methods", John Wiley & Sons, 1999
2. Curran, H.J., Gaffuri, P., Pitz, J., Westbrook, C.K., Leppard, W.R., "Autoignition Chemistry in a Motored Engine: An Experimental and Kinetic Modeling Study", Twenty-Sixth Symposium on Combustion / The Combustion Institute pp. 2669-2676, 1996
3. Franklin, M.L., Murphy, T.E., "A Study of Knock and Power Loss in the Automotive Spark Ignition Engine", SAE Paper 890161, 1989
4. Heisler, H., "Advanced Engine Technology", SAE International, 1995
5. Hewlett Packard, "The Fundamentals of Modal Analysis", Hewlett Packard Application Note 243-3, 1986
6. Hewlett Packard, "The Fundamentals of Signal Analysis", Hewlett Packard Application Note 243, 1994
7. Heywood, J., "Internal Combustion Engine Fundamentals", McGraw-Hill Series in Mechanical Engineering, 1988
8. Hollis, M.S.L, "Shock Testing of an Endevco 8511A-20K Piezoresistive Pressure Transducer", Army Research Laboratory, NTIS ARL-TN-108, 1998
9. Jost, W., "Knock Reaction", Ninth Symposium on Combustion / The Combustion Institute, pp. 1013-1022, 1962
10. Kwang, M.C, Heywood, J.B., Keck, J.C., "Prediction of Knock Occurrence in a Spark-Ignition Engine", Twenty-Second Symposium on Combustion / The Combustion Institute, pp. 455-463, 1988
11. LMS, "Digital Signal Processing", LMS N. America Training Series, 1998
12. LMS, "Fourier Monitor and Modal Analysis", LMS N. America Training Series, 2000
13. LMS, "Signature Monitor and Running Modes", LMS N. America Training Series, 2000
14. Lyons, R.H., "Machinery Noise and Diagnostics", Butterworth Publishers, 1987
15. Male, T., "Photographs at 500,000 Frames per Second of Combustion and Detonation in a Reciprocating Engine", Third Symposium on Combustion / The Combustion Institute, pp. 721-726, 1952

16. Malmberg, E.W., Smith, M.L., Bigler, J.E., Bobbit, A., "A Study of Cool Flames and Associated Reactions in an Engine", Fifth Symposium on Combustion / The Combustion Institute, pp. 385-391, 1956
17. Marvin, C., Ewers, G., "A Simple Approach to Digital Signal Processing", John Wiley & Sons, Inc, 1996
18. Rosli, U., Wolfer, P., "Piezoelectric Transducers Measure Pressures", Kistler Instrumente AG
19. Rowe, A., "Engine Defect Source Identification by Enhanced Signature Analysis", Masters Thesis, University of Windsor, Windsor, Ontario, Canada, 1999
20. Shangchun, F., Guangyu, L., Hongran, W., "Study of the Dynamic Characteristics of the Resonant Cylinder Pressure Transducer with Frequency Output Using Digital Simulation", The Institute of Scientific and Technical Information of China, NTIS, 1993
21. Smith, J.R., Green, R.M., Westbrook, C.K., Pitz, W.J., "An Experimental and Modeling Study of Engine Knock", Twentieth Symposium on Combustion / The Combustion Institute, pp. 91-100, 1984
22. Stone, R., "Introduction to Internal Combustion Engines – 2nd Edition", SAE International, 1998
23. Tjong, J., "Engine Dynamic Signal Monitoring and Diagnostics", Doctor of Philosophy Dissertation, University of Windsor, Windsor, Ontario, Canada, June 1993

LITERATURE SUMMARY CHART

Author	Year	Pressure Measurement	Vibration Measurement	Piezoelectric Pressure Transducers	Fiberoptic Transducers	Thermal Effects	Combustion Knock	Photographic/Propagation Studies	Knock Damage	Fuels	Knock Detection	Pressure-Based Knock Detection	Vibration-Based Knock Detection	Force Transducers	Spark Plug Electrode Knock Detection	Experimental	Modelling	Statistical Processing
Arrigoni, V. et al.	1978	*																
Ball, G.A.	1956						*	*										
Ball, J. et al.	2000	*																*
Beidl, C. et al.	1999		*												*			
Benedetti, G.A., Benson, J.Z.	1995	*															*	
Boccardo, Y., Kizer, T.	1984	*	*	*		*			*		*				*			
Bradley, D. et al.	1996	*		*		*									*	*		
Brunt, M.F.J. et al.	1998	*		*		*			*	*	*				*			
Burgdorf, K., Chomiak, J.	1998	*		*		*			*	*	*				*			*
Burgdorf, K., Denbratt, I.	1997	*		*		*			*	*	*				*			
Burgdorf, K., Denbratt, I.	1998	*		*		*			*	*	*				*			
Castagne, M. et al.	2003	*		*		*			*	*	*				*			
Checkel, M., Dale, J.	1986	*		*		*			*	*	*				*			
Checkel, M., Dale, J.	1989	*		*		*			*	*	*				*			
Chun, K., Heywood, J.	1989	*		*		*			*	*	*				*			
Chun, K. et al.	1988	*		*		*			*	*	*				*			
Chun, K. et al.	1993					*	*		*	*	*				*			
Collings, N. et al.	1986	*		*		*			*	*	*			*	*	*		
Daniels, C.F., Zhu, G.G.	2003	*	*	*		*			*	*	*			*	*	*		
Draper, C.S.	1933	*		*		*			*	*	*				*		*	
DSP Technology	1996	*		*		*			*	*	*				*	*	*	
Dues, S. et al.	1990		*	*		*			*	*	*				*	*	*	
Fitzpatrick, M. et al.	2000	*		*		*			*	*	*				*	*	*	
Flurry, B., Riedwyl, H.	1988																	*
Forbes, J. et al.	1995										*				*	*	*	
Geiser, F. et al.	1998			*		*	*		*	*	*				*	*	*	
Gonzalez, C.	1995								*	*	*		*		*	*	*	
He, G. et al.	1993	*		*	*	*			*	*	*				*	*	*	
He, G., Wlodarczyk, T.	1994	*		*	*	*			*	*	*				*	*	*	
Heywood, J.	1988					*	*	*	*	*	*				*	*	*	
Higuma, A. et al.	1999	*		*		*			*	*	*				*	*	*	
Hirako, O. et al.	1988		*	*		*			*	*	*				*	*	*	
Hountalas, D.T., Anestis, A.	1998	*		*		*			*	*	*				*	*	*	
Iwata, T. et al.	1989		*	*		*			*	*	*				*	*	*	*
Kaji, K. et al.	1986		*	*		*			*	*	*				*	*	*	
Kaneyasu, M. et al.	1992		*	*		*			*	*	*				*	*	*	
Knoig, G., Sheppard, C.G.W.	1990	*		*	*	*			*	*	*				*	*	*	
Kurtile, R., Marki, G.	1992	*		*		*			*	*	*				*	*	*	
Lee, J. et al.	1998	*	*	*		*			*	*	*				*	*	*	*
Lee, Y. et al.	1999	*		*		*			*	*	*				*	*	*	
Lee, W., Schaefer, H.J.	1983	*		*		*			*	*	*				*	*	*	
Leppard, W.R.	1982	*		*		*			*	*	*				*	*	*	*
Levendahl, W.J.	1956	*		*		*	*		*	*	*				*	*	*	
Leveque, R. et al.	1994					*	*		*	*	*				*	*	*	
Liiva, P. et al.	1992	*		*		*			*	*	*				*	*	*	
Livengood, J.C., Wu, P.C.	1956					*	*		*	*	*				*	*	*	
Martychenko, A. et al.	1999	*				*	*		*	*	*			*	*	*	*	
Mazoyer, Th. et al.	2003	*		*		*			*	*	*				*	*	*	
McCoy, J.J., Taylor, H.F.	1993	*		*		*			*	*	*				*	*	*	
McNally, M.J. et al.	1989					*	*		*	*	*				*	*	*	
Mobley, C.	1999	*		*		*			*	*	*				*	*	*	
Mobley, C.	2000	*		*		*			*	*	*				*	*	*	
Morris, J.	1987		*	*		*			*	*	*				*	*	*	
Muller, R. et al.	2000	*		*		*			*	*	*				*	*	*	
Nakamura, H. et al.	1987	*	*	*		*			*	*	*				*	*	*	
Nates, R., Yates, A.	1994					*	*		*	*	*				*	*	*	
Patro, T.N.	1997	*		*	*	*			*	*	*				*	*	*	
Poorman, T. et al.	1995	*		*	*	*			*	*	*				*	*	*	
Poorman, T. et al.	1997	*		*	*	*			*	*	*				*	*	*	
Powell, D.	1993	*		*		*			*	*	*				*	*	*	

Author	Year	Pressure Measurement	Vibration Measurement	Piezoelectric Pressure Transducers	Fiberoptic Transducers	Thermal Effects	Combustion Knock	Photographic/Propagation Studies	Knock Damage	Fuels	Knock Detection	Pressure-Based Knock Detection	Vibration-Based Knock Detection	Force Transducers	Spark Plug Electrode Knock Detection	Experimental	Modelling	Statistical Processing
Puzinauskas, P.	1992	*					*				*				*			
Rai, H. et al.	1999	*	*			*					*				*			
Randolph, A.	1994	*		*		*									*			
Randolph, A.	1990a	*		*		*									*			
Randolph, A.	1990b	*		*		*									*			
Renault, F.	1982					*		*							*			
Richardson, S. et al.	2004					*											*	
Rosenberger, T.E. et al.	1995	*															*	
Rossee, E. et al.	1999	*	*	*		*									*			
Roth, K.J. et al.	2002	*	*	*	*	*									*			
Samimy, B. et al.	1995	*	*	*		*				*	*	*			*			
Sawamoto, K. et al.	1987	*				*				*	*		*		*			
Schaberg, P. et al.	1990	*				*									*			
Schmillen, K.P., Rechs, M.	1991	*	*	*		*				*	*	*			*			
Scholl, D. et al.	1998	*				*				*	*	*			*		*	
Scholl, D. et al.	1997a	*	*			*				*	*	*			*		*	
Scholl, D. et al.	1997b	*	*			*				*	*	*			*		*	
Sellnau, M.C. et al.	2000	*	*			*				*	*	*			*		*	
Sharma, S.	1996																	*
Shimasaki, Y. et al.	2004	*	*	*		*				*	*	*	*		*		*	
Soylu, S., Gerpen, J.	1997		*			*				*	*	*			*		*	
Spicher, U., Kollmeier, H.	1986	*		*		*		*							*		*	
Spicher, U. et al.	1992	*		*		*		*							*		*	
Sun, L., Anderton, D.	1990	*	*		*	*									*		*	
Syrimis, M., Assanis, D.N.	1997	*	*			*				*	*				*		*	
Taguchi, G. et al.	2001																	*
Tousignant, T.E. et al.	2002	*	*	*	*	*									*		*	
Tousignant, T.E. et al.	2004	*	*	*	*	*	*			*	*				*		*	
Urlaub, M., Bohme, J.F.	2004	*	*	*		*				*	*				*	*	*	*
Vianna, J. et al.	1994	*				*				*	*				*		*	
Walsh, A.D.	1962								*									
Watanabe, E., Fukutani, I.	1986	*	*			*									*		*	
Witer, A.J., Lim, T.C.	1999		*			*						*			*		*	
Wlodarczyk, M. et al.	1998a	*	*	*	*	*									*		*	
Wlodarczyk, M. et al.	1998b	*	*	*	*	*									*		*	
Zhang, Z., Tomita, E.	2001		*			*				*	*				*		*	
Zurita, G.V. et al.	1997	*	*	*		*									*		*	*
Zurita, G.V. et al.	1999	*	*	*		*				*	*				*		*	*
Zurita, G.V.	2001	*	*	*		*				*	*				*	*	*	*
Zhu, G.G., et al.	2004	*				*				*	*			*	*	*	*	*

APPENDIX A PROCESSING SOURCE CODE

CONTENTS

A.1. Raw Data Processing	138
Summary	138
Source Code	139
A.2 Knock Intensity Calculations	145
Summary	145
Source Code	146
A.3 Supplemental Plotting	150
Summary	150
Source Code	150
A.4 MTS Calculations	152
Summary	152
Source Code	152

FIGURES

A.1 Raw Data Processing Front End	138
A.2 Intensity Processing Front End	145
A.3 Data Plotting Front End	150

A.1 Raw Data Processing

The raw data processing program completes the following tasks:

- Binary data is imported to MATLAB
- A novel resampling method is used to convert data into the position (angle) domain based on the CID channel
- In-cylinder pressure is pegged based on the reference pressure channel
- A sound file (.wav) is generated based on the data in on the MIC channel
- A large array is exported which contains all relevant knock data (resampled and offset)

DATA INPUT - READ AND RESAMPLE

File Name

File Size

	Sensitivity	Type		Sensitivity	Type
CH1	0.00488	CID ▾	CH9	0.46	ACCEL ▾
CH2	0.46	ACCEL ▾	CH10	0.46	ACCEL ▾
CH3	0.46	ACCEL ▾	CH11	0.244	PRES ▾
CH4	0.46	ACCEL ▾	CH12	0.0024	PREF ▾
CH5	0.46	ACCEL ▾	CH13	0.195	MIC ▾
CH6	0.46	ACCEL ▾	CH14	0	unused ▾
CH7	0.46	ACCEL ▾	CH15	0	unused ▾
CH8	0.46	ACCEL ▾	CH16	0	unused ▾

A. 1 - Raw Data Processing Front End

Source Code:

```
inputfigid=get(0,'currentfigure');

filename=get(findobj(inputfigid,'Tag','hfilename'),'String');
filesize=str2num(get(findobj(inputfigid,'Tag','hfilesize'),'String'));
totlen=(filesize-4096)/2;
[dummy flen]=size(file1);
cyl=str2num(file1(flen-11))

%cyl=get(findobj(inputfigid,'Tag','hcyl'),'Value');
%firint=str2num(get(findobj(inputfigid,'Tag','hfirint'),'String'));
firint=90;

%initializing
numchan=0;
preschanind=1;
k=1;
for i=1:16

evalc(['chsens(',int2str(i),')=str2num(get(findobj(',' ,int2str(inputfigid),',' ,''
Tag',' ,''chsens',int2str(i),''),'String'))']);

evalc(['chtype(',int2str(i),')=get(findobj(',' ,int2str(inputfigid),',' ,''Tag',' ,''
chtype',int2str(i),''),'Value'))'];
    if chtype(i) < 6
        numchan=numchan+1;
    end
    if chtype(i) == 1
        cidchan=i;
    end
    if chtype(i) == 2
        knkchans(k)=i;
        k=k+1;
    end
    if chtype(i) == 3
        preschan(preschanind)=i;
        preschanind=preschanind+1;
        knkchans(k)=i;
        k=k+1;
    end
    if chtype(i) == 4
        micchan=i;
    end
    if chtype(i) == 5
        prefchan=i;
    end
end

%conversion to firing order
if cyl==2
    refcyl=4
elseif cyl==3
    refcyl=2
elseif cyl==4
```

```

    refcyl=7
elseif cyl==5
    refcyl=6
elseif cyl==6
    refcyl=5
elseif cyl==7
    refcyl=3
elseif cyl==8
    refcyl=8
end

%ALLOCATE SPACE FOR LARGE VARIABLES

T='ALLOCATING SPACE...';
disp(T)
data=zeros(totlen+2048,1);
ncid=zeros(totlen,1);
chan=zeros(totlen+10000,1);

chanlen=totlen/numchan;
cyloffset=(cyl-1)*firint;

T='READING FILE....';
disp(T)

fid=fopen(filename,'r');
totlen=(filesize-4096)/2;
clear data
clear chan
data=fread(fid,totlen+2048,'short');
chan=data(2049:totlen+2048,1); %using chan as dummy here for memory purposes
data=reshape(chan,[chanlen,numchan]);

%create output filename
[dummy sfile]=size(filename);
if filename(6)=='c'
    namebegin=9;
    namend=15;
else
    namebegin=10;
    namend=17;
end

exfile1=filename(namebegin:namend);
exfile2=filename(sfile-2:sfile);
exfile=cat(2,exfile1,'_',exfile2);

%Create .wav from mic channel
soundout=cat(2,'c:\Sound\',exfile);
tmpsound=data(:,micchan);
tmpsound=tmpsound./(1.2*max(tmpsound));
evalc(['wavwrite(tmpsound,250000,','',soundout,='')']);
clear tmpsound

%Search for Zero Crossings (cidindex) after thresholds (300)

```

```

T='SEARCHING FOR ZERO CROSSINGS....';
disp(T)

i=1;
k=1;

while i<(chanlen)
    if data(i,cidchan)>300
        cidcount=1;
        while data(i,cidchan)>300
            cidcount=cidcount+1;
            i=i+1;
            if i==(chanlen-1)
                break
            end
        end
        if cidcount>20 & i<(chanlen-1)
            while data(i,cidchan)>0
                i=i+1;
                if i==(chanlen-1)
                    break
                end
            end
            cidindex(k)=i;
            k=k+1;
        end
    end
    i=i+1;
end

%Estimate resolution and offset data to begin at approximately 180 BTDC Cyl
#1

initres=720/(cidindex(2)-cidindex(1))-0.0002;

cidindexoffset=floor(cidindex-(202/initres));
if cidindexoffset(1)<0
    icid=3;
else
    icid=2;
end

%Find number of points in each cycle (index to index)
n=1;
for i=icid:k-1
    cyclen(n)=cidindexoffset(i)-cidindexoffset(i-1);
    n=n+1;
end

[dummy ncycles]=size(cyclen);
ncycles

T='DETERMINING RESOLUTION....';
disp(T)

```

```

%Find worst res cycle to determine res

[reflength,refind]=min(cyclen);
res=720/reflength %resolution based on smallest cycle

for i=1:reflength
    cyc(i)=i*res;
end

T='CREATING INDEX CYCLES...';
disp(T)

%RESAMPLING - compare cycx to reference cyc and determine which points
% can be used from the larger cycles

for n=(icid-1):ncycles
    clear newind
    tmpcyc=data((cidindexoffset(n)+1):cidindexoffset(n+1),cidchan);

    size(tmpcyc);
    xlen=size(tmpcyc,1);
    resx=720/xlen;

    for i=1:xlen
        cycx(i)=i*resx;
    end

    nk=1;
    count=0;
    for i=1:reflength
        testold=10;
        for k=nk:xlen
            count=count+1;
            test=abs(cyc(i)-cycx(k));
            if test<testold
                newind(i)=k;
                if k>1
                    nk=k-1;
                else
                    nk=k;
                end
                testold=test;
            else
                break
            end
        end
    end
    end

    junk(:,n)=transpose(newind(1,:)); %matrix of usable indices
end

T='RESAMPLING...';
disp(T)

```



```

%Reshape pre-allocated variable
clear ncid
ncid=zeros(reflength,numchan,ncycles);

%Create new array based on the the indices in junk
for n=(icid-1):ncycles
    junk2=junk(:,n);
    tmpcyc=data((cidindexoffset(n)+1):cidindexoffset(n+1),:);
    tmpcyc=tmpcyc(junk2,:);
    ncid(:,:,n)=tmpcyc;
end

clear data
clear junk
clear junk2
clear tmpcyc
clear tmpcycn

clear chan
chan=permute(ncid,[1 3 2]); %rearrange dimensions

clear ncid

T='OFFSETTING DATA...';
disp(T)

%offset to cyl1
chan=reshape(chan,[reflength*ncycles numchan]);
cylloffset=floor(202/initres)-floor(202/res); %correcting from initial
estimate
chan=chan(cylloffset+1:(reflength*ncycles-(reflength-cylloffset)),:);
ncycles=ncycles-1;
chan=reshape(chan,[reflength ncycles numchan]);

%reference pressures for each cycle

pref=chan(1,:,prefchan); %Dynamic pressure is referenced to 180 BTDC cyl 1

%offset to refcyl
if cyl ~= 1
    chan=reshape(chan,[reflength*ncycles numchan]);
    refcyloffset=floor((90*(refcyl-1))/res);
    chan=chan(refcyloffset+1:(reflength*ncycles-(reflength-refcyloffset)),:);
    ncycles=ncycles-1;
    chan=reshape(chan,[reflength ncycles numchan]);
end

if icid==3
    chan=chan(:,2:ncycles,:);
    ncycles=ncycles-1;
end

t=cyc-180;

```

```

%Sensitivity Correction

for i=1:numchan
    chan(:,:,i)=chan(:,:,i).*chsens(i);
end

%Pressure Reference Correction
for k=1:(preschanind-1)
    for i=1:ncycles
        shift=chan(1,i,preschan(k))-chan(1,i,prefchan);
        chan(:,i,preschan(k))=chan(:,i,preschan(k))-shift;
    end
end

%reduce data size to required window and knock related channels
chan=chan((floor(60/res):floor(270/res)),:,knkchans);
[dummy numchan]=size(knkchans);
t=t(floor(60/res):floor(270/res));
[dummy reflength]=size(t);

save 'c:\tempdata' chan chtype filename micchan ncycles numchan preschan res
t exfile knkchans soundout reflength file1 path1 cyl

close
clear all

T='PROCESSING COMPLETE';
disp(T)
sound(wavread('c:\tada.wav'),22050,16)
knkint

```

A.2 Knock Intensity Calculations

This intensity calculation program competes the following tasks:

- Applies a high pass Butterworth filter to all knock data
- Defines crank angle windows for single window, double window and variance intensity calculations
- Calculates knock intensities (using trapezoid function for integration)
- Exports a 5 dimensional array [cycle, channel, spark index, cylinder, head] of intensity data for each intensity calculation type
- Plots pressure and accelerometer raw and variance data

INTENSITY CALCULATIONS

Filter Settings

Order

Ratio

Single Window Method

TO

Double Window Method

TO

TO

CALCULATE

A. 2 – Intensity Program Front End

Source Code:

```
intfig=get(0,'currentfigure');
load 'c:\tempdata'

T='DEFININING WINDOWS...';
disp(T)

%DEFINE WINDOWS

singlewinstart=str2num(get(findobj(intfig,'Tag','hsinglewinstart'),'String'))
;
singlewinend=str2num(get(findobj(intfig,'Tag','hsinglewinend'),'String'));
noisewinstart=str2num(get(findobj(intfig,'Tag','hnoisewinstart'),'String'));
noisewinend=str2num(get(findobj(intfig,'Tag','hnoisewinend'),'String'));
doublewinstart=str2num(get(findobj(intfig,'Tag','hdoublewinstart'),'String'))
;
doublewinend=str2num(get(findobj(intfig,'Tag','hdoublewinend'),'String'));

%FILTER LONG WINDOW

clear chfilt chwin %single chwinnoise chwindouble

sws=floor((singlewinstart+90)/res+1);
swe=floor((singlewinend+90)/res);
nws=floor((noisewinstart+90)/res+1);
nwe=floor((noisewinend+90)/res);
dws=floor((doublewinstart+90)/res+1);
dwe=floor((doublewinend+90)/res);
nwsw=floor((-45+90)/res+1);
vws=floor((-5+90)/res+1);
vwe=floor((45+90)/res);

filtorder=get(findobj(intfig,'Tag','hfilterorder'),'Value');
filtratio=str2num(get(findobj(intfig,'Tag','hfiltratio'),'String'));
[b,a]=butter(filtorder,filtratio,'high');

T='FILTERING...';
disp(T)

prog=1*149/(numchan+1);

for i=1 : numchan
    prefilt(:, :, i)=chan(:, :, i)-repmat(mean(chan(:, :, i)), [reflength, 1]);
evalc(['chfilt(:, :, ', int2str(i), ')=filter(b, a, prefilt(:, :, ', int2str(i), ')'])
;
    prog=(1+i)*149/(numchan+1);
    %set(findobj(1,'Tag','intprog'),'Pos',[24 15 prog 9])
    %refresh
```

```

end

clear prefilt
chfilt=chfilt(floor(30/res):reflength, :, :);
chan=chan(floor(30/res):reflength, :, :);
t=t(floor(30/res):reflength);
[reflength dummy dummy]=size(chan);
T='CALCULATING INTENSITY...';
disp(T)

swin=chfilt(sws:swe, :, :);
nwin=chfilt(nws:nwe, :, :);
dwin=chfilt(dws:dwe, :, :);

%Variance (Running)
for k=1:numchan
    chrvar(:, :, k)=(chfilt(:, :, k)-
    repmat(mean(chfilt(:, :, k), 1), [reflength, 1])).^2;
    chvar(:, k)=(mean(chrvar(:, :, k), 2));
    intvarsig(k)=trapz(chvar(vws:vwe, k));
    intvarnoise(k)=trapz(chvar(1:vws, k));
    intvar(k)=intvarsig(k)/intvarnoise(k);
end

for i=1:numchan
    for m=1:ncycles
        ints(m, i)=trapz(swin(:, m, i).^2);
        pks(m, i)=max(swin(:, m, i));
        intn(m, i)=trapz(nwin(:, m, i).^2);
        pkn(m, i)=max(nwin(:, m, i));
        intd(m, i)=trapz(dwin(:, m, i).^2);
        pkd(m, i)=max(dwin(:, m, i));
    end
end
intdn=intd./intn;
pkdn=pkd./pkn;

%Statistics
[dummy maxindpks]=max(mean(pks, 2));
maxpks=pks(maxindpks, :);
[dummy maxindpkdn]=max(mean(pkdn, 2));
maxpkdn=pkdn(maxindpkdn);
medpks=median(mean(pks, 2));
medindpks=find(mean(pks, 2) > (medpks-0.0001) & mean(pks, 2) <
(medpks+0.0001));

[dummy minindpks]=min(mean(pks, 2));

T='EXPORTING DATA...';
disp(T)

```

```

[dummy flen]=size(file1);
[dummy plen]=size(path1);
sparktext=file1(flen-1:flen);
sparkind=str2num(sparktext);
speed=file1(flen-9:flen-8);

if file1(3)=='c'
    headend=2;
else
    headend=3;
end
head=str2num(file1(2:headend));

if speed == '10'
    savecycles=75;
elseif speed == '15'
    savecycles=115;
elseif speed == '25'
    savecycles=200;
elseif speed == '35'
    savecycles=280;
elseif speed == '45'
    savecycles == 360;
end

load(['c:\IntensityData\ints', speed]);
matints(:,1:numchan,sparkind,cyl,head)=ints(1:savecycles,:);
evalc(['save 'c:\IntensityData\ints', speed, '' matints']);

load(['c:\IntensityData\pks', speed]);
matpks(:,1:numchan,sparkind,cyl,head)=pks(1:savecycles,:);
evalc(['save 'c:\IntensityData\pks', speed, '' matpks']);

load(['c:\IntensityData\intdn', speed]);
matintdn(:,1:numchan,sparkind,cyl,head)=intdn(1:savecycles,:);
evalc(['save 'c:\IntensityData\intdn', speed, '' matintdn']);

load(['c:\IntensityData\pkdn', speed]);
matpkdn(:,1:numchan,sparkind,cyl,head)=pkdn(1:savecycles,:);
evalc(['save 'c:\IntensityData\pkdn', speed, '' matpkdn']);

load(['c:\IntensityData\intv', speed]);
matintv(1:numchan,sparkind,cyl,head)=intv;
evalc(['save 'c:\IntensityData\intv', speed, '' matintv']);

T='PROCESSING COMPLETE...';
disp(T)

sound(wavread('c:\tada.wav'),22050,16)

tagind=1;
pcyc=maxindpks;
figname='Maximum Peak Cycle';
figfilename1=cat(2,'c:\Figures\Raw\',file1(1:(2+headend)),'_',speed,'_',spark
text);

```

```

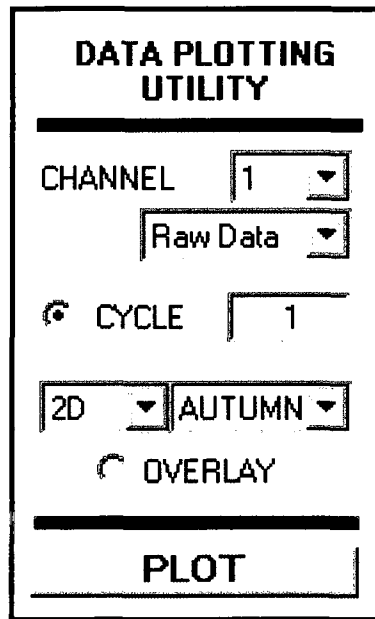
plotform
saveas(gcf,figfilename1,'tif');
figfilename2=cat(2,'c:\Figures\Variance\',file1(1:(2+headend)),'_',speed,'_',
sparktext);
plotformvar
saveas(gcf,figfilename2,'tif');

runplot
close(intfig)

```

A.3 Supplemental Plotting Program

This program is utilized for observation of data not plotted in the standard format.



A. 3 - Data Plotting Front End

Source Code:

```

overlay=get(findobj(gcf,'Tag','hoverlay'),'Value');
singlecolor={'k';'r';'b';'g';'c';'m';'y'};
%plot(chan(:,1,1),char(singlecolor(2)))
if overlay==1
    scolorind=scolorind+1;
    if scolorind > 6
        scolorind=1;
    end
end

```

```

    end
    figure(findobj('Tag',temptag))
else
    scolorind=1
    tagind=tagind+1;
    temptag=int2str(tagind);
    figure('Tag',temptag)
    hold
end

plotchan=get(findobj(gcf,'Tag','hplotchan'),'Value');
indivcycle=get(findobj(gcf,'Tag','hindivcycle'),'Value');
plotcycle=str2num(get(findobj(gcf,'Tag','hplotcycle'),'String'));
datatype=get(findobj(gcf,'Tag','hdatatype'),'Value');
plottype=get(findobj(gcf,'Tag','hplottype'),'Value');
cval=get(findobj(gcf,'Tag','hplotcolor'),'Value');
cstr=get(findobj(gcf,'Tag','hplotcolor'),'String');

if datatype==1
    if indivcycle ==1
        plot(t,chan(:,plotcycle,plotchan),char(singlecolor(scolorind)))
    else
        if plottype ==1
            plot(t,chan(:, :, plotchan))
        else
            mesh(1:ncycles,t,chan(:, :, plotchan))
        end
    end
elseif datatype == 2
    if indivcycle ==1
        plot(t,chfilt(:,plotcycle,plotchan),char(singlecolor(scolorind)))
    else
        if plottype ==1
            plot(t,chfilt(:, :, plotchan))
        else
            mesh(1:ncycles,t,chfilt(:, :, plotchan))
        end
    end
elseif datatype == 3
    set(findobj(gcf,'Tag','hplotcycle'),'Visible','off')
    if indivcycle ==1 %indicating mean in this case
        plot(t,chvar(:,plotchan),char(singlecolor(scolorind)))
    else
        if plottype ==1
            plot(t,chrvar(:, :, plotchan))
        else
            mesh(1:ncycles,t,chrvar(:, :, plotchan))
        end
    end
end
end

%Formatting

if plottype==1
    set(gca,'XLim',[-90 90],'XTick',(-90:15:90),'FontSize',8)

```



```

XLabel('Relative Crank Angle (deg)')
if plotchan==10
    YLabel('Pressure (kPa)')
else
    YLabel('Acceleration (m/s^2)')
end
else
    view(115,14)
    grid on
    colormap(cstr{cval})
end
end

```

A.4 MTS Calculations

The MTS program completes the following tasks (Shown here only for IntS):

- Imports intensity data
- Classifies data as knocking or non-knocking based on the intensity of the pressure channel
- Creates baseline based on good (non-knocking) data
- Based on bad sample, completes Taguchi signal to noise ratio analysis and Main effects analysis to determine which channels exhibit main effects for each cylinder
- Generates an accelerometer usage array based on the result of main effects analysis
- Calculated Mahalanobis Distance for complete sample, utilizing only those accelerometers listed in the usage array for each cylinder
- Exports intensity, Mahalanobis Distance and usage arrays as well as results of signal to noise ratio analysis and main effects analysis

Source Code:

```

speedarray=get(findobj(gcf,'Tag','hspeed'),'String');
speedval=get(findobj(gcf,'Tag','hspeed'),'Value');
speed=char(speedarray(speedval))
if speed == '10'

```

```

    load('c:\IntensityData\ints10')
    usedheads=[2 3 5 6 7 8 9 10 12 14 15];
    goodthresh=50;
    badthresh=50;
elseif speed == '15'
    load('c:\IntensityData\ints15')
    usedheads=[2 3 5 6 7 8 10 11 12 14 15];
    goodthresh=50;
    badthresh=50;
elseif speed == '25'
    load('c:\IntensityData\ints25')
    usedheads=[2 3 5 6 7 8 9 10 11 12 14 15];
    goodthresh=50;
    badthresh=50;
elseif speed == '35'
    load('c:\IntensityData\ints35')
    usedheads=[2 3 5 6 7 8 9 10 11 12 14 15];
    goodthresh=50;
    badthresh=50;
elseif speed == '45'
    load('c:\IntensityData\ints45')
    usedheads=[2 3 5 6 7 8 9 10 11 12 14 15];
    goodthresh=50;
    badthresh=50;
end
[dummy heads]=size(usedheads);

%%%BY MEAN

totalsample=squeeze(mean(matints,1));

%%%good/bad ind2d to be used at end result to evaluate MD and int (gives BL
in format of final result)
totalsample=squeeze(mean(matints,1));
%rearrange totalsample to [samples x 8cyls x 10chans]
samplesize=10*heads;
sample=permute(reshape(permute(totalsample(1:10,:,:),usedheads),[1 3 2 4]),[10
8 samplesize]),[3 2 1]);
for cyl=1:8
    k=1;
    kk=1;
    for i=1:samplesize
        if sample(i,cyl,10)>0
            if sample(i,cyl,10)<goodthresh
                goodind2d(k,cyl)=i;
                k=k+1;
            else
                badind2d(kk,cyl)=i;
                kk=kk+1;
            end
        end
    end
end
end
end
end

```

```

%goodind same as goodind2d, but not separated by cylinder (good sample groups
all heads and cyls together)
samplesize=10*8*heads;
sample=(reshape(totalsample(1:10, :, :, usedheads), [10, samplesize]))';
k=1;
for i=1:samplesize
    if sample(i,10)<goodthresh & sample(i,10)>0 %GOOD ESTIMATE (BASED ON CYL
PRES INTS)
        goodind(k)=i;
        k=k+1;
    end
end

sample=sample(goodind,1:9);
[samplesize dummy]=size(sample);

m=mean(sample);
rm= repmat(m, [samplesize, 1]);
s=std(sample);
rs= repmat(s, [samplesize, 1]);
normsample=(sample-rm)./rs;
covmat=cov(normsample);
invcov=inv(covmat);
mdspace=normsample*invcov*normsample'/9;
for i=1:samplesize
    md(i)=mdspace(i,i);
end

%bad

orth=[1 1 1 1 1 1 1 1 1 1 1;1 1 1 1 1 2 2 2 2 2 2;1 1 2 2 2 1 1 1 2 2 2;1 2 1
2 2 1 2 2 1 1 2;1 2 2 1 2 2 1 2 1 2 1;1 2 2 2 1 2 2 1 2 1 1;2 1 2 2 1 1 2 2 1
2 1;2 1 2 1 2 2 2 1 1 1 2;2 1 1 2 2 2 1 2 2 1 1 ;2 2 2 1 1 1 1 2 2 1 2;2 2 1
2 1 2 1 1 1 2 2;2 2 1 1 2 1 2 1 2 2 1];
orth9=orth(:,1:9);

clear cpsample cmdsample
csnsamplesize=10*heads; %indiv cylinder SNR sample
for cyl=1:8

csnsample=(reshape(totalsample(1:10, :, cyl, usedheads), [10, csnsamplesize]))';
clear badind
k=1;
for i=1:csnsamplesize
    if csnsample(i,10)>badthresh%CONSERVATIVE BAD ESTIMATE
        badind(k)=i;
        k=k+1;
    end
end

[dummy csamplesize(cyl)]=size(badind);
cmdsample(1:csamplesize(cyl), :, cyl)=csnsample(badind,1:9);
cpsample(1:csamplesize(cyl), :, cyl)=csnsample(badind,10);

for i=1:12

```

```

clear used mdsnsample mdsnspace normsns mdsnspace mdsn snrind

k=1;
for j=1:9
    if orth9(i,j)==1
        used(k)=j;
        k=k+1;
    end
end
[dummy sizeused]=size(used);

%recalculate for used variables from orthogonal array(still based on
good)
m=mean(sample(:,used));
rm= repmat(m, [samplesize,1]);
s=std(sample(:,used));
rs= repmat(s, [samplesize,1]);
normsample=(sample(:,used)-rm)./rs;
covmat=cov(normsample);
invcov=inv(covmat);

mdsnsample=reshape(nonzeros(cmdsample(:,used,cyl)), [csamplesize(cyl)
sizeused]);

[dummy mdsnspace]=size(used);

for p=1:csamplesize(cyl)
    normsns(p,:)=(mdsnsample(p,:)-m)./s;
end

mdsnspace=normsns*invcov*normsns'/mdsnspace;

for p=1:csamplesize(cyl)
    mdsn(p)=double(mdsnspace(p,p));
    snrind(p)=double(1/(mdsn(p)^2));
end
MDbefore(i,1:csamplesize(cyl),cyl)=mdsn;
SNR(i,cyl)=-10*log10(sum(snrind)/csamplesize(cyl));

end

for i=1:9

clear L1 L2

k=1;
kk=1;
for j=1:12
    if orth9(j,i)==1
        L1(k)=j;
        k=k+1;
    else
        L2(kk)=j;
        kk=kk+1;
    end
end
end

```

```

        ME(i,cyl)=sum(SNR(L1,cyl))-sum(SNR(L2,cyl));
    end

end

%use only positive main effects

for cyl=1:8
    k=1;
    for i=1:9
        if ME(i,cyl)>0
            usedarray(k,cyl)=i;
            k=k+1;
        end
    end
end

%recalculate improved (based on only positive effects) ON BAD SAMPLE
for cyl=1:8

    clear used mdsnsample mdsnsize norms n mdsnspace mdsn snrind

    used=nonzeros(usedarray(:,cyl))';
    [dummy sizeused]=size(used);

    %recalculate for used variables from orthogonal array(still based on good)
    m=mean(sample(:,used));
    rm=repmat(m,[samplesize,1]);
    s=std(sample(:,used));
    rs=repmat(s,[samplesize,1]);
    normsample=(sample(:,used)-rm)./rs;
    covmat=cov(normsample);
    invcov=inv(covmat);

    mdsnsample=reshape(nonzeros(cmdsample(:,used,cyl)),[csamplesize(cyl)
sizeused]);

    [dummy mdsnsize]=size(used);

    for p=1:csamplesize(cyl)
        norms n(p,:)=(mdsnsample(p,:)-m)./s;
    end

    mdsnspace=norms n*invcov*norms n'/mdsnsize;

    for p=1:csamplesize(cyl)
        mdsn(p)=double(mdsnspace(p,p));
        snrind(p)=double(1/(mdsn(p)^2));
    end
end

```

```

MDafter7(1:csamplesize(cyl),cyl)=mdsn';
SNRafter7(cyl)=-10*log10(sum(snrind)/csamplesize(cyl));

end

%recalculate improved (based on only positive effects)for WHOLE SAMPLE

clear cmdsample cpsample csamplesize csample

for cyl=1:8

    clear mdsnsample mdsnsize norms n mdsn space mdsn snrind

    csamplesize=10*1*heads;

    csample(:, :, cyl)=(reshape(totalsample(1:10, 1:10, cyl, usedheads), [10, csamplesize]))';
    cmdsample(:, :, cyl)=csample(:, 1:9, cyl);
    cpsample(:, cyl)=csample(:, 10, cyl);

    clear used

    used=nonzeros(usedarray(:, cyl))';

    %recalculate for used variables(still based on good)
    m=mean(sample(:, used));
    rm=repmat(m, [samplesize, 1]);
    s=std(sample(:, used));
    rs=repmat(s, [samplesize, 1]);
    norms=sample(:, used)-rm)./rs;
    covmat=cov(norms);
    invcov=inv(covmat);

    mdsnsample=cmdsample(:, used, cyl);
    [dummy mdsnsize]=size(used);

    for p=1:csamplesize
        norms(p, :)=(mdsnsample(p, :)-m)./s;
    end

    mdsn space=norms*invcov*norms'/mdsnsize;

    for p=1:csamplesize
        mdsn(p)=double(mdsn space(p, p));
        snrind(p)=double(1/(mdsn(p)^2));
    end
    MDafter(:, cyl)=mdsn';
    SNRafter(cyl)=-10*log10(sum(snrind)/csamplesize);

end

```

```

%calculate knocking to non-knocking ratios of MD and int magnitudes
for cyl=1:8

    baseMD=mean(MDafter(nonzeros(goodind2d(:,cyl)),cyl));
    knockMD=mean(MDafter(nonzeros(badind2d(:,cyl)),cyl));
    snrMD(cyl)=knockMD/baseMD;

    basePint=mean(cpsample(nonzeros(goodind2d(:,cyl)),cyl));
    knockPint=mean(cpsample(nonzeros(badind2d(:,cyl)),cyl));
    snrPint(cyl)=knockPint/basePint;

    baseint=mean(cmdsample(nonzeros(goodind2d(:,cyl)),:,cyl));
    knockint=mean(cmdsample(nonzeros(badind2d(:,cyl)),:,cyl));
    snrint(:,cyl)=(knockint./baseint)';

end

snrintMD=snrint;
snrintMD(10,:)=snrPint;
snrintMD(11,:)=snrMD;

outputintMD=cmdsample;
outputintMD(:,10,:)=cpsample;
outputintMD(:,11,:)=MDafter;

wklwrite('c:\ME',ME)
wklwrite('c:\SNR',SNR)
wklwrite('c:\usedarray',usedarray)
wklwrite('c:\snrintMD',snrintMD)
wklwrite('c:\gdind',goodind2d)
wklwrite('c:\intMD_c1',outputintMD(:, :, 1))
wklwrite('c:\intMD_c2',outputintMD(:, :, 2))
wklwrite('c:\intMD_c3',outputintMD(:, :, 3))
wklwrite('c:\intMD_c4',outputintMD(:, :, 4))
wklwrite('c:\intMD_c5',outputintMD(:, :, 5))
wklwrite('c:\intMD_c6',outputintMD(:, :, 6))
wklwrite('c:\intMD_c7',outputintMD(:, :, 7))
wklwrite('c:\intMD_c8',outputintMD(:, :, 8))

```

APPENDIX B
SUPPLEMENTAL DATA – TRANSDUCER VALIDATION

FIGURES

B.1 Pressure Traces 1000 RPM / PT 163

a. 6123 Offset / 6117 (Cyl #6)	161
b. 6123 Offset / 6117 (Cyl #7)	161
c. 6123 Offset / AutoPSI Central (Cyl #6)	162
d. 6123 Offset / AutoPSI Central (Cyl #6)	162
e. 6125 Central / 6123 Offset (Cyl #2)	163
f. 6125 Central / 6123 Offset (Cyl #3)	163
g. 6125 Offset / 6123 Central (Cyl #6)	164
h. 6125 Offset / 6123 Central (Cyl #7)	164
i. 6125 Central / 6117 (Cyl #2)	165
j. 6125 Central / 6117 (Cyl #3)	165
k. 6125 Offset / 6117 (Cyl #6)	166
l. 6125 Offset / 6117 (Cyl #7)	166

B.2 Pressure Traces 1000 RPM / WOT **167**

a. 6123 Offset / 6117 (Cyl #6)	167
b. 6123 Offset / 6117 (Cyl #7)	167
c. 6123 Offset / AutoPSI Central (Cyl #6)	168
d. 6123 Offset / AutoPSI Central (Cyl #6)	168
e. 6125 Central / 6123 Offset (Cyl #2)	169
f. 6125 Central / 6123 Offset (Cyl #3)	169
g. 6125 Offset / 6123 Central (Cyl #6)	170
h. 6125 Offset / 6123 Central (Cyl #7)	170
i. 6125 Central / 6117 (Cyl #2)	171
j. 6125 Central / 6117 (Cyl #3)	171
k. 6125 Offset / 6117 (Cyl #6)	172

l. 6125 Offset / 6117 (Cyl #7)	172
--------------------------------	-----

B.3 Pressure Traces 2500 RPM / PT 175

a. 6123 Offset / 6117 (Cyl #6)	173
b. 6123 Offset / 6117 (Cyl #7)	173
c. 6123 Offset / AutoPSI Central (Cyl #6)	174
d. 6123 Offset / AutoPSI Central (Cyl #6)	174
e. 6125 Central / 6123 Offset (Cyl #2)	175
f. 6125 Central / 6123 Offset (Cyl #3)	175
g. 6125 Offset / 6123 Central (Cyl #6)	176
h. 6125 Offset / 6123 Central (Cyl #7)	176
i. 6125 Central / 6117 (Cyl #2)	177
j. 6125 Central / 6117 (Cyl #3)	177
k. 6125 Offset / 6117 (Cyl #6)	178
l. 6125 Offset / 6117 (Cyl #7)	178

B.4 Pressure Traces 2500 RPM / WOT 181

a. 6123 Offset / 6117 (Cyl #6)	179
b. 6123 Offset / 6117 (Cyl #7)	179
c. 6123 Offset / AutoPSI Central (Cyl #6)	180
d. 6123 Offset / AutoPSI Central (Cyl #6)	180
e. 6125 Central / 6123 Offset (Cyl #2)	181
f. 6125 Central / 6123 Offset (Cyl #3)	181
g. 6125 Offset / 6123 Central (Cyl #6)	182
h. 6125 Offset / 6123 Central (Cyl #7)	182
i. 6125 Central / 6117 (Cyl #2)	183
j. 6125 Central / 6117 (Cyl #3)	183
k. 6125 Offset / 6117 (Cyl #6)	184
l. 6125 Offset / 6117 (Cyl #7)	184

B.5 Pressure Traces 4500 RPM / PT 187

a. 6123 Offset / 6117 (Cyl #6)	185
b. 6123 Offset / 6117 (Cyl #7)	185
c. 6123 Offset / AutoPSI Central (Cyl #6)	186
d. 6123 Offset / AutoPSI Central (Cyl #6)	186
e. 6125 Central / 6123 Offset (Cyl #2)	187
f. 6125 Central / 6123 Offset (Cyl #3)	187
g. 6125 Offset / 6123 Central (Cyl #6)	188
h. 6125 Offset / 6123 Central (Cyl #7)	188
i. 6125 Central / 6117 (Cyl #2)	189
j. 6125 Central / 6117 (Cyl #3)	189
k. 6125 Offset / 6117 (Cyl #6)	190
l. 6125 Offset / 6117 (Cyl #7)	190

B.6 Pressure Traces 4500 RPM / WOT 191

a. 6123 Offset / 6117 (Cyl #6)	191
b. 6123 Offset / 6117 (Cyl #7)	191
c. 6123 Offset / AutoPSI Central (Cyl #6)	192
d. 6123 Offset / AutoPSI Central (Cyl #6)	192
e. 6125 Central / 6123 Offset (Cyl #2)	193
f. 6125 Central / 6123 Offset (Cyl #3)	193
g. 6125 Offset / 6123 Central (Cyl #6)	194
h. 6125 Offset / 6123 Central (Cyl #7)	194
i. 6125 Central / 6117 (Cyl #2)	195
j. 6125 Central / 6117 (Cyl #3)	195
k. 6125 Offset / 6117 (Cyl #6)	196
l. 6125 Offset / 6117 (Cyl #7)	196

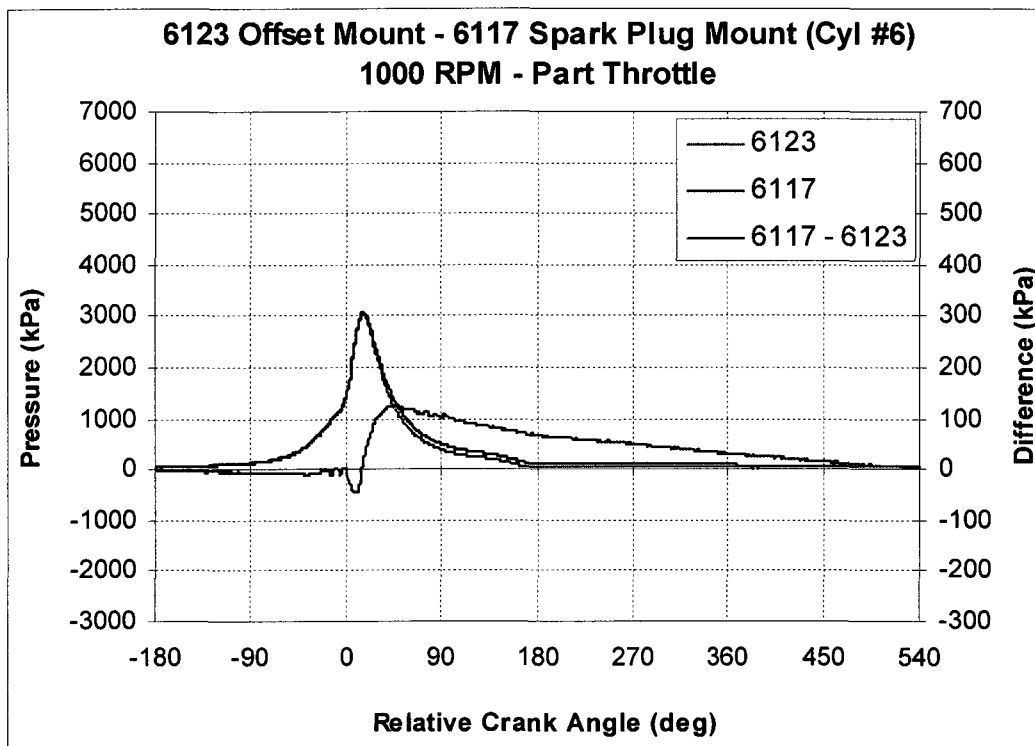


Figure B.1 a – Pressure Traces – 6123 Offset / 6117 (Cyl #6) – 1000 RPM / PT

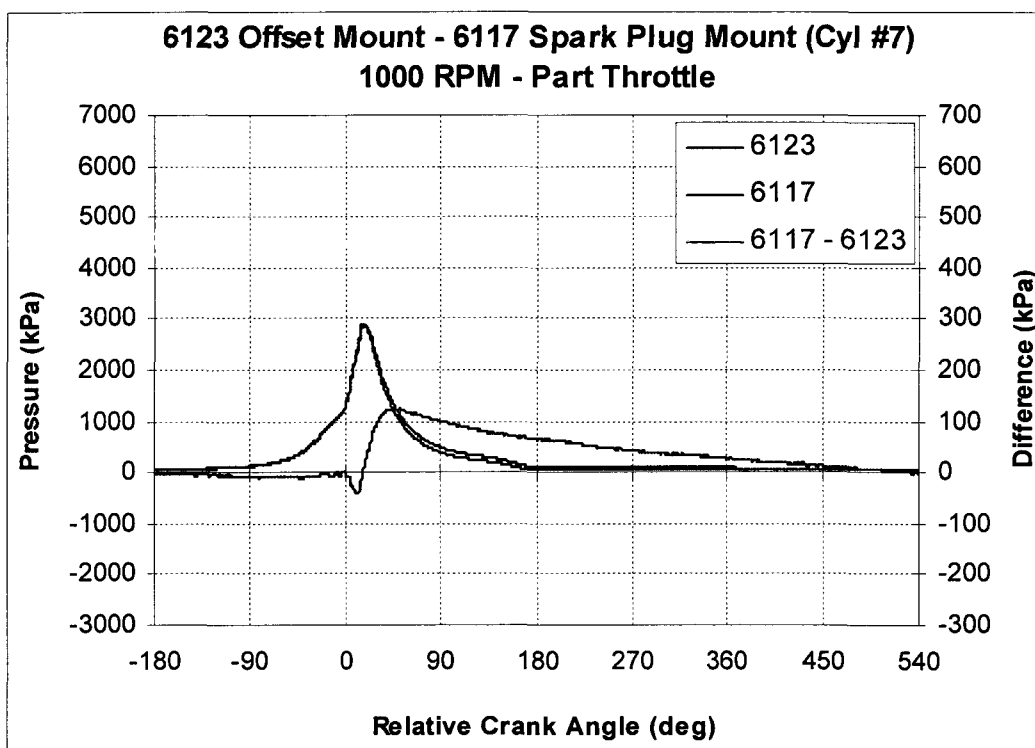


Figure B.1 b – Pressure Traces - 6123 Offset / 6117 (Cyl #7) – 1000 RPM / PT

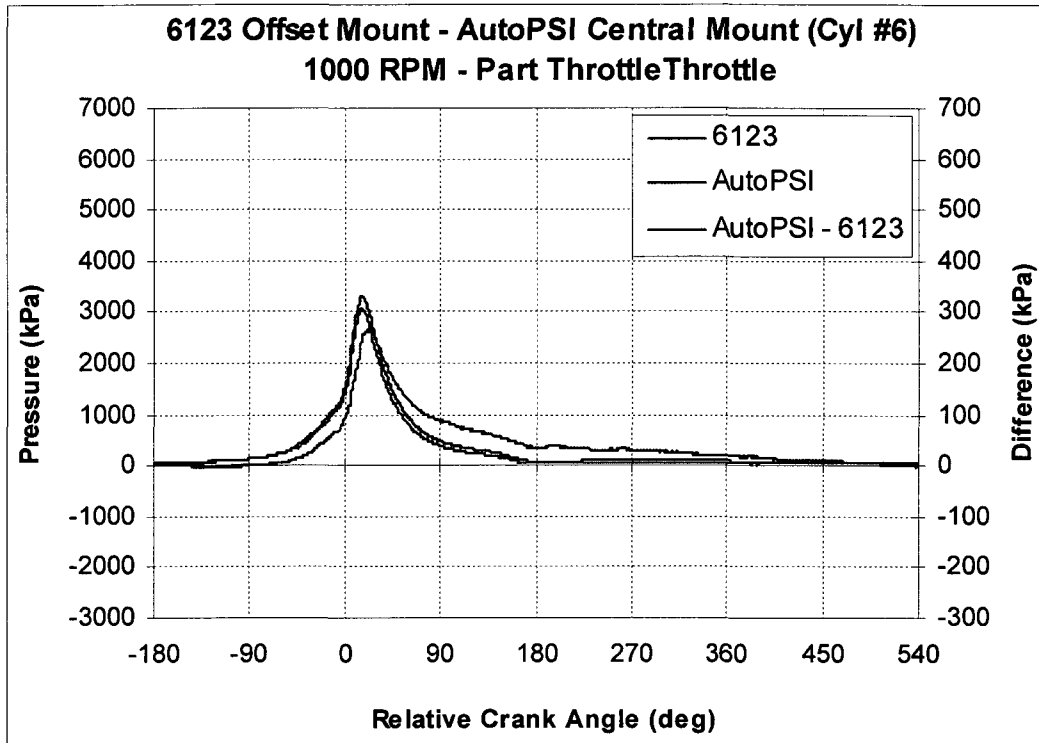


Figure B.1 c – Pressure Traces - 6123 Offset / AutoPSI Central (Cyl #6) – 1000 RPM / PT

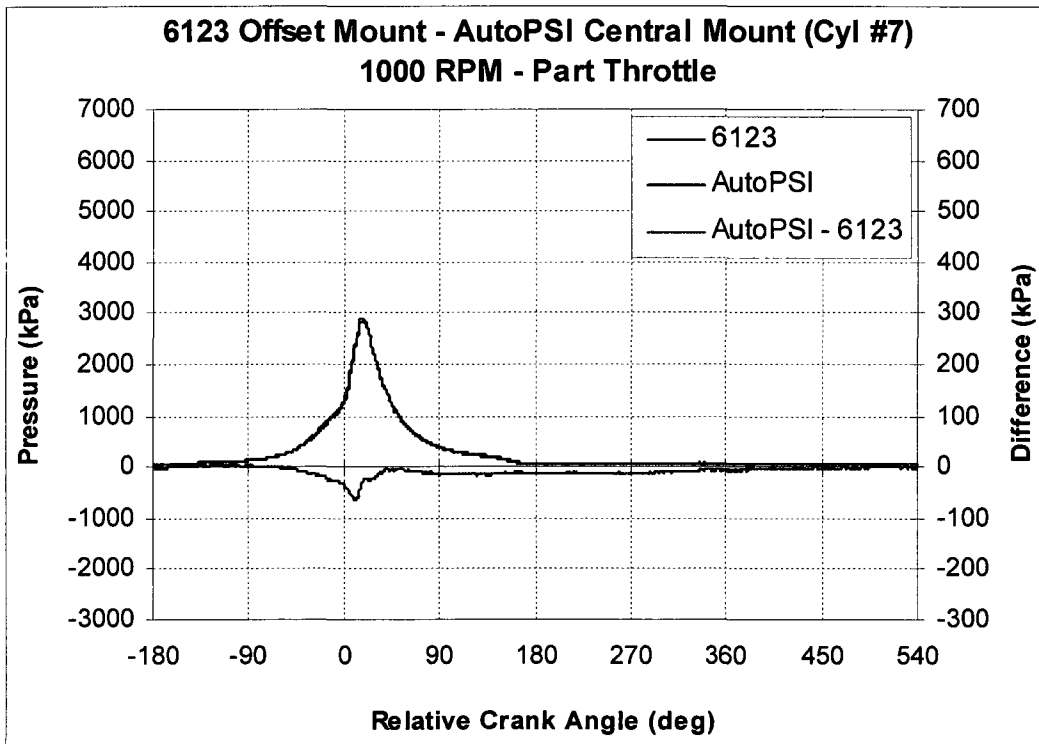


Figure B.1 d – Pressure Traces - 6123 Offset / AutoPSI Central (Cyl #6) – 1000 RPM / PT

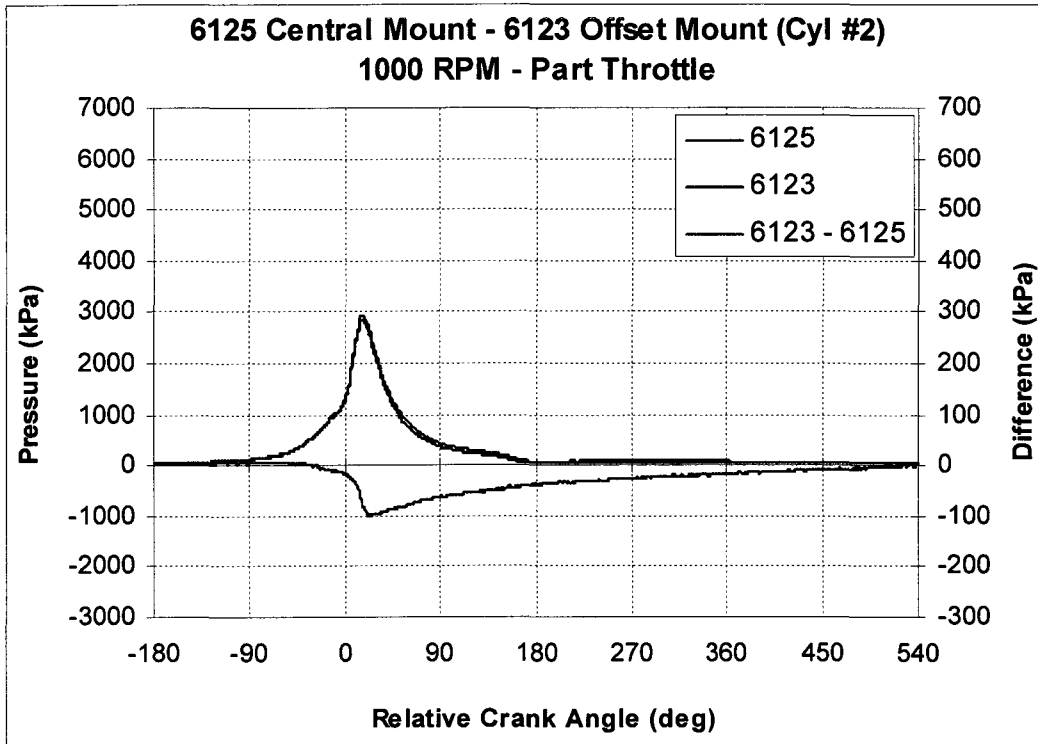


Figure B.1 e – Pressure Traces – 6125 Central / 6123 Offset (Cyl #2) – 1000 RPM / PT

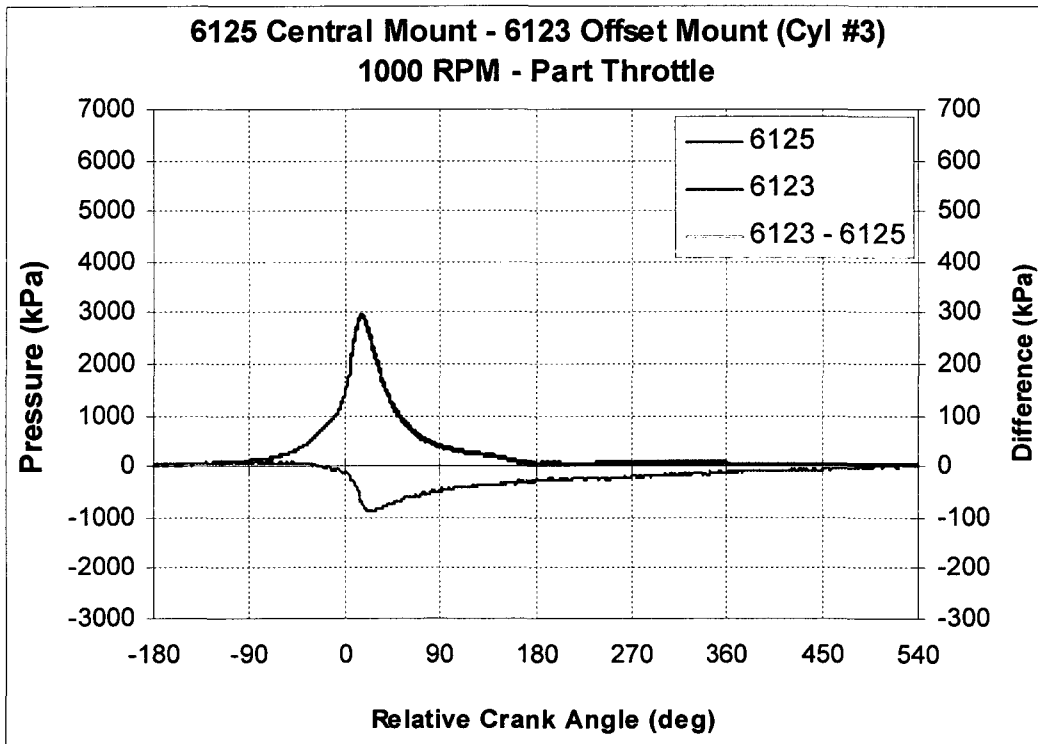


Figure B.1 f – Pressure Traces – 6125 Central / 6123 Offset (Cyl #3) – 1000 RPM / PT

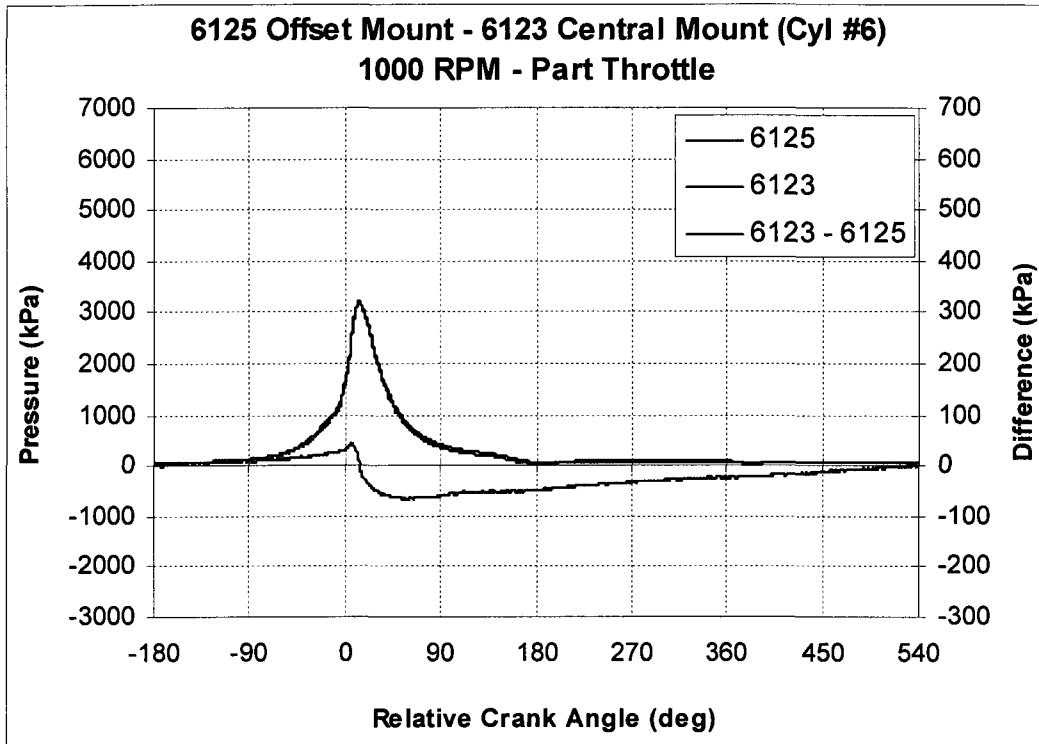


Figure B.1 g – Pressure Traces – 6125 Offset / 6123 Central (Cyl #6) – 1000 RPM / PT

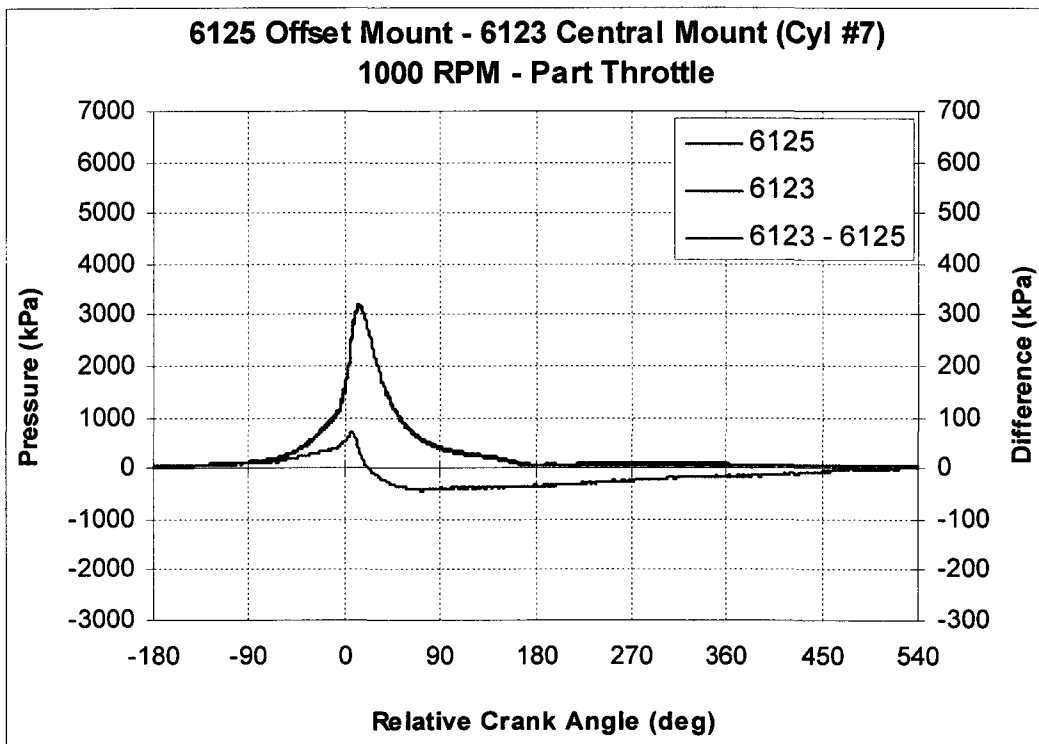


Figure B.1 h – Pressure Traces – 6125 Offset / 6123 Central (Cyl #7) – 1000 RPM / PT

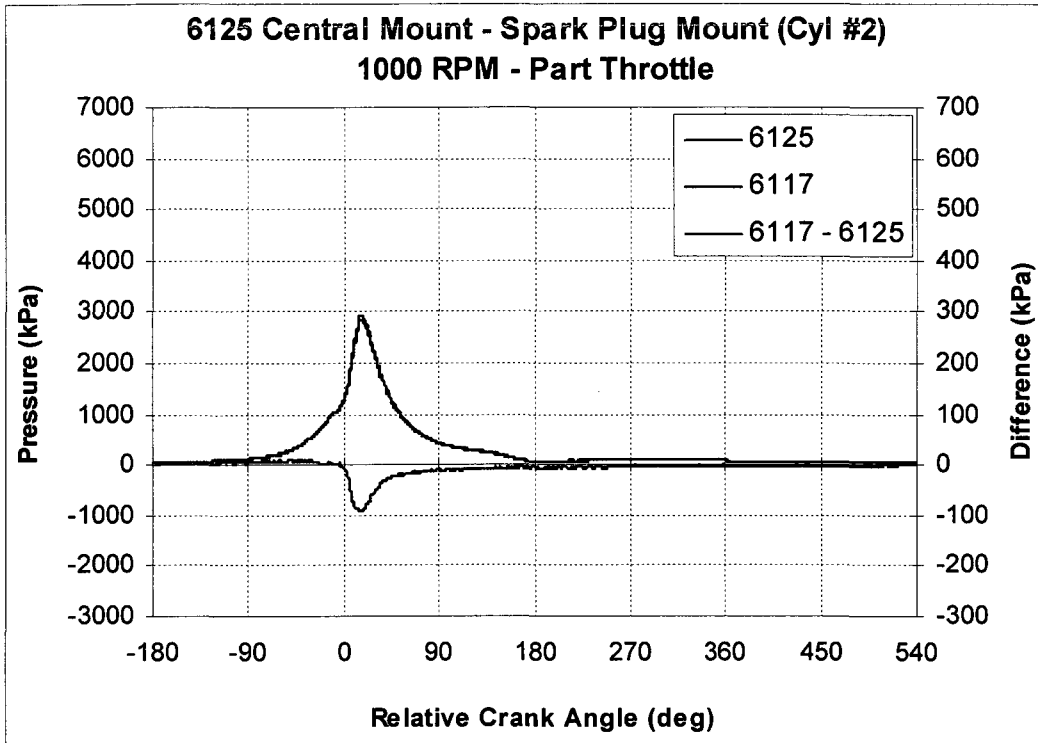


Figure B.1 i – Pressure Traces – 6125 Central / 6117 (Cyl #2) – 1000 RPM / PT

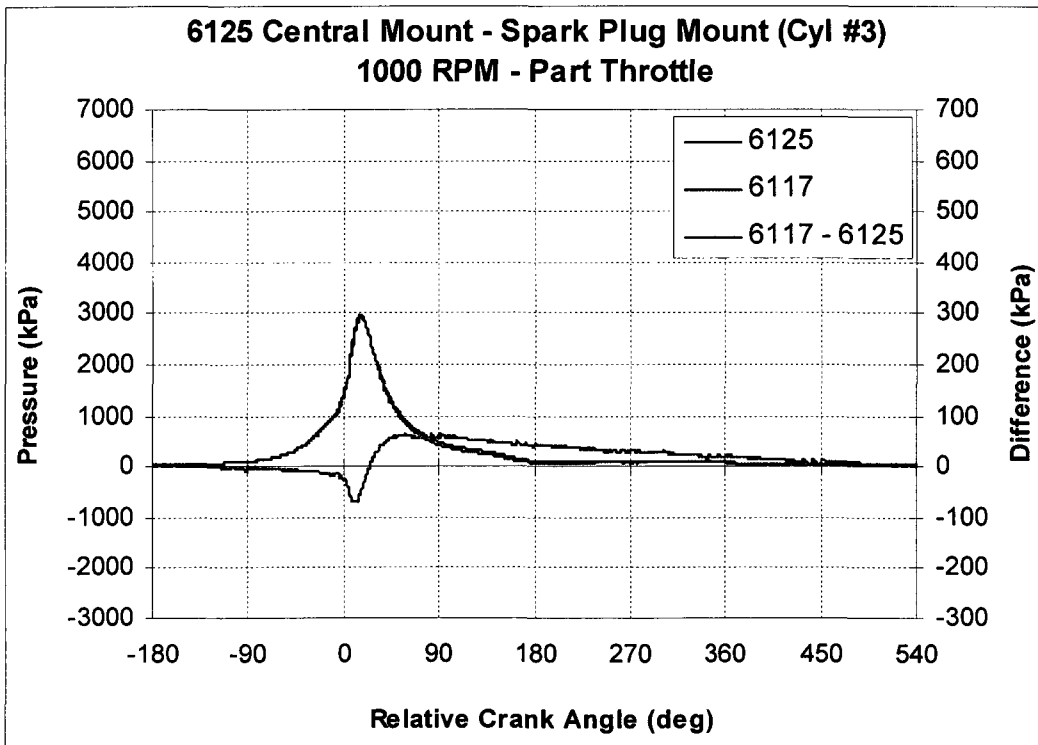


Figure B.1 j – Pressure Traces – 6125 Central / 6117 (Cyl #3) – 1000 RPM / PT

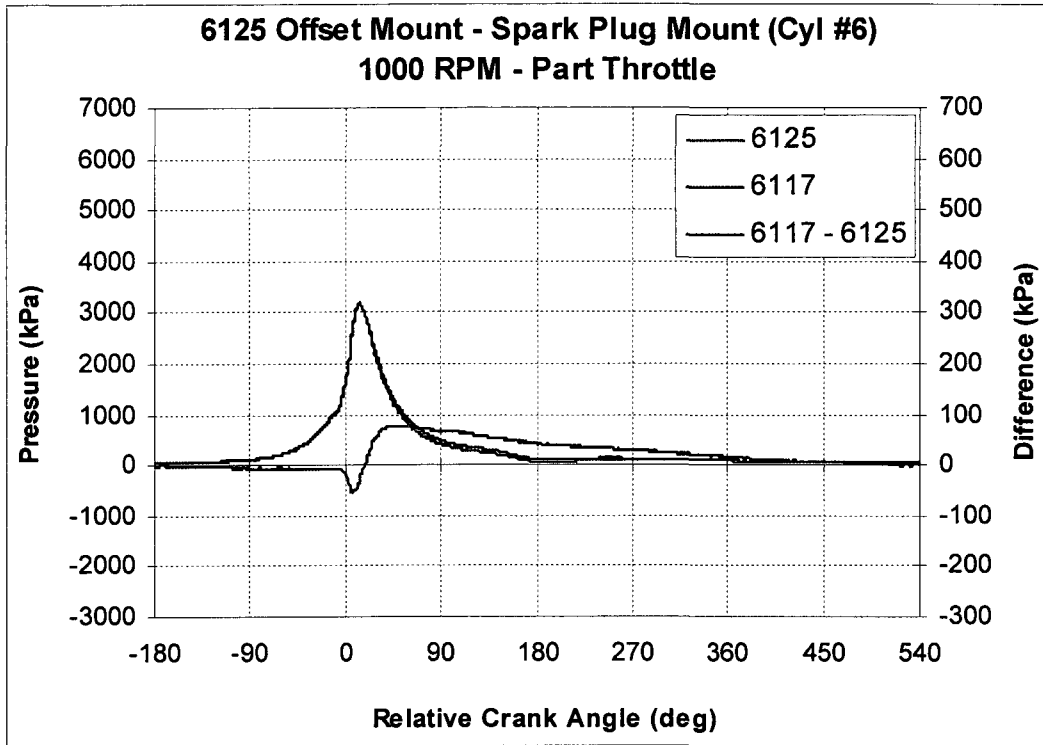


Figure B.1 k – Pressure Traces – 6125 Offset / 6117 (Cyl #6) – 1000 RPM / PT

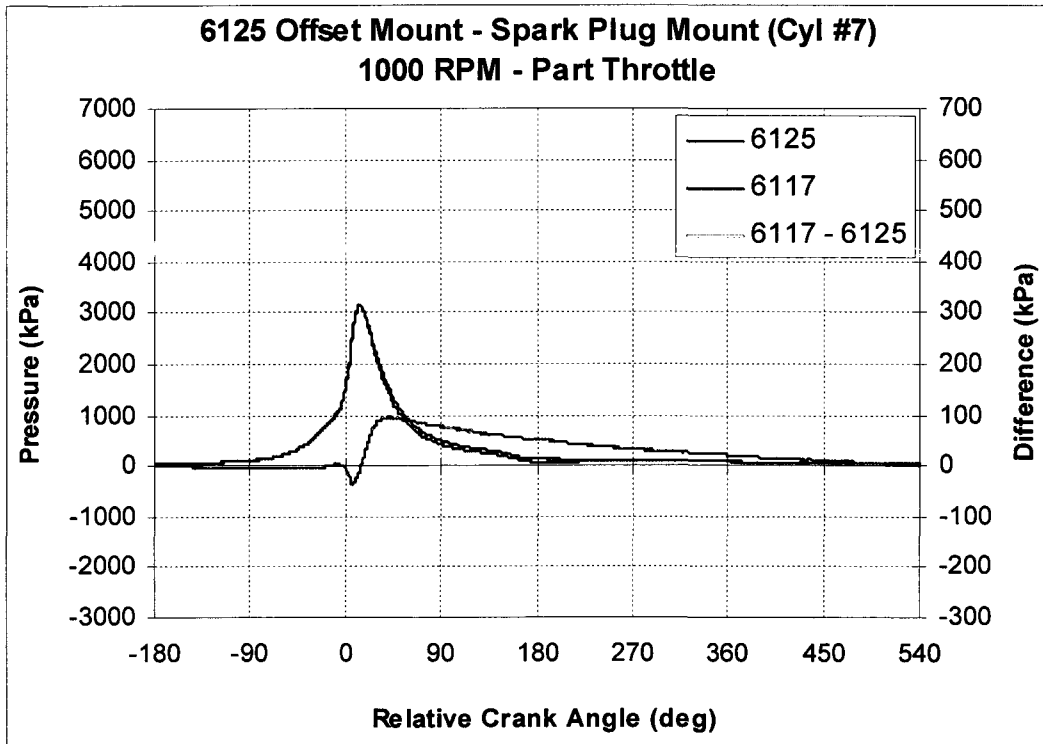


Figure B.1 l – Pressure Traces – 6125 Offset / 6117 (Cyl #7) – 1000 RPM / PT

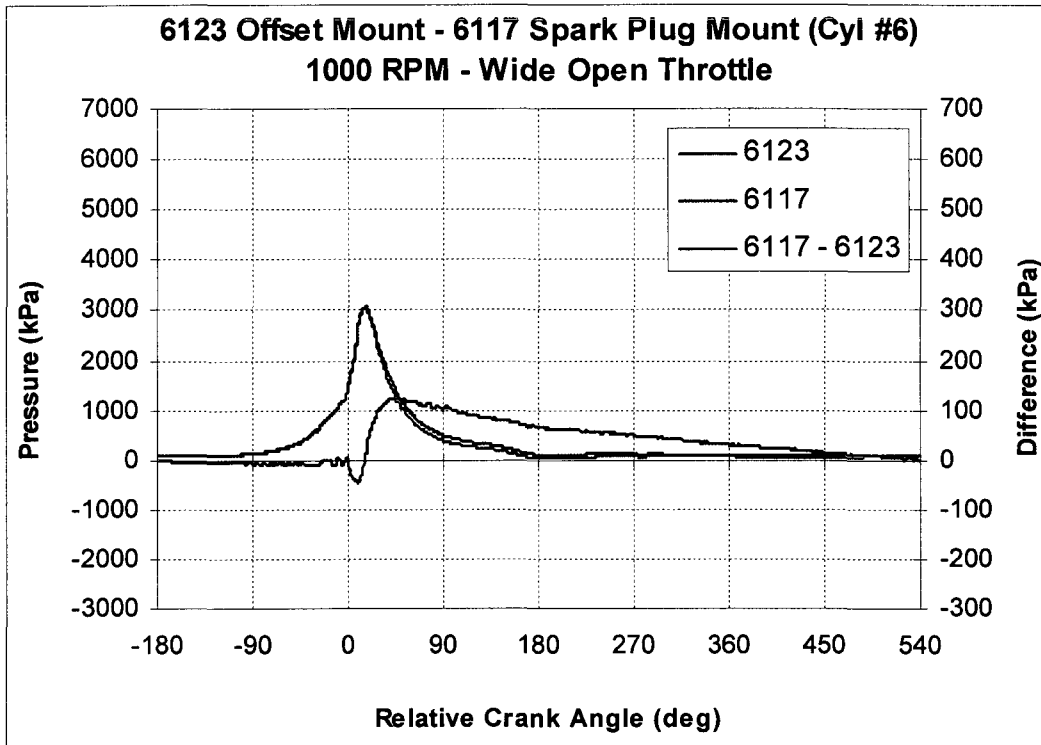


Figure B.2 a – Pressure Traces - 6123 / 6117 (Cyl #6) – 1000 RPM / WOT

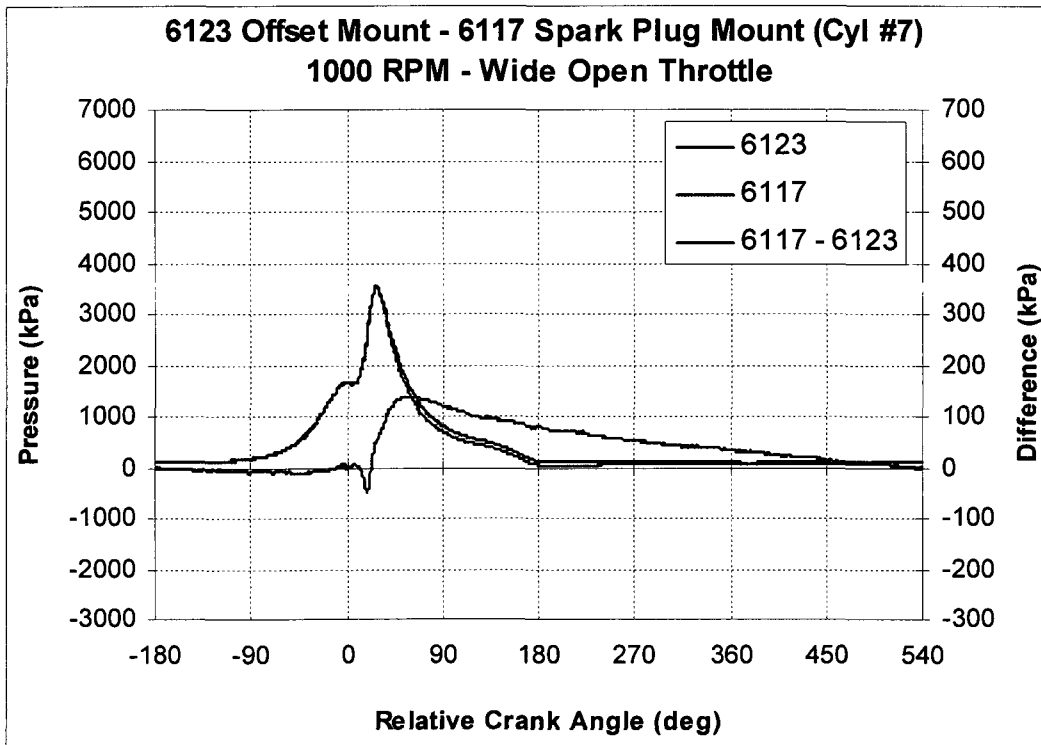


Figure B.2 b – Pressure Traces - 6123 Offset / 6117 (Cyl #7) – 1000 RPM / WOT

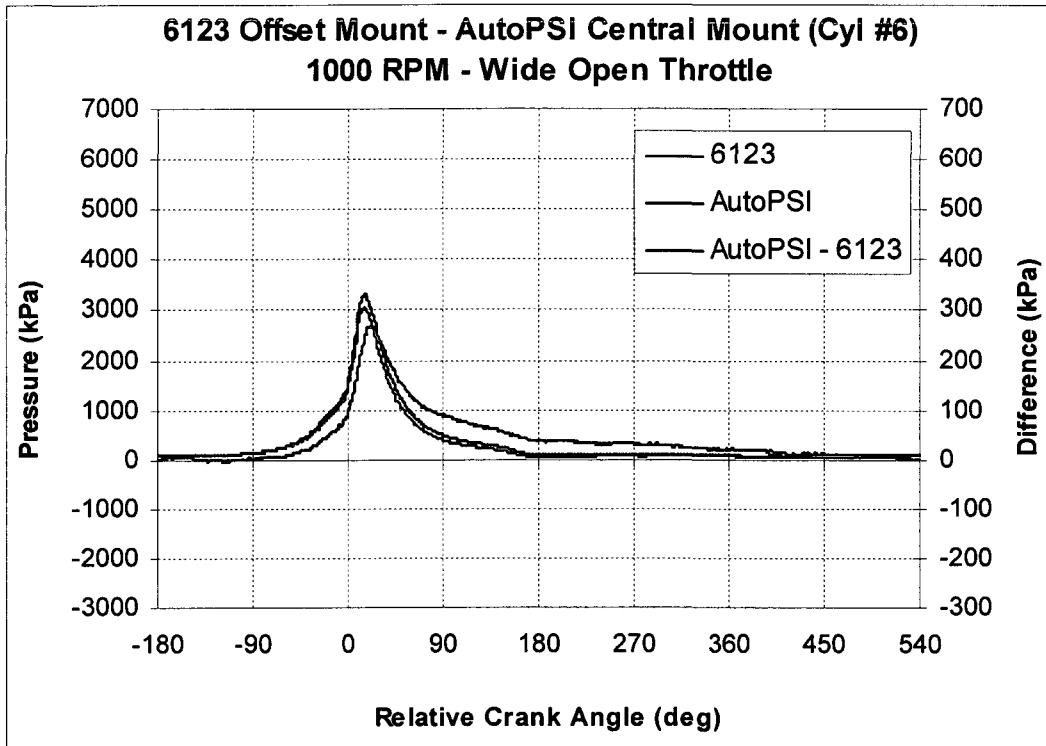


Figure B.2 c – Pressure Traces – 6123 Offset / AutoPSI Central (Cyl #6) – 1000 RPM / WOT

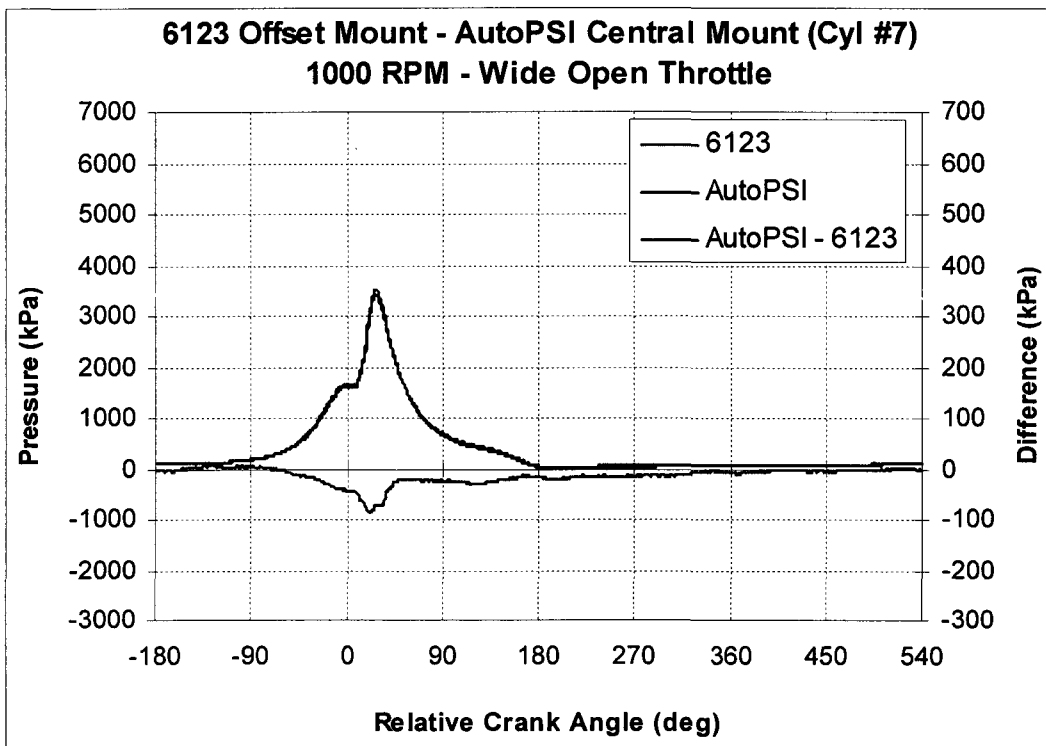


Figure B.2 d – Pressure Traces – 6123 Offset / AutoPSI Central (Cyl #7) – 1000 RPM / WOT

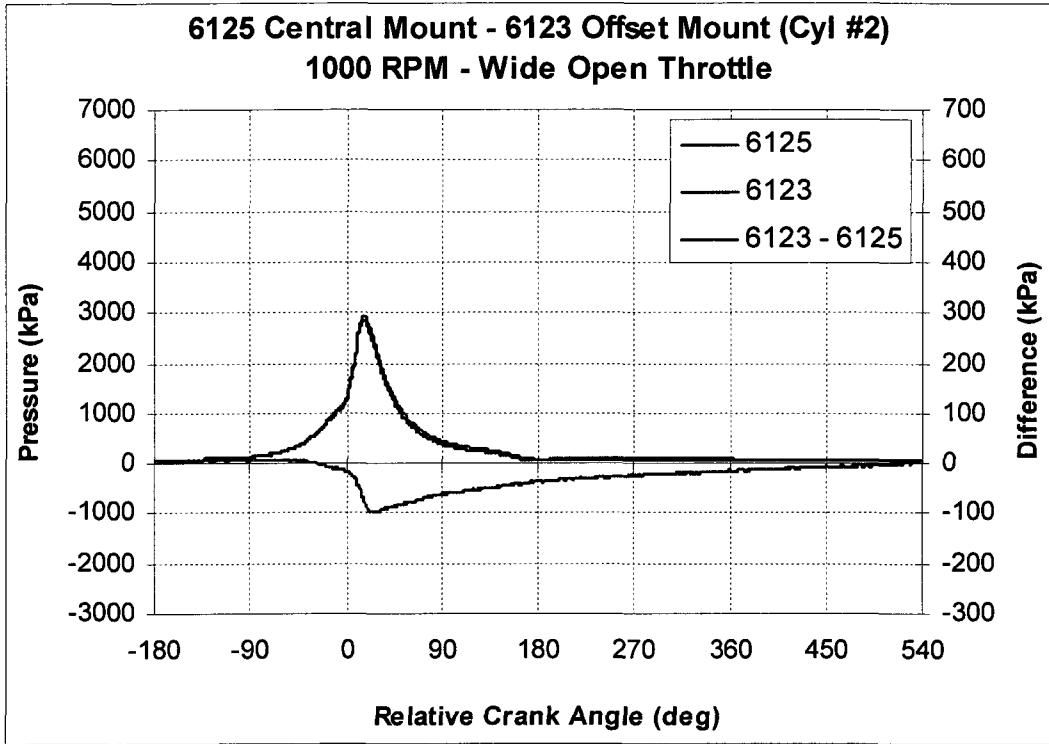


Figure B.2 e – Pressure Traces – 6125 Central / 6123 Offset (Cyl #2) – 1000 RPM / WOT

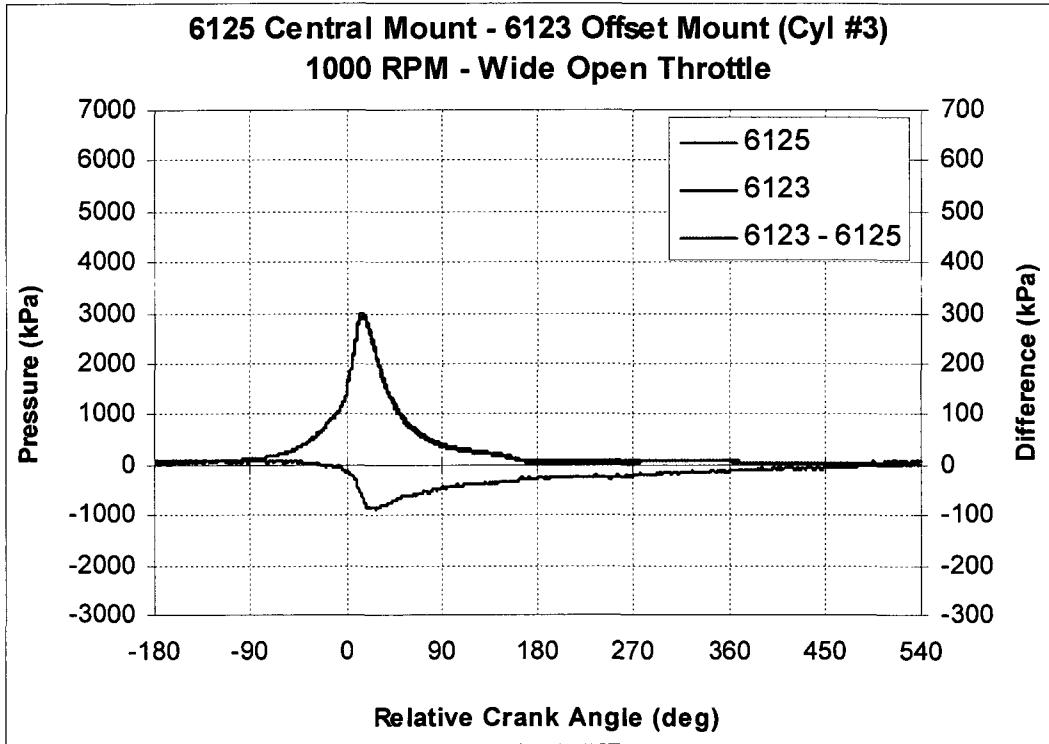


Figure B.2 f – Pressure Traces – 6125 Central / 6123 Offset (Cyl #3) – 1000 RPM / WOT

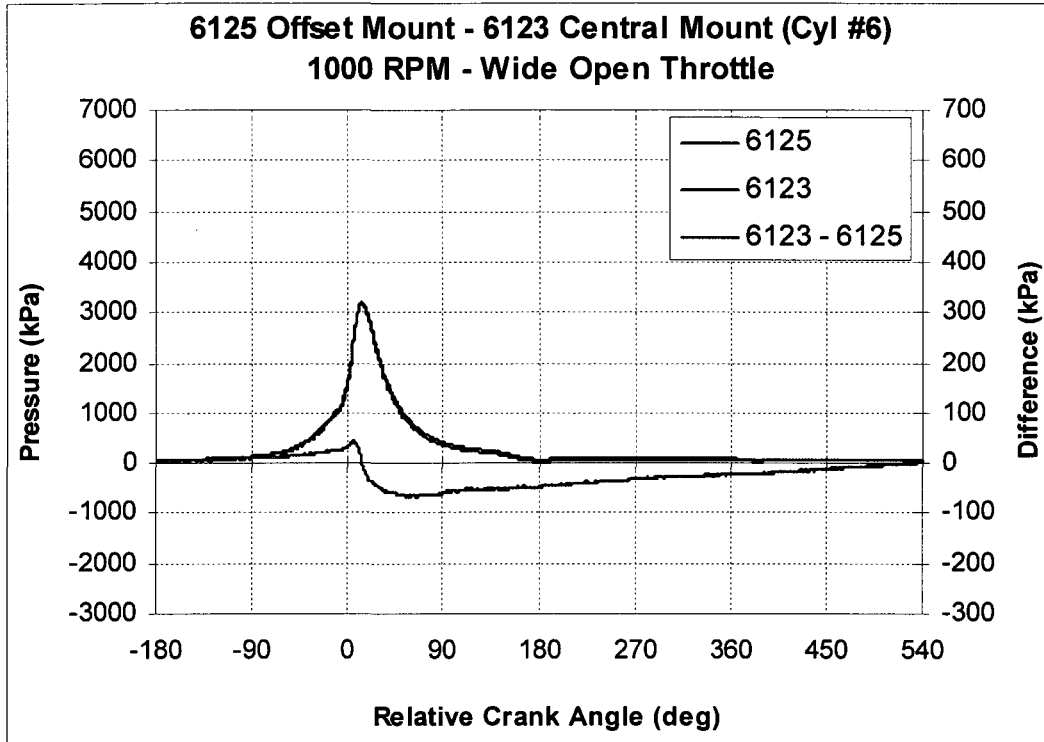


Figure B.2 g – Pressure Traces – 6125 Offset / 6123 Central (Cyl #6) – 1000 RPM / WOT

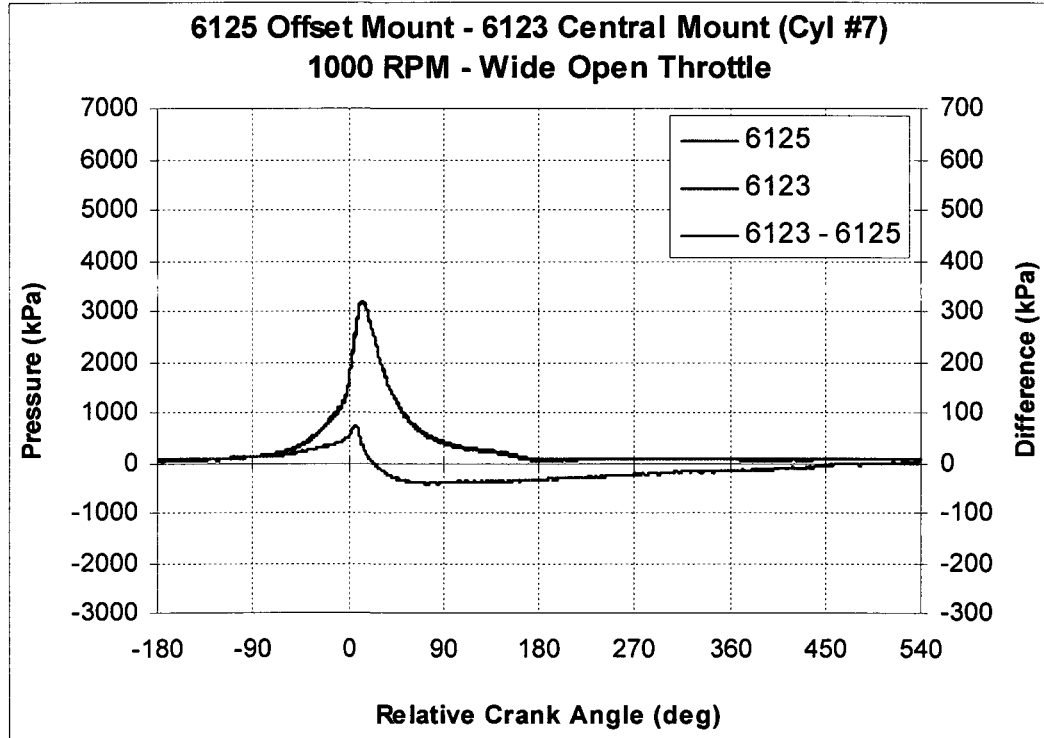


Figure B.2 h – Pressure Traces – 6125 Offset / 6123 Central (Cyl #7) – 1000 RPM / WOT

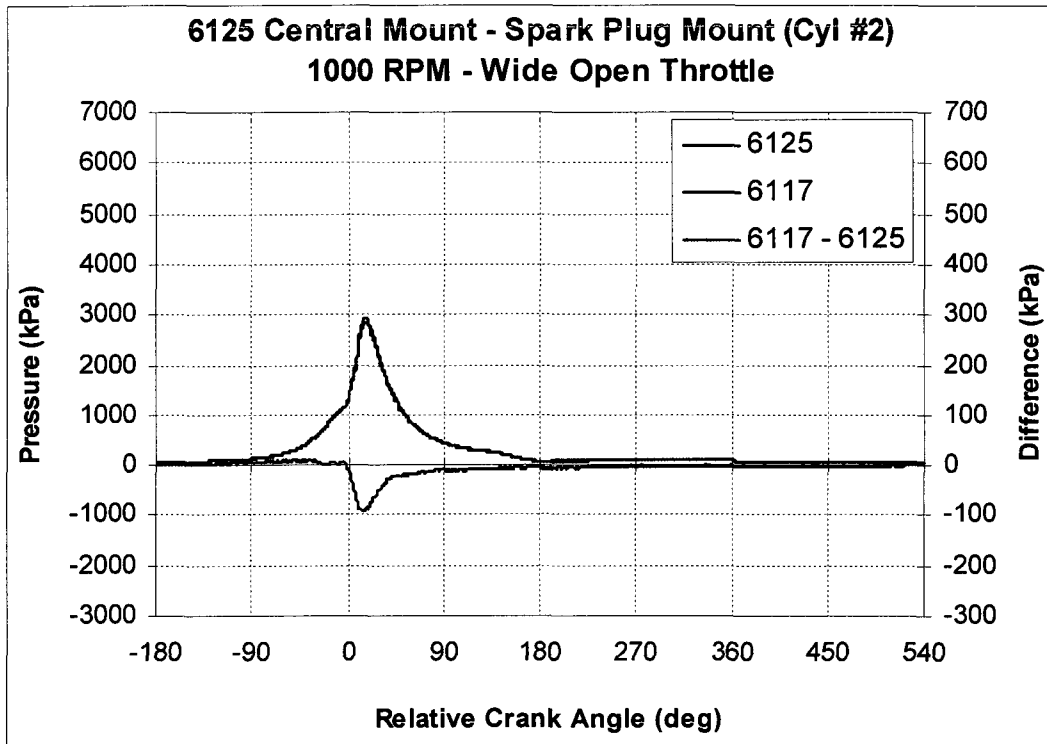


Figure B.2 i – Pressure Traces – 6125 Central / 6117 (Cyl #2) – 1000 RPM / WOT

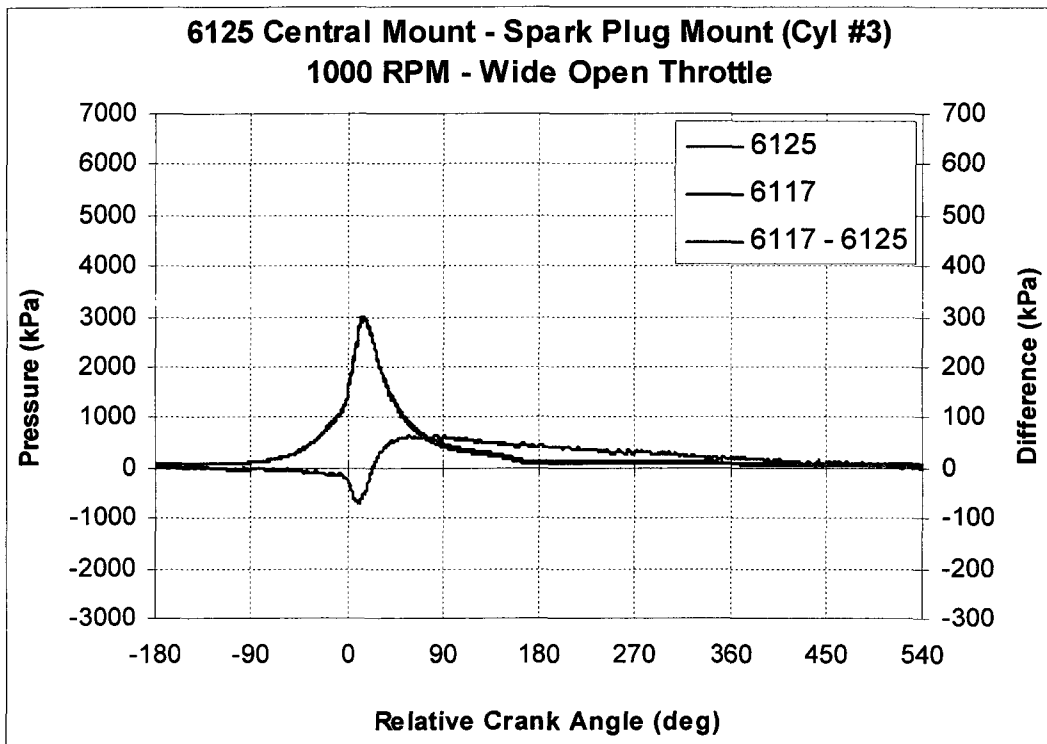


Figure B.2 j – Pressure Traces – 6125 Central / 6117 (Cyl #3) – 1000 RPM / WOT

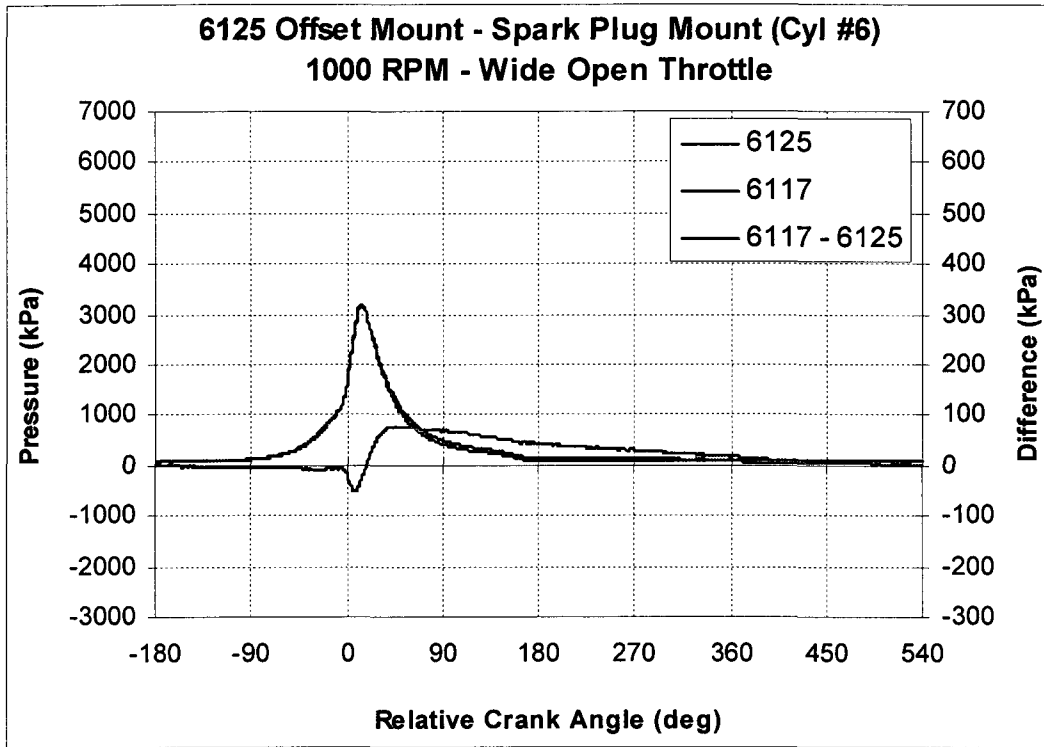


Figure B.2 k – Pressure Traces – 6125 Offset / 6117 (Cyl #6) – 1000 RPM / WOT

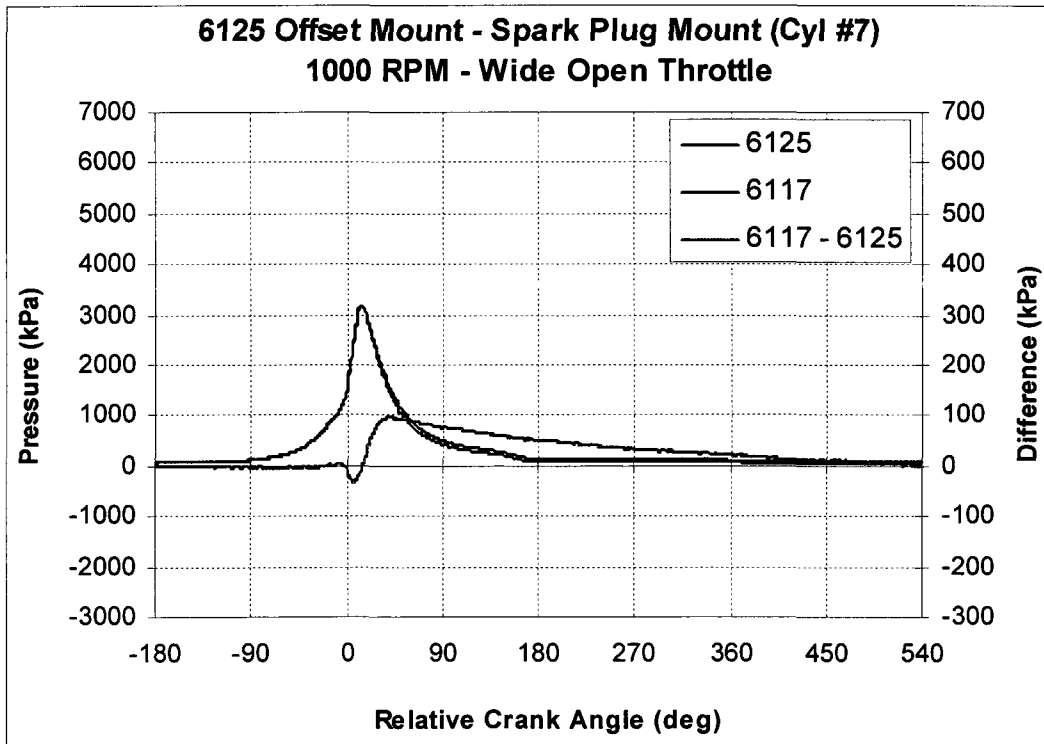
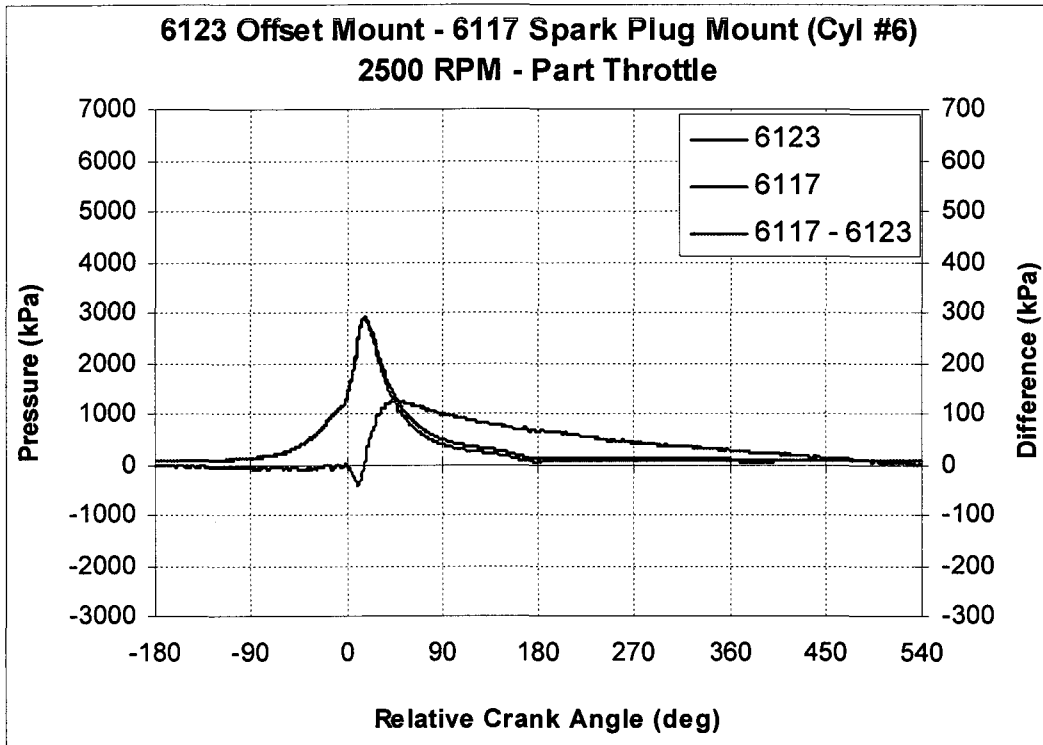
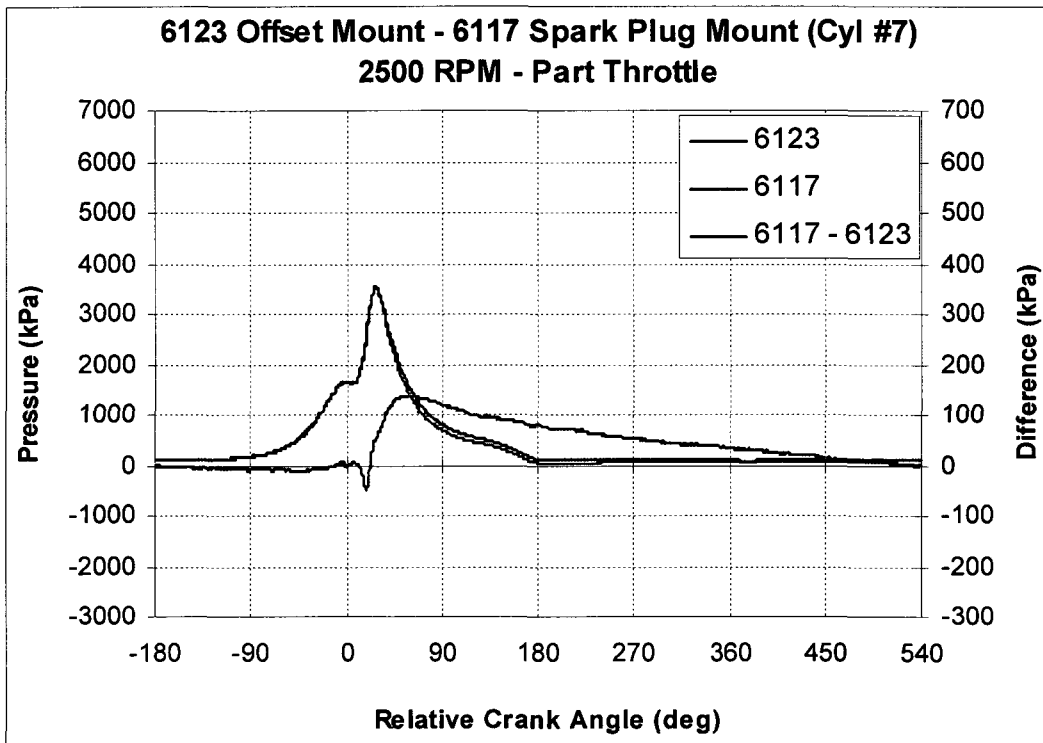


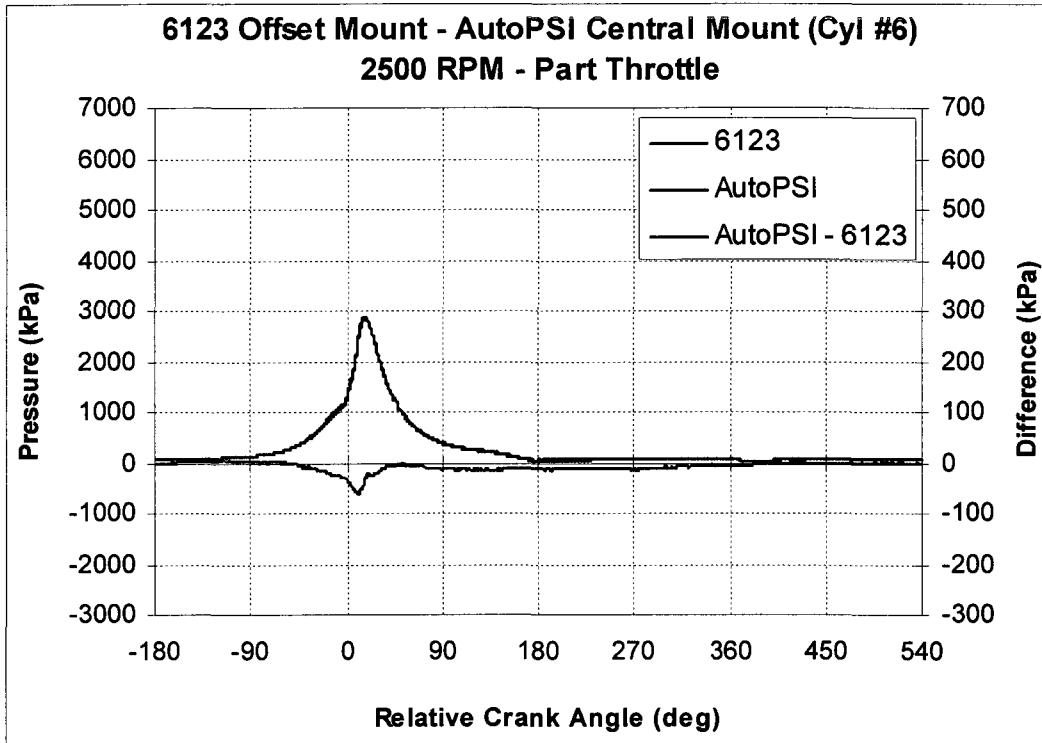
Figure B.2 l – Pressure Traces – 6125 Offset / 6117 (Cyl #7) – 1000 RPM / WOT



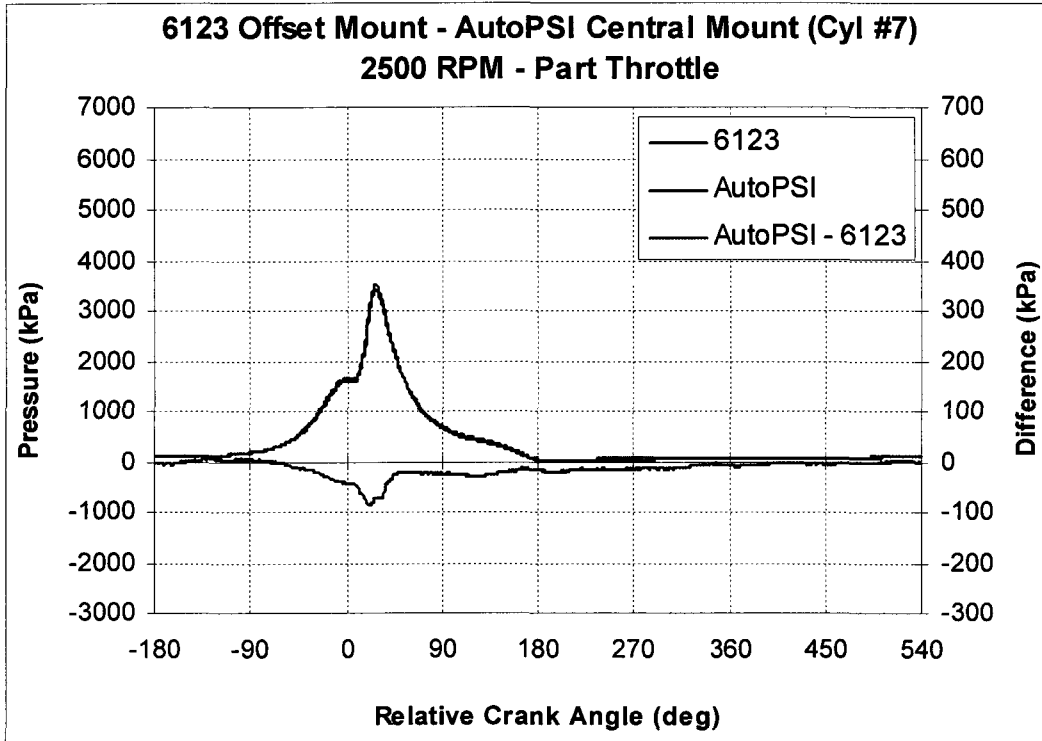
B.3 a – Pressure Traces - 6123 Offset / 6117 (Cyl #6) – 2500 RPM / PT



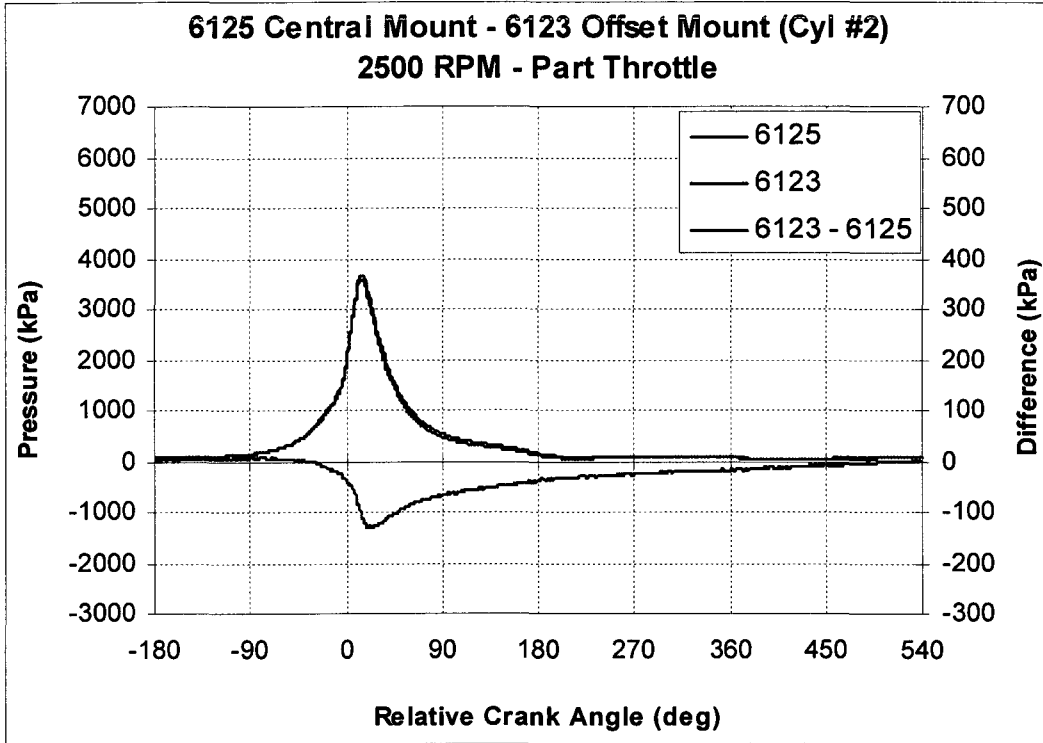
B.3 b – Pressure Traces - 6123 Offset / 6117 (Cyl #7) – 2500 RPM / PT



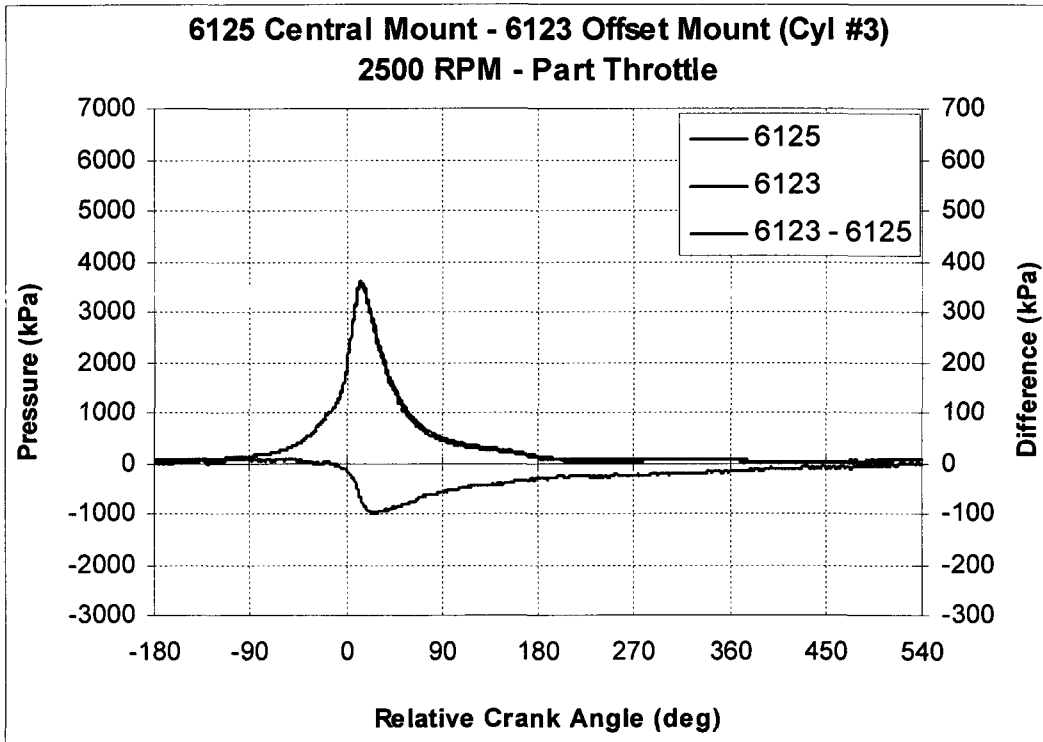
B.3 c – Pressure Traces – 6123 Offset / AutoPSI Central (Cyl #6) – 2500 RPM / PT



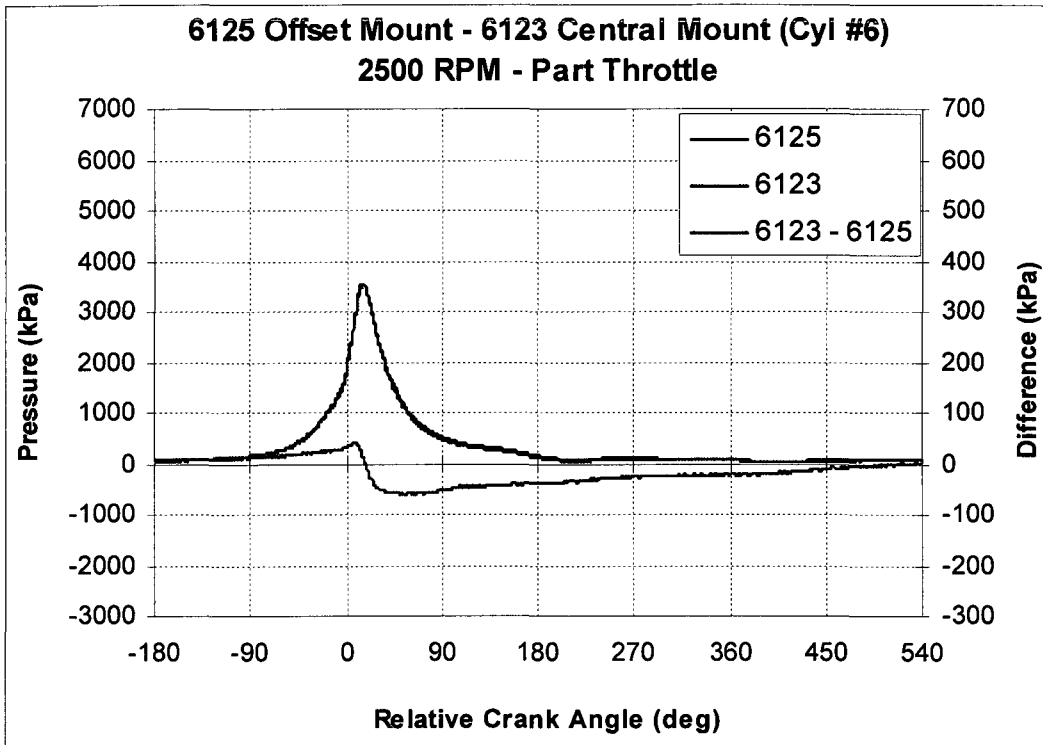
B.3 d – Pressure Traces – 6123 Offset / AutoPSI Central (Cyl #7) – 2500 RPM / PT



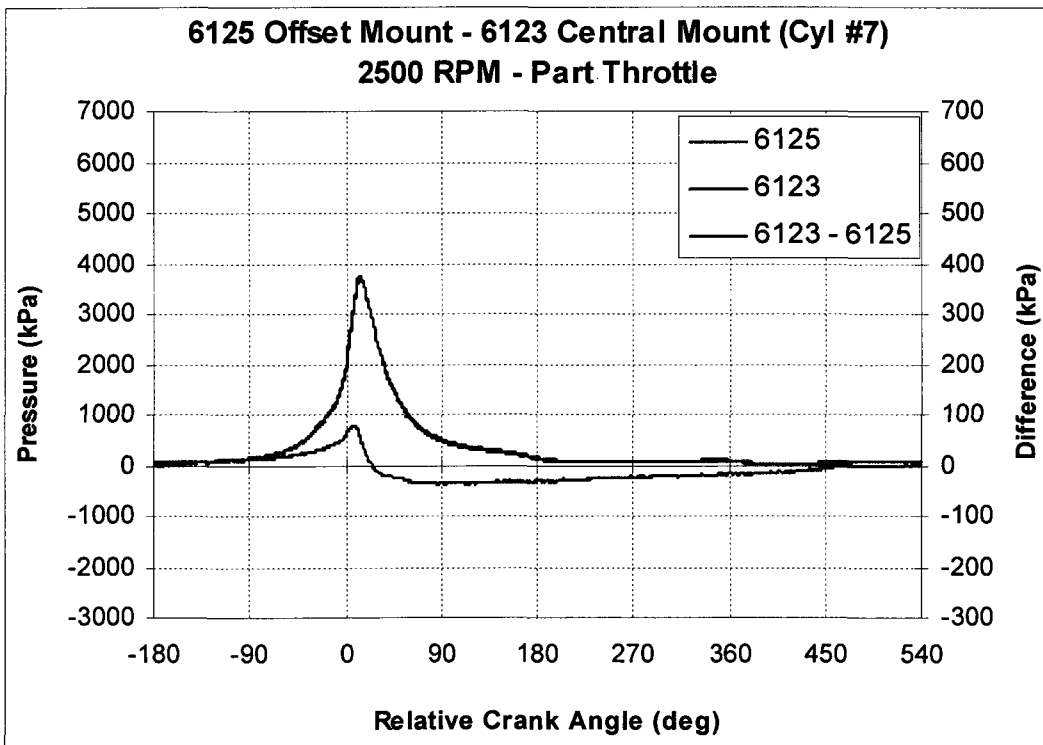
B.3 e – Pressure Traces – 6125 Central / 6123 Offset (Cyl #2) – 2500 RPM / PT



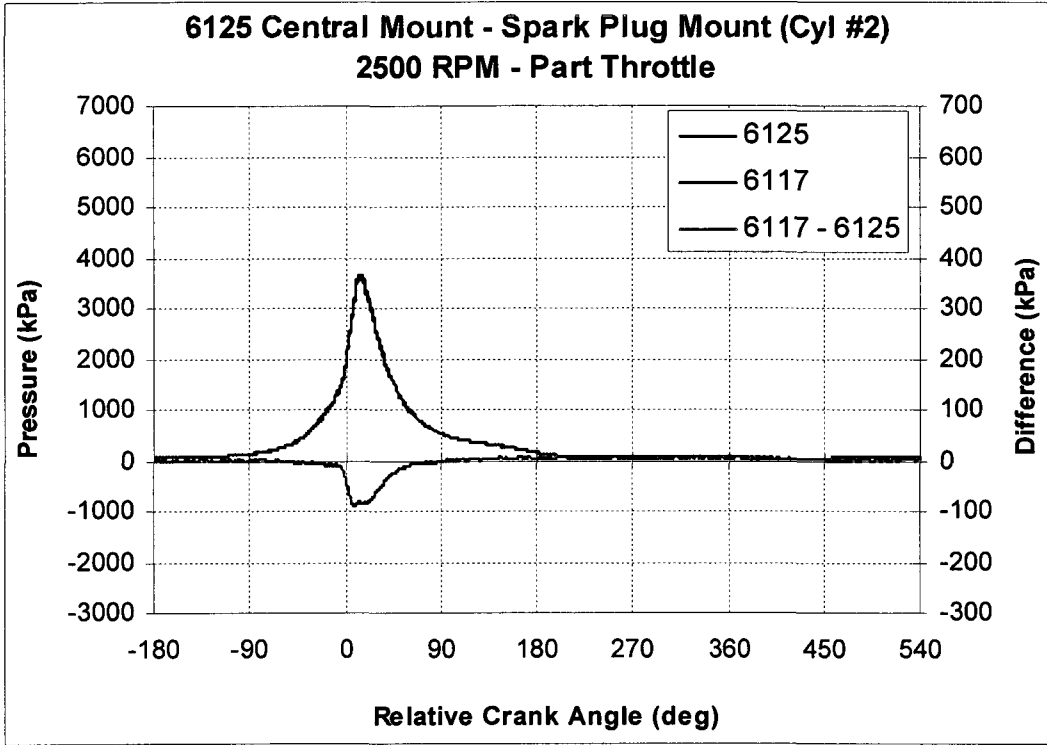
B.3 f – Pressure Traces – 6125 Central / 6123 Offset (Cyl #3) – 2500 RPM / PT



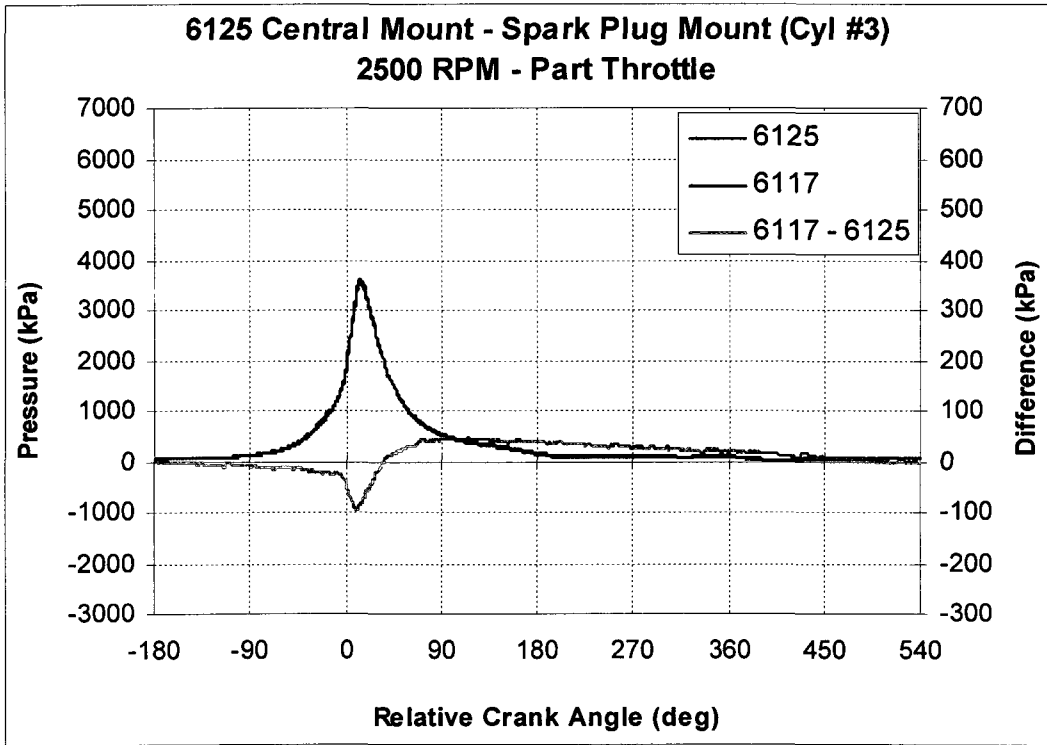
B.3 g – Pressure Traces – 6125 Offset / 6123 Central (Cyl #6) – 2500 RPM / PT



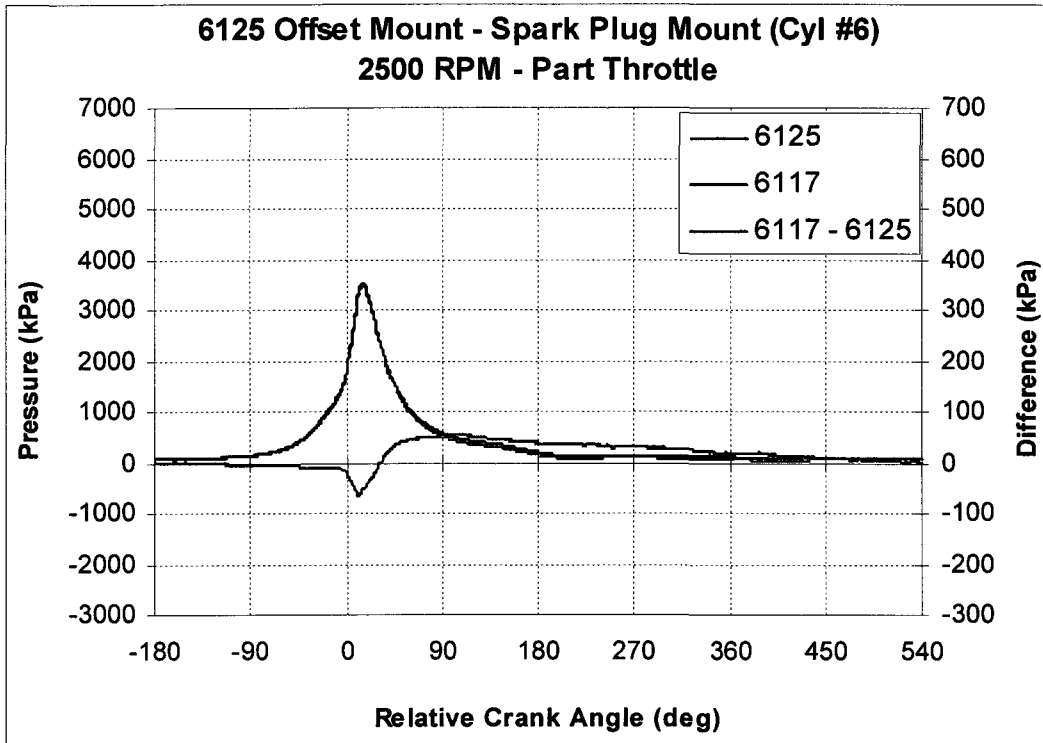
B.3 h – Pressure Traces – 6125 Offset / 6123 Central (Cyl #7) – 2500 RPM / PT



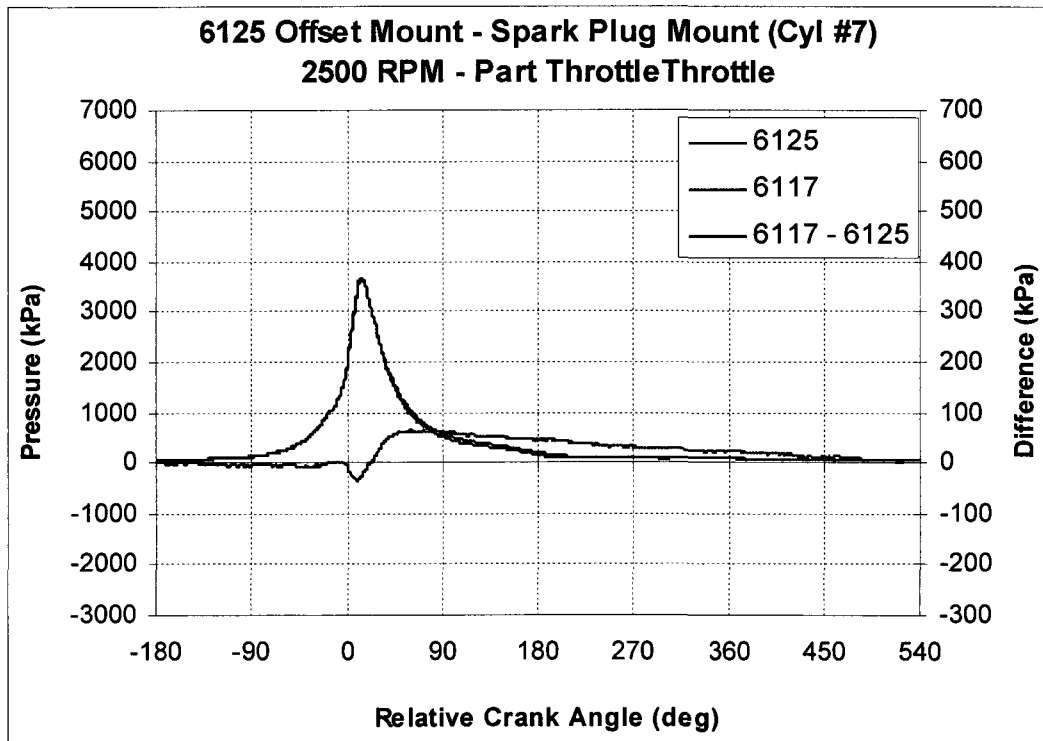
B.3 i – Pressure Traces – 6125 Central / 6117 (Cyl #2) – 2500 RPM / PT



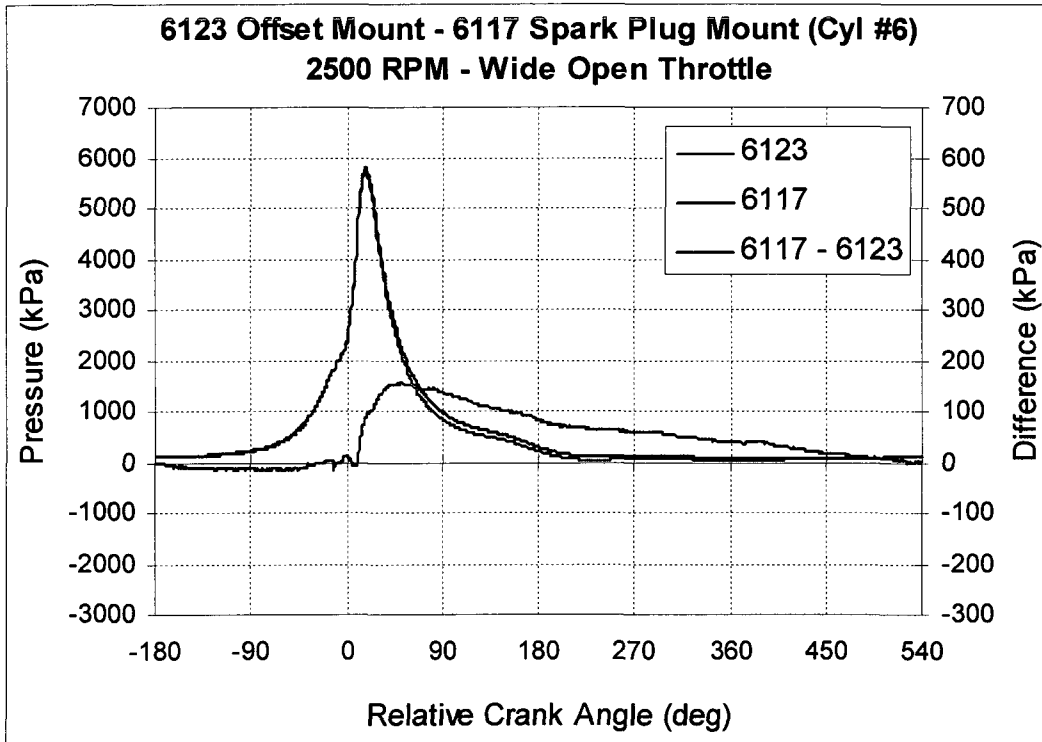
B.3 j – Pressure Traces – 6125 Central / 6117 (Cyl #3) – 2500 RPM / PT



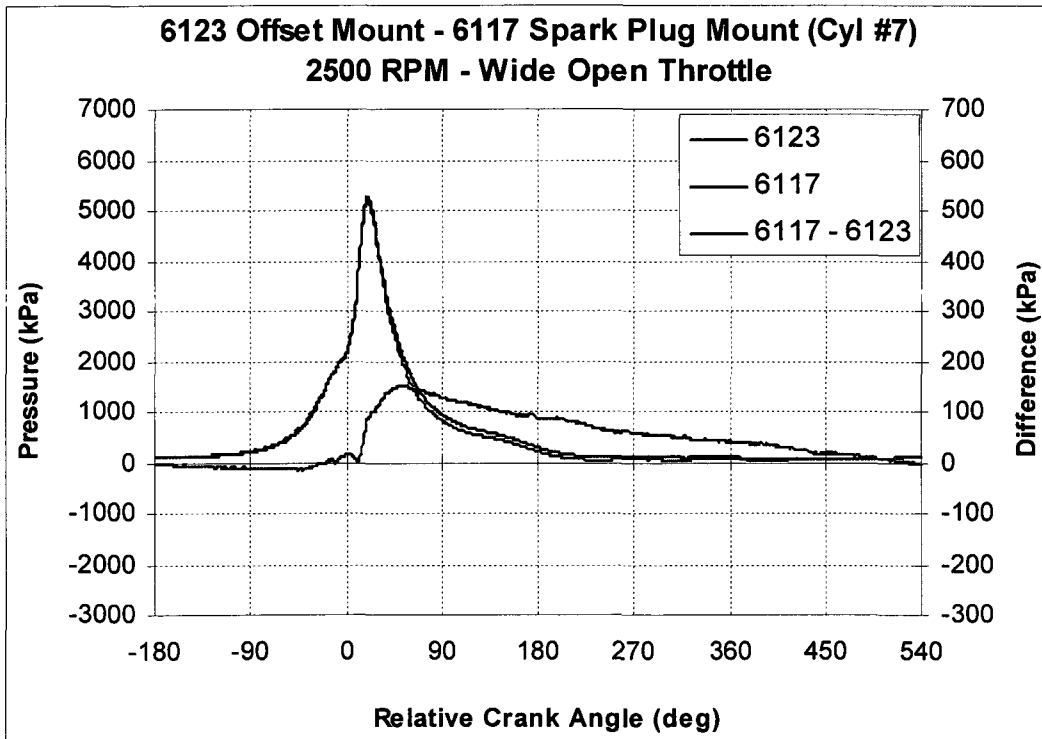
B.3 k – Pressure Traces – 6125 Offset / 6117 (Cyl #6) – 2500 RPM / PT



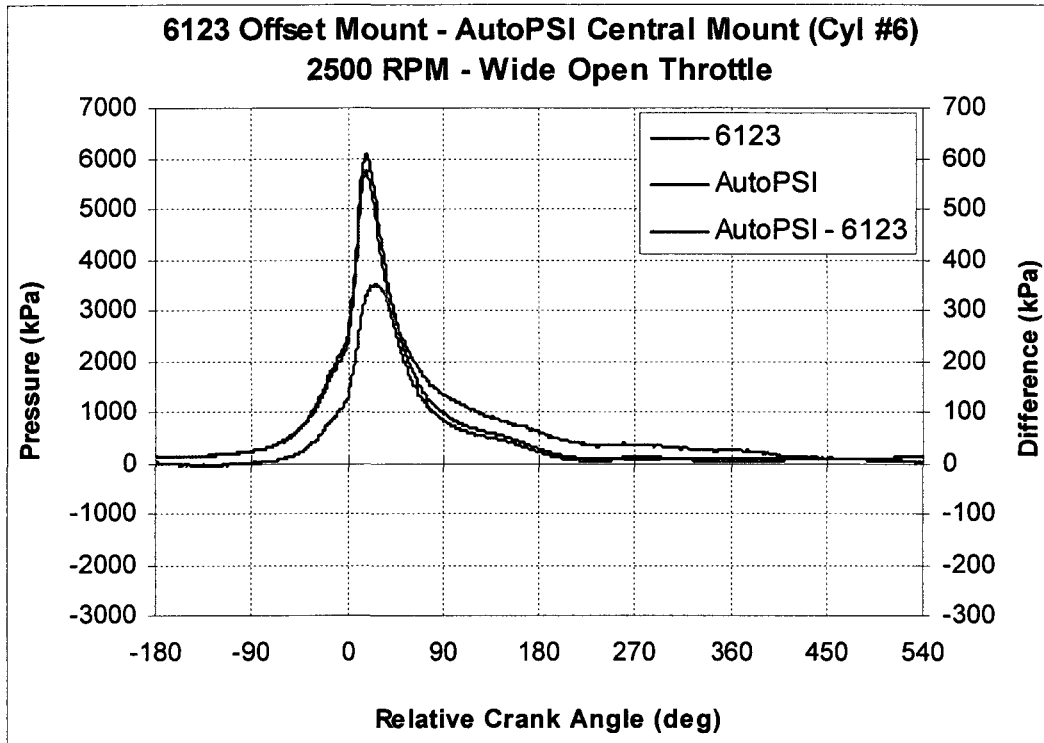
B.3 l – Pressure Traces – 6125 Offset / 6117 (Cyl #7) – 2500 RPM / PT



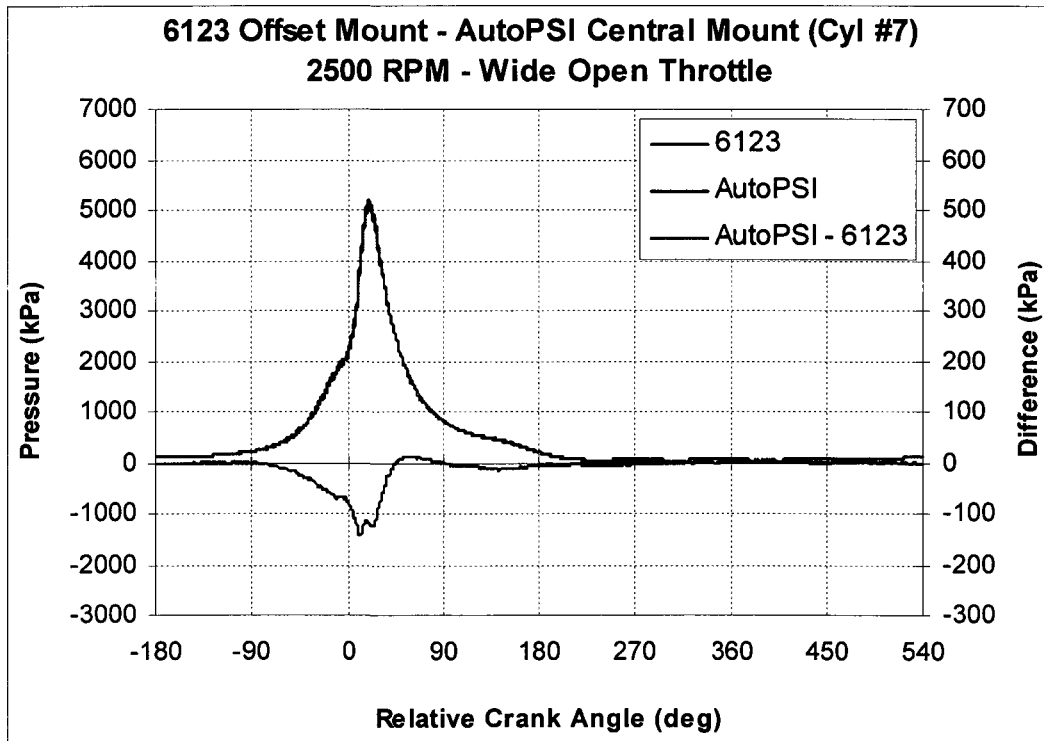
B.4 a – Pressure Traces - 6123 Offset / 6117 (Cyl #6) – 2500 RPM / WOT



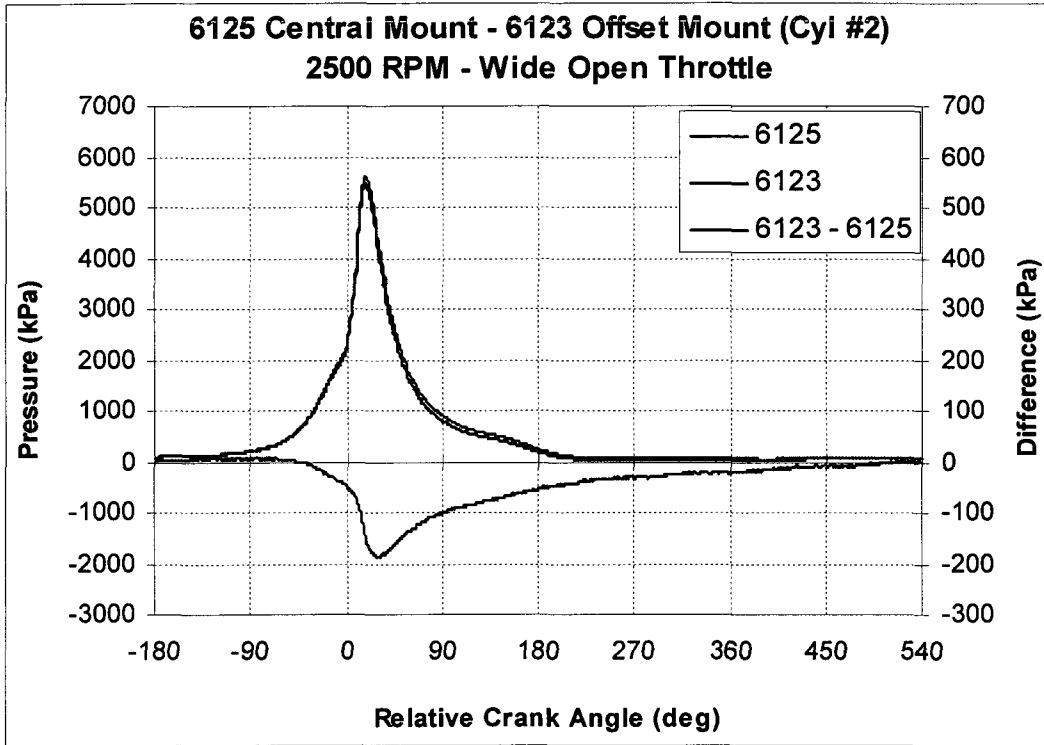
B.4 b – Pressure Traces - 6123 Offset / 6117 (Cyl #7) – 2500 RPM / WOT



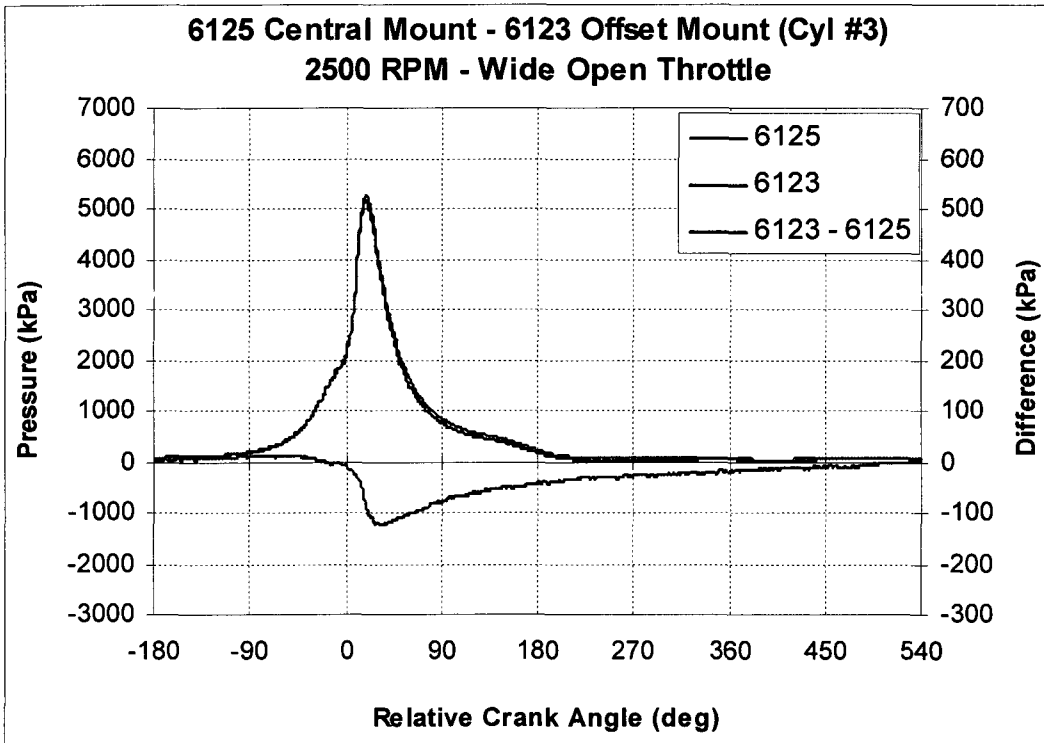
B.4 c – Pressure Traces – 6123 Offset / AutoPSI Central (Cyl #6) – 2500 RPM / WOT



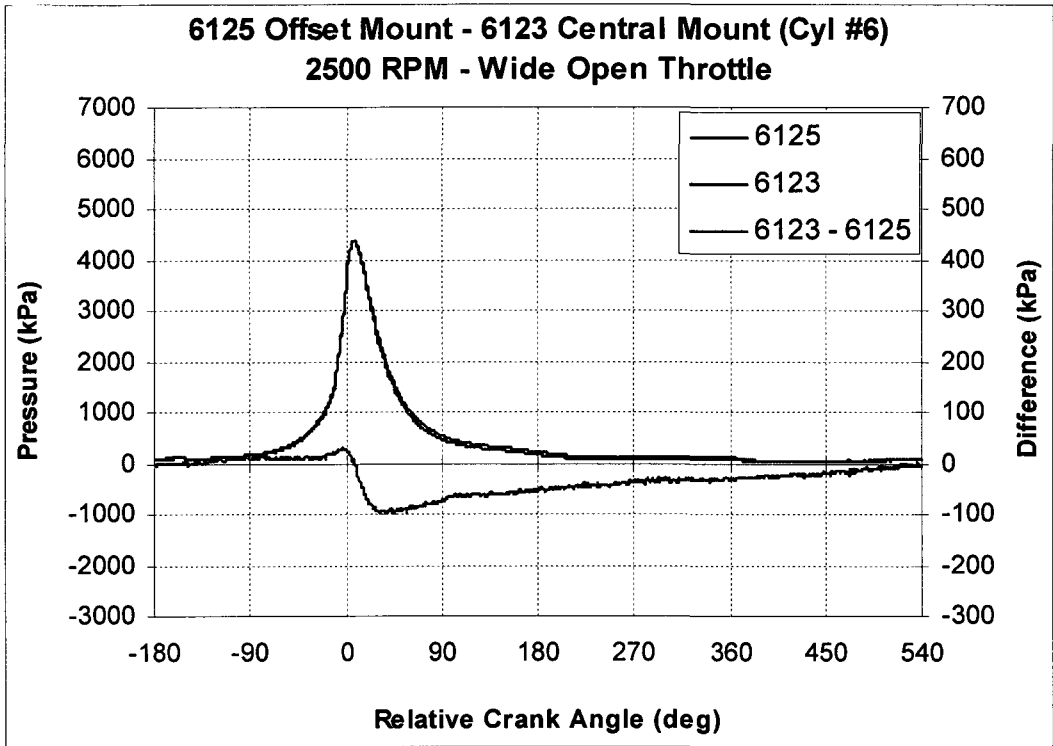
B.4 d – Pressure Traces – 6123 Offset / AutoPSI Central (Cyl #7) – 2500 RPM / WOT



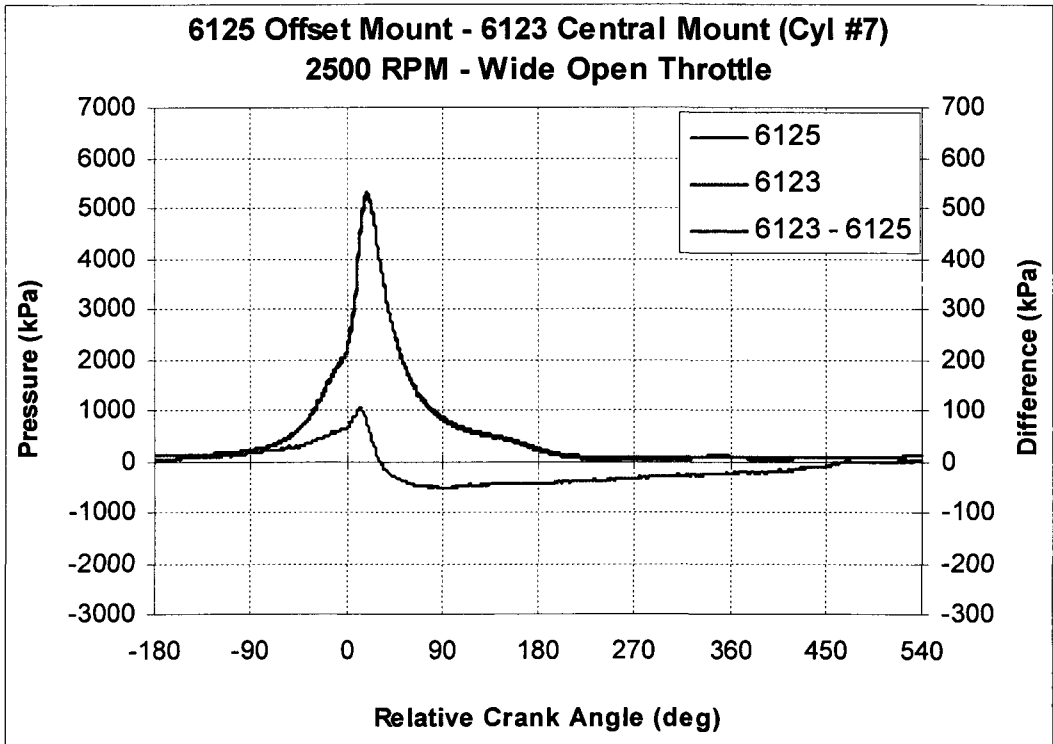
B.4 e – Pressure Traces – 6125 Central / 6123 Offset (Cyl #2) – 2500 RPM / WOT



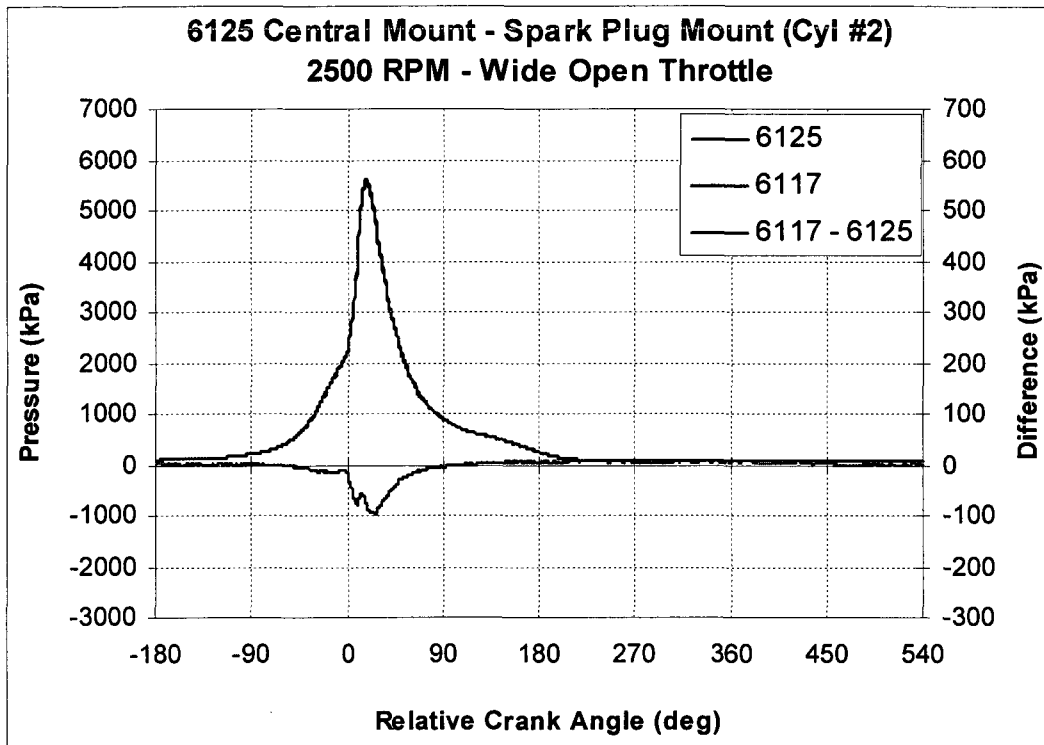
B.4 f – Pressure Traces – 6125 Central / 6123 Offset (Cyl #3) – 2500 RPM / WOT



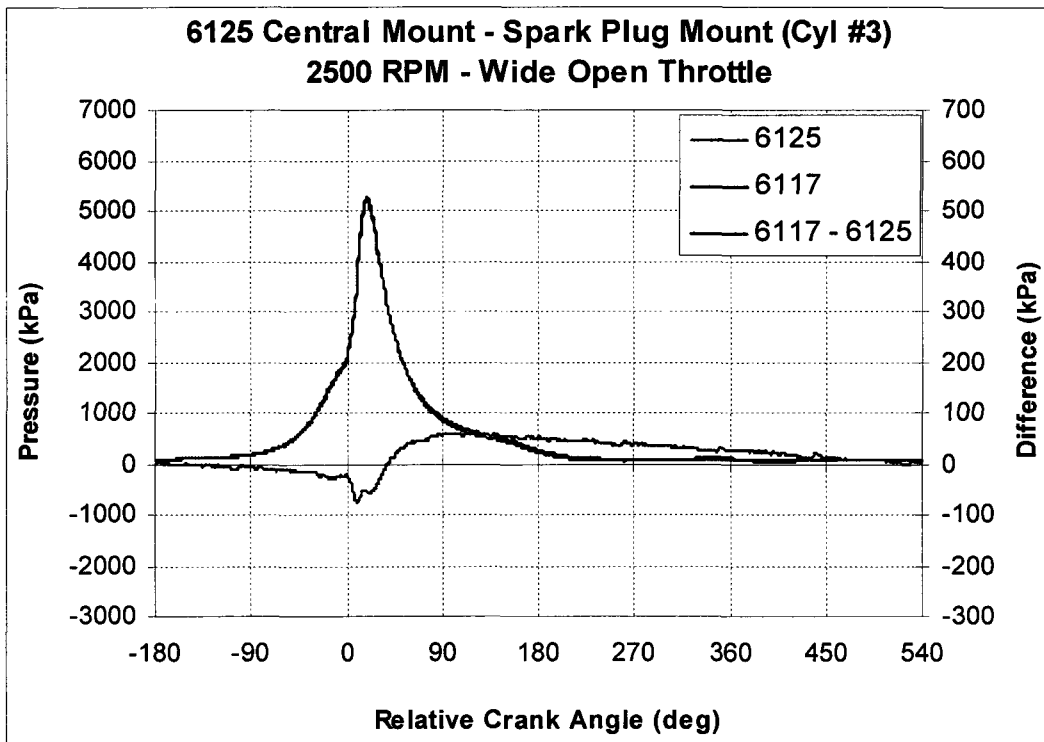
B.4 g – Pressure Traces – 6125 Offset / 6123 Central (Cyl #6) – 2500 RPM / WOT



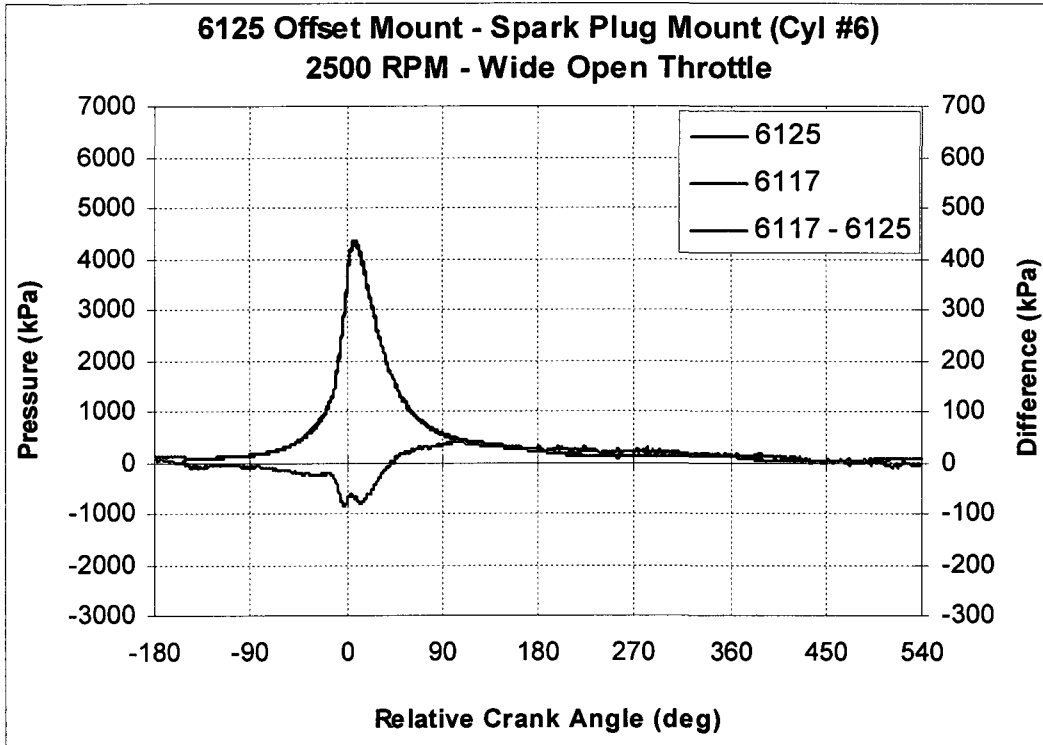
B.4 h – Pressure Traces – 6125 Offset / 6123 Central (Cyl #7) – 2500 RPM / WOT



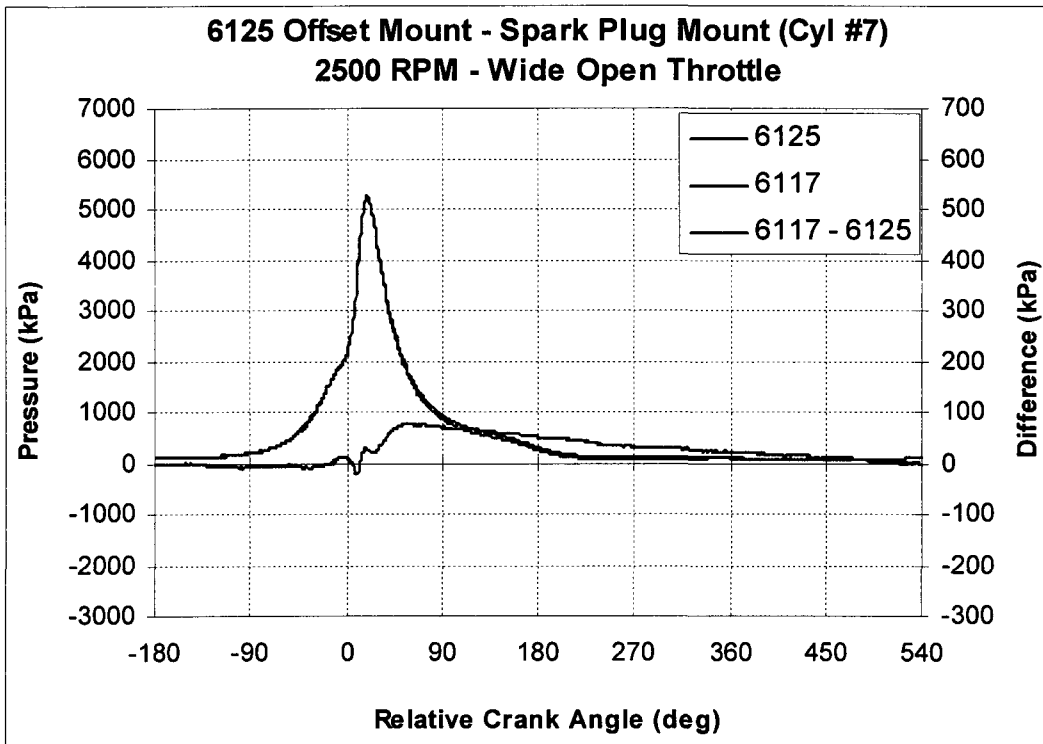
B.4 i – Pressure Traces – 6125 Central / 6117 (Cyl #2) – 2500 RPM / WOT



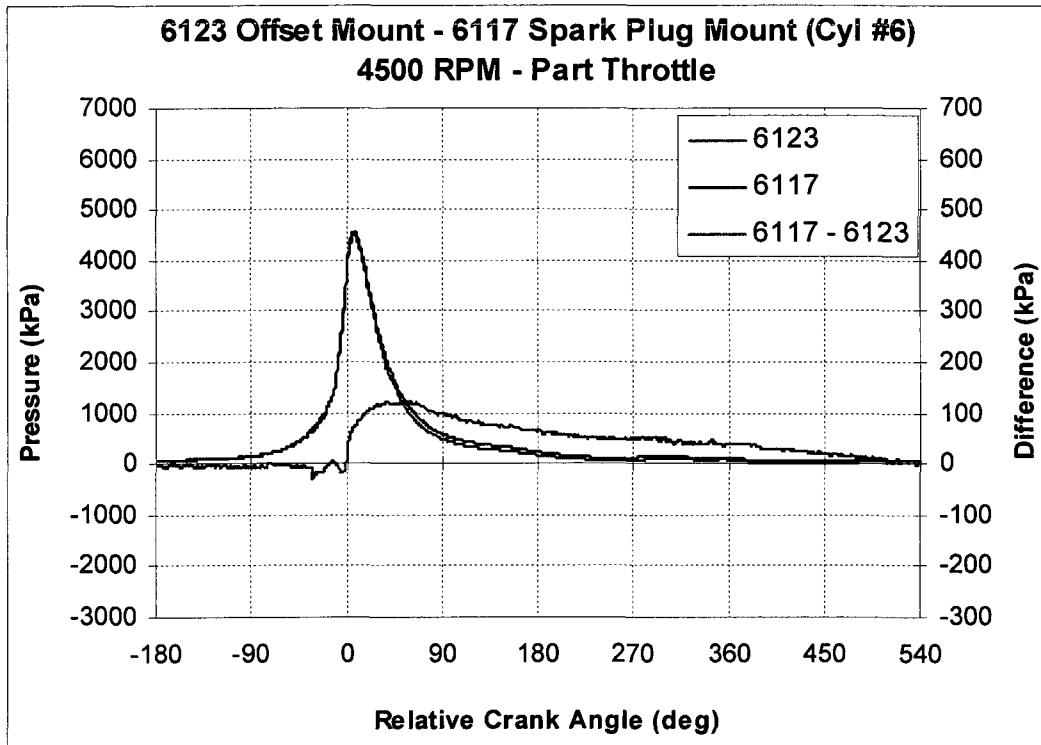
B.4 j – Pressure Traces – 6125 Central / 6117 (Cyl #3) – 2500 RPM / WOT



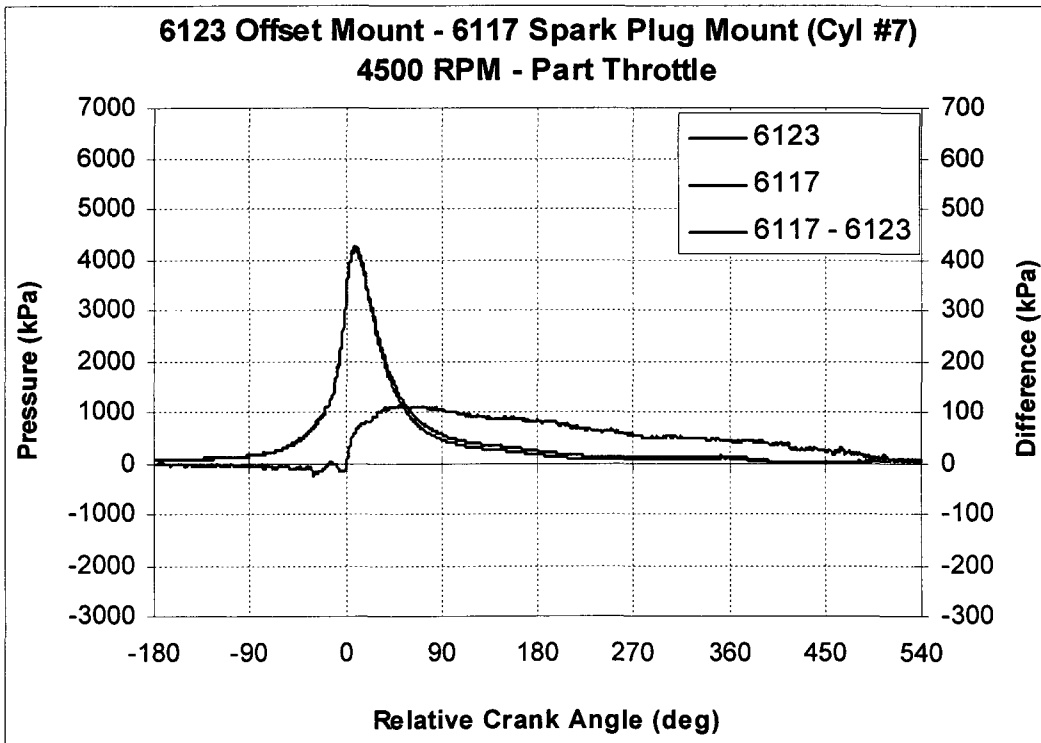
B.4 k – Pressure Traces – 6125 Offset / 6117 (Cyl #6) – 2500 RPM / WOT



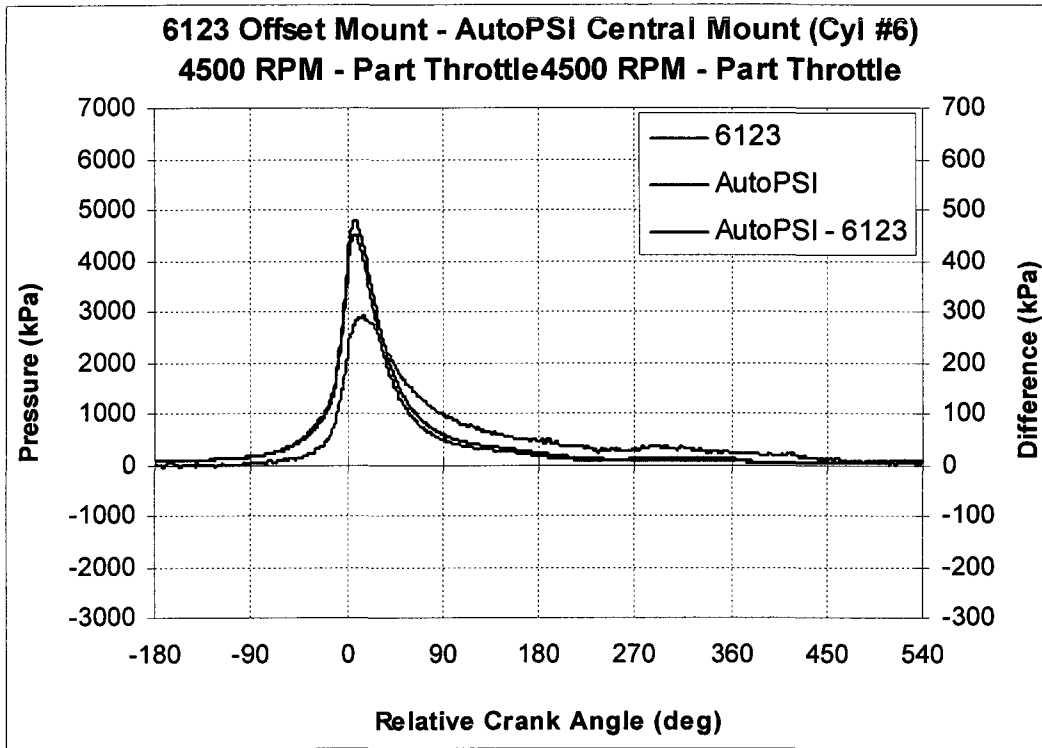
B.4 l – Pressure Traces – 6125 Offset / 6117 (Cyl #7) – 2500 RPM / WOT



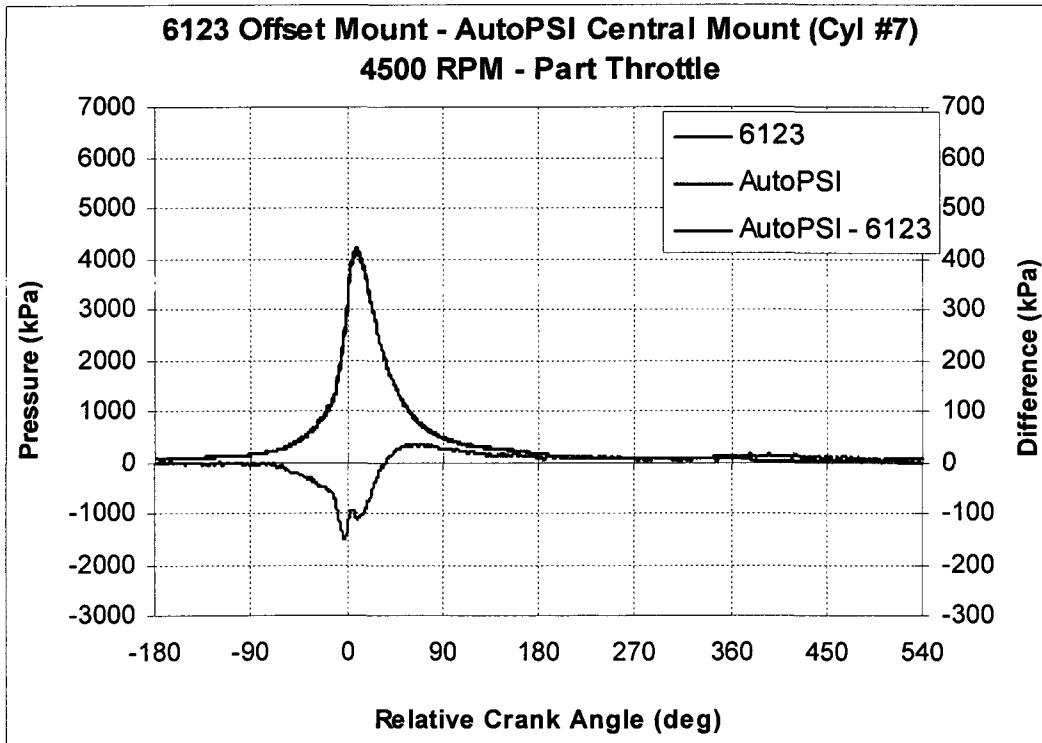
B.5 a – Pressure Traces - 6123 Offset / 6117 (Cyl #6) – 4500 RPM / PT



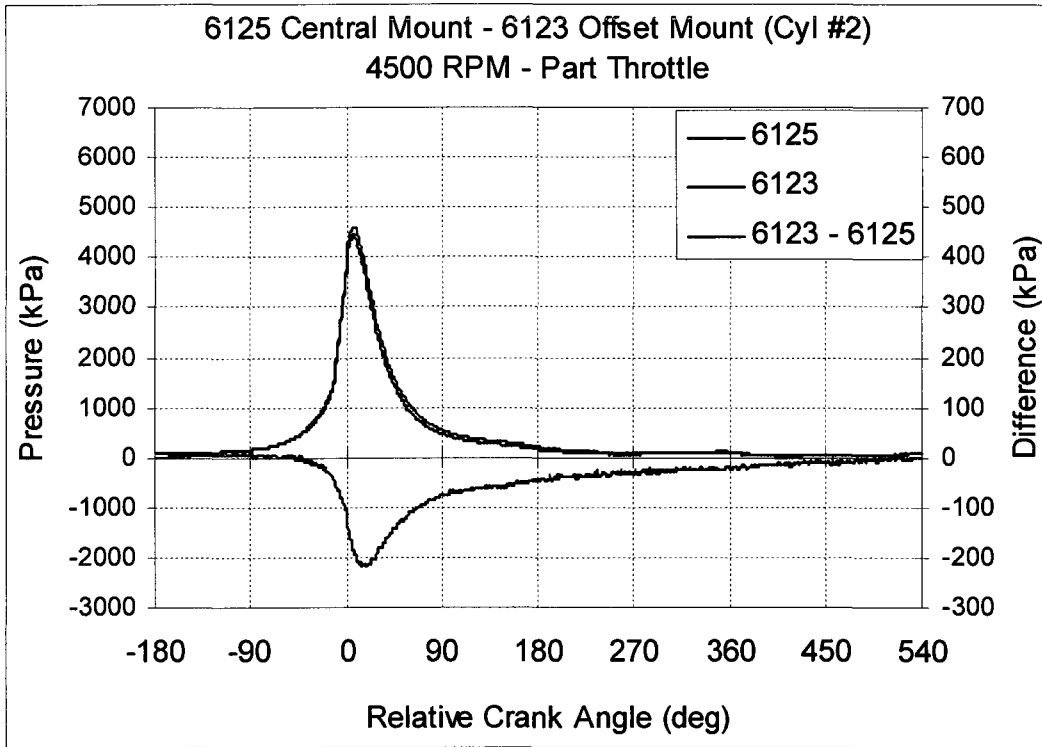
B.5 b – Pressure Traces - 6123 Offset / 6117 (Cyl #7) – 4500 RPM / PT



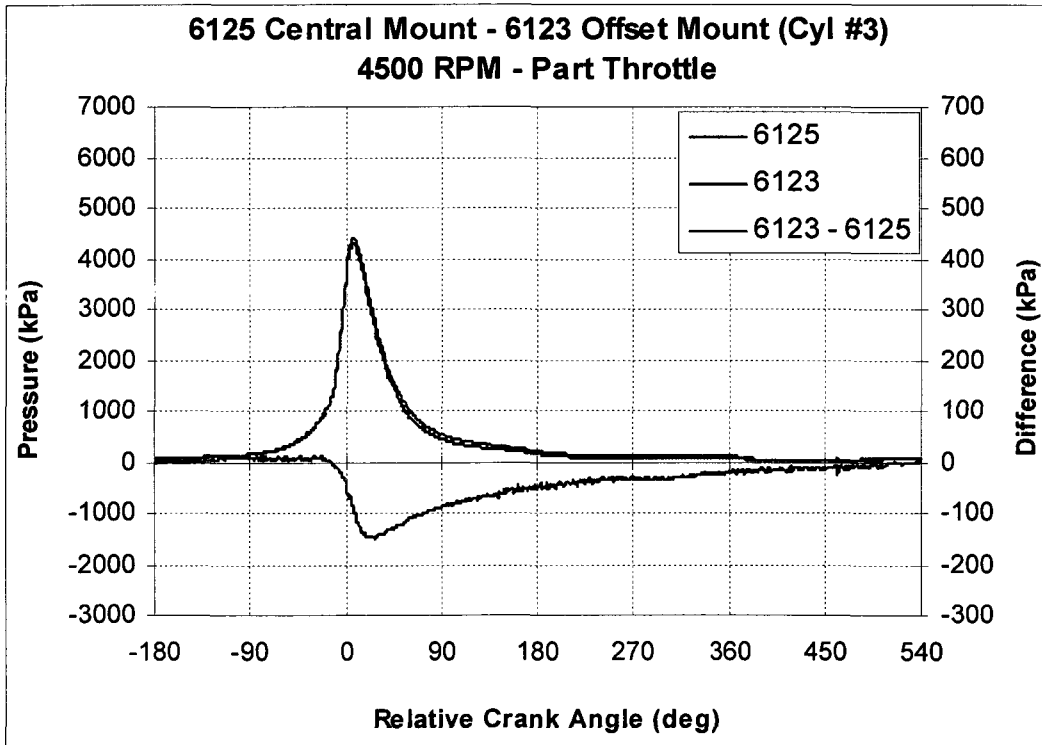
B.5 c – Pressure Traces – 6123 Offset / AutoPSI Central (Cyl #6) – 4500 RPM / PT



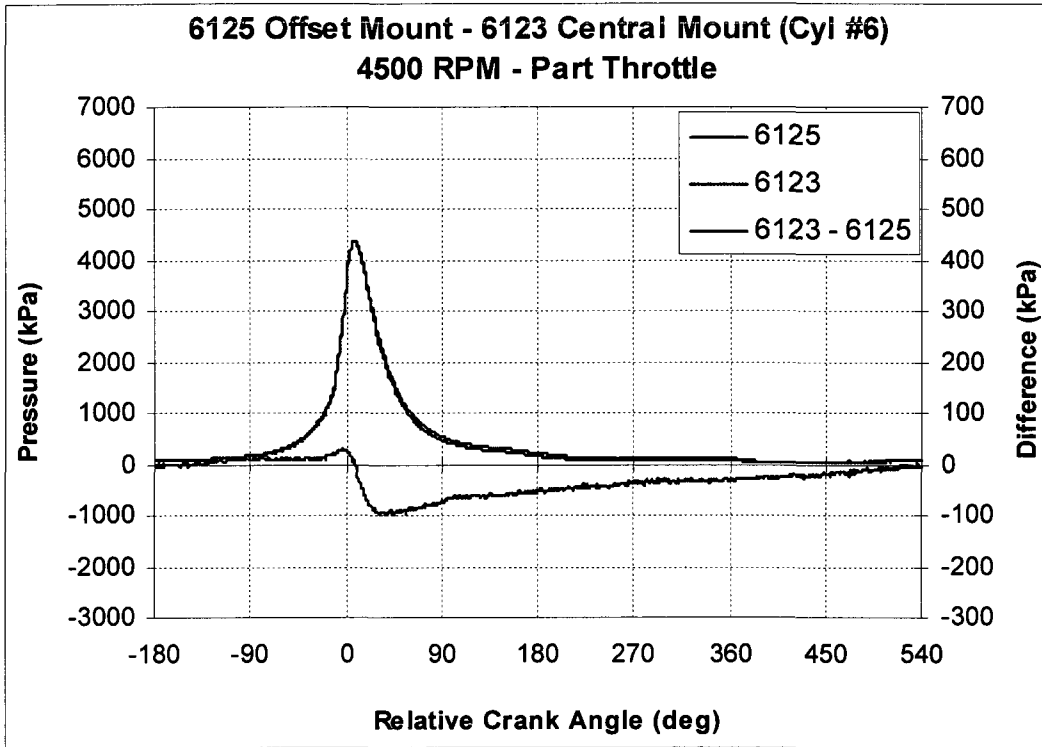
B.5 d – Pressure Traces – 6123 Offset / AutoPSI Central (Cyl #7) – 4500 RPM / PT



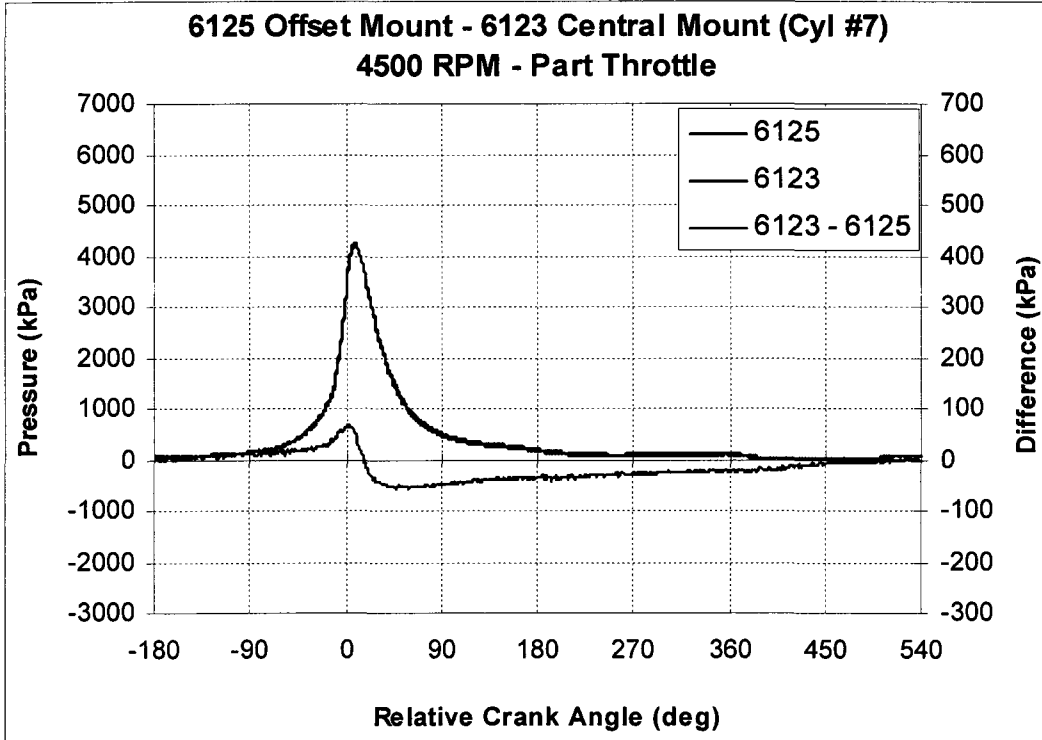
B.5 e – Pressure Traces – 6125 Central / 6123 Offset (Cyl #2) – 4500 RPM / PT



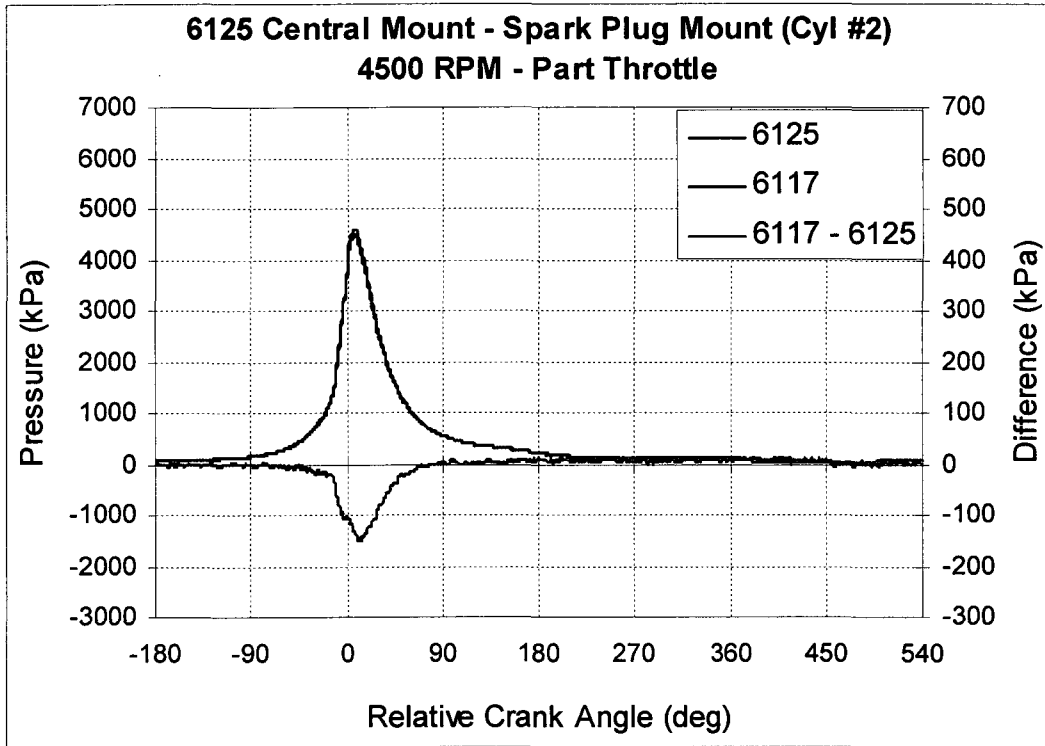
B.5 f – Pressure Traces – 6125 Central / 6123 Offset (Cyl #3) – 4500 RPM / PT



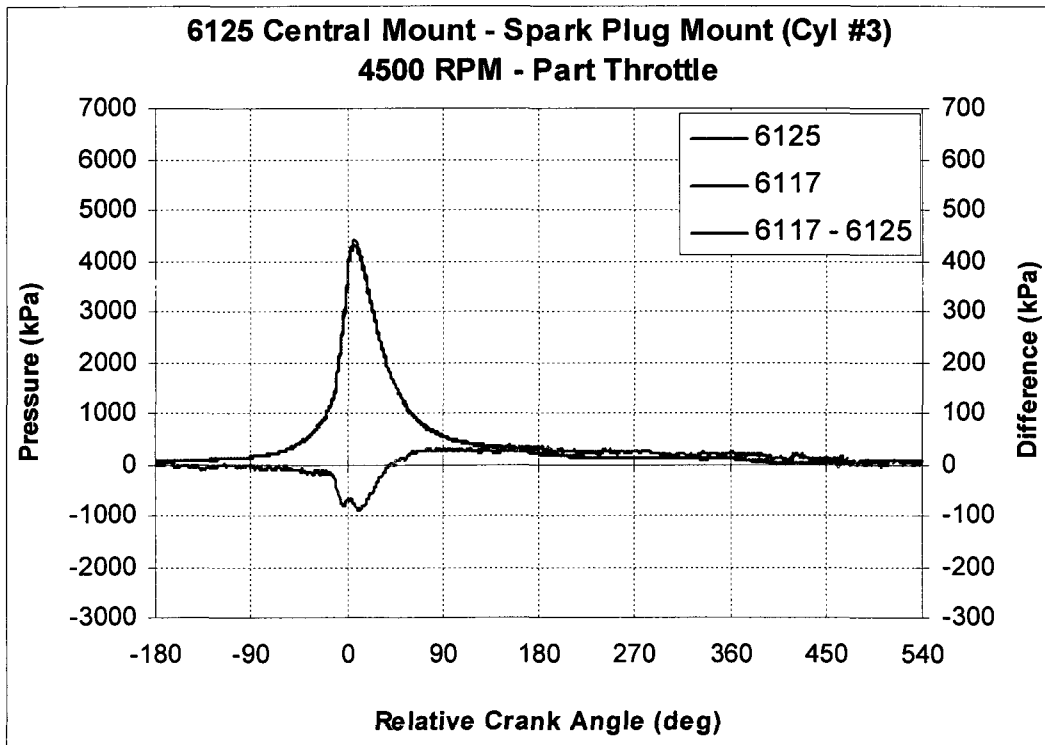
B.5 g – Pressure Traces – 6125 Offset / 6123 Central (Cyl #6) – 4500 RPM / PT



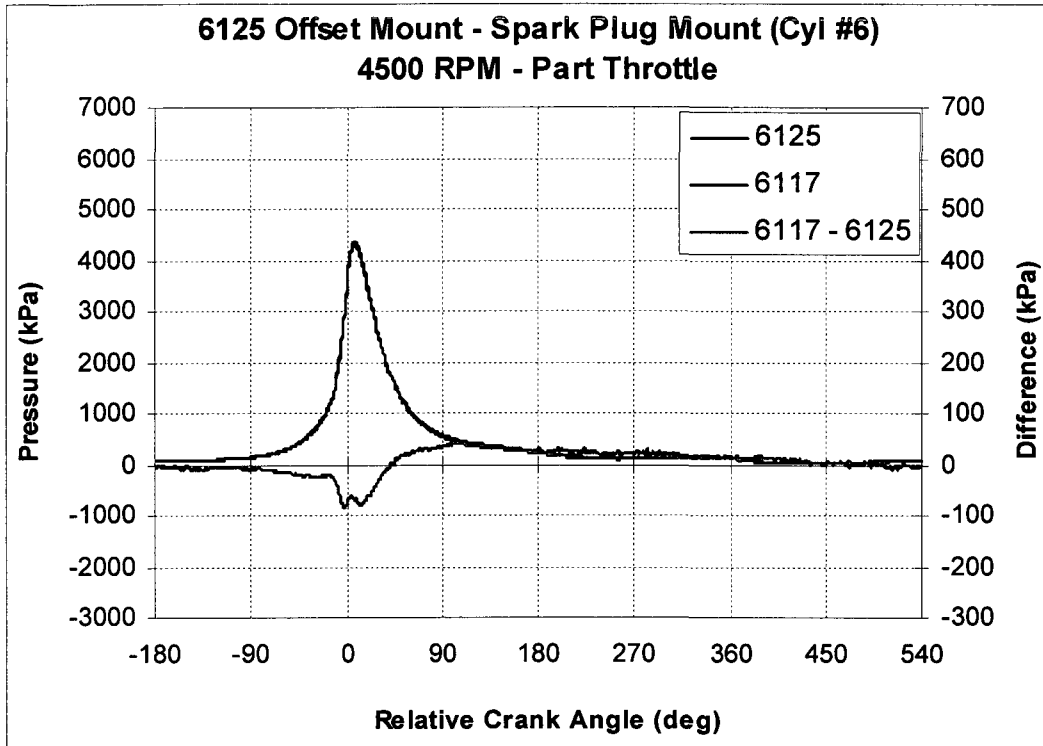
B.5 h – Pressure Traces – 6125 Offset / 6123 Central (Cyl #7) – 4500 RPM / PT



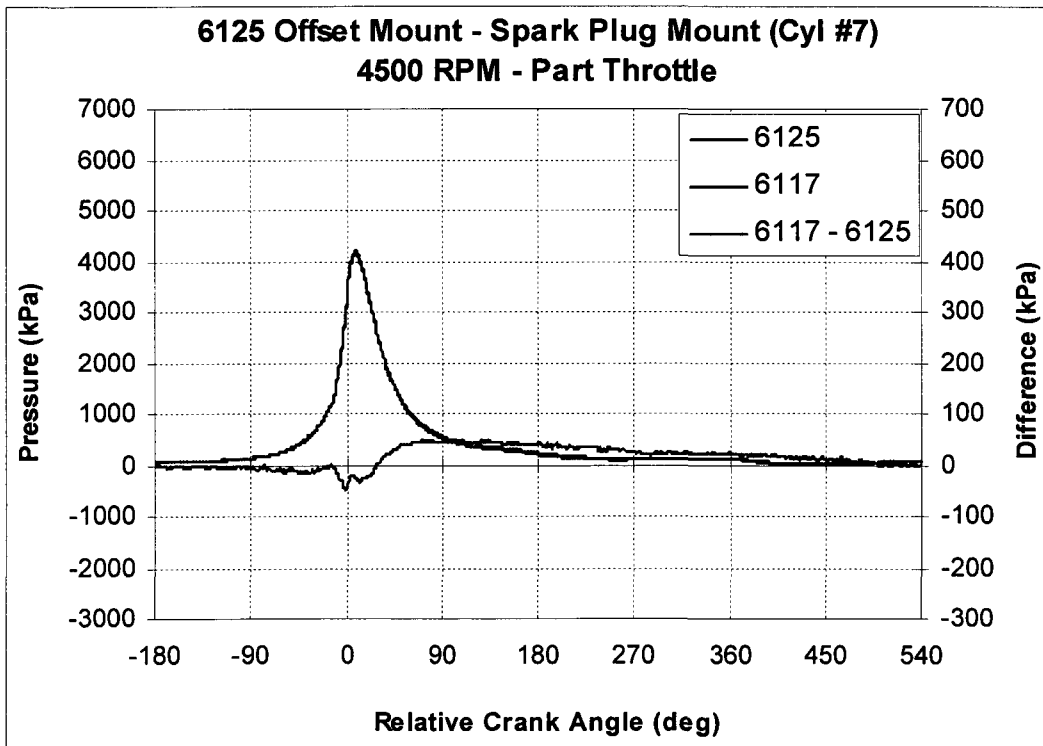
B.5 i – Pressure Traces – 6125 Central / 6117 (Cyl #2) – 4500 RPM / PT



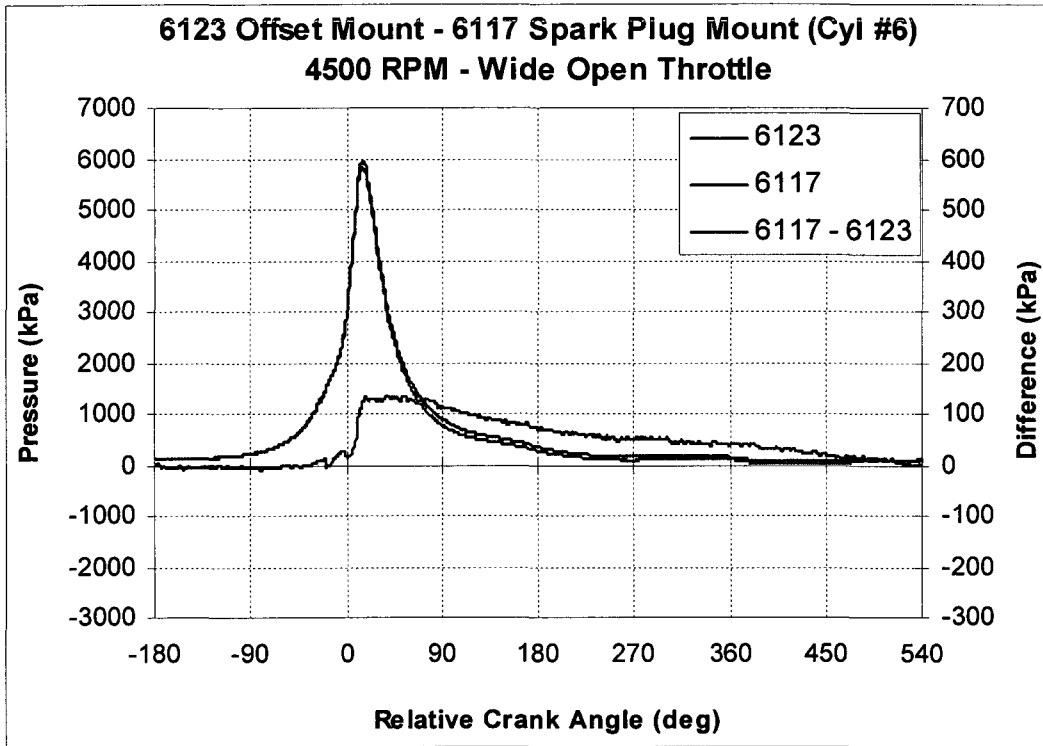
B.5 j – Pressure Traces – 6125 Central / 6117 (Cyl #3) – 4500 RPM / PT



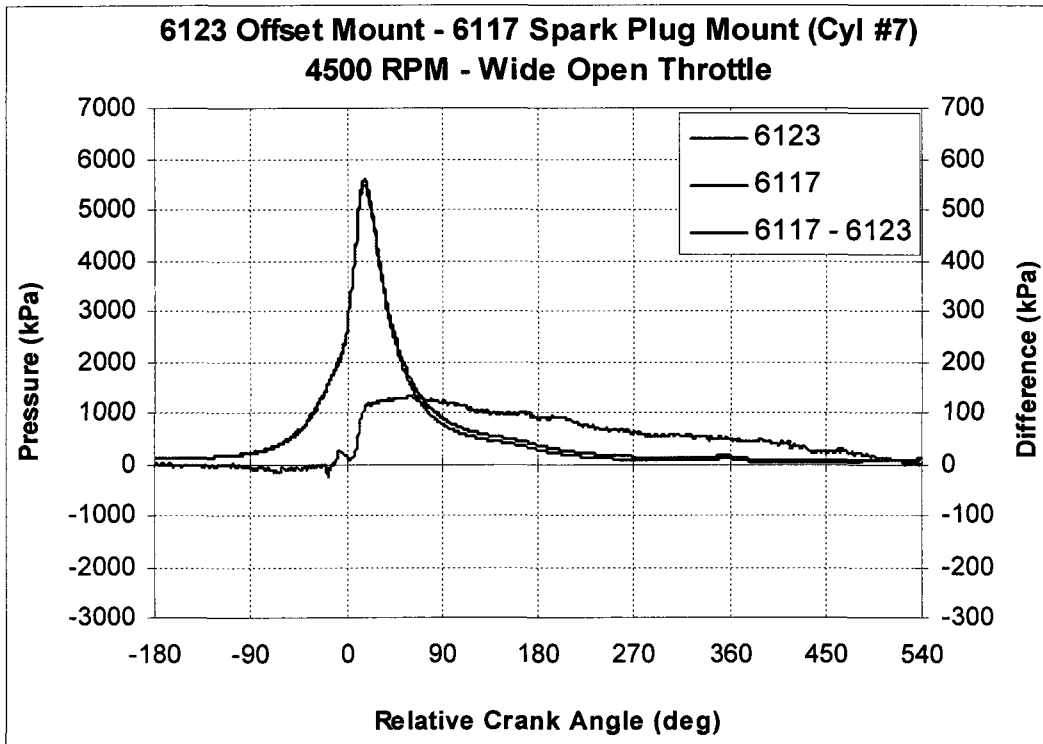
B.5 k – Pressure Traces – 6125 Offset / 6117 (Cyl #6) – 4500 RPM / PT



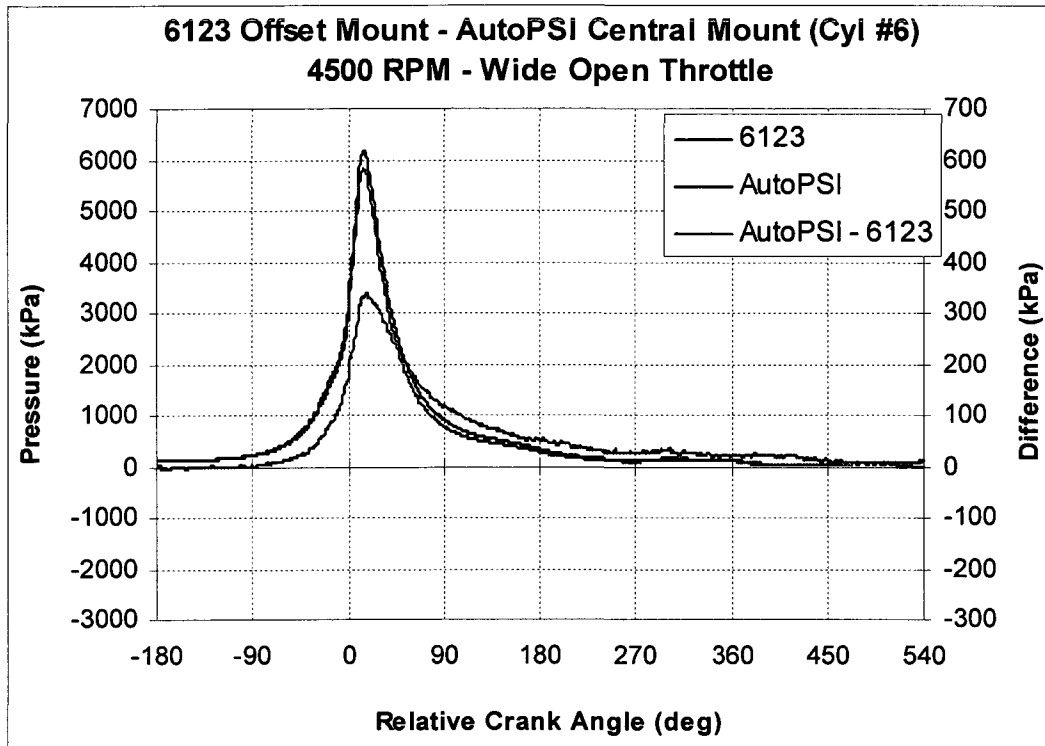
B.5 l – Pressure Traces – 6125 Offset / 6117 (Cyl #7) – 4500 RPM / PT



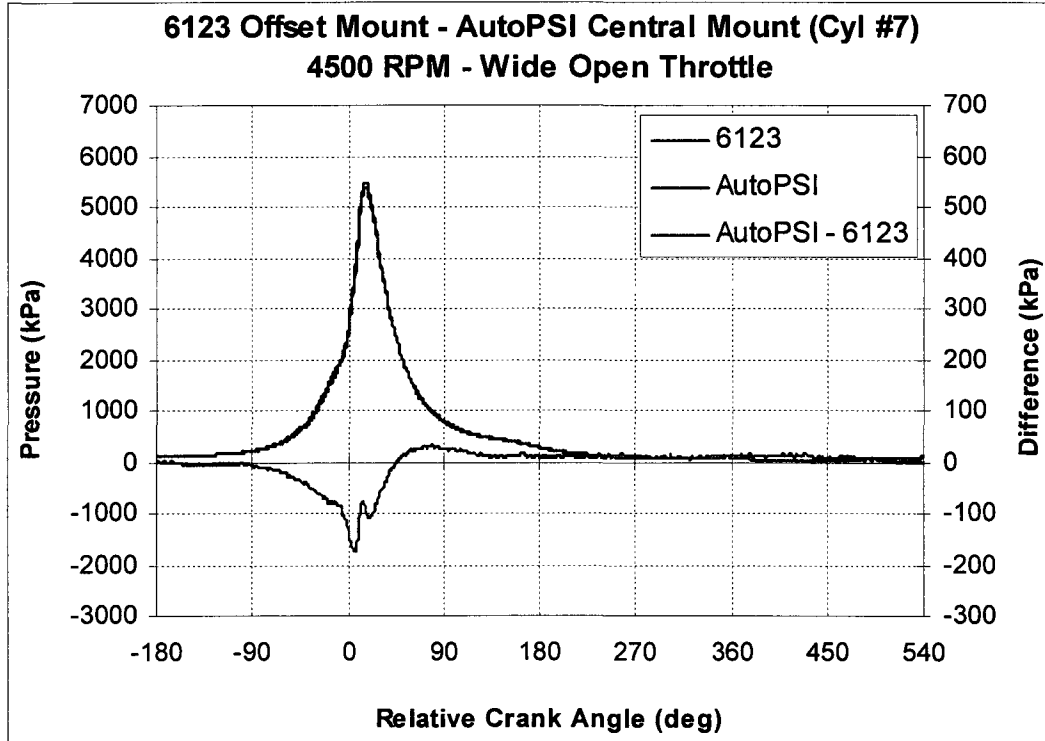
B.6 a – Pressure Traces - 6123 Offset / 6117 (Cyl #6) – 4500 RPM / WOT



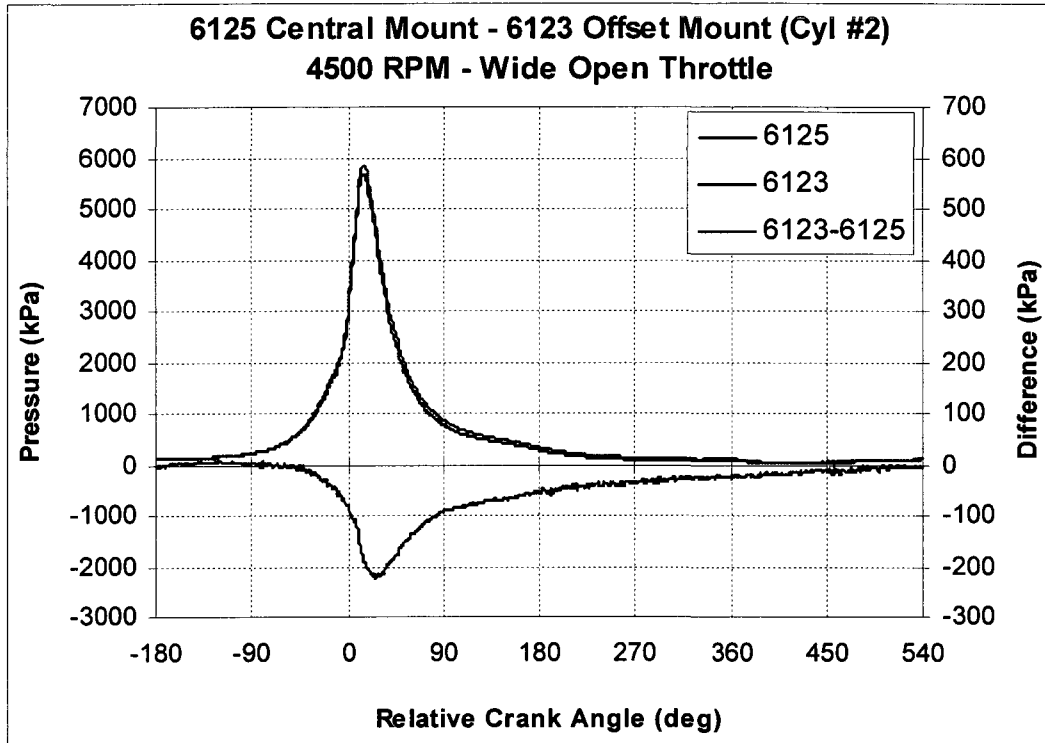
B.6 b – Pressure Traces - 6123 Offset / 6117 (Cyl #7) – 4500 RPM / WOT



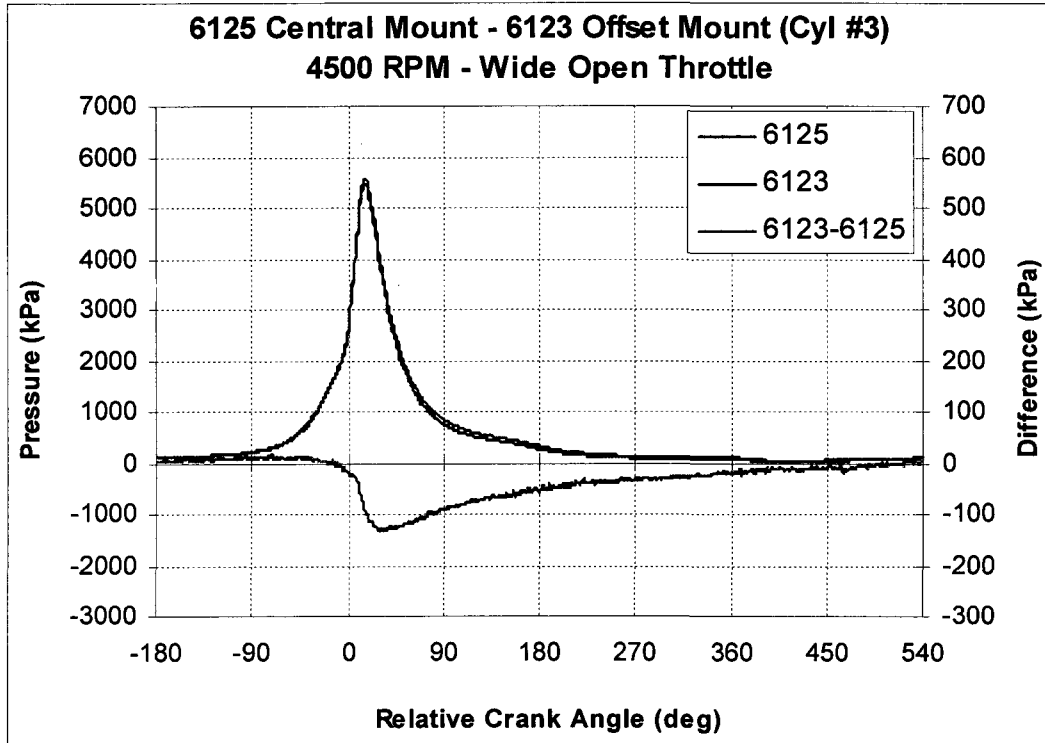
B.6 c – Pressure Traces – 6123 Offset / AutoPSI Central (Cyl #6) – 4500 RPM / WOT



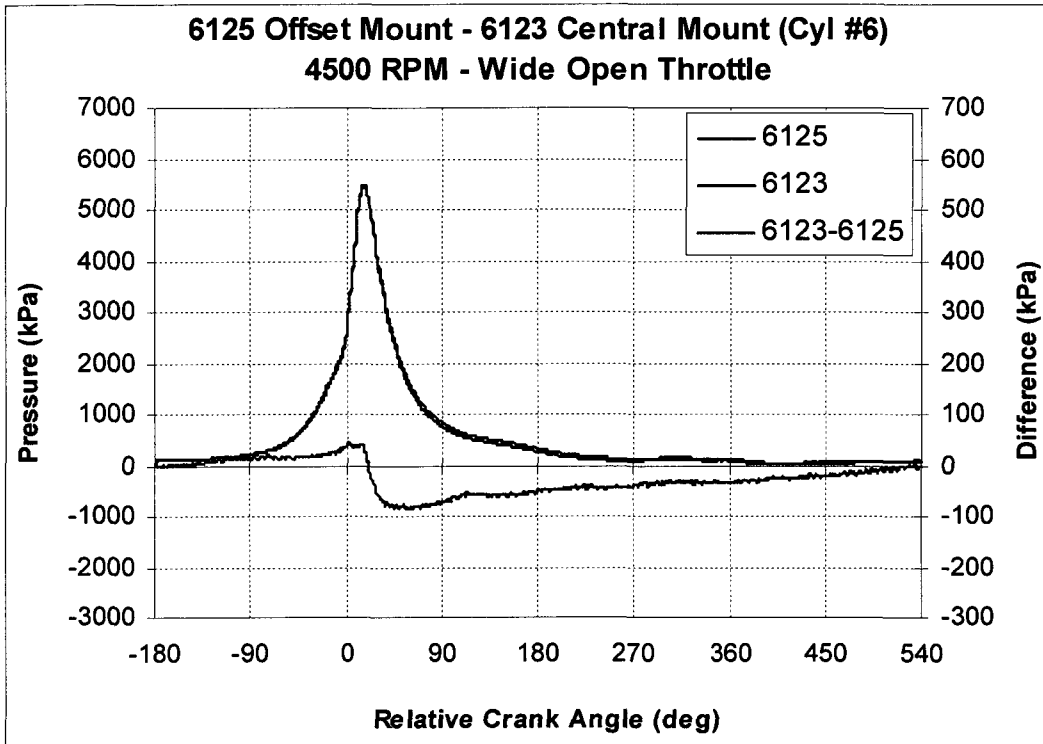
B.6 d – Pressure Traces – 6123 Offset / AutoPSI Central (Cyl #7) – 4500 RPM / WOT



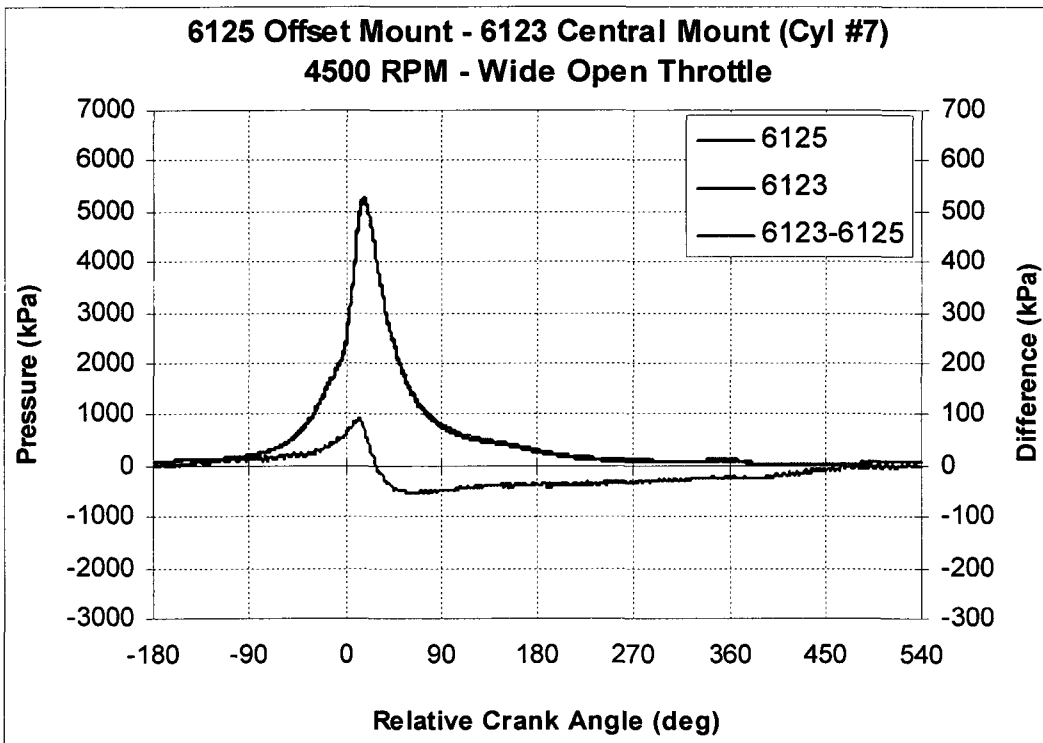
B.6 e – Pressure Traces – 6125 Central / 6123 Offset (Cyl #2) – 4500 RPM / WOT



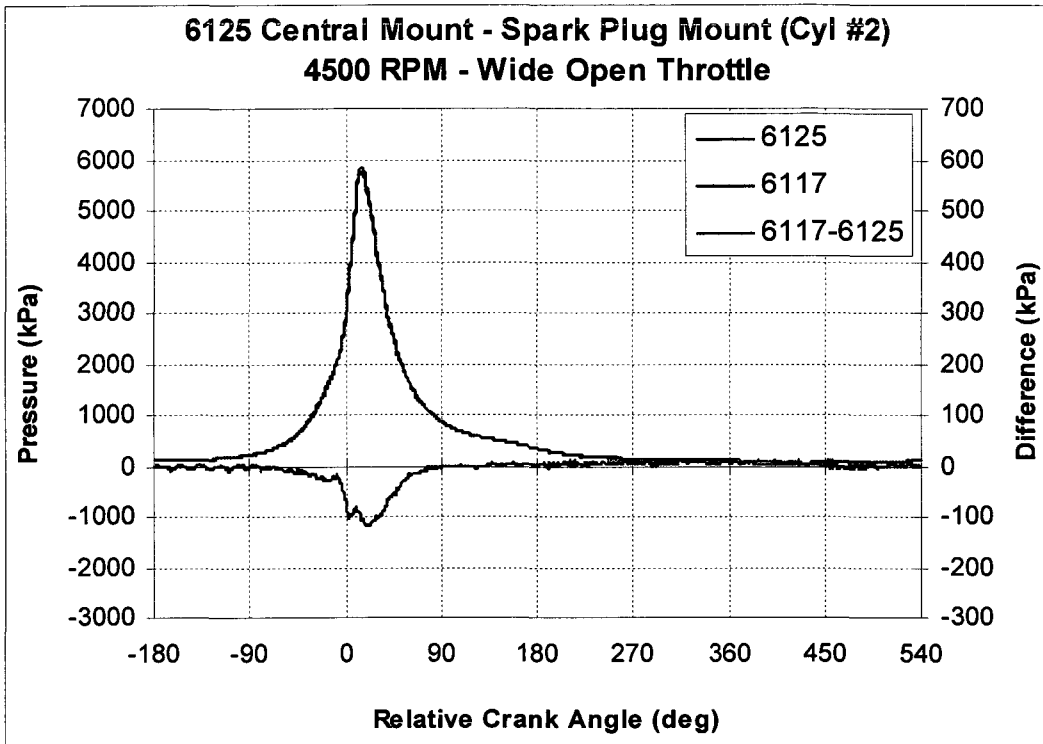
B.6 f – Pressure Traces – 6125 Central / 6123 Offset (Cyl #3) – 4500 RPM / WOT



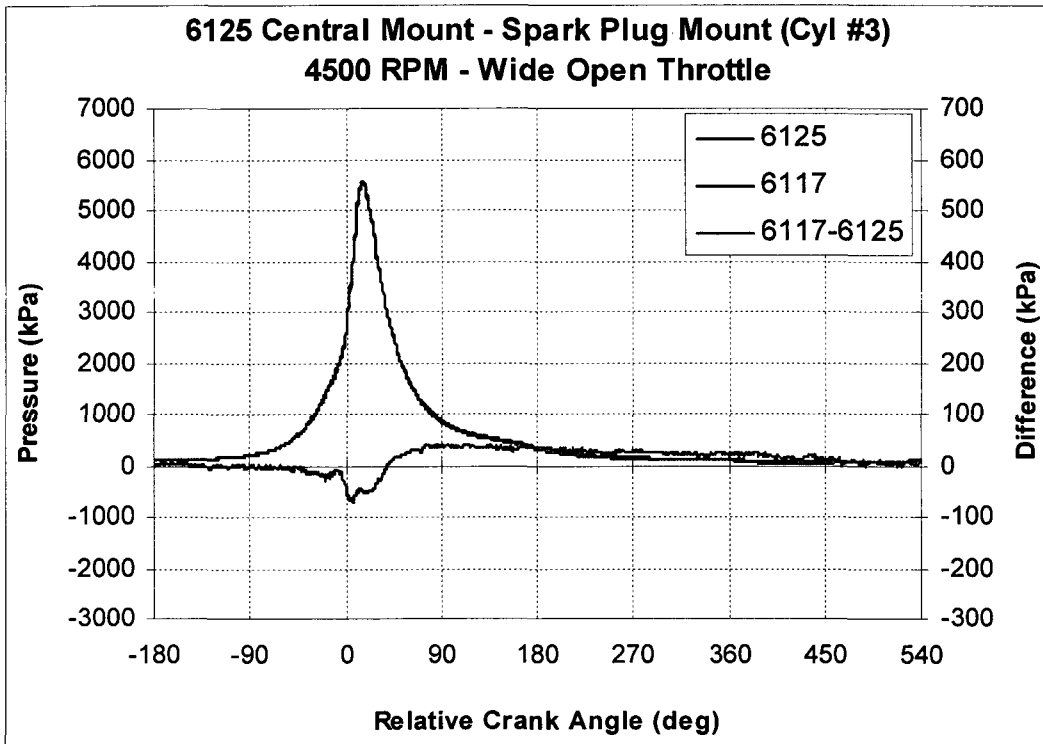
B.6 g – Pressure Traces – 6125 Offset / 6123 Central (Cyl #6) – 4500 RPM / WOT



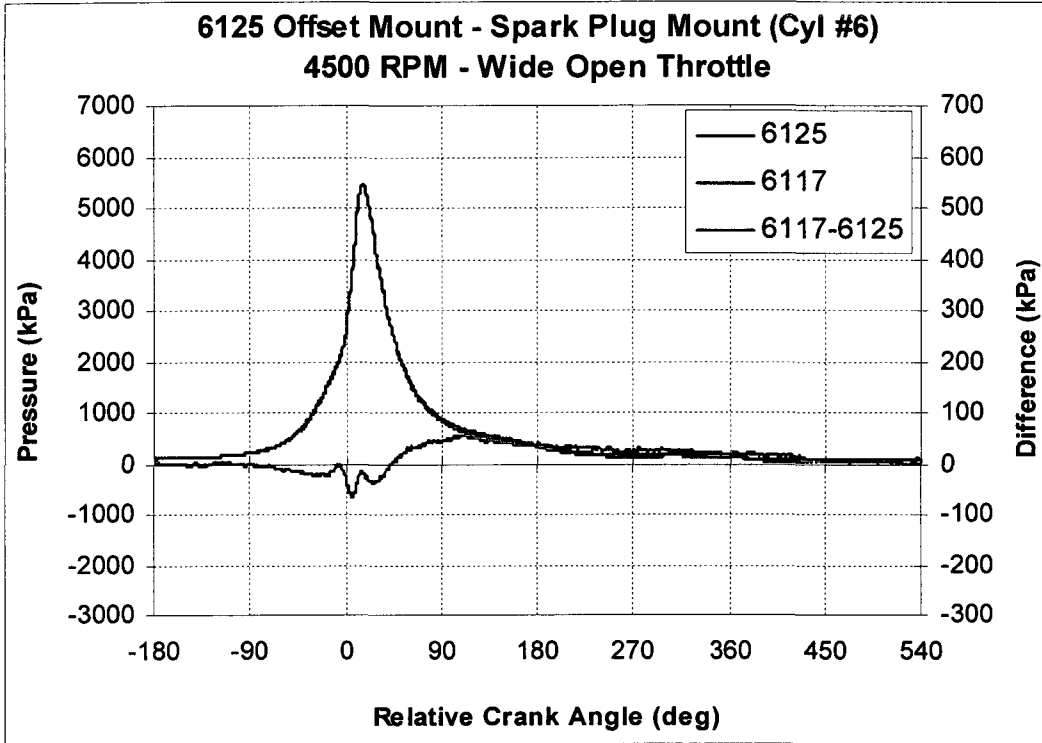
B.6 h – Pressure Traces – 6125 Offset / 6123 Central (Cyl #7) – 4500 RPM / WOT



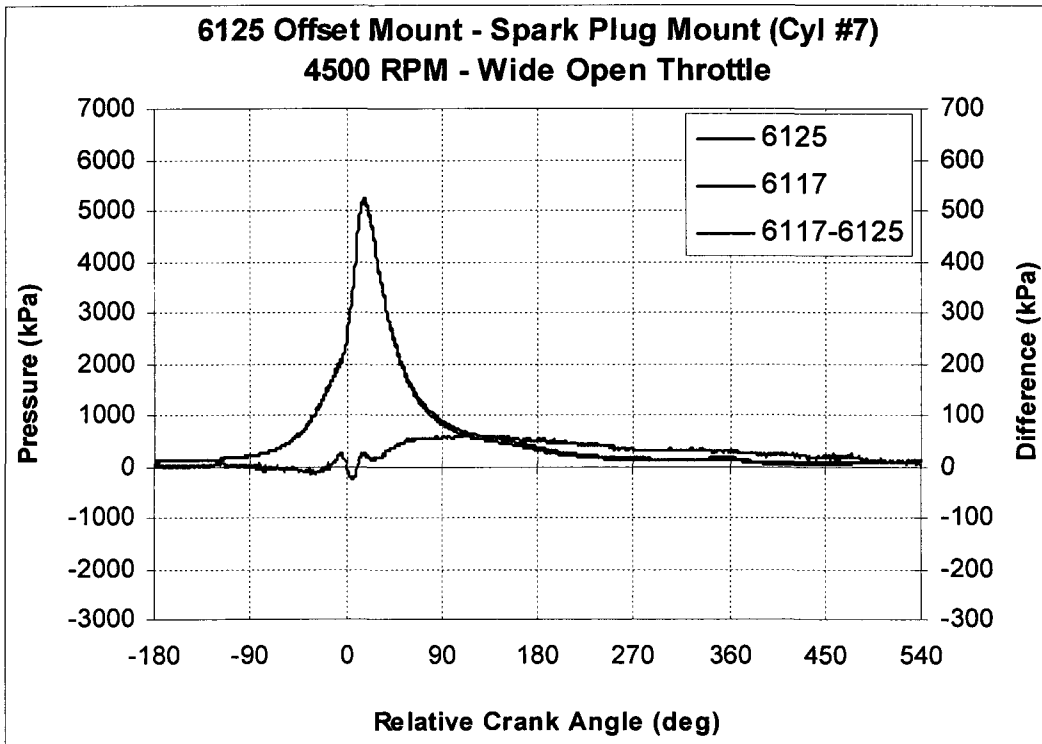
B.6 i – Pressure Traces – 6125 Central / 6117 (Cyl #2) – 4500 RPM / WOT



B.6 j – Pressure Traces – 6125 Central / 6117 (Cyl #3) – 4500 RPM / WOT



B.6 k – Pressure Traces – 6125 Offset / 6117 (Cyl #6) – 4500 RPM / WOT



B.6 l – Pressure Traces – 6125 Offset / 6117 (Cyl #7) – 4500 RPM / WOT

APPENDIX C

SUPPLEMENTAL DATA – KNOCK VALIDATION

TABLES

C.1	Signal to Noise Ratio Results	203
C.2	Main Effects Results	204
C.3	Accelerometer Usage Table	205

FIGURES

C.1 MD / IntS Sweeps – 1000 RPM, Cylinder #1 208

a.	Head #2	206
b.	Head #3	206
c.	Head #5	206
d.	Head #6	207
e.	Head #7	207
f.	Head #8	207
g.	Head #9	208
h.	Head #10	208
i.	Head #12	208
j.	Head #14	209
k.	Head #15	209

C.2 MD / Int Sweeps – 1000 RPM, Head #2212

a.	IntS, Cylinder #1	210
b.	IntD, Cylinder #1	210
c.	IntV, Cylinder #1	210
d.	IntS, Cylinder #2	211
e.	IntD, Cylinder #2	211
f.	IntV, Cylinder #2	211

g. IntS, Cylinder #3	212
h. IntD, Cylinder #3	212
i. IntV, Cylinder #3	212
j. IntS, Cylinder #4	213
k. IntD, Cylinder #4	213
l. IntV, Cylinder #4	213
m. IntS, Cylinder #5	214
n. IntD, Cylinder #5	214
o. IntV, Cylinder #5	214
p. IntS, Cylinder #6	215
q. IntD, Cylinder #6	215
r. IntV, Cylinder #6	215
s. IntS, Cylinder #7	216
t. IntD, Cylinder #7	216
u. IntV, Cylinder #7	216
v. IntS, Cylinder #8	217
w. IntD, Cylinder #8	217
x. IntV, Cylinder #8	217

C.3 MD / IntS Sweeps – Head #2 220

a. 1500 RPM, Cylinder #1	218
b. 1500 RPM, Cylinder #2	218
c. 1500 RPM, Cylinder #3	219
d. 1500 RPM, Cylinder #4	219
e. 1500 RPM, Cylinder #5	220
f. 1500 RPM, Cylinder #6	220
g. 1500 RPM, Cylinder #7	221
h. 1500 RPM, Cylinder #8	221
i. 2500 RPM, Cylinder #1	222
j. 2500 RPM, Cylinder #2	222
k. 2500 RPM, Cylinder #3	223

l. 2500 RPM, Cylinder #4	223
m. 2500 RPM, Cylinder #5	224
n. 2500 RPM, Cylinder #6	224
o. 2500 RPM, Cylinder #7	225
p. 2500 RPM, Cylinder #8	225
q. 3500 RPM, Cylinder #1	226
r. 3500 RPM, Cylinder #2	226
s. 3500 RPM, Cylinder #3	227
t. 3500 RPM, Cylinder #4	227
u. 3500 RPM, Cylinder #5	228
v. 3500 RPM, Cylinder #6	228
w. 3500 RPM, Cylinder #7	229
x. 3500 RPM, Cylinder #8	229
y. 4500 RPM, Cylinder #1	230
z. 4500 RPM, Cylinder #2	230
aa. 4500 RPM, Cylinder #3	231
bb. 4500 RPM, Cylinder #4	231
cc. 4500 RPM, Cylinder #5	232
dd. 4500 RPM, Cylinder #6	232
ee. 4500 RPM, Cylinder #7	233
ff. 4500 RPM, Cylinder #8	233

C.4 MD / IntS Normalized Sweeps – 1000 RPM, Cyl. #1 236

a. Head #2	234
b. Head #3	234
c. Head #5	234
d. Head #6	235
e. Head #7	235
f. Head #8	235
g. Head #9	236
h. Head #10	236

i. Head #12	236
j. Head #14	237
k. Head #15	237
C.5 MD / Int Normalized Sweeps – 1000 RPM, Head #2	238
a. IntS, Cylinder #1	238
b. IntD, Cylinder #1	238
c. IntV, Cylinder #1	238
d. IntS, Cylinder #2	239
e. IntD, Cylinder #2	239
f. IntV, Cylinder #2	239
g. IntS, Cylinder #3	240
h. IntD, Cylinder #3	240
i. IntV, Cylinder #3	240
j. IntS, Cylinder #4	241
k. IntD, Cylinder #4	241
l. IntV, Cylinder #4	241
m. IntS, Cylinder #5	242
n. IntD, Cylinder #5	242
o. IntV, Cylinder #5	242
p. IntS, Cylinder #6	243
q. IntD, Cylinder #6	243
r. IntV, Cylinder #6	243
s. IntS, Cylinder #7	244
t. IntD, Cylinder #7	244
u. IntV, Cylinder #7	244
v. IntS, Cylinder #8	245
w. IntD, Cylinder #8	245
x. IntV, Cylinder #8	245

C.6 MD / IntS Normalized Sweeps - Head #2 248

a. 1500 RPM, Cylinder #1	246
b. 1500 RPM, Cylinder #2	246
c. 1500 RPM, Cylinder #3	247
d. 1500 RPM, Cylinder #4	247
e. 1500 RPM, Cylinder #5	248
f. 1500 RPM, Cylinder #6	248
g. 1500 RPM, Cylinder #7	249
h. 1500 RPM, Cylinder #8	249
i. 2500 RPM, Cylinder #1	250
j. 2500 RPM, Cylinder #2	250
k. 2500 RPM, Cylinder #3	251
l. 2500 RPM, Cylinder #4	251
m. 2500 RPM, Cylinder #5	252
n. 2500 RPM, Cylinder #6	252
o. 2500 RPM, Cylinder #7	253
p. 2500 RPM, Cylinder #8	253
q. 3500 RPM, Cylinder #1	254
r. 3500 RPM, Cylinder #2	254
s. 3500 RPM, Cylinder #3	255
t. 3500 RPM, Cylinder #4	255
u. 3500 RPM, Cylinder #5	256
v. 3500 RPM, Cylinder #6	256
w. 3500 RPM, Cylinder #7	257
x. 3500 RPM, Cylinder #8	257
y. 4500 RPM, Cylinder #1	258
z. 4500 RPM, Cylinder #2	258
aa. 4500 RPM, Cylinder #3	259
bb. 4500 RPM, Cylinder #4	259
cc. 4500 RPM, Cylinder #5	260
dd. 4500 RPM, Cylinder #6	260

ee. 4500 RPM, Cylinder #7	261
ff. 4500 RPM, Cylinder #8	261

C.7 Normalized Intensity 264

a. IntS, 1000 RPM	262
b. IntD, 1000 RPM	262
c. IntV, 1000 RPM	262
d. IntS, 1500 RPM	263
e. IntD, 1500 RPM	263
f. IntV, 1500 RPM	263
g. IntS, 2500 RPM	264
h. IntD, 2500 RPM	264
i. IntV, 2500 RPM	264
j. IntS, 3500 RPM	265
k. IntD, 3500 RPM	265
l. IntV, 3500 RPM	265
m. IntS, 4500 RPM	266
n. IntD, 4500 RPM	266
o. IntV, 4500 RPM	266

Table C. 1 – Signal to Noise Ratio Results

SPEED	Cyl Used	INTS								INTD								INTV							
		C1	C2	C3	C4	C5	C6	C7	C8	C1	C2	C3	C4	C5	C6	C7	C8	C1	C2	C3	C4	C5	C6	C7	C8
1000	11111111	26.0	26.5	29.3	28.5	33.4	30.7	34.1	29.7	26.7	22.4	28.7	25.2	30.8	28.1	33.9	19.7	27.7	22.8	28.3	24.2	30.4	25.9	31.0	18.6
	11111000	29.1	30.1	33.9	32.6	36.3	16.2	7.2	-1.4	30.6	23.6	33.0	30.1	33.0	12.9	3.0	-3.2	32.1	24.7	33.0	28.5	29.0	8.8	1.6	2.0
	11000110	26.9	28.8	20.8	7.4	28.8	27.9	38.6	34.5	30.7	12.2	31.6	13.6	29.1	23.2	36.6	23.8	32.0	18.3	29.5	20.7	30.7	19.5	34.2	22.8
	10100101	29.6	28.1	32.0	25.8	29.4	32.5	25.6	17.2	32.5	20.4	29.8	26.2	28.3	24.7	29.1	-7.0	32.8	20.2	30.4	29.0	28.6	24.9	28.9	-2.4
	00100101	26.6	25.6	21.1	34.0	26.3	17.9	36.8	23.2	30.8	16.8	23.6	27.6	22.1	24.4	35.4	7.4	32.0	19.2	21.4	29.8	25.2	25.0	33.5	8.3
	10001001	25.9	20.1	7.2	-12.1	40.7	18.8	32.6	35.1	32.1	16.4	24.4	14.2	37.4	15.3	28.8	22.8	34.0	20.1	21.4	11.6	35.6	8.5	32.0	21.4
	01001100	27.6	29.9	25.2	-9.1	39.6	33.5	28.5	20.4	23.2	10.6	33.3	15.7	36.3	27.8	31.7	2.2	27.7	21.0	29.8	23.8	35.5	25.7	31.3	1.7
	01010011	27.5	29.3	24.5	34.0	29.2	10.4	30.2	33.1	22.4	12.3	33.7	27.5	20.2	24.2	26.3	20.1	27.2	21.7	30.2	29.8	23.6	24.1	29.6	19.1
	01100010	30.3	31.9	33.4	30.1	18.0	18.9	38.3	21.7	25.6	23.9	35.3	31.4	15.0	8.9	37.3	9.6	29.2	26.7	33.6	31.1	15.8	1.9	35.2	7.6
	00011100	1.8	8.5	17.7	33.4	39.6	33.0	37.8	21.2	9.1	-3.5	10.1	27.4	35.2	32.3	37.7	11.3	9.3	3.6	11.5	29.7	38.1	28.1	35.5	13.5
	00101011	18.5	24.2	29.4	24.8	37.1	25.9	36.7	33.9	20.6	-0.4	26.9	24.3	34.3	23.1	36.4	24.2	26.1	16.3	28.4	27.1	33.7	20.3	33.0	22.9
	00110101	16.5	21.2	33.3	33.8	29.4	29.6	30.8	33.2	1.2	-6.9	32.4	27.9	29.8	23.1	27.8	22.3	4.5	5.8	33.9	30.2	31.0	19.1	30.5	21.9
1500	11111111	23.0	23.8	23.8	27.2	25.5	28.1	29.5	32.3	24.2	18.5	26.0	24.5	26.4	23.4	29.0	28.1	24.6	20.9	24.6	24.1	25.6	25.1	29.9	29.3
	11111000	26.8	28.0	28.5	30.2	28.9	18.1	1.2	-5.6	26.6	14.3	29.9	29.0	29.5	12.8	-1.7	-9.1	28.3	23.1	29.5	28.4	26.4	11.5	-0.7	-3.6
	11000110	23.4	27.9	20.9	11.9	16.8	30.9	34.3	37.2	27.3	13.1	28.1	13.2	23.9	23.3	33.5	32.9	27.6	20.1	26.8	14.5	20.6	26.0	33.5	34.0
	10100101	26.3	26.9	28.6	25.3	19.2	33.4	18.2	9.9	28.9	18.1	28.4	22.4	23.9	24.0	26.6	-6.1	29.9	21.8	29.1	19.3	22.7	24.8	27.7	4.3
	10010010	24.8	24.2	18.5	33.2	13.1	26.8	33.8	25.6	28.2	16.6	18.3	29.1	15.5	22.1	34.7	3.9	29.5	21.2	19.1	28.8	17.8	23.7	33.2	12.2
	00100101	21.8	19.4	0.3	-3.3	33.1	22.2	29.0	39.4	29.4	15.7	17.1	7.0	33.9	16.6	31.0	30.7	31.1	22.5	8.5	4.1	31.7	15.7	30.1	31.7
	01001100	24.1	29.0	23.0	12.1	32.1	34.3	19.2	12.2	21.7	15.8	29.6	13.9	32.5	25.1	32.1	-1.8	24.9	23.1	27.5	16.3	11.6	24.7	30.9	9.0
	01010011	24.6	29.5	23.3	33.3	5.8	20.4	26.6	37.3	21.8	15.6	30.0	29.3	11.7	21.3	28.4	27.4	25.0	23.9	27.2	28.9	14.4	22.5	27.9	29.6
	01100010	28.5	31.6	30.7	28.3	11.8	27.9	35.2	26.8	22.9	19.9	32.4	26.5	14.0	9.0	36.6	6.2	26.9	27.2	31.9	19.7	15.4	4.2	32.4	12.4
	00111100	-9.0	1.9	16.7	33.3	31.7	37.7	35.0	26.9	3.9	-9.7	10.9	29.0	32.4	28.6	35.0	6.9	3.3	-1.5	17.1	27.9	31.6	29.2	34.2	12.9
	00101011	16.8	22.4	26.4	22.9	29.9	28.6	32.7	37.1	19.6	14.0	26.3	21.3	30.4	19.6	33.7	32.9	20.8	19.4	27.1	16.5	28.6	19.9	33.7	34.0
	00110101	6.8	24.3	29.3	33.7	18.5	32.6	26.9	37.5	6.6	-8.4	30.1	29.3	23.3	22.7	29.4	30.6	5.5	8.4	30.0	29.3	21.4	21.6	28.4	31.6
2500	11111111	20.3	25.0	21.1	23.6	21.1	25.1	19.8	18.9	12.8	17.4	17.8	20.5	18.8	11.1	22.2	16.6	15.2	22.2	17.3	21.6	18.8	17.5	23.6	12.7
	11111000	24.5	27.7	24.4	27.0	24.4	18.2	2.1	-10.3	15.2	18.5	17.4	23.4	21.6	6.1	-0.8	-8.4	15.7	24.7	20.4	24.1	21.5	7.3	-3.4	-8.3
	11000110	20.1	27.6	19.4	5.4	11.4	28.2	22.5	22.7	15.1	16.7	-1.1	1.5	12.9	10.8	23.6	21.5	15.0	24.8	8.0	8.6	11.9	19.7	26.3	17.6
	10100101	15.5	20.2	23.9	14.5	12.0	30.0	16.1	5.5	18.3	15.6	13.0	4.6	10.3	13.2	18.7	-4.5	18.0	23.8	13.6	8.9	-12.7	20.6	19.4	-7.1
	10010010	15.5	18.3	12.6	25.6	1.3	19.9	25.0	18.4	14.7	17.0	15.5	22.0	1.7	4.1	25.3	7.9	17.4	24.5	18.1	22.2	-0.6	2.2	28.0	-3.4
	00100101	14.1	11.4	-14.2	-10.2	28.5	20.9	19.8	26.3	15.0	18.6	-1.9	-3.3	25.1	5.6	19.9	21.7	14.4	26.2	-0.9	-9.3	26.1	11.3	22.2	17.8
	01001100	20.3	27.8	18.1	5.6	26.5	29.8	14.8	7.1	5.2	18.1	12.2	4.9	24.1	7.8	19.9	-3.9	6.5	24.0	11.2	6.5	24.0	21.0	27.7	1.9
	01010011	20.9	28.2	19.3	25.6	-17.5	9.3	18.2	24.6	3.9	20.7	19.2	21.9	1.0	0.5	18.2	20.7	3.2	25.5	19.1	22.4	-2.8	1.4	20.4	17.0
	01100010	25.2	30.5	25.7	13.9	-17.8	20.4	26.8	19.5	11.8	23.3	-3.9	5.7	-5.8	2.5	26.4	8.1	9.6	28.4	14.6	5.9	-2.1	-0.9	29.2	-6.4
	00111100	-3.8	1.3	11.7	26.7	27.2	29.1	25.0	18.8	4.6	-12.3	13.0	22.1	24.1	5.9	25.4	9.3	4.3	-2.1	15.8	23.2	24.2	20.7	27.5	-1.7
	00101011	11.0	17.2	22.0	12.8	24.3	22.7	23.6	22.8	8.4	8.9	6.6	4.0	22.8	3.9	24.8	22.1	5.3	15.6	6.8	9.5	22.6	11.8	26.9	17.1
	00110101	1.1	16.8	24.7	28.2	11.9	26.7	19.8	24.4	5.8	9.9	14.8	23.8	10.2	4.9	20.2	20.9	0.6	13.8	20.3	24.9	10.8	19.4	21.8	16.8
3500	11111111	12.9	11.3	11.1	13.0	18.7	12.3	0.9	4.5	8.3	19.7	22.2	12.6	20.2	6.8	19.8	3.6	10.6	20.5	20.9	6.6	21.3	7.3	12.0	3.3
	11111000	16.9	12.7	10.0	16.2	19.2	11.9	-0.6	-5.5	8.9	23.3	25.6	12.8	16.3	-1.1	0.0	-6.5	12.1	23.2	22.2	3.9	18.3	2.0	1.5	-5.6
	11000110	13.4	12.2	6.6	-2.9	2.0	15.8	0.9	4.5	9.1	18.9	19.1	1.2	0.6	6.5	23.4	1.8	7.3	17.7	20.6	0.6	0.7	9.4	11.7	3.7
	10100101	6.1	4.3	10.1	5.0	0.9	17.3	0.1	-5.2	7.3	12.6	27.3	-4.5	1.4	8.9	1.9	-4.7	8.9	12.8	22.9	-3.6	1.2	6.2	9.8	-4.8
	10010010	2.6	1.4	-0.7	15.9	-0.9	7.7	4.3	-2.2	3.0	12.9	18.6	11.9	0.8	3.8	18.0	3.3	0.9	12.5	7.6	4.9	-7.8	3.3	16.1	-4.9
	00100101	8.9	4.5	-2.5	-11.0	22.3	11.9	2.4	5.0	-3.3	15.1	3.3	-6.4	19.9	1.4	11.2	2.9	8.7	14.7	-10.8	-12.3	22.4	5.5	11.5	1.3
	01001100	13.5	13.2	11.4	-5.8	22.8	11.5	-13.3	-4.6	4.7	19.5	15.0	-2.6	22.5	9.1	4.1	-6.2	8.3	19.0	17.6	-6.3	25.9	7.3	3.4	-12.5
	01010011	10.1	14.5	1.3	15.4	-1.5	1.5	3.0	6.6	-3.2	20.0	20.8	12.9	0.0	2.5	10.7	4.5	-3.5	19.1	16.7	6.7	-12.3	1.0	12.5	0.5
	01100010	14.5	14.2	7.3	3.8	-6.5	4.8	-2.0	-0.4	-0.3	23.8	28.1	-0.3	-7.7	4.0	16.7	-2.4	-1.1	23.0	20.8	-20.4	-11.1	4.5	13.2	-17.9
	00111100	-3.0	-0.4	3.7	16.0	23.5	9.8	0.5	0.3	2.5	-6.8	18.9	9.5	20.2	2.3	17.5	1.1	3.0	-4.0	10.2	0.2	22.6	6.4	11.1	-13.8
	00101011	-2.3	4.0	10.8	2.5	19.5	1.7	-4.2	4.0	2.8	5.5	25.5	-1.9	20.2	4.3	20.7	-7.2	3.1	8.1	21.8	-6.5	21.6	-1.3	15.0	1.1
	00110101	-3.9	5.0	8.4	18.1	-0.1	8.6	0.8	7.1	0.9	8.3	25.5	12.8	0.0	-2.0	11.2	2.8	-7.1	7.0	21.7	7.4	-0.8	5.1	13.1	0.5
4500	11111111	4.9	18.5	14.5	7.9	3.9	2.6	3.4	3.4	4.9	13.7	16.7	-5.7	-5.2	-0.3	10.1	5.1	7.3	14.6	19.6	3.7	-4.1	3.4	11.6	0.2
	11111000	7.2	19.9	17.9	10.0	0.8	-0.8	-2.8	-10.1	5.7	12.9	16.6	-13.5	-16.1	-8.9	-5.0	-5.3	9.2	17.4	23.2	0.4	-4.1	-1.9	-1.3	-8.7
	11000110	0.2	21.7	4.0	-6.6	-4.4	-2.5	4.6	1.0	3.6	17.7	9.8	-4.9	-5.0	-2.7	14.3	7.3	4.1	18.3	9.1	-7.3	-8.9	4.9	13.0	1.2
	10100101	4.3	8.0	12.7	1.6	-0.9	4.1	-2.6	-4.9	4.2	15.2	21.5	-8.2	-10.7	-4.9	6.0	1.1	1.1	15.6	20.9	-6.8	-8.3	-2.2	4.0	-11.3
	10010010	3.5	6.2	5.0	11.4	-2.3	1.2	4.2	0.3	-7.7	14.2	7.6	-4.9	-21.6	-10.5	13.4	6.6	3.0	15.8	14.7	-0.9	-9.3	1.1	13.7	-8.0</

Table C. 2 - Main Effects Results

SPEED	Cyl Accel	INTS								INTD								INTV							
		C1	C2	C3	C4	C5	C6	C7	C8	C1	C2	C3	C4	C5	C6	C7	C8	C1	C2	C3	C4	C5	C6	C7	C8
1000	A1	41.9	14.4	-19.2	-30.8	2.2	-7.3	-27.4	-25.3	81.3	75.7	-0.6	-17.2	7.8	-10.7	-30.4	-26.1	66.6	30.0	-3.4	-27.8	4.0	-6.4	-33.9	-16.0
	A2	48.7	48.8	26.3	-16.1	-17.2	-20.2	-23.2	-25.8	32.8	62.1	48.5	-4.1	-22.7	-17.8	-26.4	-8.9	37.3	49.7	37.4	0.9	-25.1	-20.0	-30.5	-13.7
	A3	13.7	19.9	74.8	88.0	-20.5	12.3	-31.8	-33.1	-10.9	18.2	29.3	39.0	-9.1	-26.3	-28.9	-22.1	-9.9	12.3	43.8	24.7	-18.3	-29.9	-36.1	-16.1
	A4	-31.3	-21.7	11.8	129.3	0.6	-19.8	-23.2	-23.9	-43.9	-18.3	-19.7	40.3	-9.3	22.2	-35.8	2.0	-49.2	-24.6	-14.7	28.9	-4.7	30.2	-32.8	9.3
	A5	-28.5	-25.7	-22.3	-66.9	66.7	20.8	-23.5	-24.0	-0.9	-9.6	-30.2	-17.3	62.6	11.1	-20.9	0.9	-0.8	-3.1	-26.6	-25.9	45.2	2.7	-27.6	2.8
	A6	-29.5	-18.1	8.8	-23.4	12.7	79.0	13.6	10.6	-38.7	-37.4	-11.0	-19.2	27.5	50.4	29.6	-8.7	-46.6	-36.8	-4.5	-0.4	29.4	54.6	26.4	-5.2
	A7	-26.2	-13.0	-4.4	53.2	-21.5	13.4	67.4	26.7	1.5	-5.0	-30.4	7.9	-16.5	12.1	70.9	38.8	-1.9	-6.3	-25.9	9.8	-11.5	9.7	48.5	29.9
	A8	-3.8	-4.1	-18.9	-30.3	9.4	-8.6	28.8	97.4	-18.0	-35.9	12.5	-25.8	9.8	5.9	15.6	112.5	-11.6	-10.7	11.9	-28.4	14.6	3.0	24.3	95.9
	A9	25.3	23.0	15.3	12.7	2.1	6.3	6.6	13.1	27.0	16.6	9.2	1.8	-9.5	36.7	21.7	-20.1	32.5	21.6	5.7	11.9	-1.2	69.8	18.2	-21.2
1500	A1	54.3	11.4	-29.0	-37.2	6.8	-17.8	-29.7	-39.0	68.2	48.1	-12.4	-24.3	8.8	-4.1	-40.3	-21.7	64.5	29.1	-23.3	-19.5	2.0	4.5	-33.8	-21.5
	A2	63.0	50.9	30.5	-0.3	-24.8	-17.7	-29.6	-36.2	27.8	50.2	44.0	-1.6	-21.4	-18.8	-34.5	-15.2	37.3	46.5	36.7	6.2	-19.6	-20.7	-33.4	-16.2
	A3	18.4	25.1	64.5	48.9	1.2	0.3	-34.2	-40.6	-3.4	6.4	38.1	31.5	-2.6	-25.3	-39.2	-17.5	-5.5	11.5	46.0	16.8	-7.5	-34.7	-38.5	-21.3
	A4	-44.0	-25.5	10.1	96.5	-19.4	-17.5	-15.7	-8.6	-38.5	-48.6	-17.9	66.0	-19.8	13.4	-40.8	-6.9	-44.9	-38.3	-3.4	76.9	-13.3	18.1	-35.2	-13.3
	A5	-30.8	-40.0	-32.6	-41.4	96.2	-7.1	-28.4	-32.2	-10.1	-5.3	-28.4	-25.0	73.0	3.5	-32.0	-7.2	-11.4	-15.0	-29.9	-23.1	63.1	3.3	-25.1	-10.8
	A6	-48.7	-21.4	14.5	-2.9	21.3	49.1	4.5	-4.6	-35.8	-47.7	-1.8	-9.8	27.4	45.6	24.9	-1.3	-45.8	-44.5	11.8	5.1	19.4	53.8	28.0	4.6
	A7	-23.0	-25.3	4.0	23.8	-8.8	15.0	79.6	65.3	-8.9	2.2	-24.3	12.5	-12.1	3.6	54.7	39.3	-12.2	-15.5	-5.2	5.4	-8.4	7.4	62.5	32.1
	A8	-4.9	5.6	-21.9	-38.4	-7.2	-11.3	36.3	125.1	-3.5	-7.5	7.0	-25.3	1.8	6.4	19.7	182.7	-8.0	0.4	-10.0	-22.9	-2.9	12.7	25.8	142.9
	A9	41.5	22.6	17.5	18.2	-15.2	6.3	-1.7	-7.7	27.7	52.7	9.2	6.4	-16.5	22.6	22.6	-13.6	32.1	30.4	11.0	10.0	-6.2	32.6	25.3	-0.5
2500	A1	35.3	8.6	-34.3	-27.0	44.1	2.1	-22.8	-36.6	53.5	36.1	-1.2	-13.6	15.1	25.7	-25.9	-20.3	66.0	40.9	-11.4	-18.2	13.2	5.2	-31.6	-15.5
	A2	77.7	81.3	47.2	3.5	-57.0	-20.2	-25.0	-33.9	-0.7	57.0	0.5	4.6	-22.5	1.0	-24.8	-20.7	5.4	47.9	16.9	12.1	-24.2	-20.2	-28.0	-5.0
	A3	10.6	23.0	74.9	41.3	-1.4	7.9	-17.4	-37.2	11.7	14.8	8.8	13.0	-11.9	7.1	-20.8	-20.3	3.8	5.6	21.5	19.1	1.6	-0.6	-28.6	-24.5
	A4	-27.7	-17.1	19.0	114.9	-16.2	-21.9	-13.7	-9.3	-14.5	-30.2	72.7	116.3	-12.9	-10.9	-23.0	4.1	-12.6	-34.3	57.7	110.1	-23.8	-15.0	-27.8	-7.8
	A5	-11.7	-31.5	-42.4	-27.6	150.7	9.1	-23.3	-31.4	-10.4	-33.8	7.5	-7.8	107.3	4.2	-21.0	-15.3	-2.5	-30.2	-23.1	-15.3	107.3	27.0	-26.5	5.1
	A6	-37.7	-14.8	29.0	9.2	66.9	59.5	2.5	-3.9	-5.2	-41.7	16.9	3.6	33.1	30.7	16.3	-10.1	-6.2	-38.4	8.1	17.1	37.7	85.9	17.0	6.2
	A7	-8.1	-12.0	16.3	17.2	-18.5	8.5	51.9	43.6	2.0	-30.5	-27.0	0.7	-18.7	0.3	51.6	41.1	8.6	-24.6	-2.9	15.7	-18.0	-10.0	69.3	-2.1
	A8	-9.8	0.7	-24.1	-27.8	6.1	-12.5	13.9	80.6	-10.9	12.0	-11.6	-14.4	15.6	-2.5	14.0	117.0	-18.0	4.8	-22.9	-10.8	7.6	10.1	18.8	124.0
	A9	22.3	21.2	25.3	16.7	-17.9	-8.6	1.5	-4.0	-6.1	23.0	46.0	4.6	-10.3	4.6	14.3	-12.4	5.8	19.9	8.0	11.7	-18.3	-3.1	16.3	2.6
3500	A1	32.0	-4.2	-8.1	-13.7	4.4	39.0	23.0	-11.9	25.8	32.3	-17.7	-3.7	4.0	6.1	-6.4	7.9	45.7	29.3	-27.4	18.9	10.3	10.5	-5.6	34.9
	A2	73.0	59.3	17.9	-6.8	-10.6	0.9	-15.1	-3.7	14.3	77.6	11.8	14.0	-10.7	9.0	-5.7	-3.3	16.1	71.4	47.4	1.2	-16.3	6.1	-22.2	-7.8
	A3	-1.4	6.2	38.0	30.9	-16.3	-1.8	-2.7	-5.1	15.0	13.4	58.5	6.1	-13.6	-4.5	-14.8	-21.6	1.8	15.5	70.4	-6.4	-1.1	9.1	-1.7	2.2
	A4	-18.4	-8.0	-10.1	103.1	-2.1	-11.3	25.0	7.5	0.0	-17.9	13.3	88.0	0.6	-21.8	-0.8	24.7	-19.1	-17.0	4.5	78.1	-19.6	-6.5	1.8	9.1
	A5	4.2	-6.4	11.6	-24.4	132.0	3.4	-21.3	-6.8	7.2	-20.2	-28.6	-9.1	124.2	-1.0	-8.6	-17.7	40.4	-10.5	-30.6	-9.9	162.4	-2.3	-22.0	-3.2
	A6	-11.6	-5.6	25.2	0.6	15.6	35.9	-13.0	-1.0	24.8	-28.3	6.1	-1.0	15.5	16.5	0.6	3.9	10.8	-27.5	33.4	28.8	39.8	26.8	-8.7	1.9
	A7	-13.8	-11.5	0.0	10.4	-7.2	-10.6	8.0	7.4	10.0	-24.7	14.7	7.1	-5.7	6.9	77.0	7.5	-3.5	-18.0	13.6	-10.3	-7.3	2.5	27.4	-7.8
	A8	-11.4	6.2	-6.1	-15.9	1.8	-11.2	14.5	49.3	-11.6	2.3	-17.1	3.3	7.4	-7.5	38.8	23.7	-13.1	0.7	-12.4	23.8	3.7	-2.8	20.6	70.1
	A9	-3.9	0.7	10.4	5.7	-0.8	-10.9	-11.3	-7.8	5.1	7.6	9.0	-0.2	15.8	24.4	-4.8	-6.5	5.4	10.3	20.7	22.4	-2.3	-9.1	6.8	14.6
4500	A1	37.8	-0.5	-13.8	-12.6	-10.6	6.2	-0.9	2.1	39.7	24.5	7.5	1.7	12.5	30.5	-0.9	17.6	66.7	22.8	-27.3	-11.9	19.1	28.5	-6.8	41.7
	A2	0.7	89.4	3.9	-10.0	-4.5	-11.7	-11.6	-9.6	-12.0	42.5	6.5	-5.8	40.7	15.5	-12.1	-5.3	0.7	43.8	24.2	-0.6	-10.7	-13.3	-20.7	-22.6
	A3	-6.5	5.8	46.6	10.3	-1.6	4.5	-17.0	-28.9	18.8	5.6	43.1	9.4	28.1	-8.2	-21.8	-26.3	-17.2	-7.6	82.4	5.0	-19.9	-19.8	-22.5	-8.0
	A4	2.8	-15.3	9.3	77.0	8.1	23.4	9.4	13.0	-18.4	-33.6	-18.5	-11.5	-18.7	-29.8	-24.9	-20.2	1.8	-21.6	45.6	82.7	-5.1	20.5	7.6	18.6
	A5	20.2	-15.7	18.3	-7.8	35.9	-2.2	-3.4	4.7	46.9	-33.5	0.8	-24.1	4.1	40.8	-12.0	3.6	46.3	-20.2	-41.1	-0.2	77.9	11.0	-12.4	25.2
	A6	-5.3	-10.5	9.0	-3.5	18.7	27.9	-7.5	14.9	41.2	-26.9	0.2	-17.4	36.5	23.0	-5.0	-11.4	5.4	-21.2	16.2	34.8	26.6	33.8	-5.6	29.0
	A7	-13.8	-14.4	-11.4	-4.3	0.2	-0.6	11.5	-1.6	-3.7	-20.4	-24.9	14.6	26.9	33.6	48.7	34.0	-7.6	-17.7	13.6	-1.5	11.0	6.0	16.3	7.3
	A8	-6.6	10.4	-6.9	-12.3	-7.8	-12.3	29.7	42.2	-2.9	14.4	9.2	28.1	10.9	-16.1	13.3	10.2	2.6	-5.0	-27.2	7.8	-13.4	13.0	48.0	58.9
	A9	5.5	3.0	5.4	10.3	13.8	8.9	-1.5	29.1	-17.5	20.6	29.2	2.7	37.9	21.4	4.1	8.7	6.8	9.1	23.7	23.2	16.0	-6.1	11.0	10.4

Table C. 3 - Accelerometer Usage Table

SPEED	INTS								INTD								INTV							
	C1	C2	C3	C4	C5	C6	C7	C8	C1	C2	C3	C4	C5	C6	C7	C8	C1	C2	C3	C4	C5	C6	C7	C8
1000	1	1	2	3	1	3	6	6	1	1	2	3	1	4	6	4	1	1	2	2	1	4	6	4
	2	2	3	4	4	5	7	7	2	2	3	4	5	5	7	5	2	2	3	3	5	5	7	5
	3	3	4	7	5	6	8	8	7	3	8	7	6	6	8	7	9	3	8	4	6	6	8	7
	9	9	6	9	6	7	9	9	9	9	9	9	8	7	9	8		9	9	7	8	7	9	8
			9		8	9								8						9		8		
					9									9								9		
1500	1	1	2	3	1	3	6	7	1	1	2	3	1	4	6	7	1	1	2	2	1	1	6	6
	2	2	3	4	3	6	7	8	2	2	3	4	5	5	7	8	2	2	3	3	5	4	7	7
	3	3	4	7	5	7	8		9	3	8	7	6	6	8		9	3	6	4	6	5	8	8
	9	8	6	9	6	9				7	9	9	8	7	9			8	9	6		6	9	
		9	7							9				8				9		7		7		
			9											9						9		8		
2500	1	1	2	2	1	1	6	7	1	1	2	2	1	1	6	4	1	1	2	2	1	1	6	5
	2	2	3	3	5	3	7	8	3	2	3	3	5	2	7	7	2	2	3	3	3	5	7	6
	3	3	4	4	6	5	8		7	3	4	4	6	3	8	8	3	3	4	4	5	6	8	8
	9	8	6	6	8	6	9			8	5	6	8	5	9		7	8	6	6	6	8	9	9
		9	7	7		7				9	6	7		6			9	9	9	7	8			
			9	9							9	9		7						9				
3500	1	2	2	3	1	1	1	4	1	1	2	2	1	1	6	1	1	1	2	1	1	1	4	1
	2	3	3	4	5	2	4	7	2	2	3	3	4	2	7	4	2	2	3	2	5	2	7	3
	5	8	5	6	6	5	7	8	3	3	4	4	5	6	8	6	3	3	4	4	6	6	8	4
		9	6	7	8	6	8		4	8	6	7	6	7		7	5	8	6	6	8	7	9	6
			7	9					5	9	7	8	8	9		8	6	9	7	8				8
			9						6		9		9				9		9	9				9
4500	1	2	2	3	4	1	4	1	1	1	1	1	1	1	7	1	1	1	2	3	1	1	4	1
	2	3	3	4	5	3	7	4	3	2	2	3	2	2	8	5	2	2	3	4	5	4	7	4
	4	8	4	9	6	4	8	5	5	3	3	7	3	5	9	7	4	9	4	6	6	5	8	5
	5	9	5		7	6		6	6	8	5	8	5	6		8	5		6	8	7	6	9	6
	9		6		9	9		8		9	6	9	6	7		9	6		7	9	9	7		7
			9					9			8		7	9			8		9			8		8
										9		8				9							9	
												9												

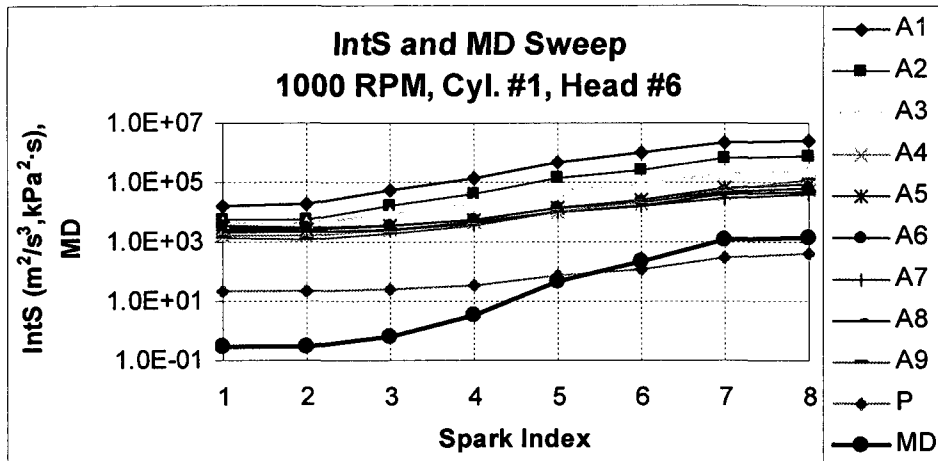


Figure C.1 d - MD / IntS Sweep - 1000 RPM, Cyl. #1, Head #6

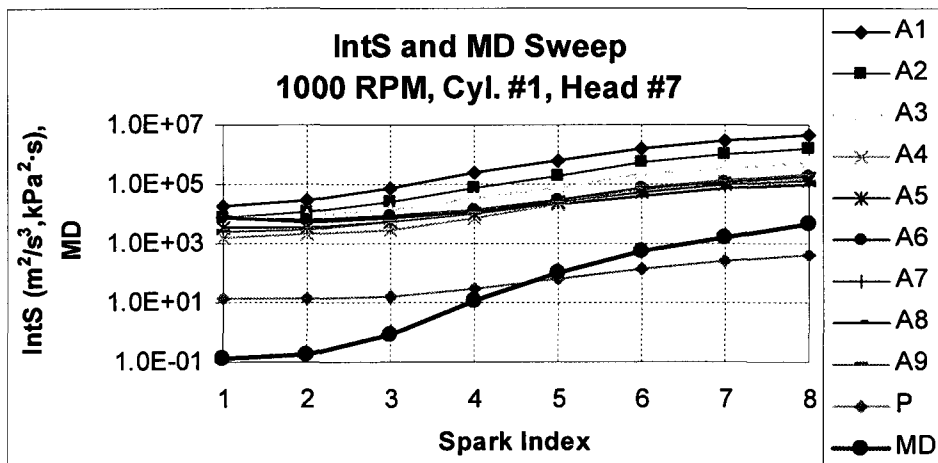


Figure C.1 e - MD / IntS Sweep - 1000 RPM, Cyl. #1, Head #7

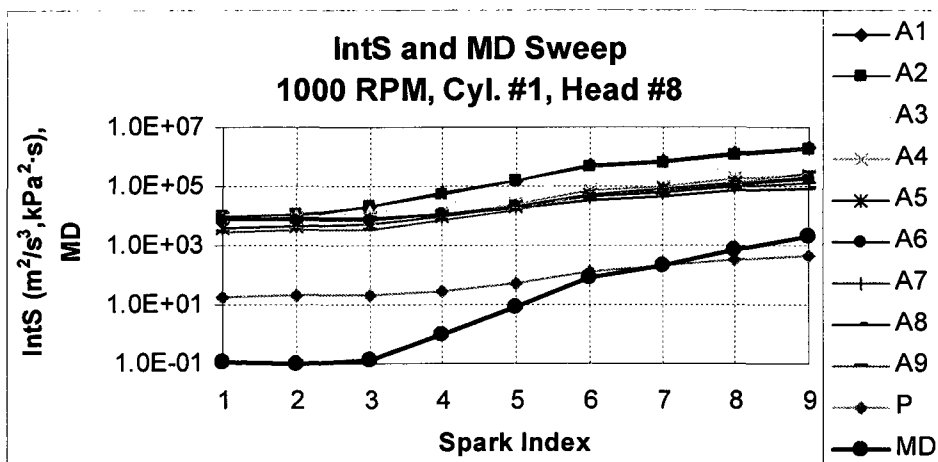


Figure C.1 f - MD / IntS Sweep - 1000 RPM, Cyl. #1, Head #8

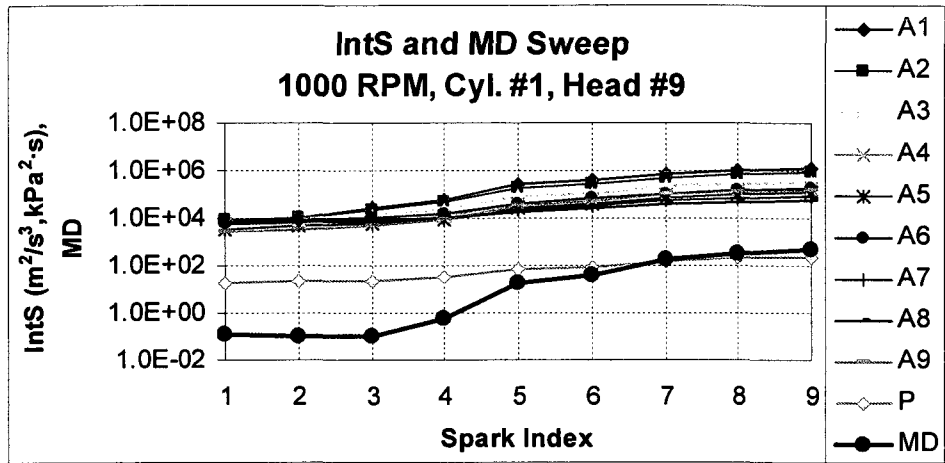


Figure C.1 g - MD / IntS Sweep - 1000 RPM, Cyl. #1, Head #9

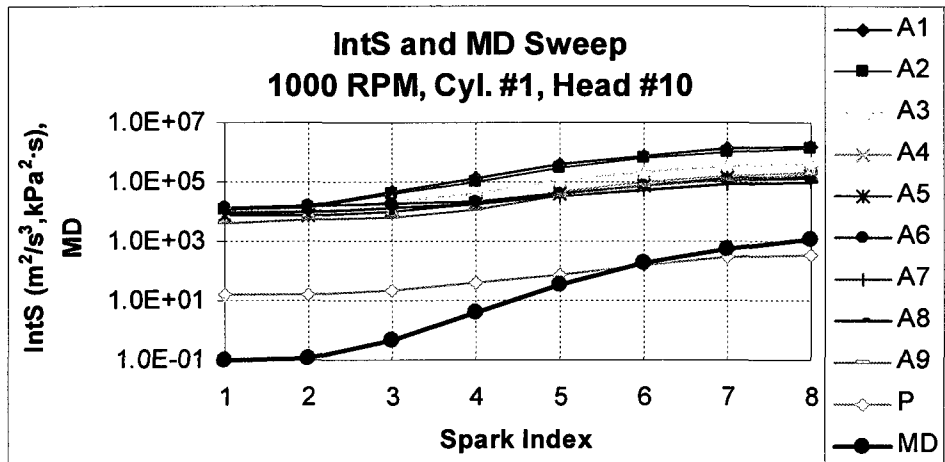


Figure C.1 h - MD / IntS Sweep - 1000 RPM, Cyl. #1, Head #10

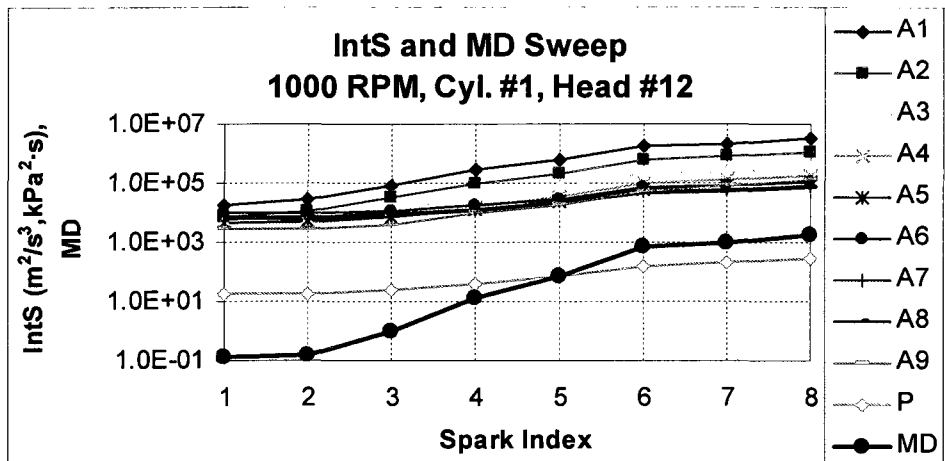


Figure C.1 i - MD / IntS Sweep - 1000 RPM, Cyl. #1, Head #12

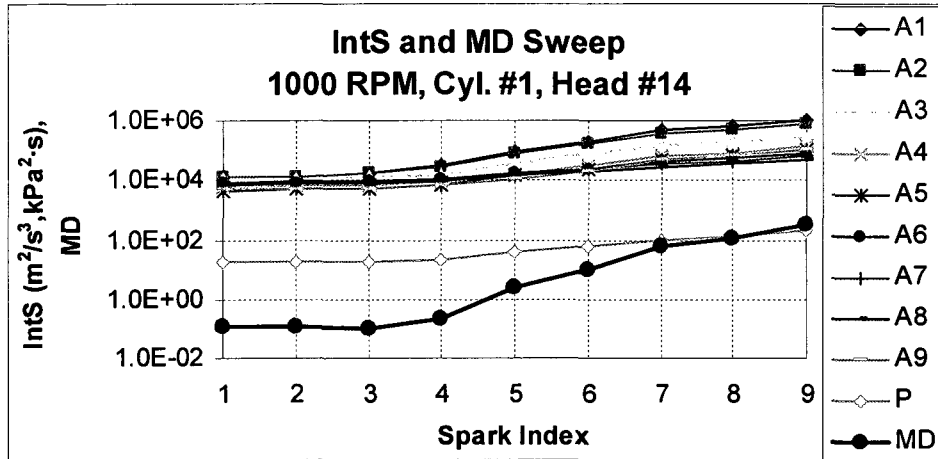


Figure C.1 j - MD / IntS Sweep - 1000 RPM, Cyl. #1, Head #14

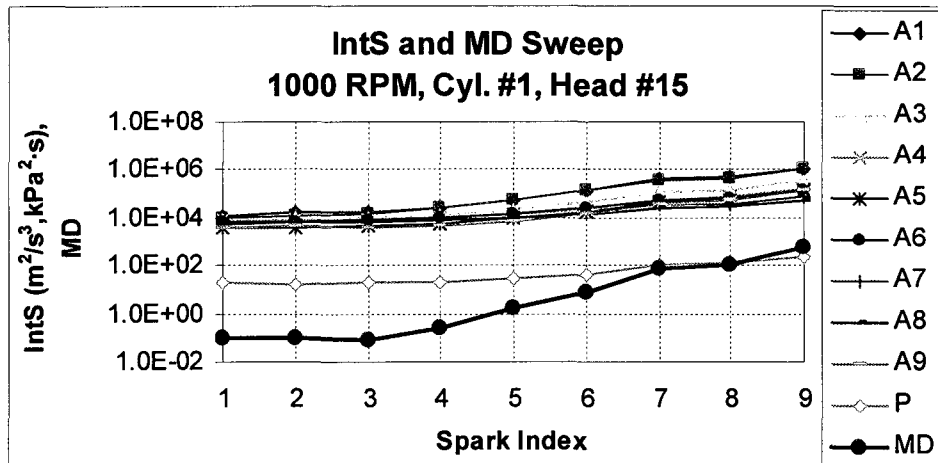
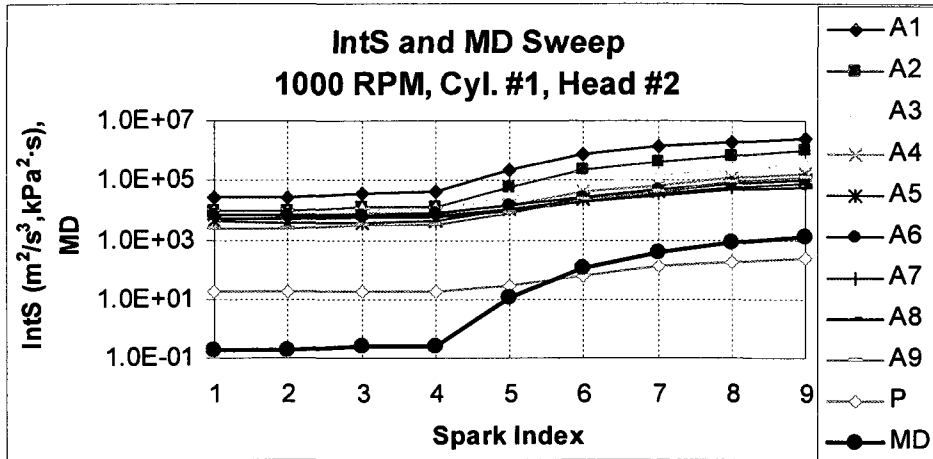
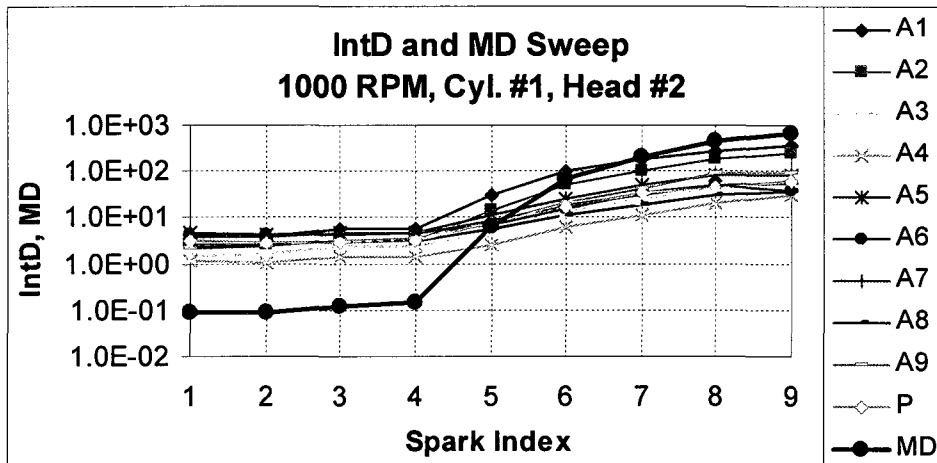


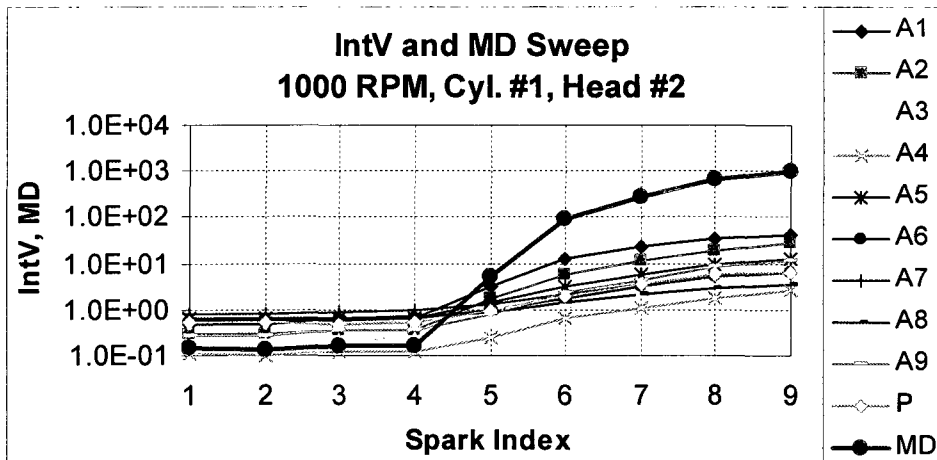
Figure C.1 k - MD / IntS Sweep - 1000 RPM, Cyl. #1, Head #15



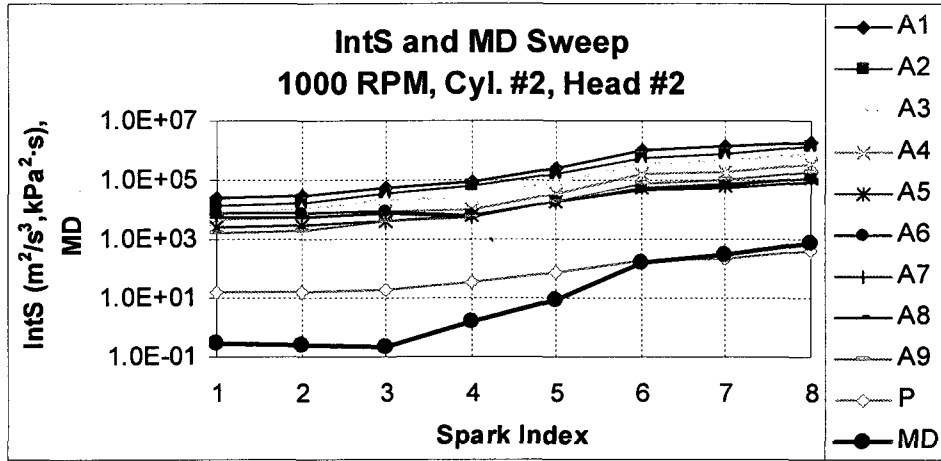
C.2 a - MD / IntS Sweep - 1000 RPM, Cyl. #1, Head #2



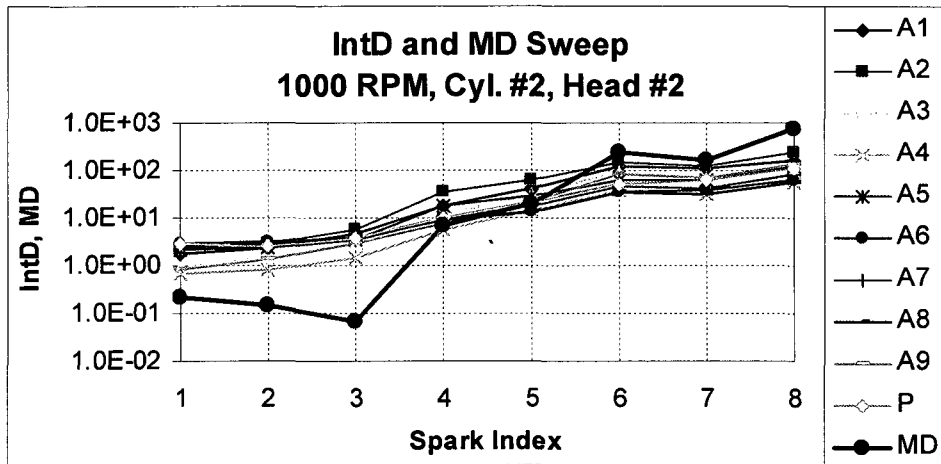
C.2 b - MD / IntD Sweep - 1000 RPM, Cyl. #1, Head #2



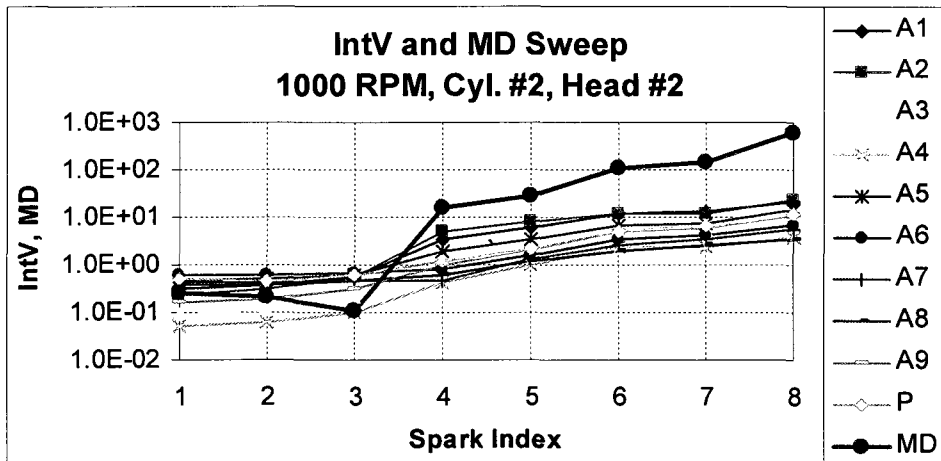
C.2 c - MD / IntV Sweep - 1000 RPM, Cyl. #1, Head #2



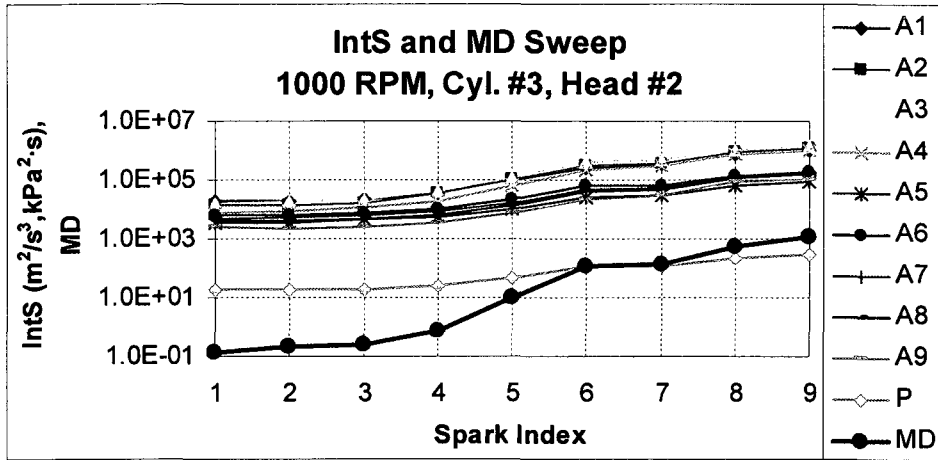
C.2 d - MD / IntS Sweep - 1000 RPM, Cyl. #2, Head #2



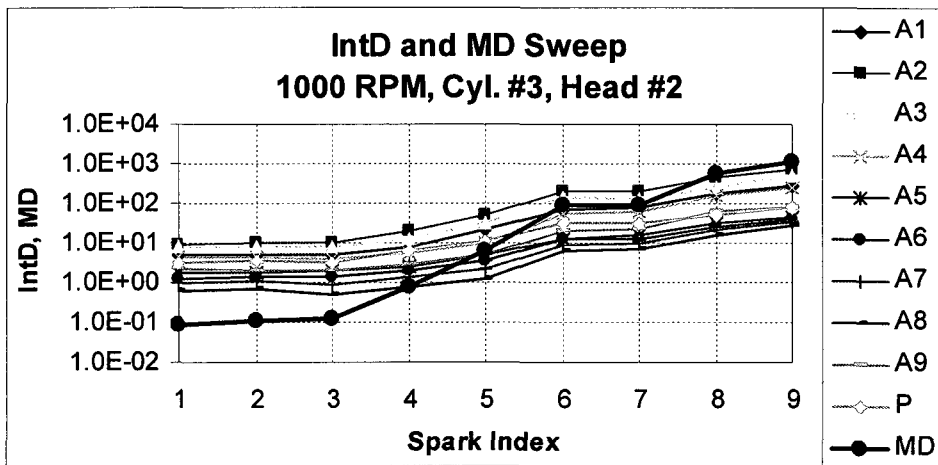
C.2 e - MD / IntD Sweep - 1000 RPM, Cyl. #2, Head #2



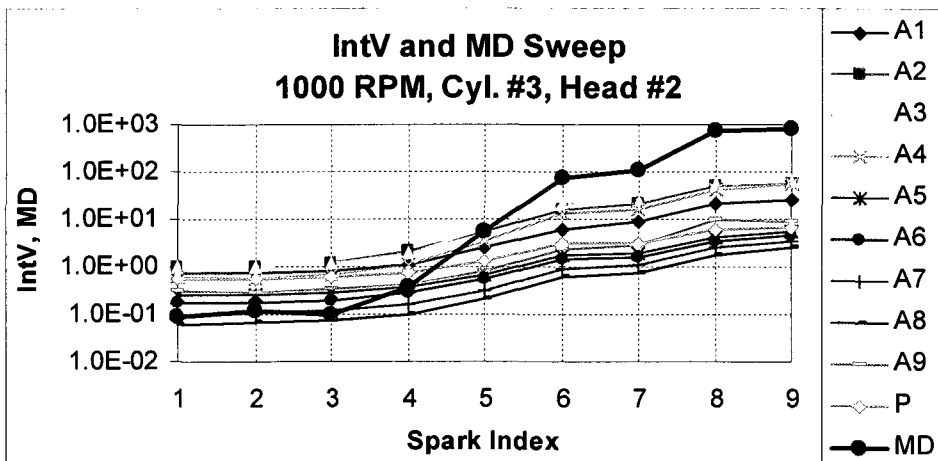
C.2 f - MD / IntV Sweep - 1000 RPM, Cyl. #2, Head #2



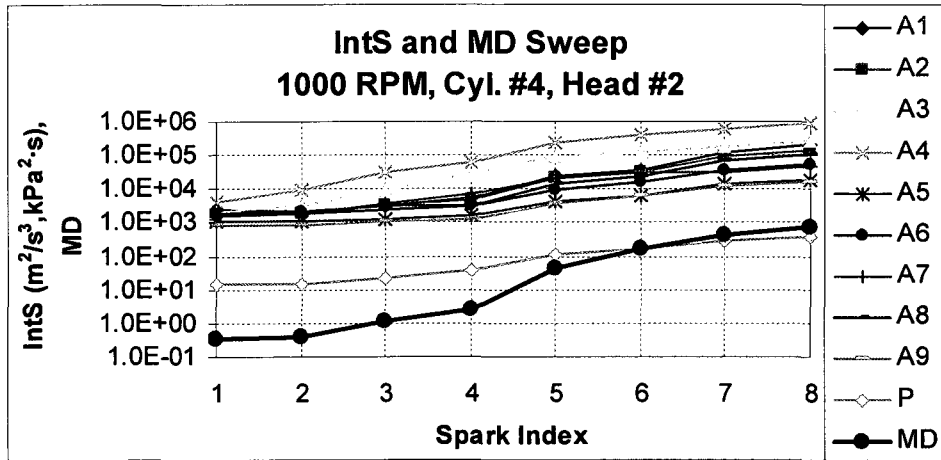
C.2 g - MD / IntS Sweep - 1000 RPM, Cyl. #3, Head #2



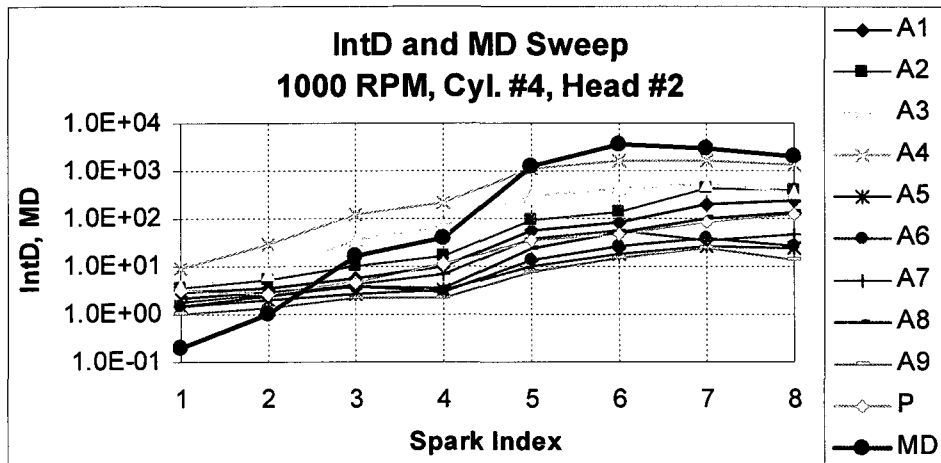
C.2 h - MD / IntD Sweep - 1000 RPM, Cyl. #3, Head #2



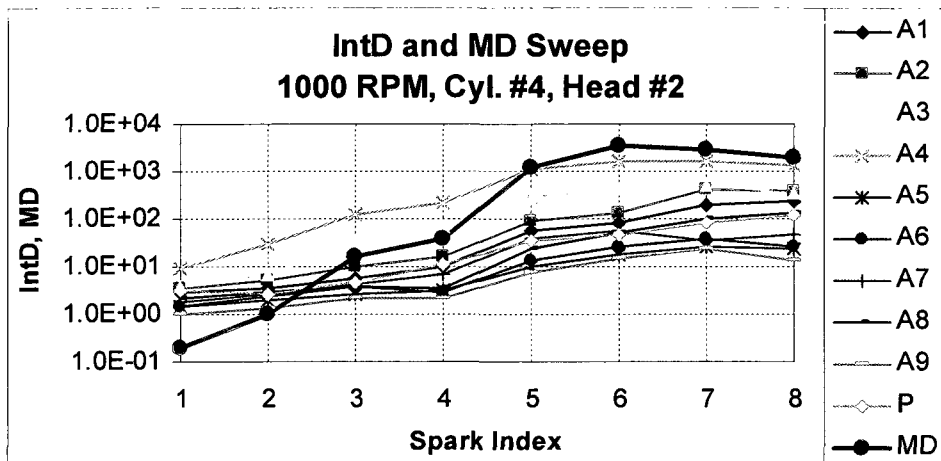
C.2 i - MD / IntV Sweep - 1000 RPM, Cyl. #3, Head #2



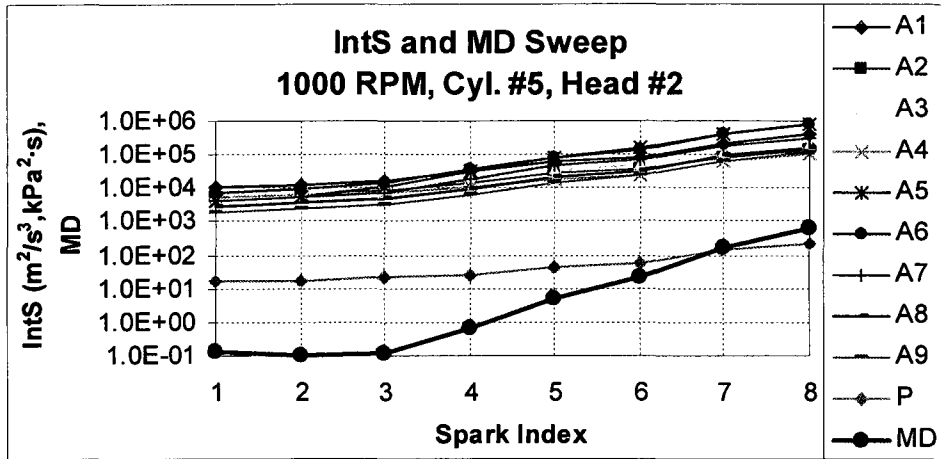
C.2 j - MD / IntS Sweep - 1000 RPM, Cyl. #4, Head #2



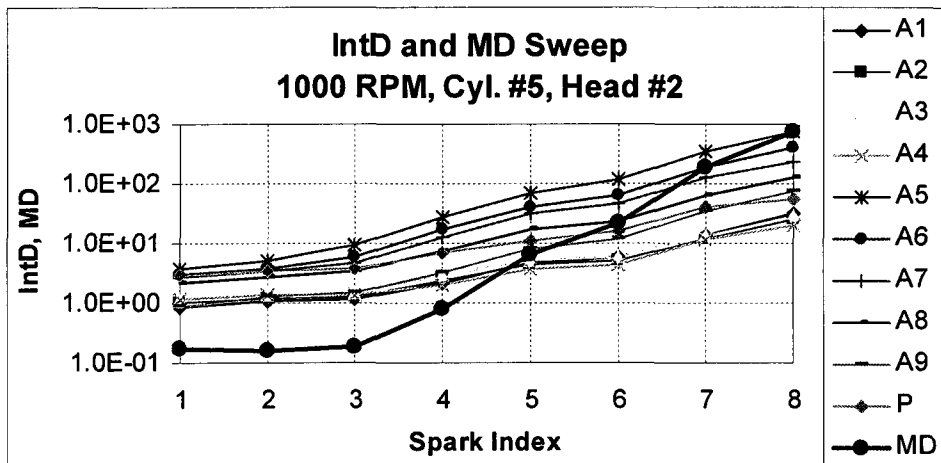
C.2 k - MD / IntD Sweep - 1000 RPM, Cyl. #4, Head #2



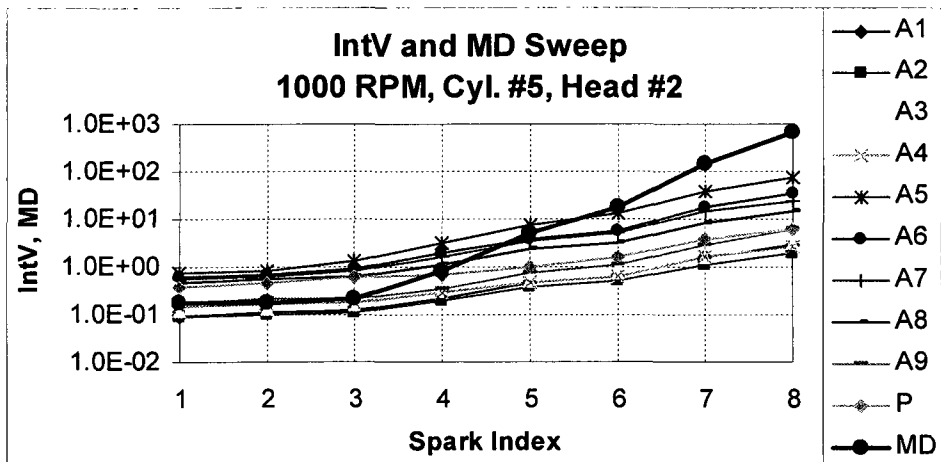
C.2 l - MD / IntV Sweep - 1000 RPM, Cyl. #4, Head #2



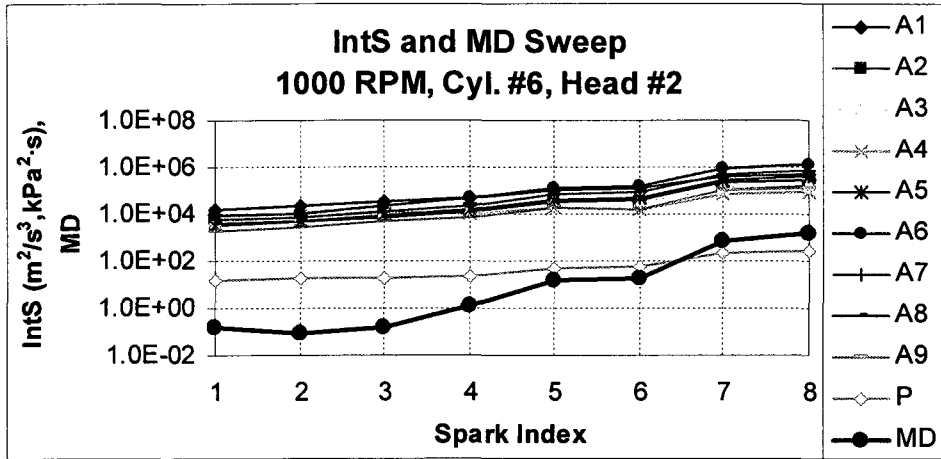
C.2 m - MD / IntS Sweep - 1000 RPM, Cyl. #5, Head #2



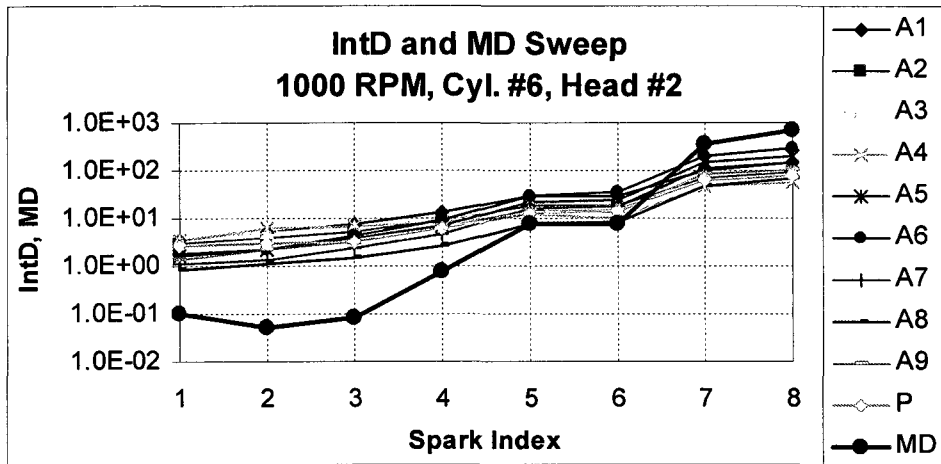
C.2 n - MD / IntD Sweep - 1000 RPM, Cyl. #5, Head #2



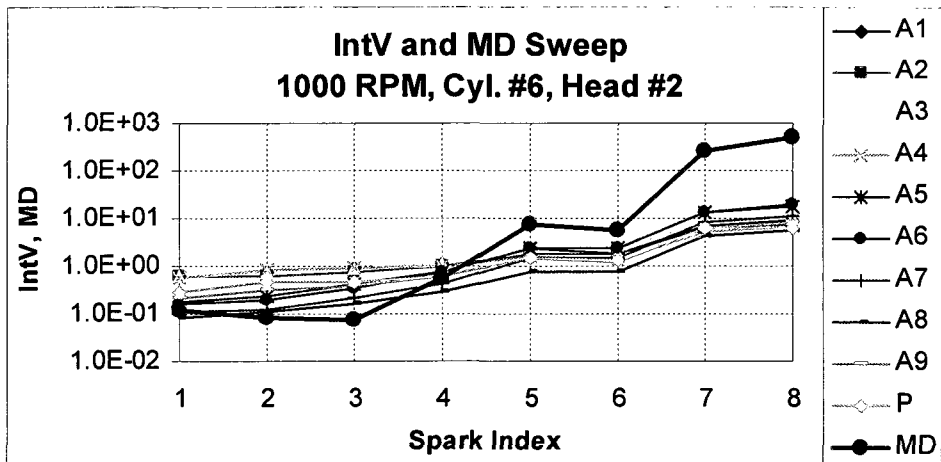
C.2 o - MD / IntV Sweep - 1000 RPM, Cyl. #5, Head #2



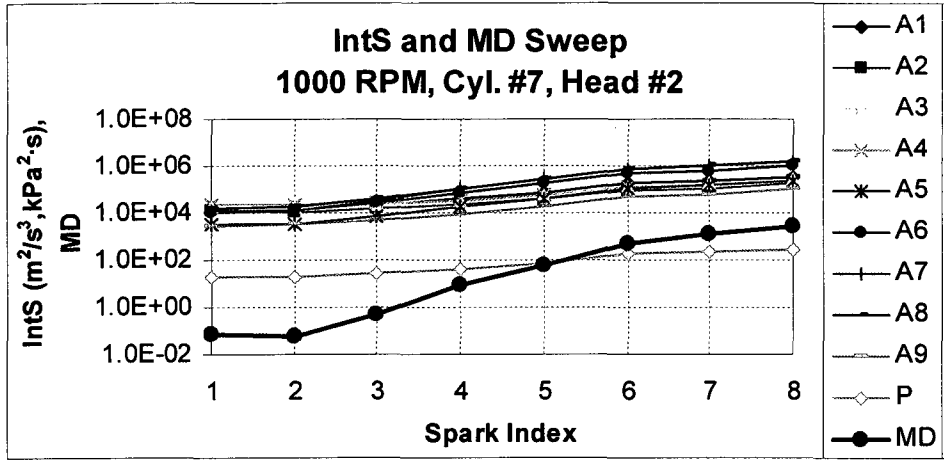
C.2 p - MD / IntS Sweep - 1000 RPM, Cyl. #6, Head #2



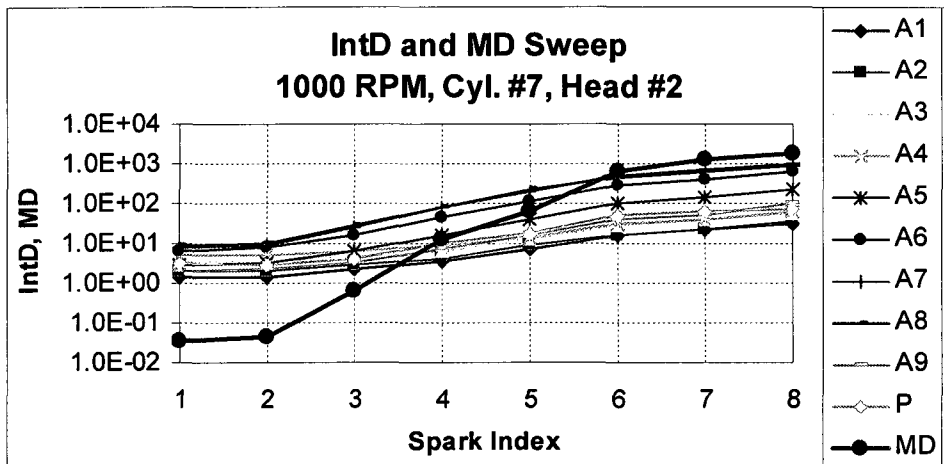
C.2 q - MD / IntD Sweep - 1000 RPM, Cyl. #6, Head #2



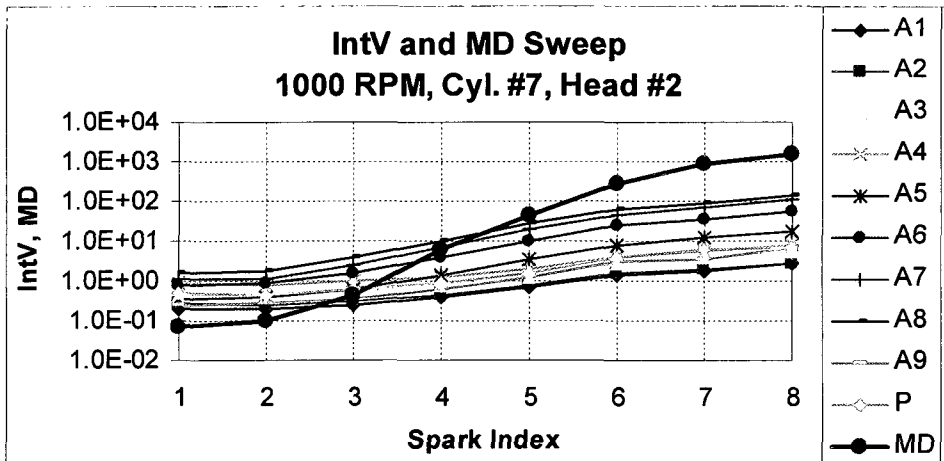
C.2 r - MD / IntV Sweep - 1000 RPM, Cyl. #6, Head #2



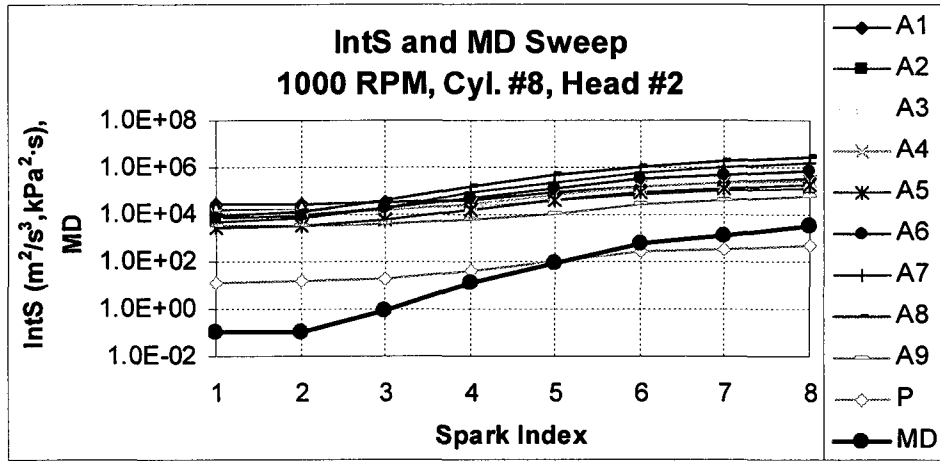
C.2 s - MD / IntS Sweep - 1000 RPM, Cyl. #7, Head #2



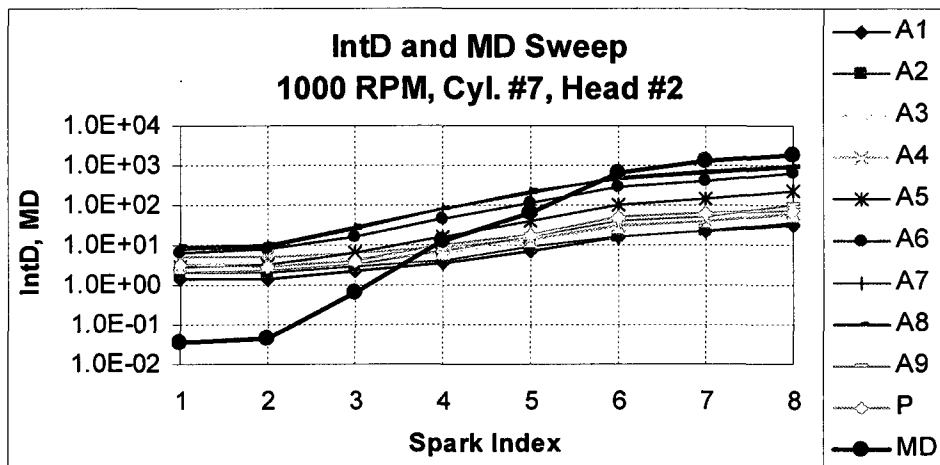
C.2 t - MD / IntD Sweep - 1000 RPM, Cyl. #7, Head #2



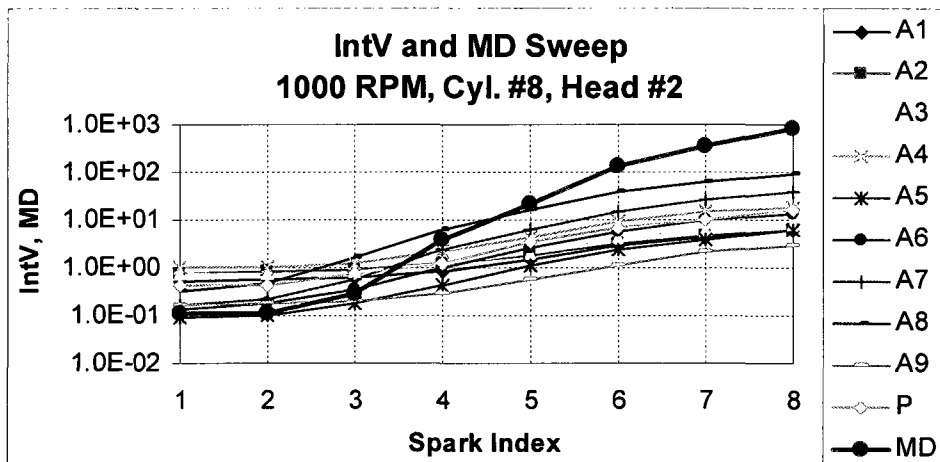
C.2 u - MD / IntV Sweep - 1000 RPM, Cyl. #7, Head #2



C.2 v - MD / IntS Sweep - 1000 RPM, Cyl. #8, Head #2



C.2 w - MD / IntD Sweep - 1000 RPM, Cyl. #8, Head #2



C.2 x - MD / IntV Sweep - 1000 RPM, Cyl. #8, Head #2

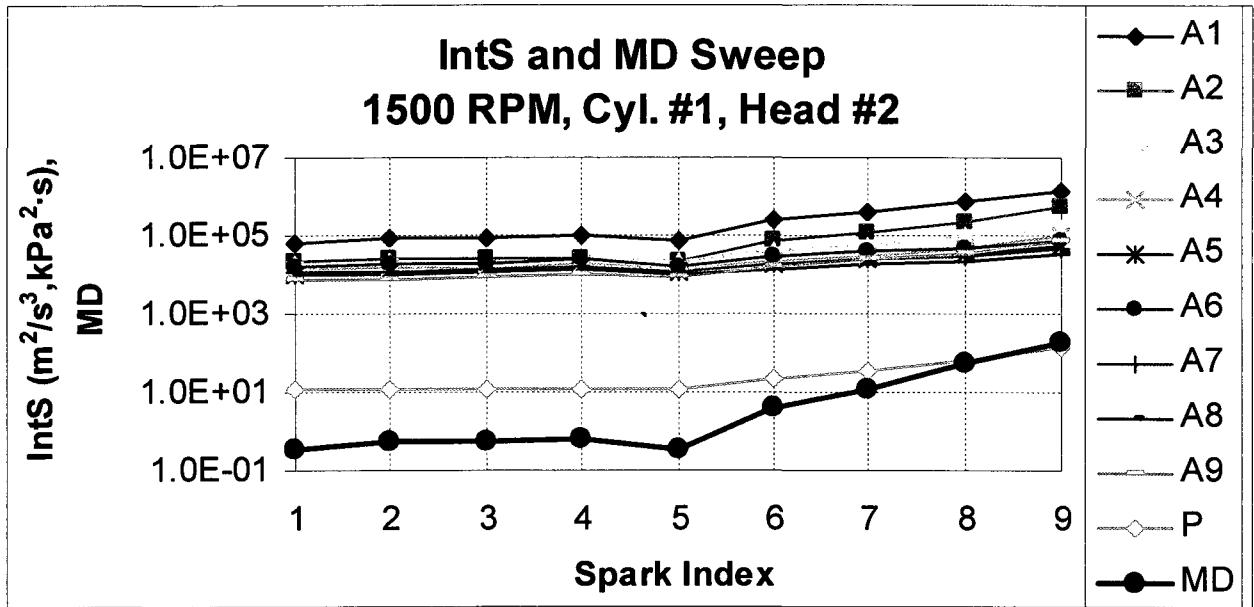


Figure C.3 a - MD / IntS Sweep - 1500 RPM, Cyl. #1, Head #2

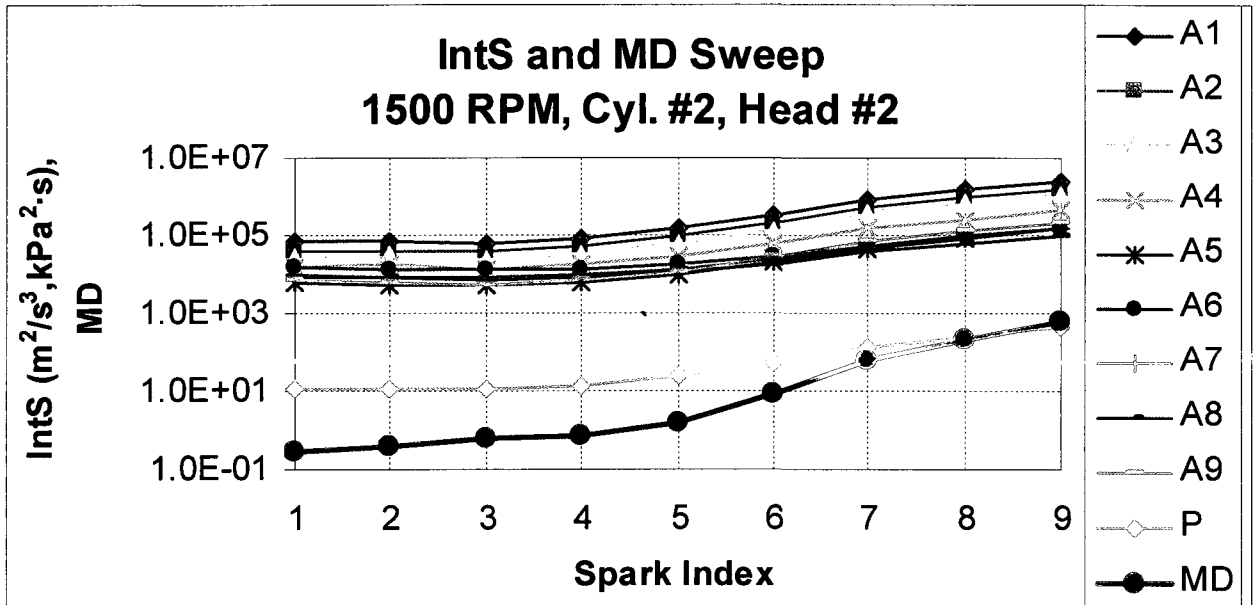


Figure C.3 b - MD / IntS Sweep - 1500 RPM, Cyl. #2, Head #2

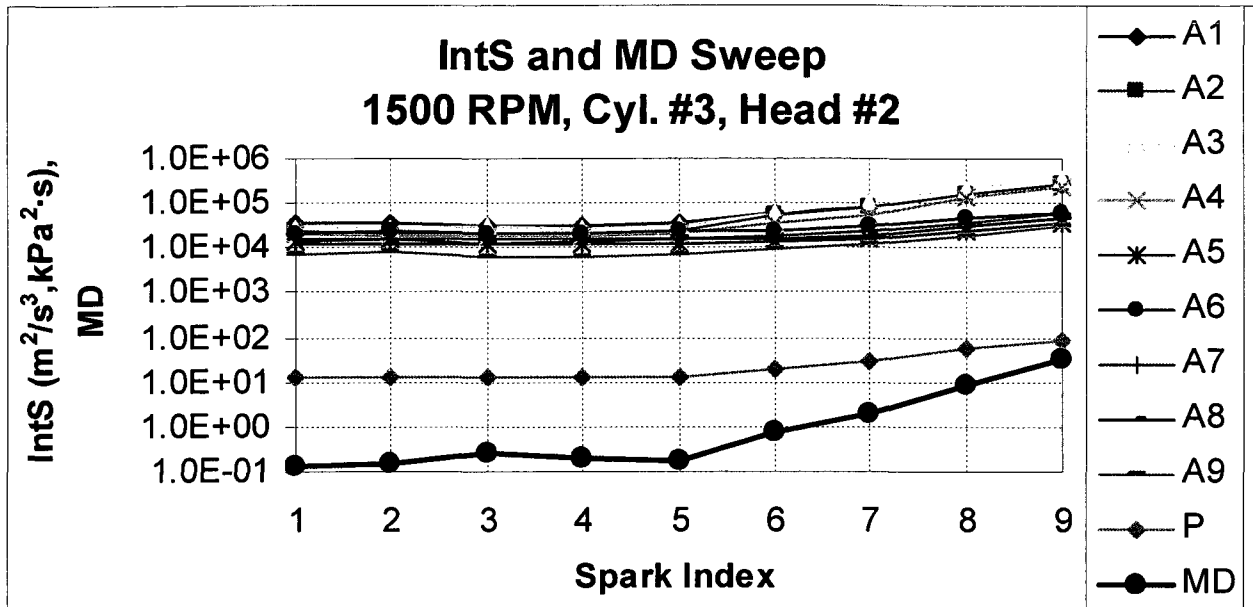


Figure C.3 c - MD / IntS Sweep - 1500 RPM, Cyl. #3, Head #2

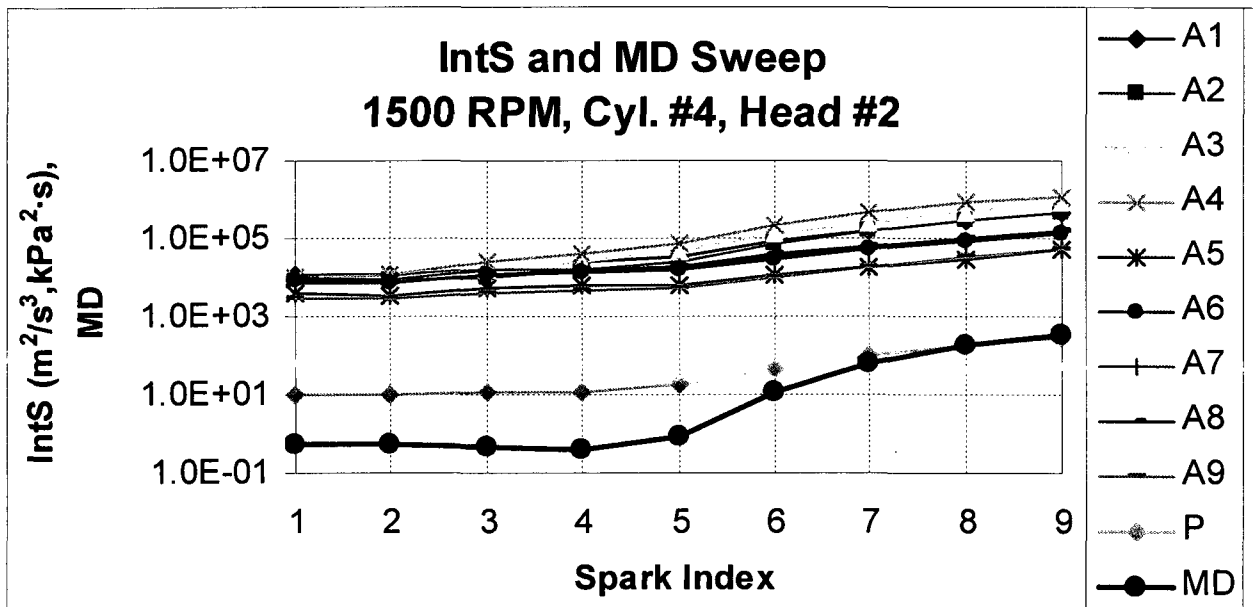


Figure C.3 d - MD / IntS Sweep - 1500 RPM, Cyl. #4, Head #2

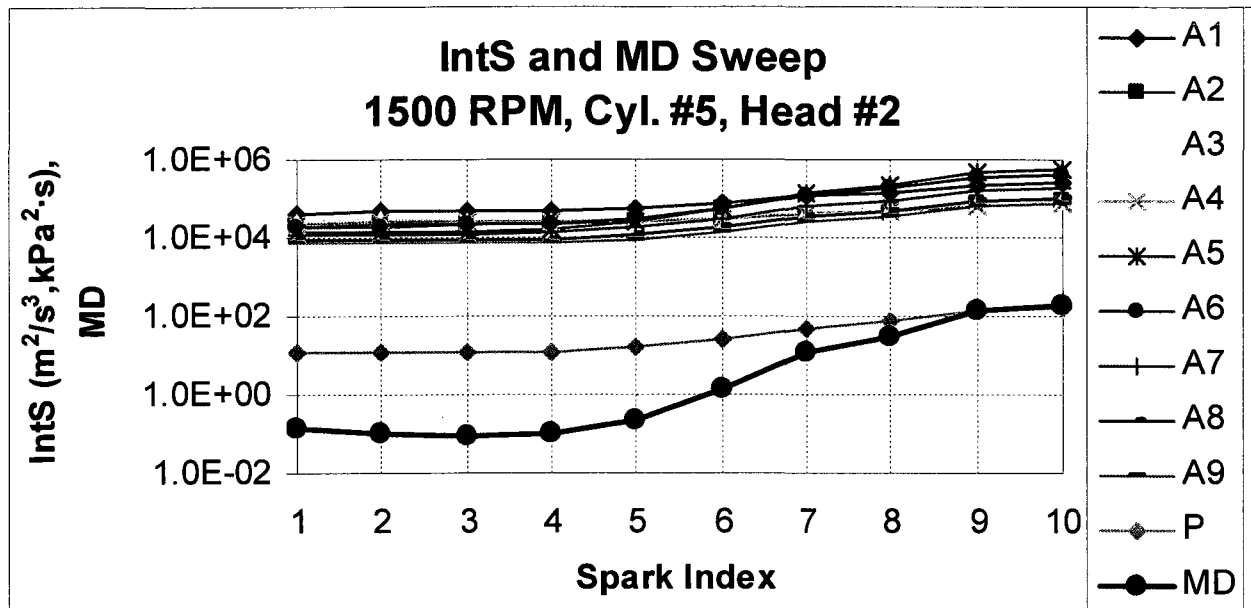


Figure C.3 e - MD / IntS Sweep - 1500 RPM, Cyl. #5, Head #2

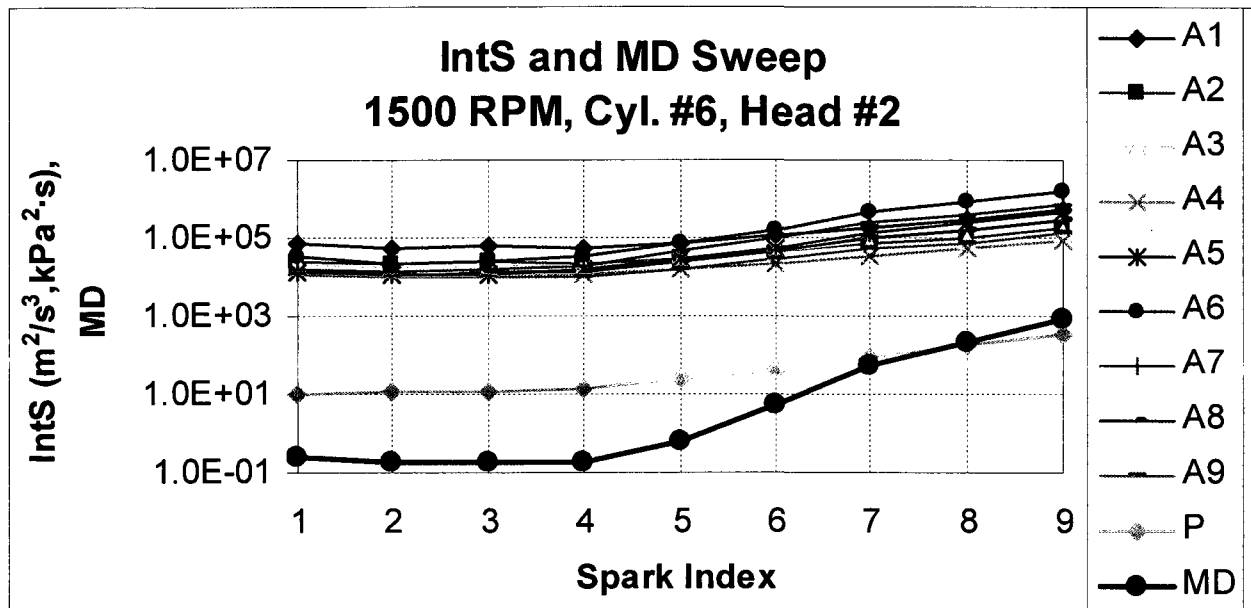


Figure C.3 f - MD / IntS Sweep - 1500 RPM, Cyl. #6, Head #2

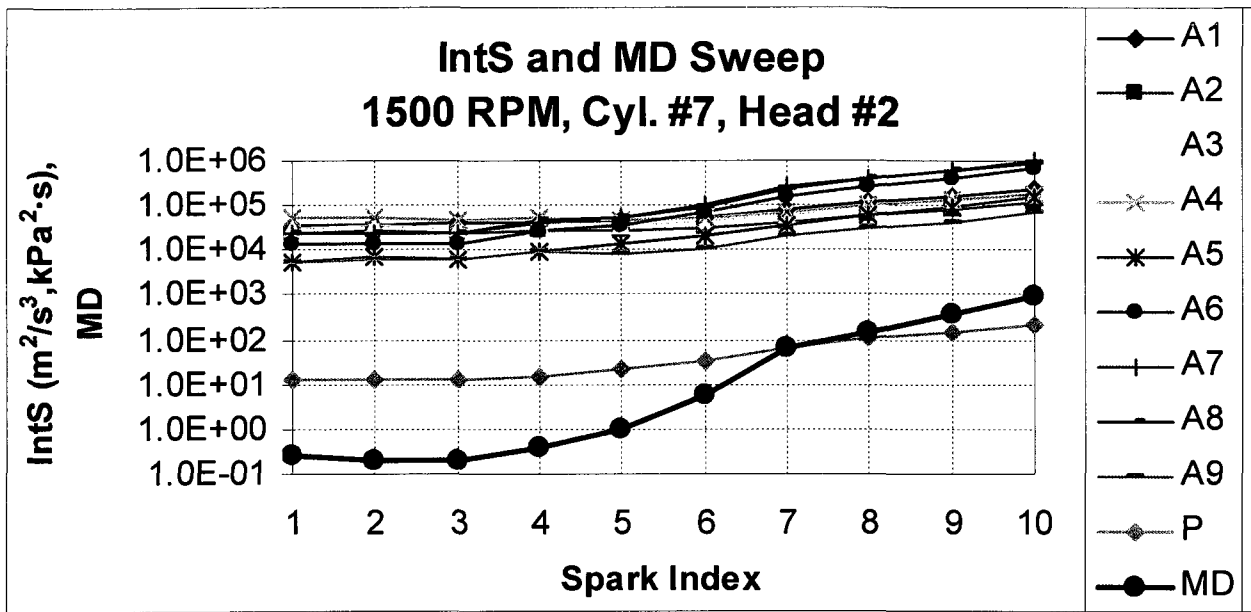


Figure C.3 g - MD / IntS Sweep - 1500 RPM, Cyl. #7, Head #2

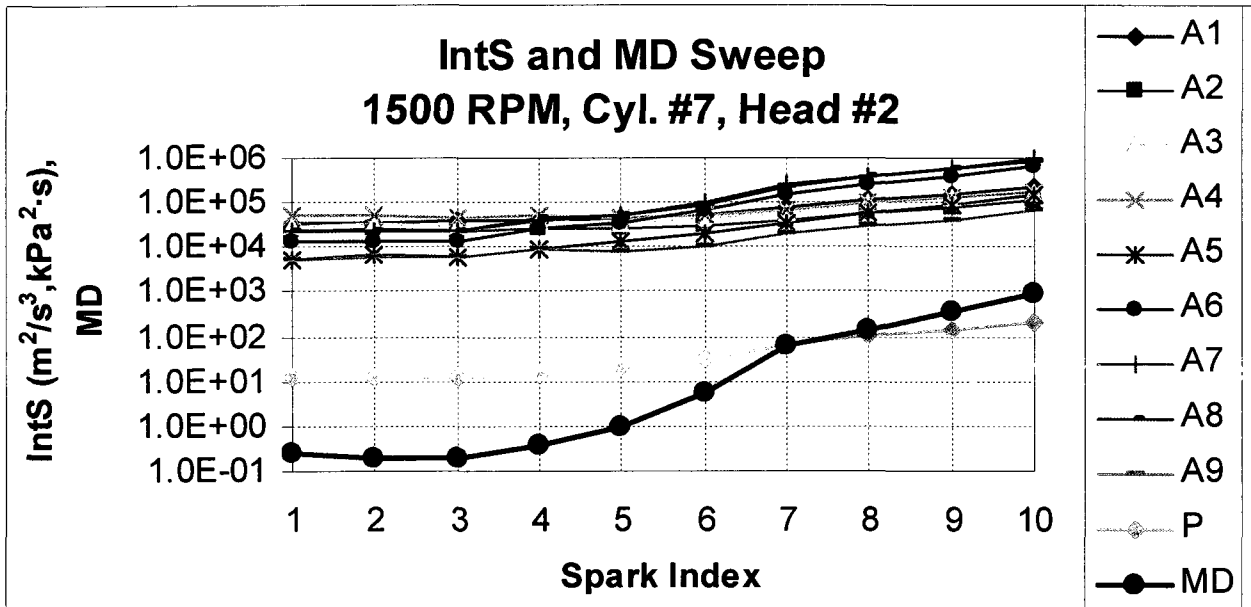


Figure C.3 h - MD / IntS Sweep - 1500 RPM, Cyl. #8, Head #2

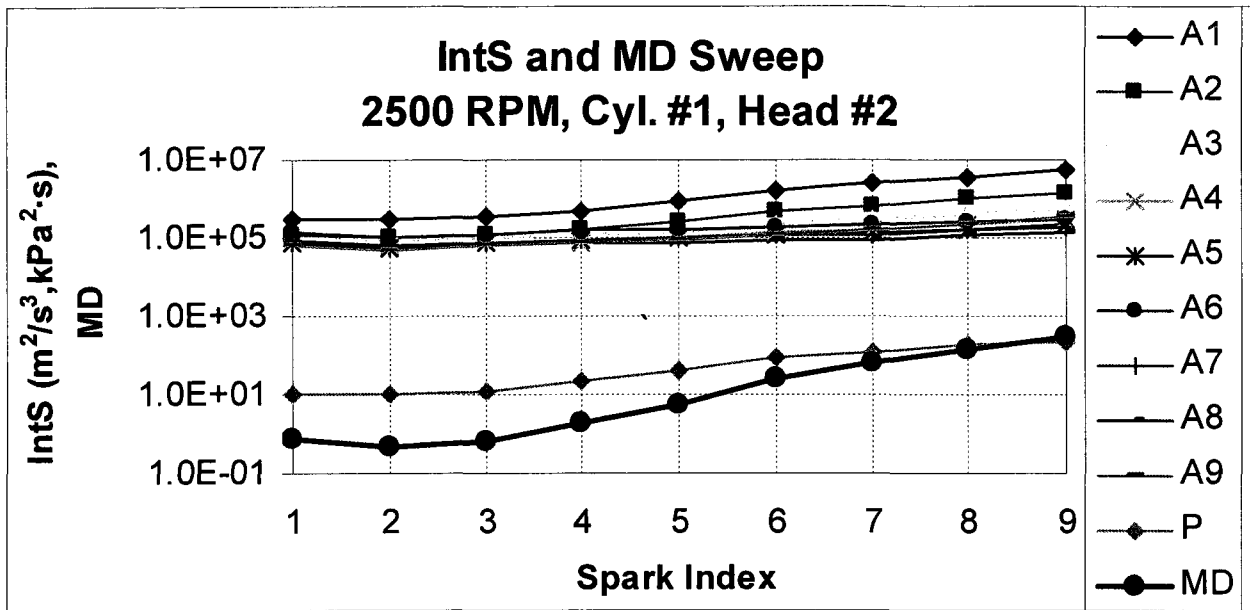


Figure C.3 i - MD / IntS Sweep - 2500 RPM, Cyl. #1, Head #2

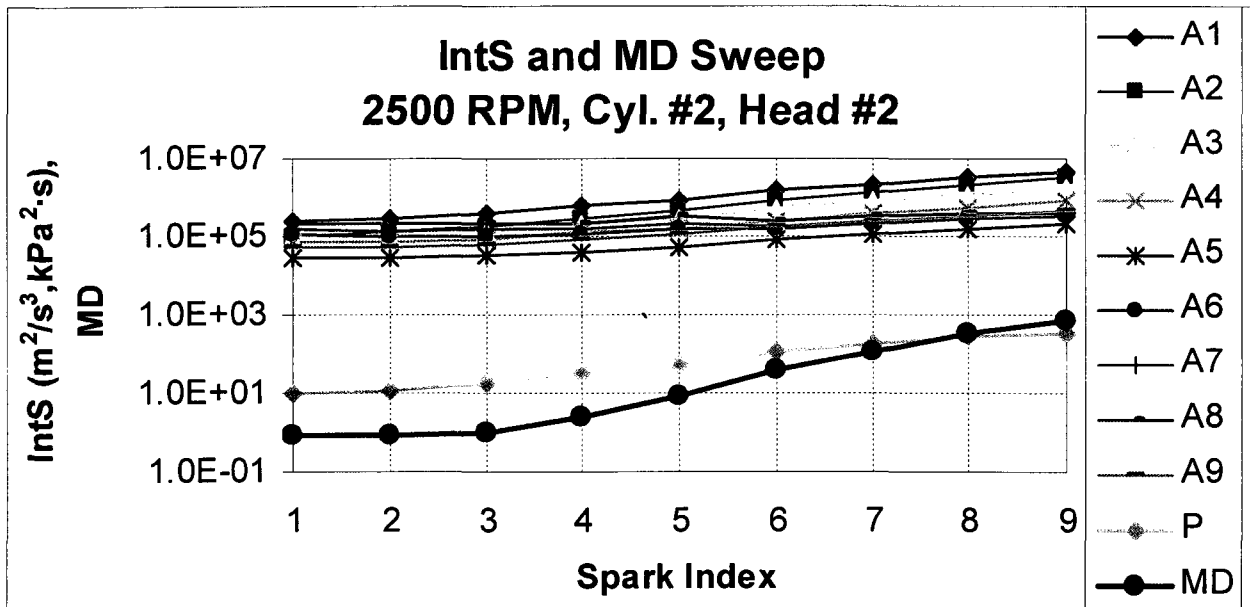


Figure C.3 j - MD / IntS Sweep - 2500 RPM, Cyl. #2, Head #2

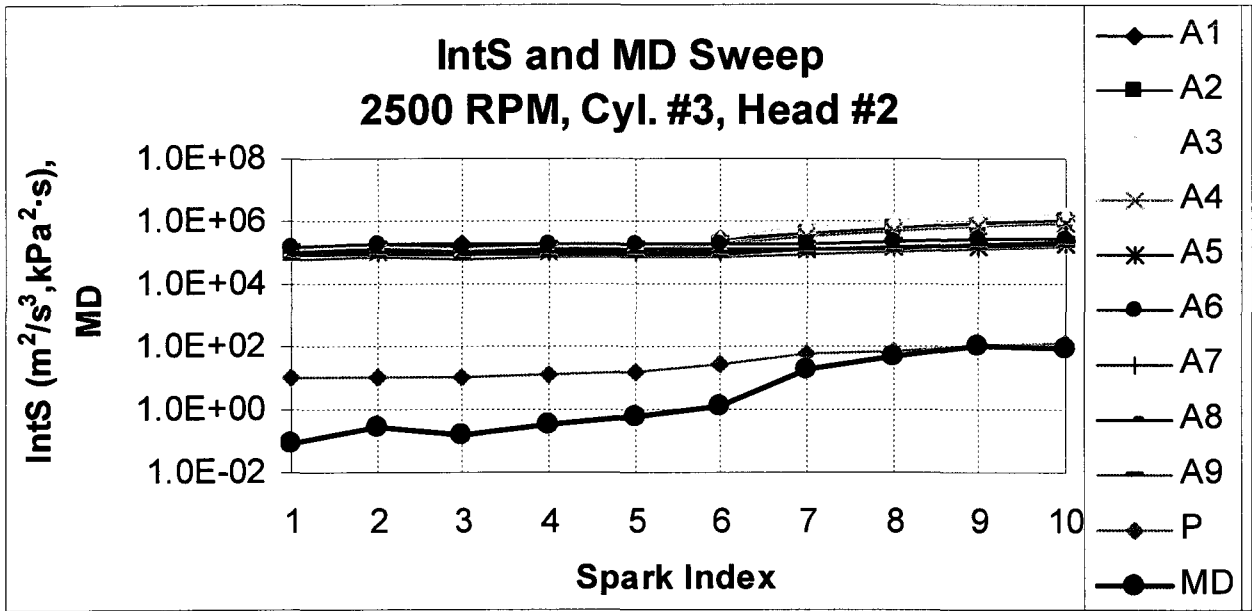


Figure C.3 k - MD / IntS Sweep - 2500 RPM, Cyl. #3, Head #2

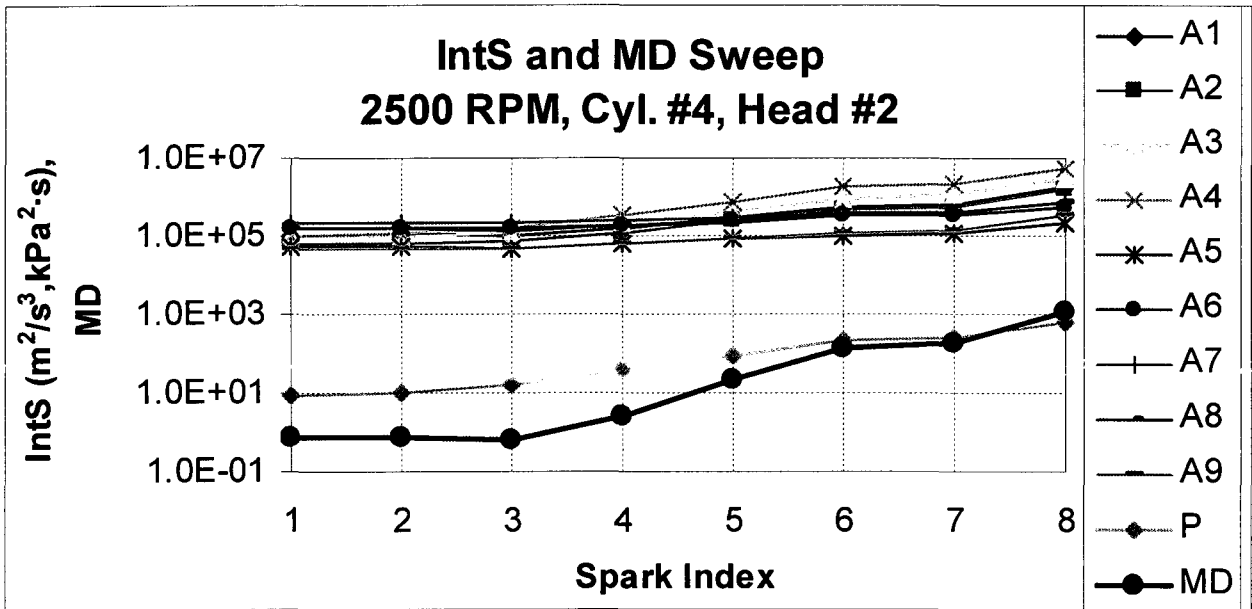


Figure C.3 l - MD / IntS Sweep - 2500 RPM, Cyl. #4, Head #2

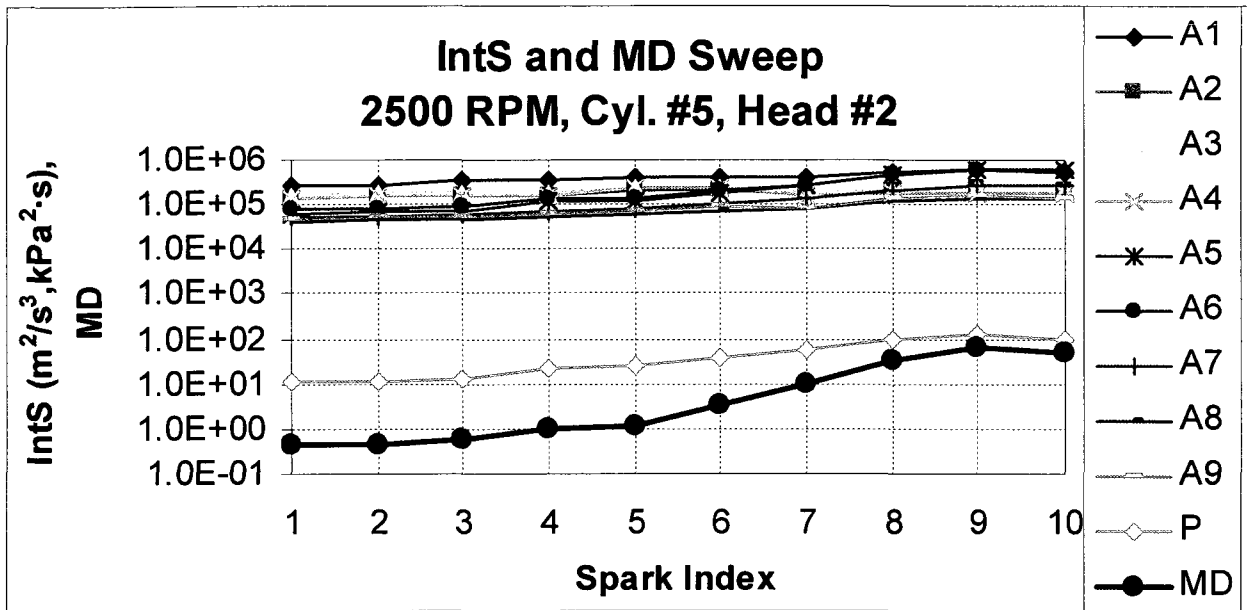


Figure C.3 m - MD / IntS Sweep - 2500 RPM, Cyl. #5, Head #2

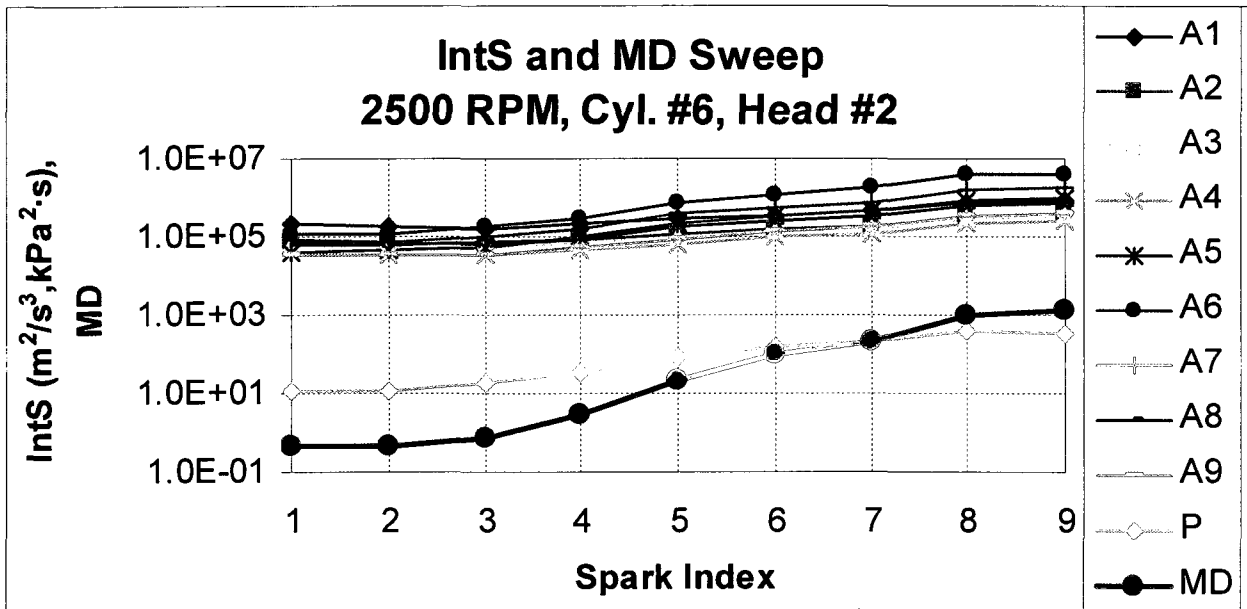


Figure C.3 n - MD / IntS Sweep - 2500 RPM, Cyl. #6, Head #2

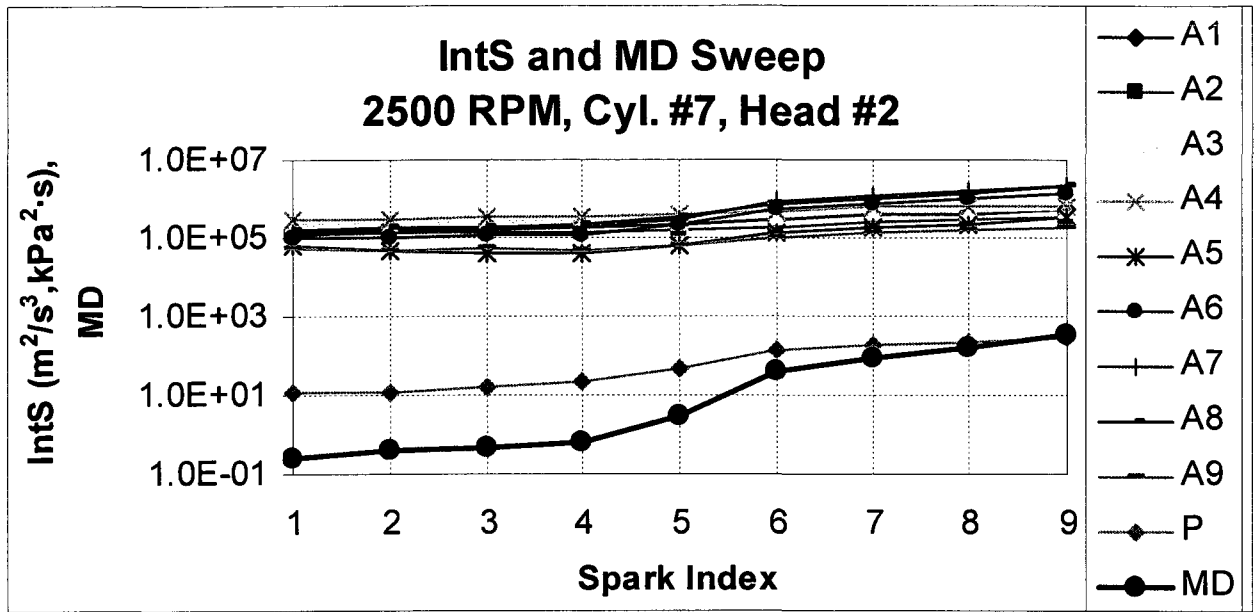


Figure C.3 o - MD / IntS Sweep - 2500 RPM, Cyl. #7, Head #2

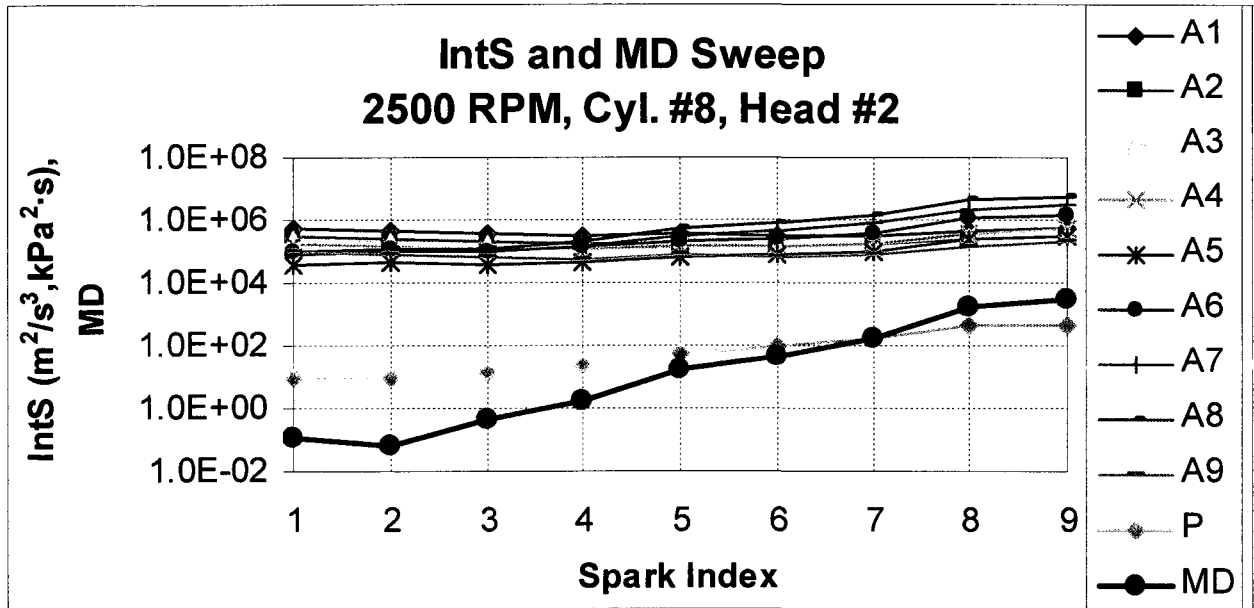


Figure C.3 p - MD / IntS Sweep - 2500 RPM, Cyl. #8, Head #2

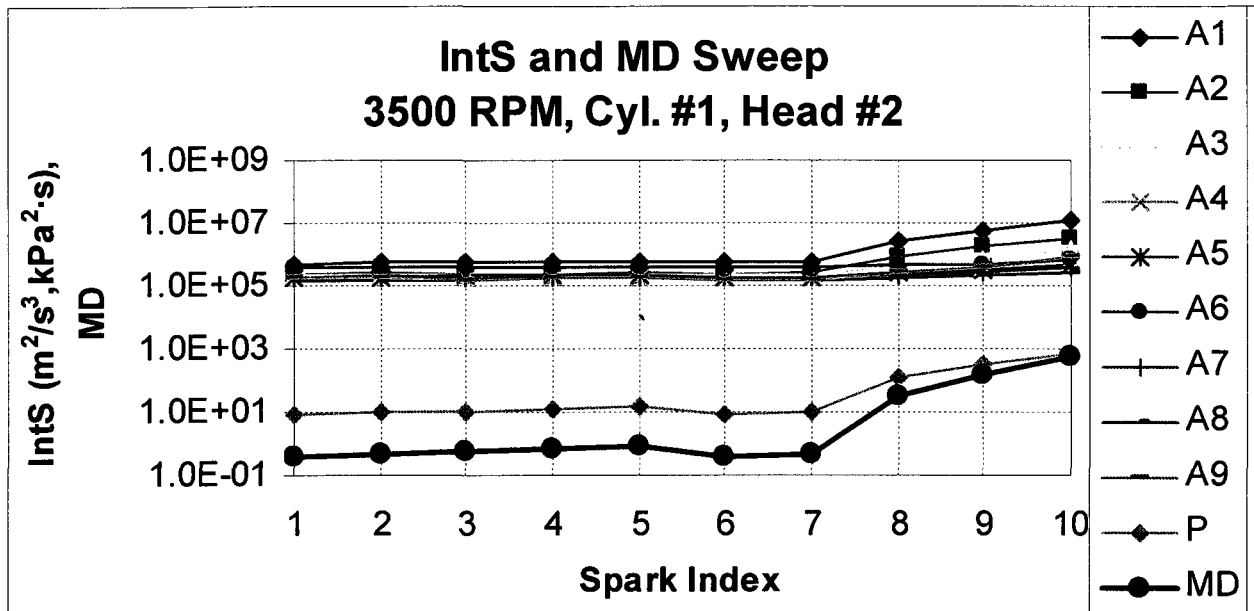


Figure C.3 q - MD / IntS Sweep - 3500 RPM, Cyl. #1, Head #2

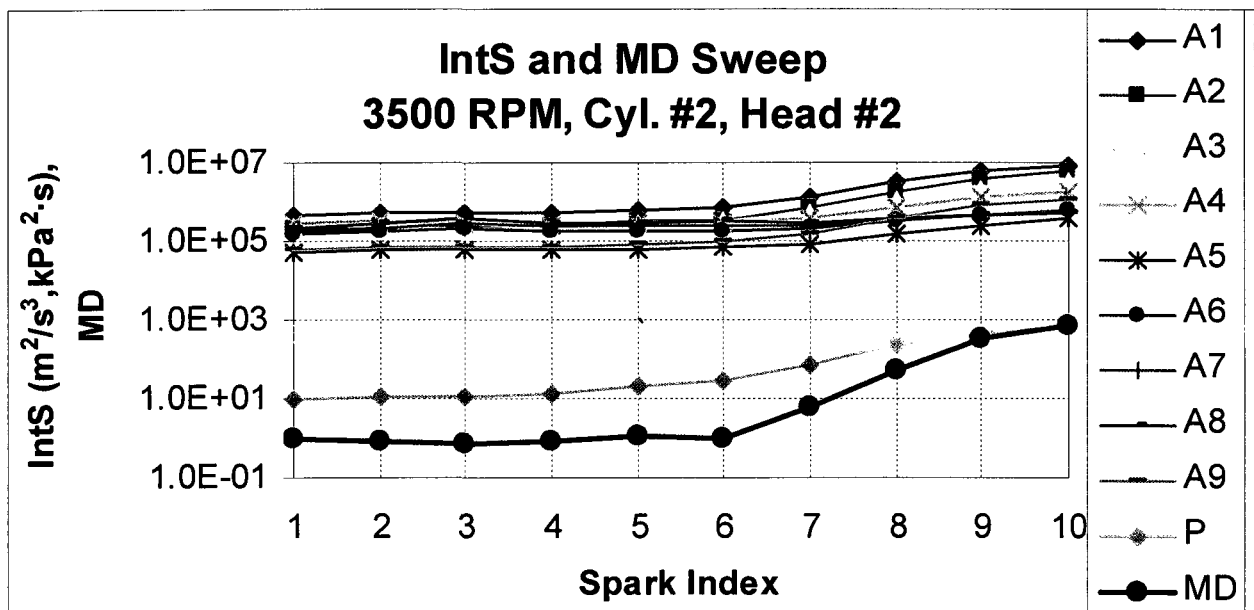


Figure C.3 r - MD / IntS Sweep - 3500 RPM, Cyl. #2, Head #2

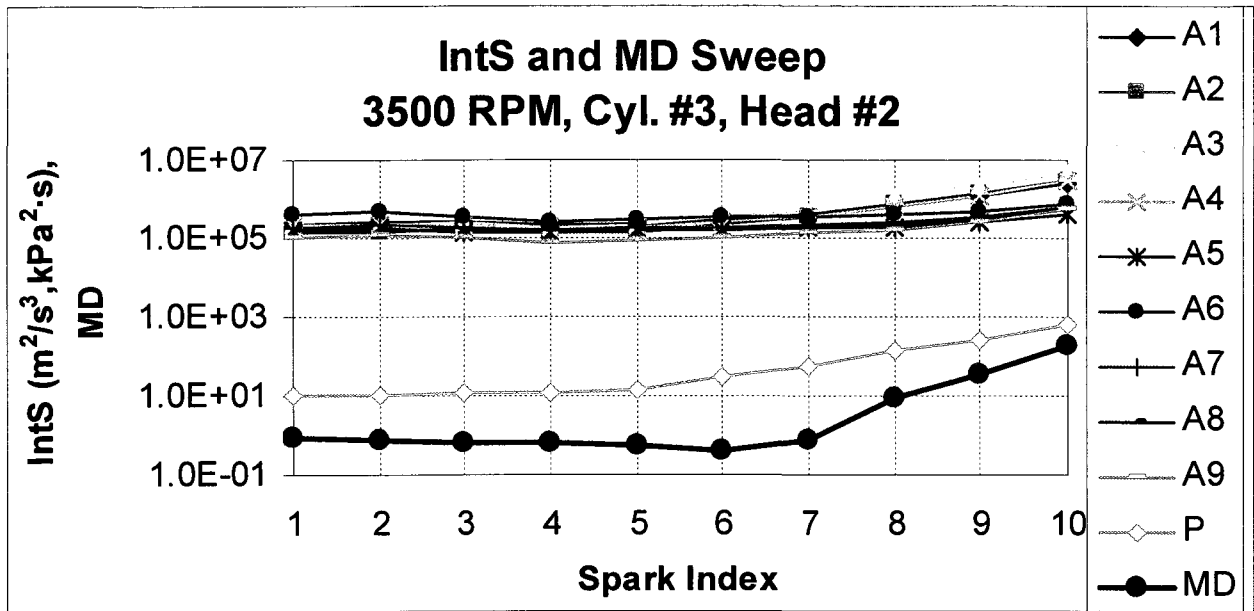


Figure C.3 s - MD / IntS Sweep - 3500 RPM, Cyl. #3, Head #2

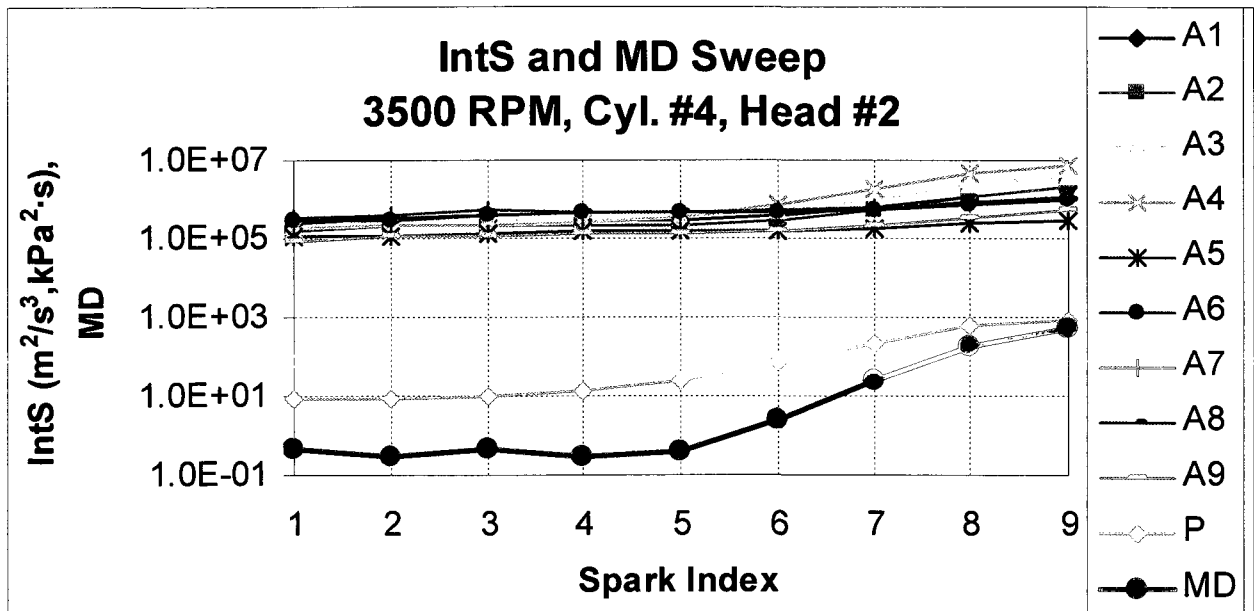


Figure C.3 t - MD / IntS Sweep - 3500 RPM, Cyl. #4, Head #2

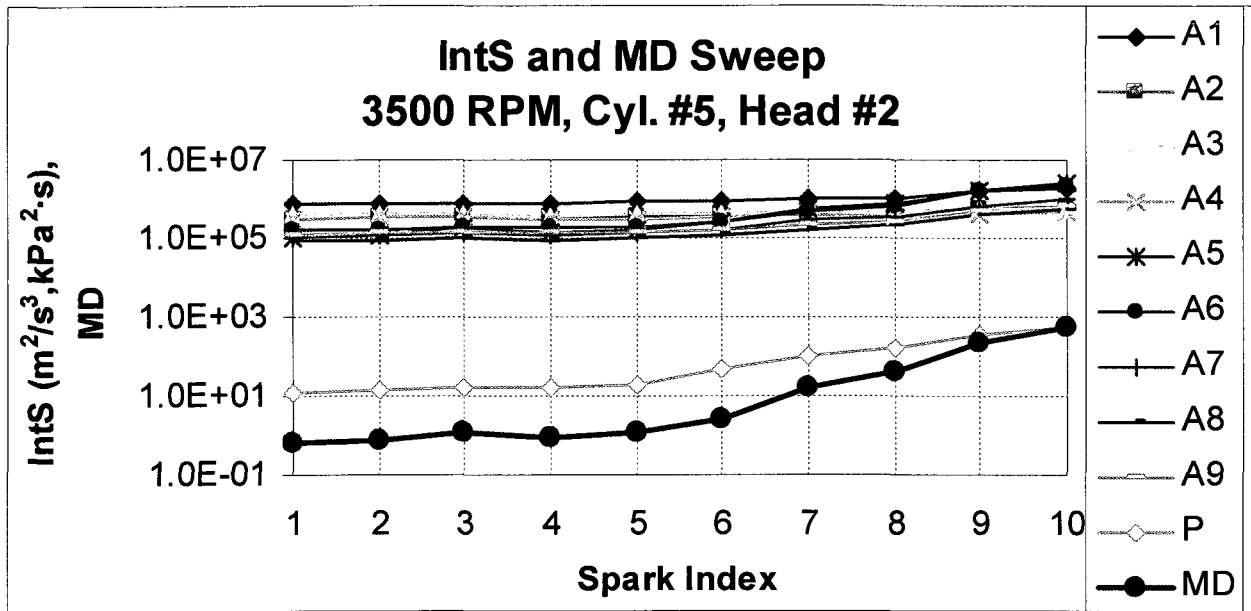


Figure C.3 u - MD / IntS Sweep - 3500 RPM, Cyl. #5, Head #2

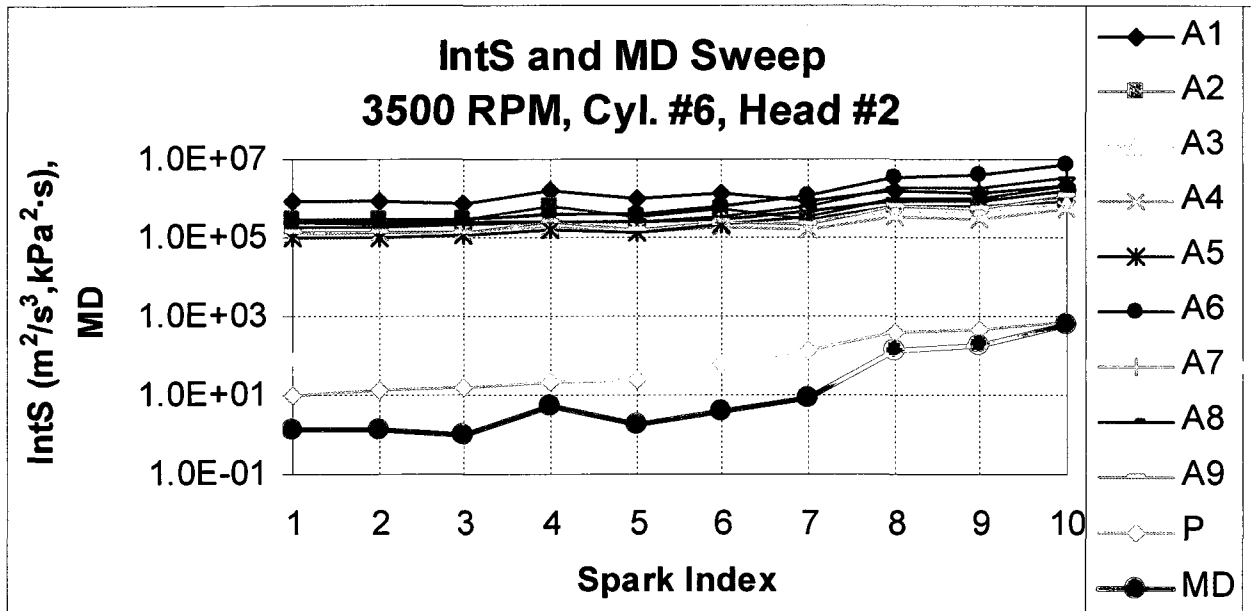


Figure C.3 v - MD / IntS Sweep - 3500 RPM, Cyl. #6, Head #2

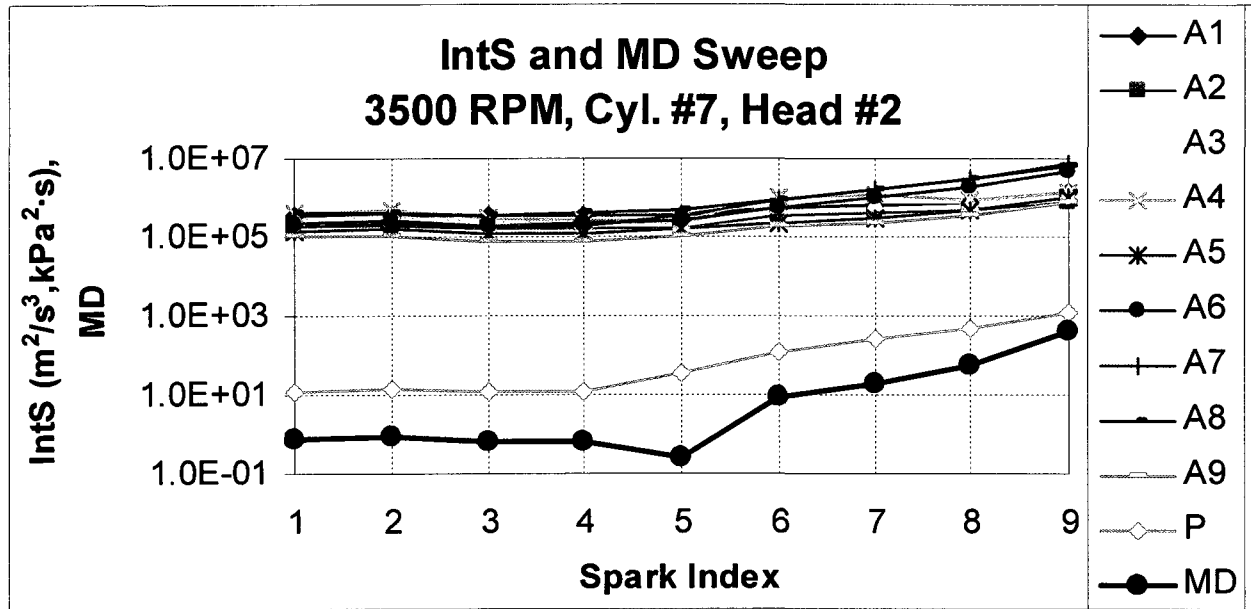


Figure C.3 w - MD / IntS Sweep - 3500 RPM, Cyl. #7, Head #2

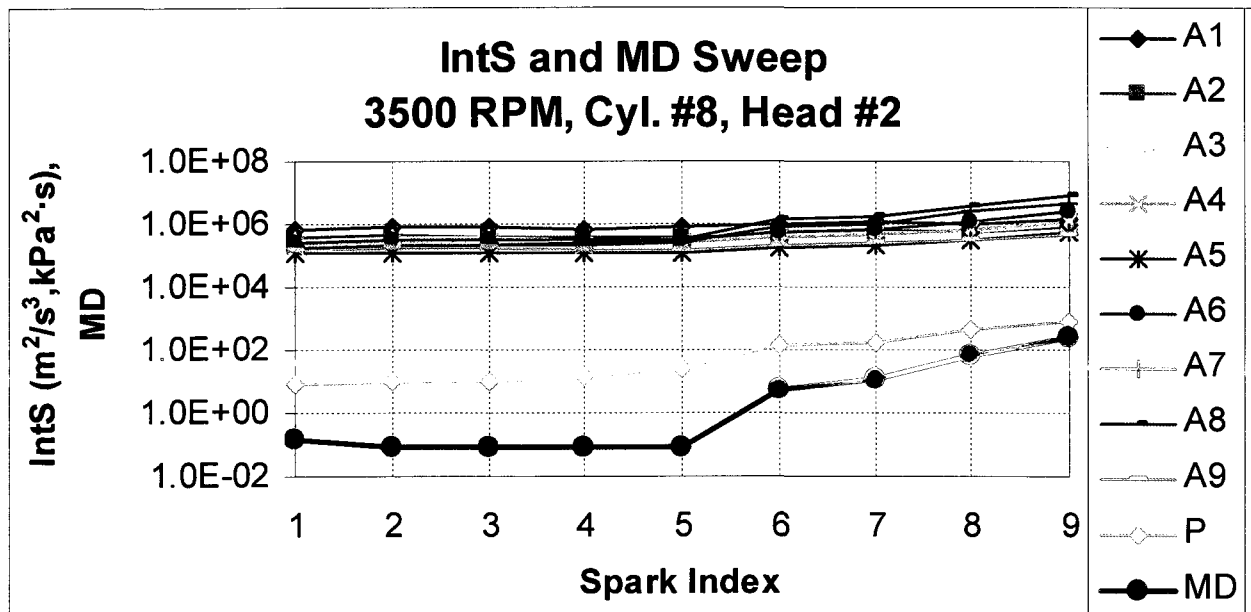


Figure C.3 x - MD / IntS Sweep - 3500 RPM, Cyl. #8, Head #2

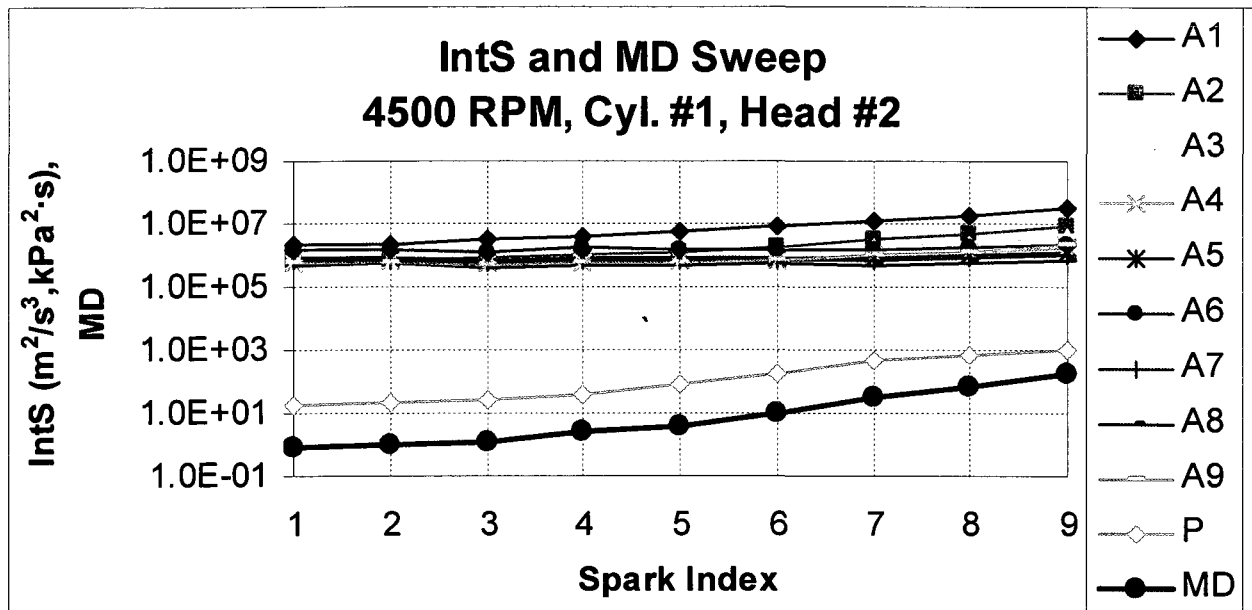


Figure C.3 y - MD / IntS Sweep - 4500 RPM, Cyl. #1, Head #2

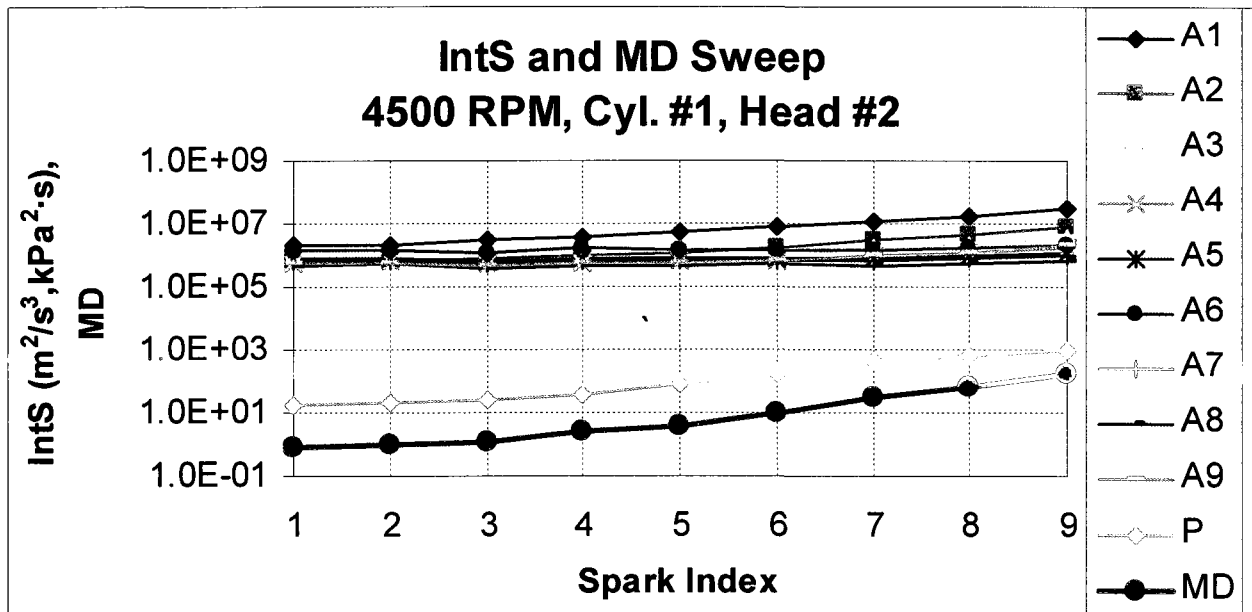


Figure C.3 z - MD / IntS Sweep - 4500 RPM, Cyl. #2, Head #2

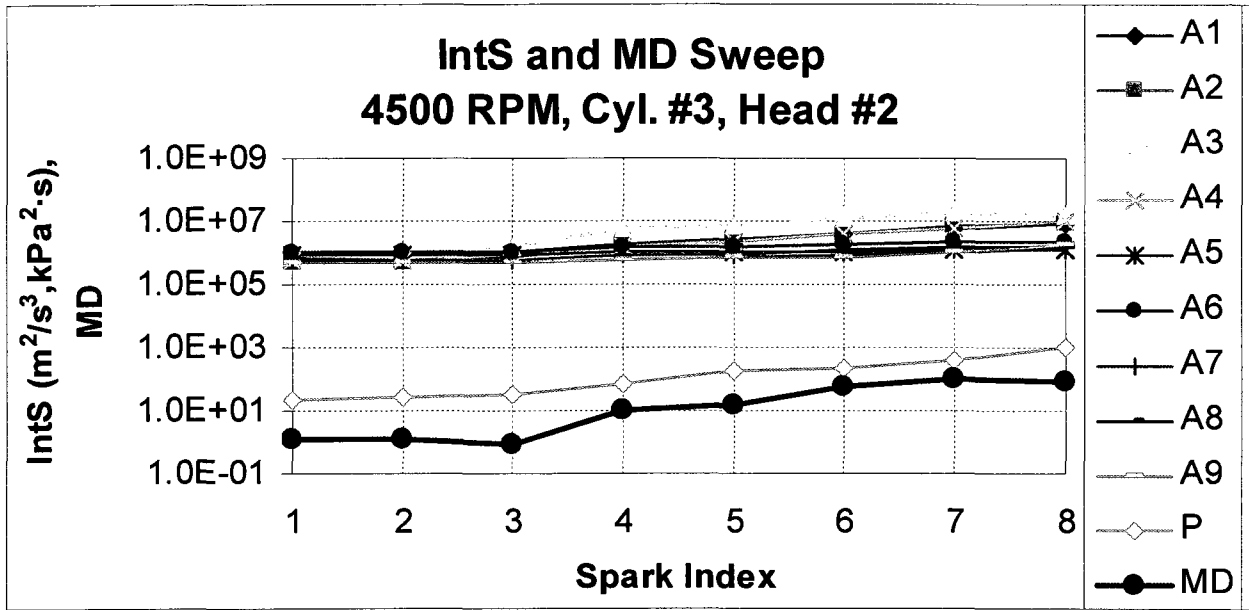


Figure C.3 aa - MD / IntS Sweep - 4500 RPM, Cyl. #3, Head #2

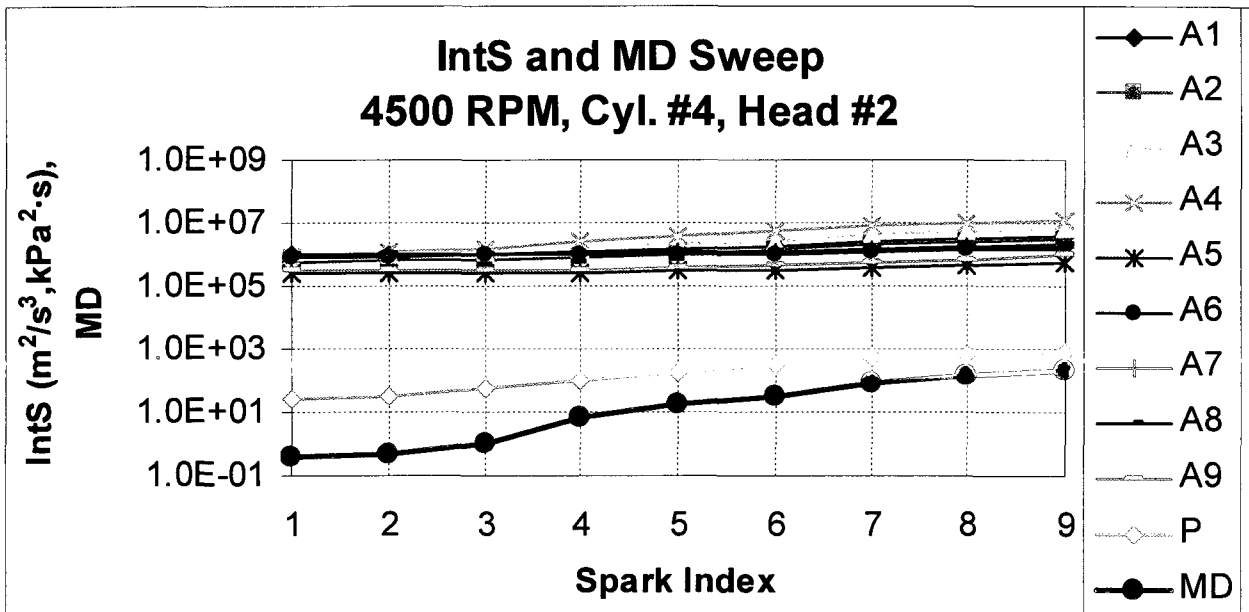


Figure C.3 bb - MD / IntS Sweep - 4500 RPM, Cyl. #4, Head #2

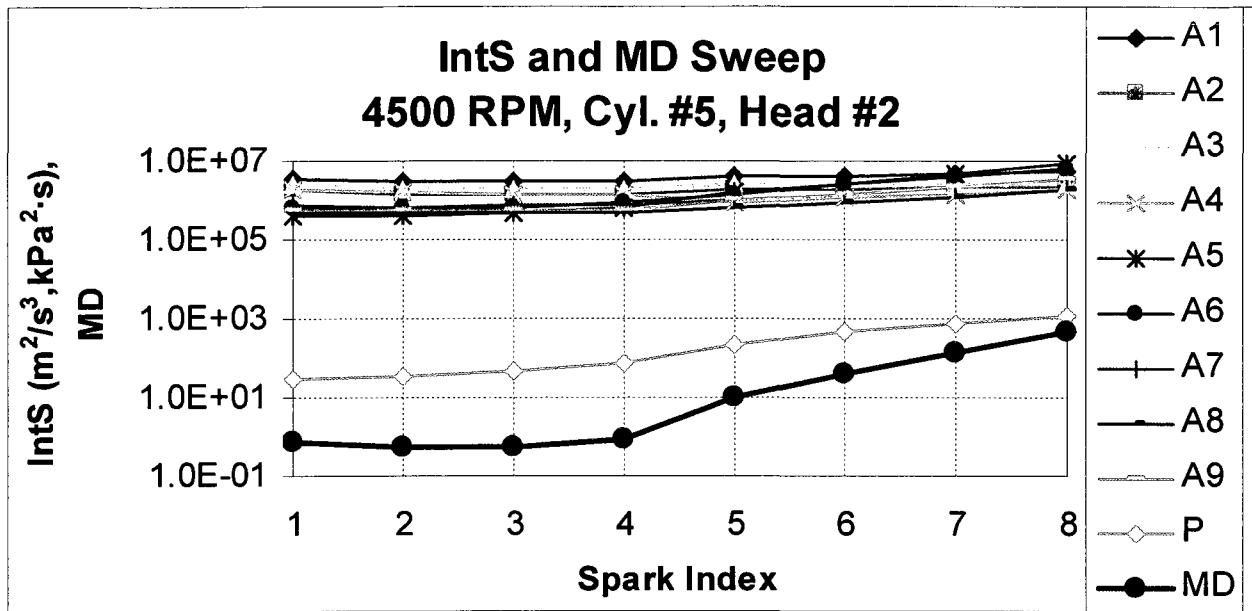


Figure C.3 cc - MD / IntS Sweep - 4500 RPM, Cyl. #5, Head #2

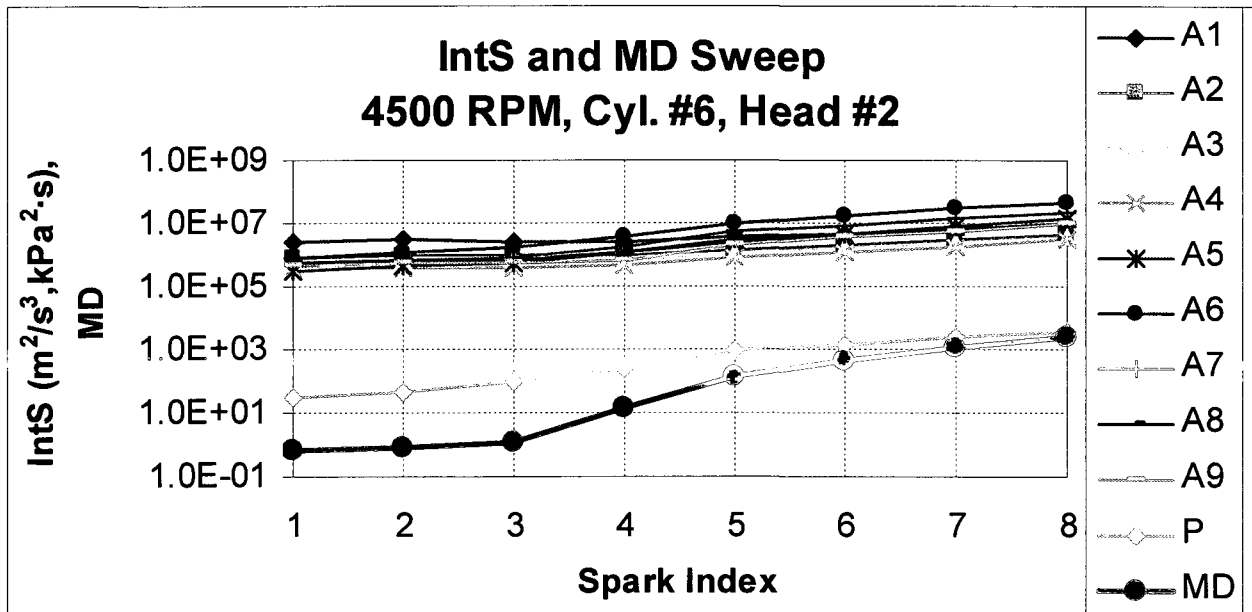


Figure C.3 dd - MD / IntS Sweep - 4500 RPM, Cyl. #6, Head #2

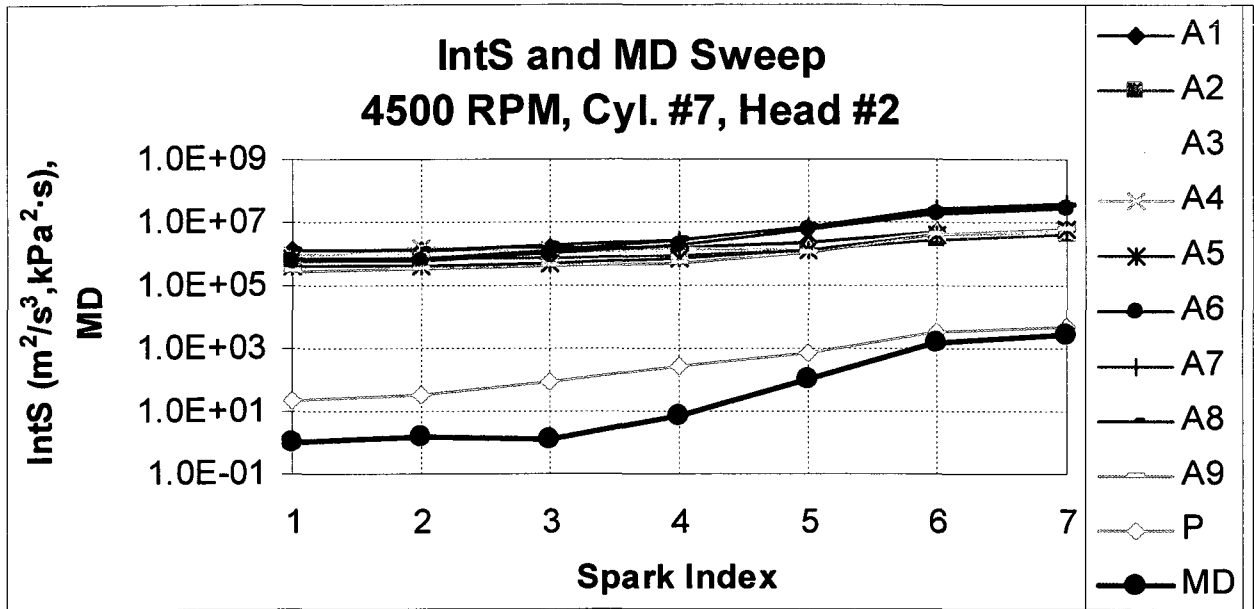


Figure C.3 ee - MD / IntS Sweep - 4500 RPM, Cyl. #7, Head #2

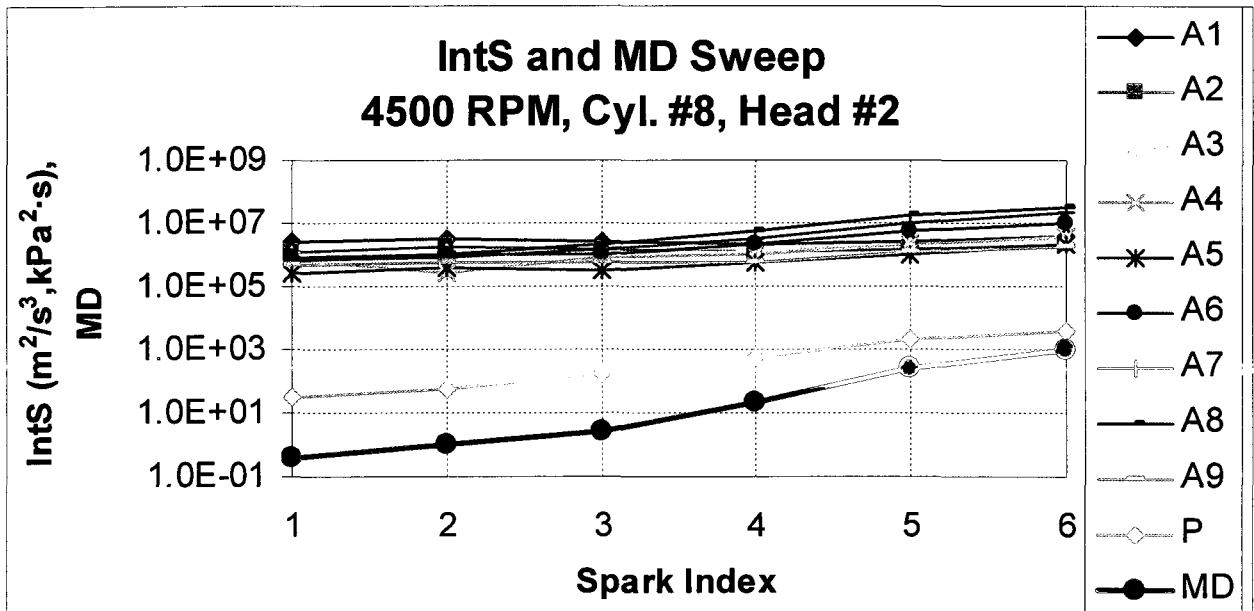


Figure C.3 ff - MD / IntS Sweep - 4500 RPM, Cyl. #8, Head #2

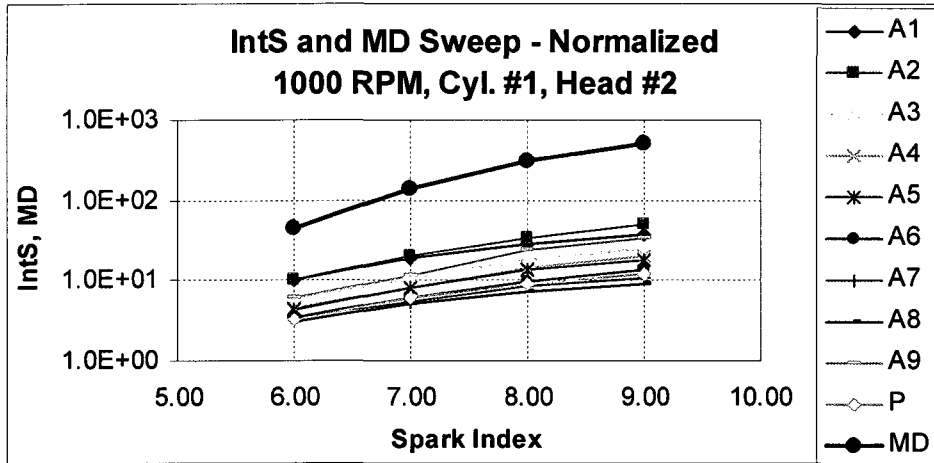


Figure C.4 a - MD / IntS Sweep (Normalized) - 1000 RPM, Cyl. #1, Head #2

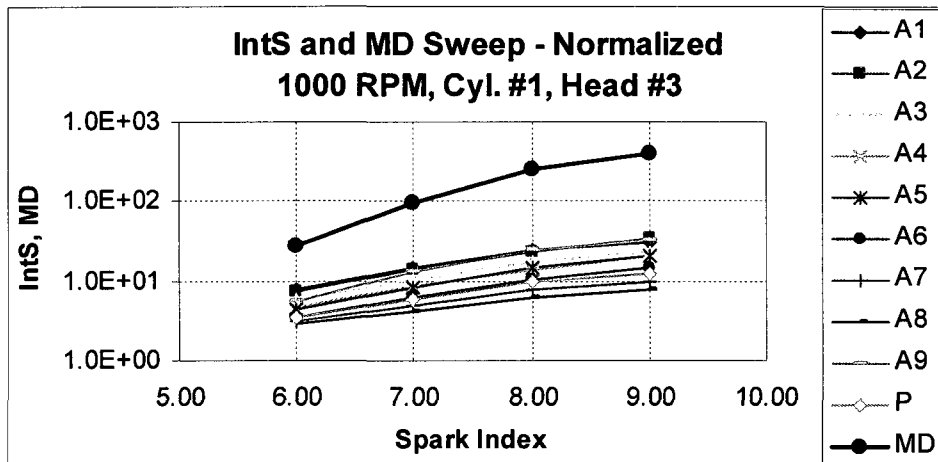


Figure C.4 b - MD / IntS Sweep (Normalized) - 1000 RPM, Cyl. #1, Head #3

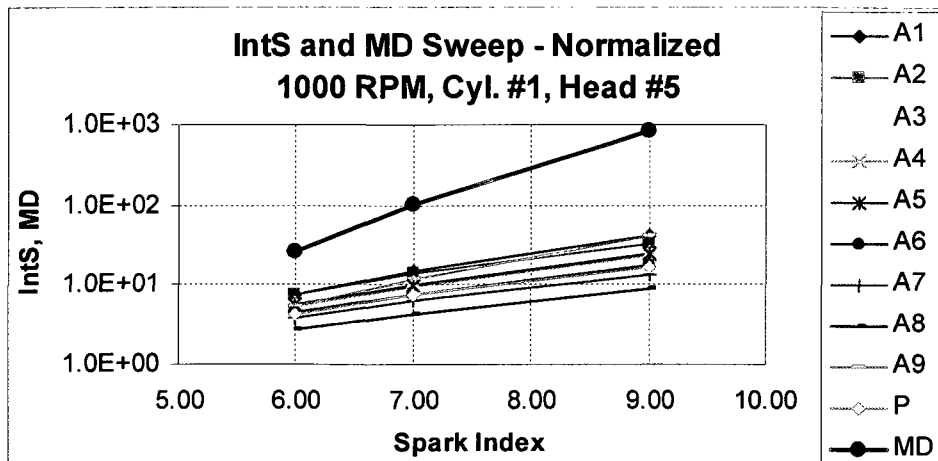


Figure C.4 c - MD / IntS Sweep (Normalized) - 1000 RPM, Cyl. #1, Head #5

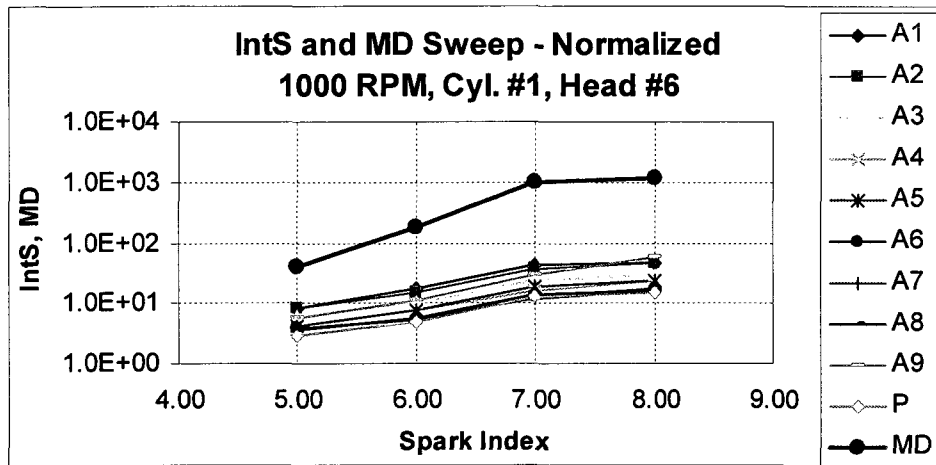


Figure C.4 d - MD / IntS Sweep (Normalized) - 1000 RPM, Cyl. #1, Head #6

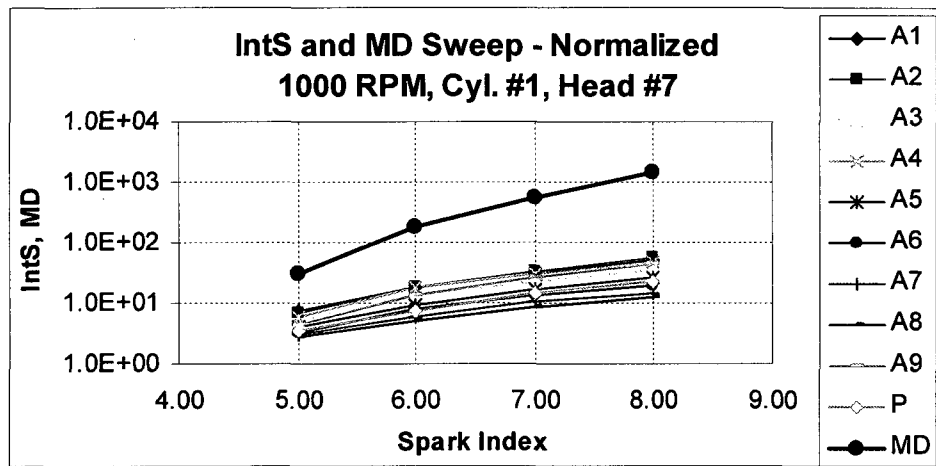


Figure C.4 e - MD / IntS Sweep (Normalized) - 1000 RPM, Cyl. #1, Head #7

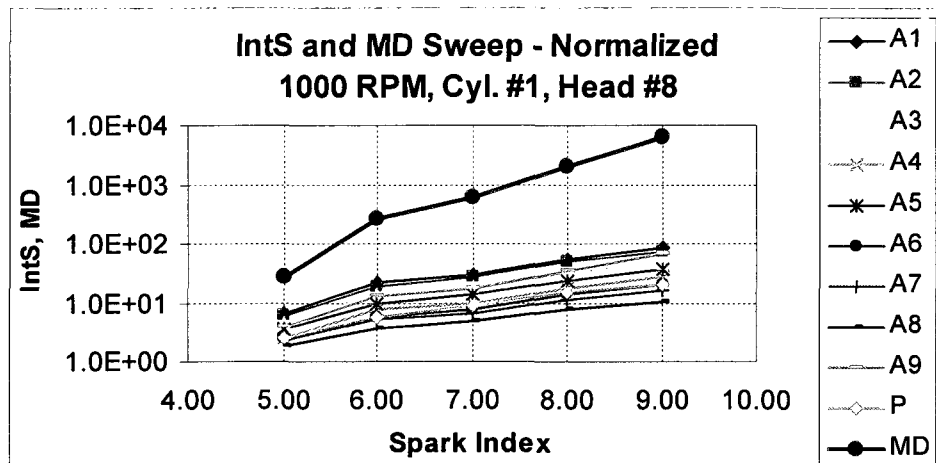


Figure C.4 f - MD / IntS Sweep (Normalized) - 1000 RPM, Cyl. #1, Head #8

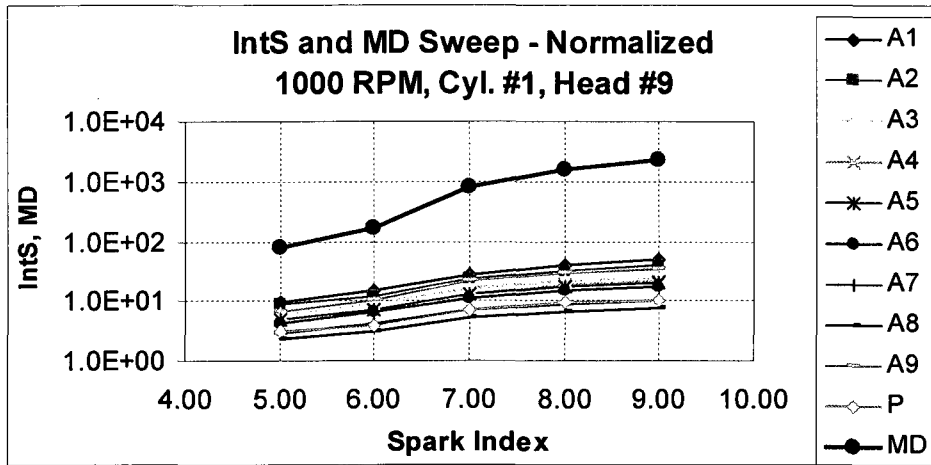


Figure C.4 g - MD / IntS Sweep (Normalized) - 1000 RPM, Cyl. #1, Head #9

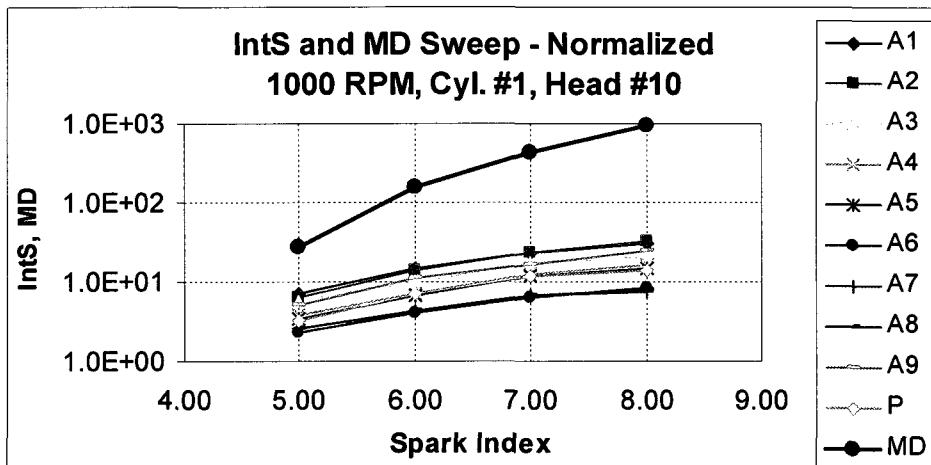


Figure C.4 h - MD / IntS Sweep (Normalized) - 1000 RPM, Cyl. #1, Head #10

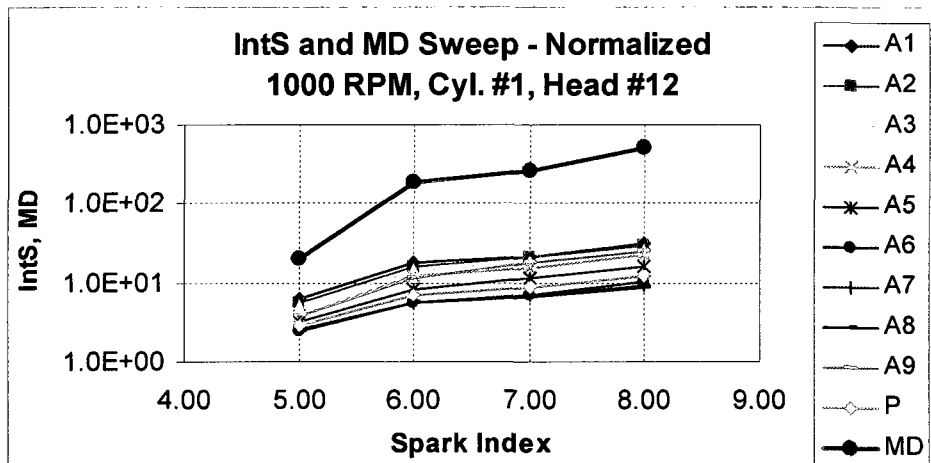


Figure C.4 i - MD / IntS Sweep (Normalized) - 1000 RPM, Cyl. #1, Head #12

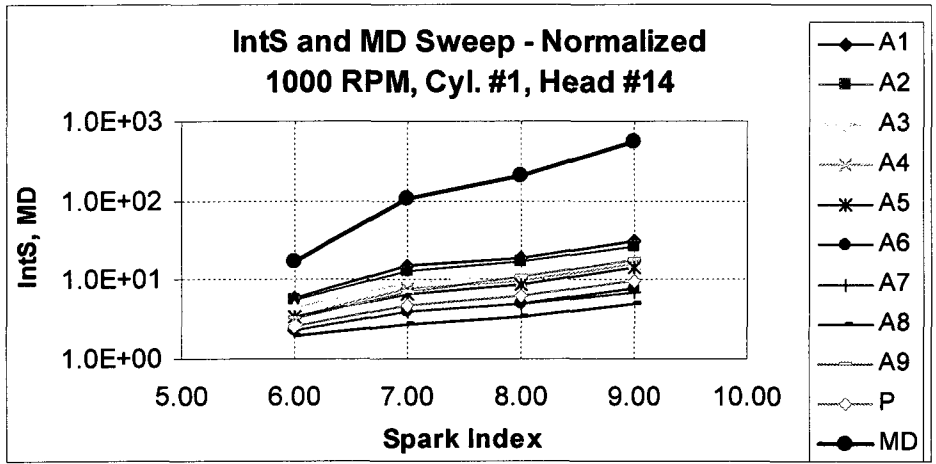


Figure C.4 j - MD / IntS Sweep (Normalized) - 1000 RPM, Cyl. #1, Head #14

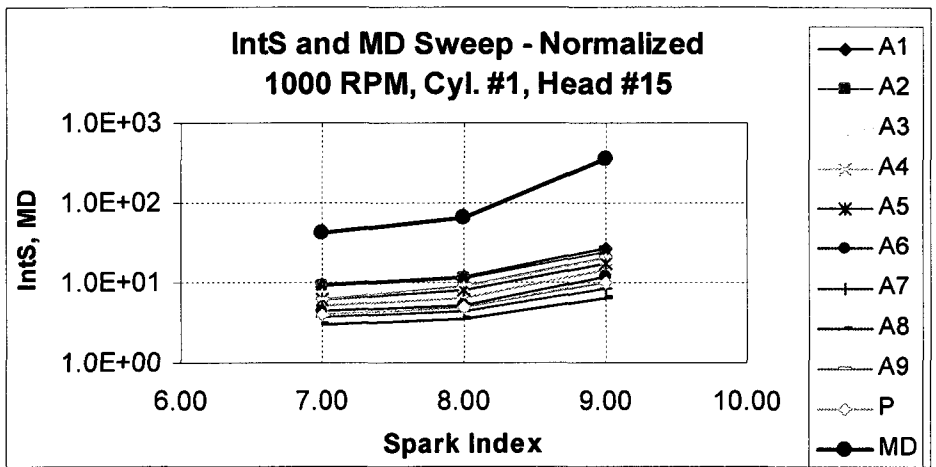


Figure C.4 k - MD / IntS Sweep (Normalized) - 1000 RPM, Cyl. #1, Head #15

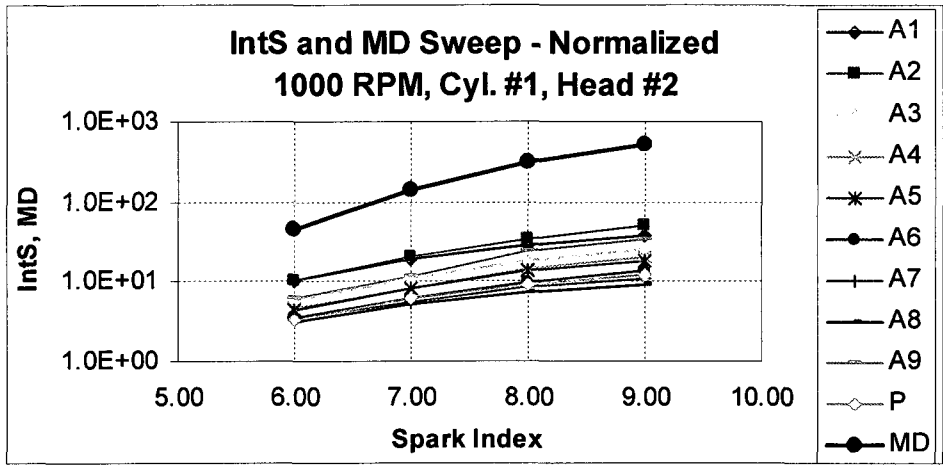


Figure C.5 a - MD / IntS Sweep (Normalized) - 1000 RPM, Cyl. #1, Head #2

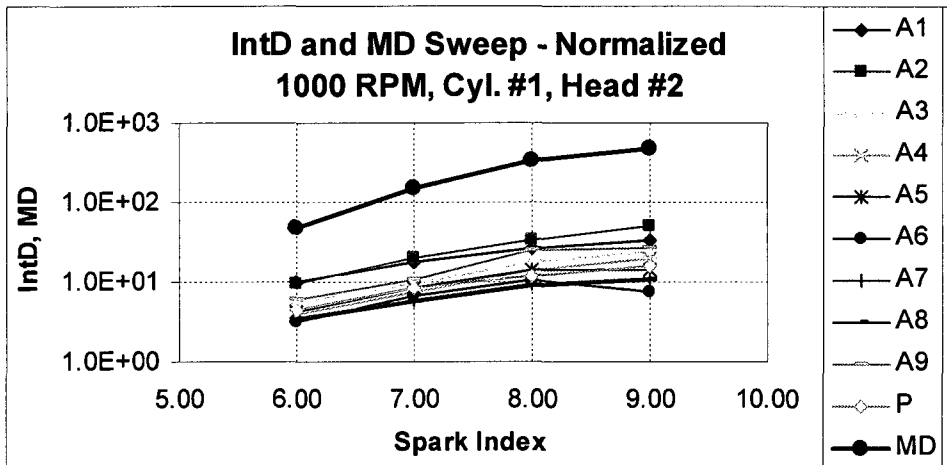


Figure C.5 b - MD / IntD Sweep (Normalized) - 1000 RPM, Cyl. #1, Head #2

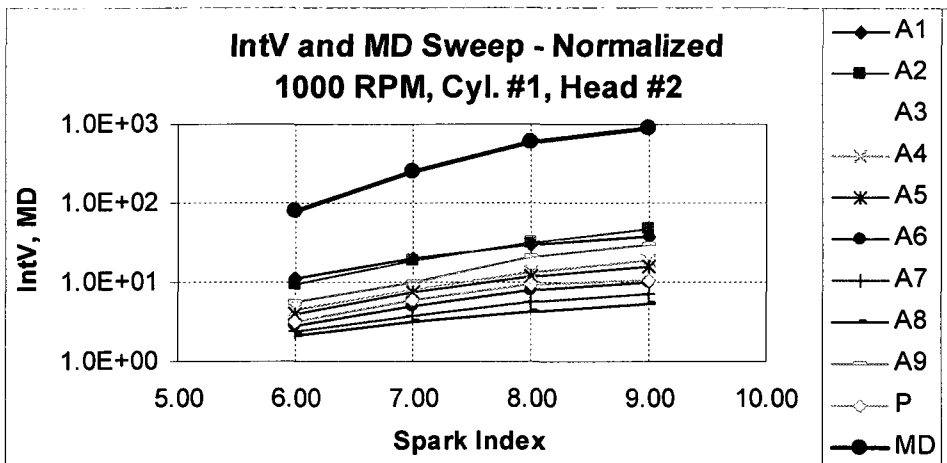


Figure C.5 c - MD / IntV Sweep (Normalized) - 1000 RPM, Cyl. #1, Head #2

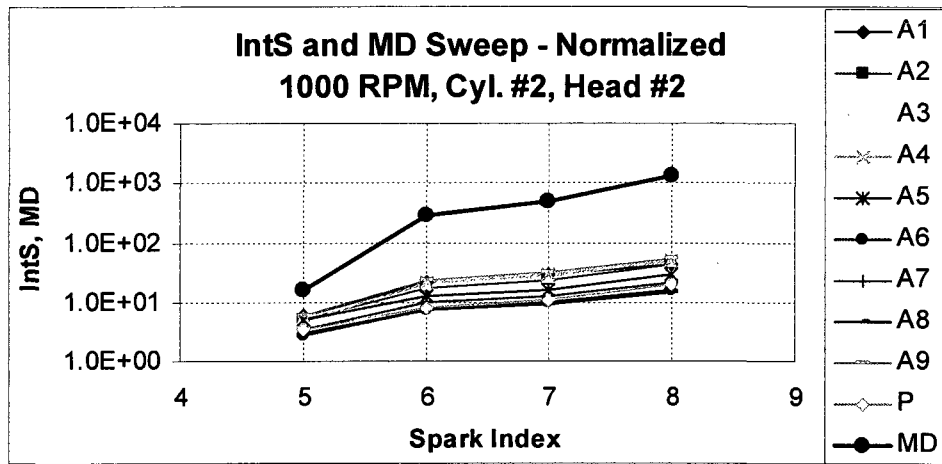


Figure C.5 d - MD / IntS Sweep (Normalized) - 1000 RPM, Cyl. #2, Head #2

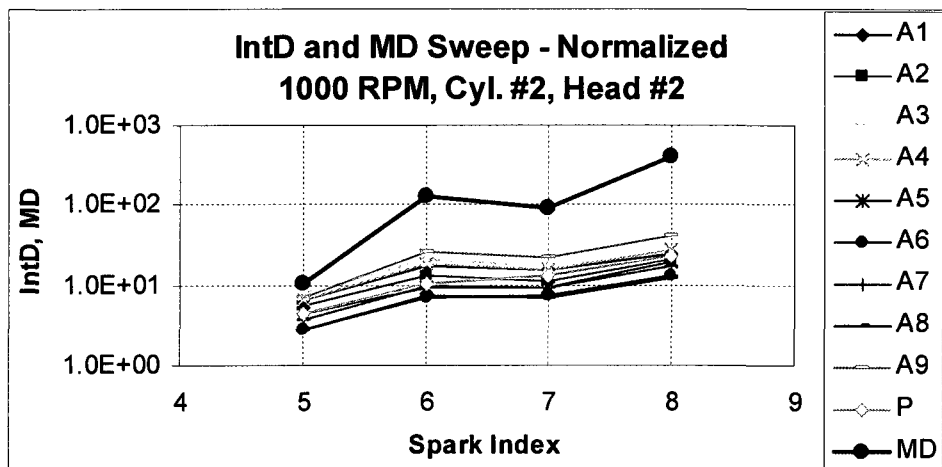


Figure C.5 e - MD / IntD Sweep (Normalized) - 1000 RPM, Cyl. #2, Head #2

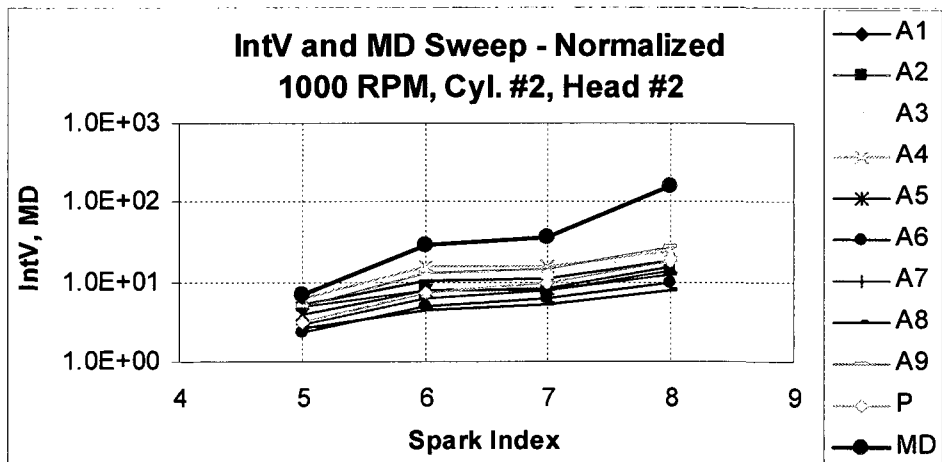


Figure C.5 f - MD / IntV Sweep (Normalized) - 1000 RPM, Cyl. #2, Head #2

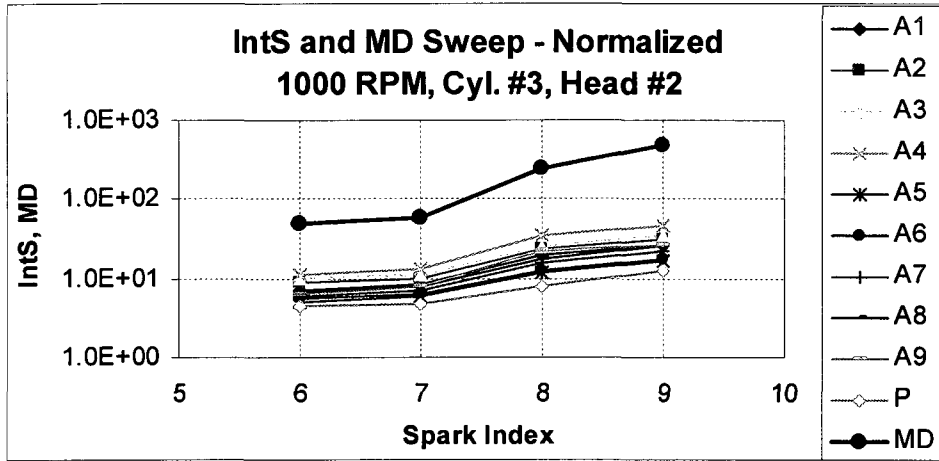


Figure C.5 g - MD / IntS Sweep (Normalized) - 1000 RPM, Cyl. #3, Head #2

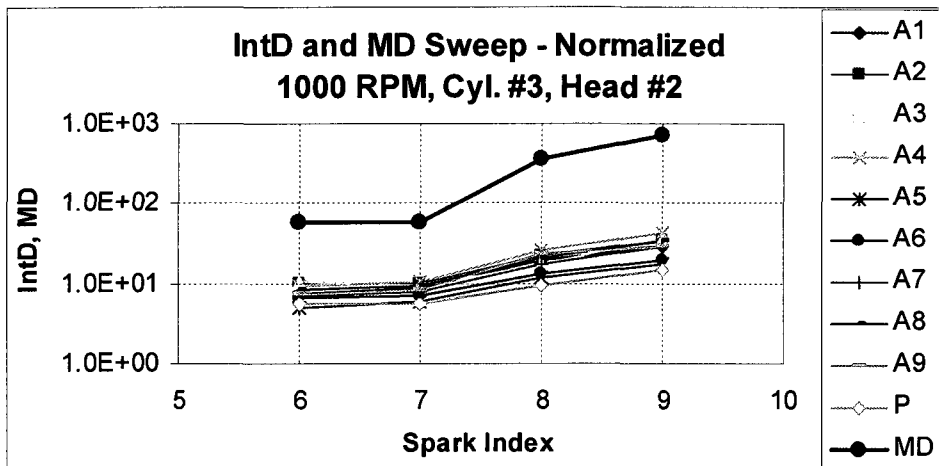


Figure C.5 h - MD / IntD Sweep (Normalized) - 1000 RPM, Cyl. #3, Head #2

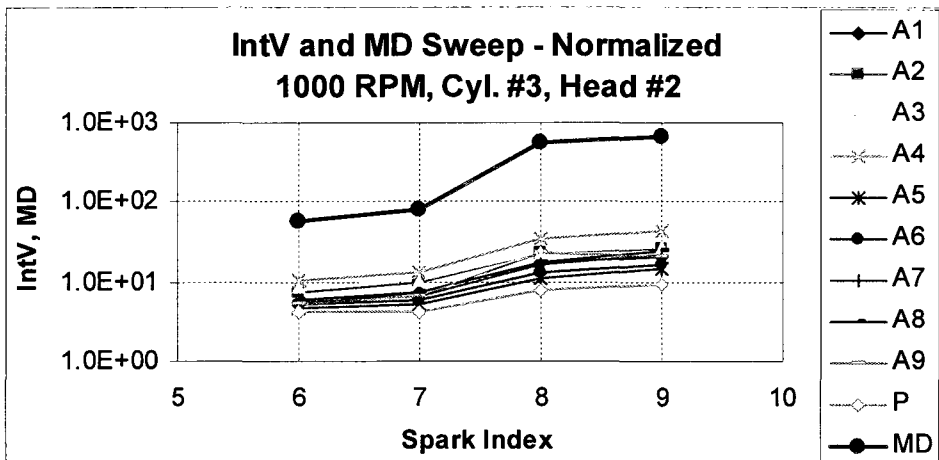


Figure C.5 i - MD / IntV Sweep (Normalized) - 1000 RPM, Cyl. #3, Head #2

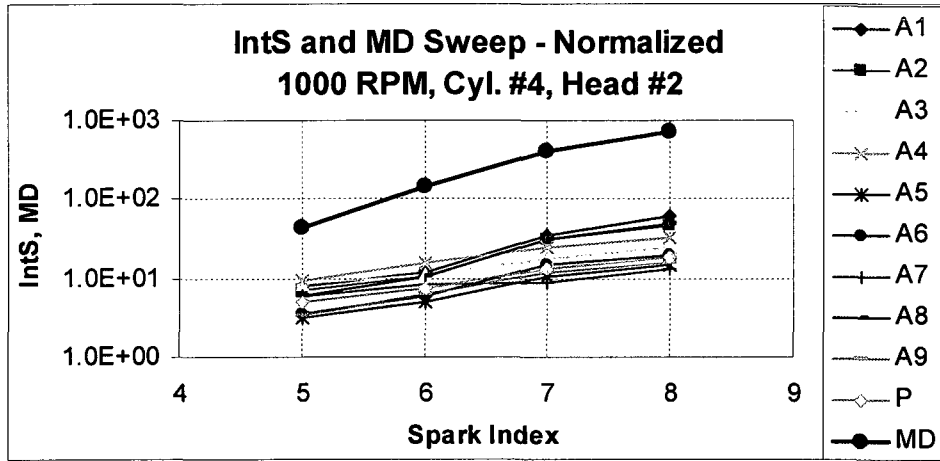


Figure C.5 j - MD / IntS Sweep (Normalized) - 1000 RPM, Cyl. #4, Head #2

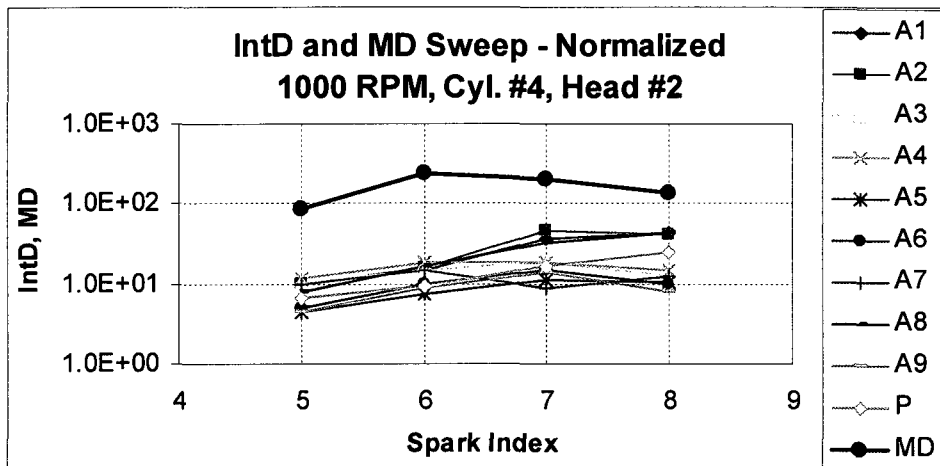


Figure C.5 k - MD / IntD Sweep (Normalized) - 1000 RPM, Cyl. #4, Head #2

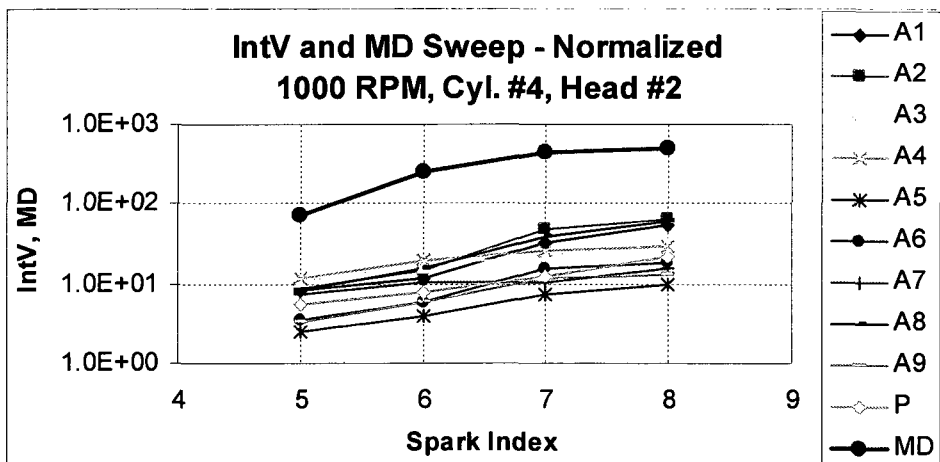


Figure C.5 l - MD / IntV Sweep (Normalized) - 1000 RPM, Cyl. #4, Head #2

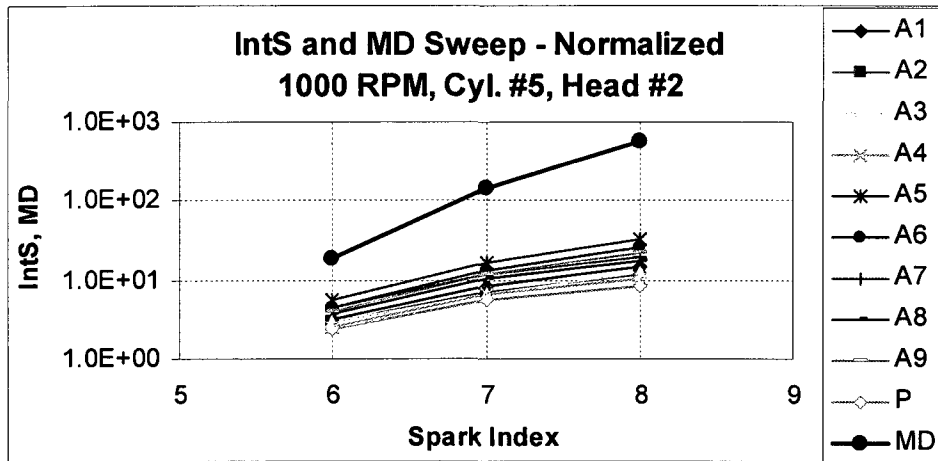


Figure C.5 m - MD / IntS Sweep (Normalized) - 1000 RPM, Cyl. #5, Head #2

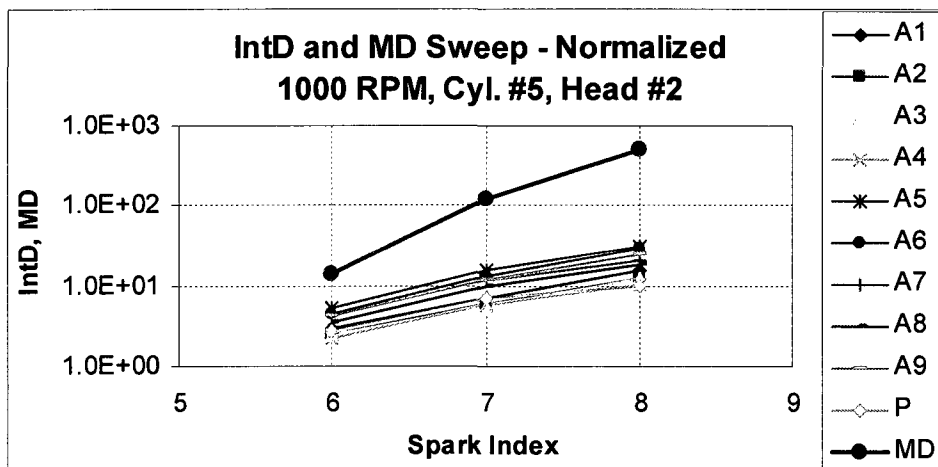


Figure C.5 n - MD / IntD Sweep (Normalized) - 1000 RPM, Cyl. #5, Head #2

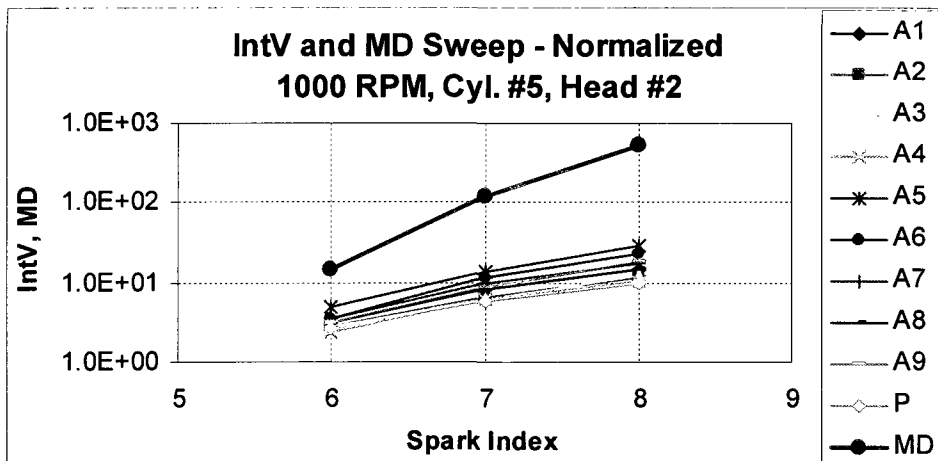


Figure C.5 o - MD / IntV Sweep (Normalized) - 1000 RPM, Cyl. #5, Head #2

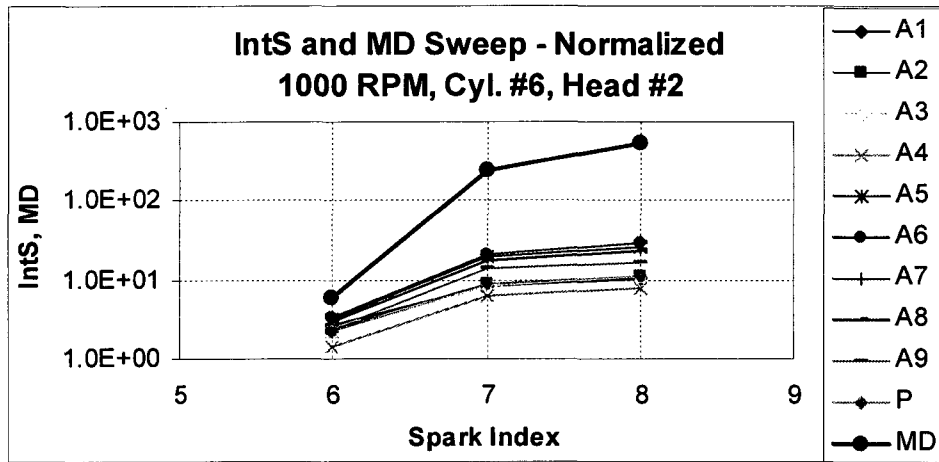


Figure C.5 p - MD / IntS Sweep (Normalized) - 1000 RPM, Cyl. #6, Head #2

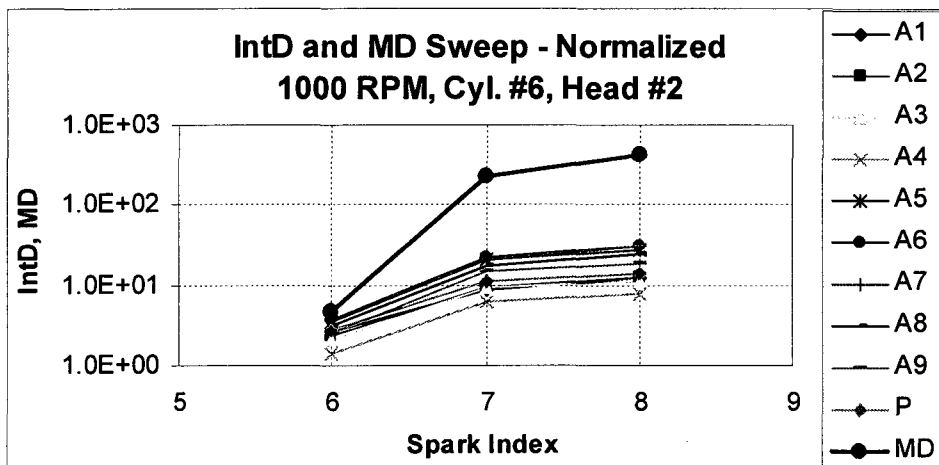


Figure C.5 q - MD / IntD Sweep (Normalized) - 1000 RPM, Cyl. #6, Head #2

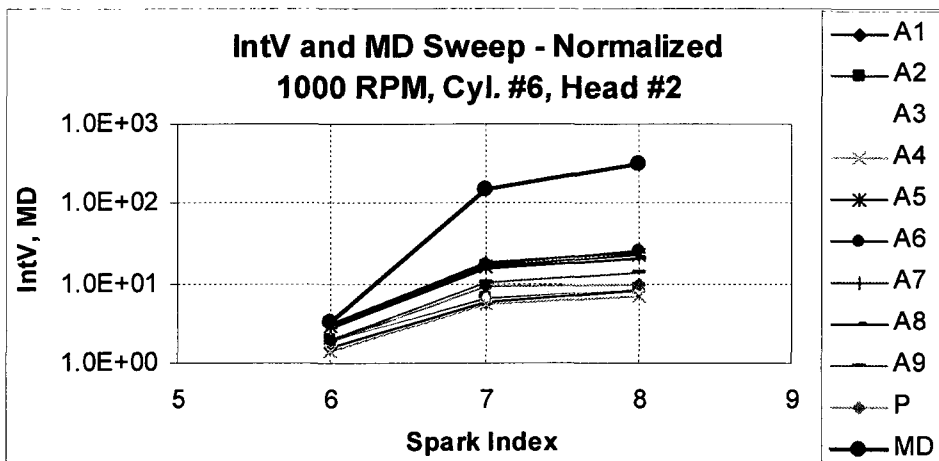


Figure C.5 r - MD / IntV Sweep (Normalized) - 1000 RPM, Cyl. #6, Head #2

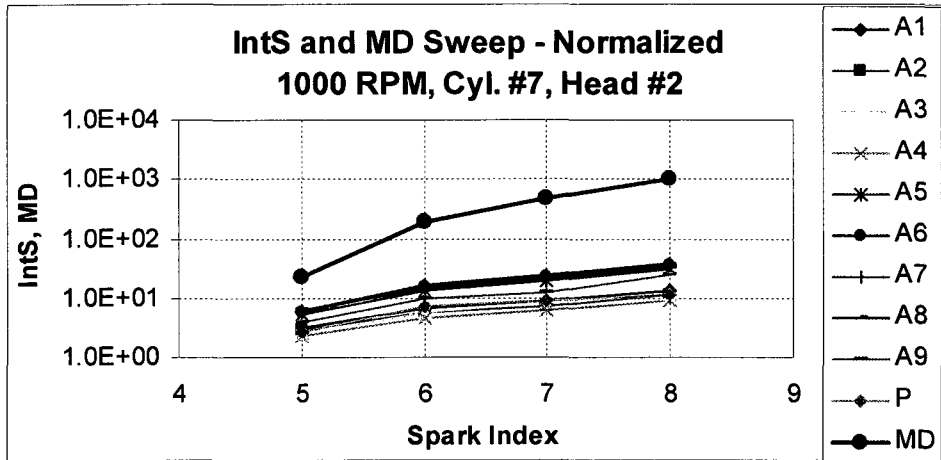


Figure C.5 s - MD / IntS Sweep (Normalized) - 1000 RPM, Cyl. #7, Head #2

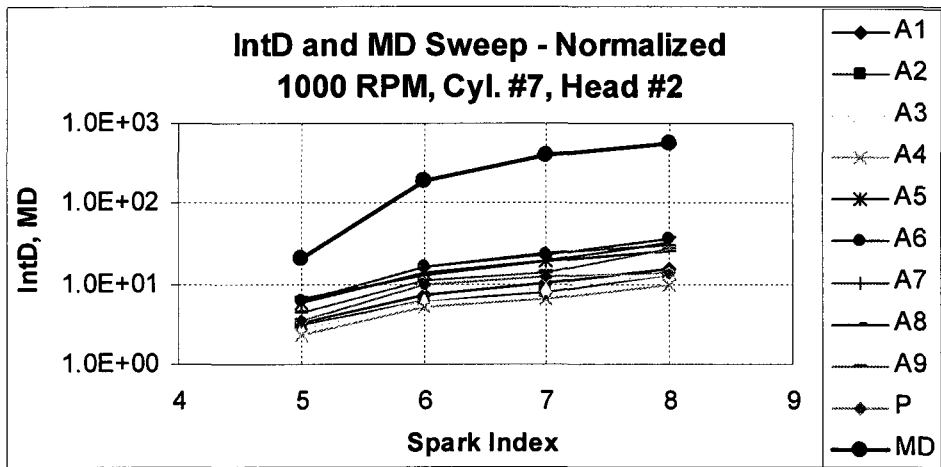


Figure C.5 t - MD / IntD Sweep (Normalized) - 1000 RPM, Cyl. #7, Head #2

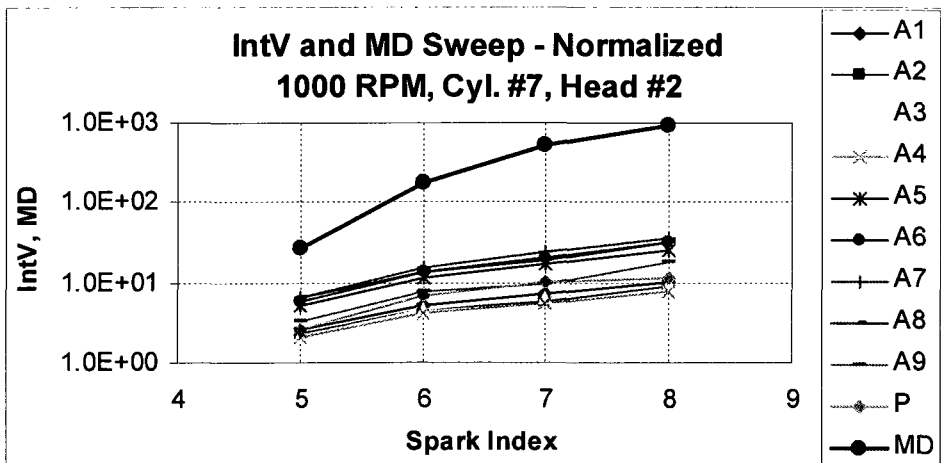


Figure C.5 u - MD / IntV Sweep (Normalized) - 1000 RPM, Cyl. #7, Head #2

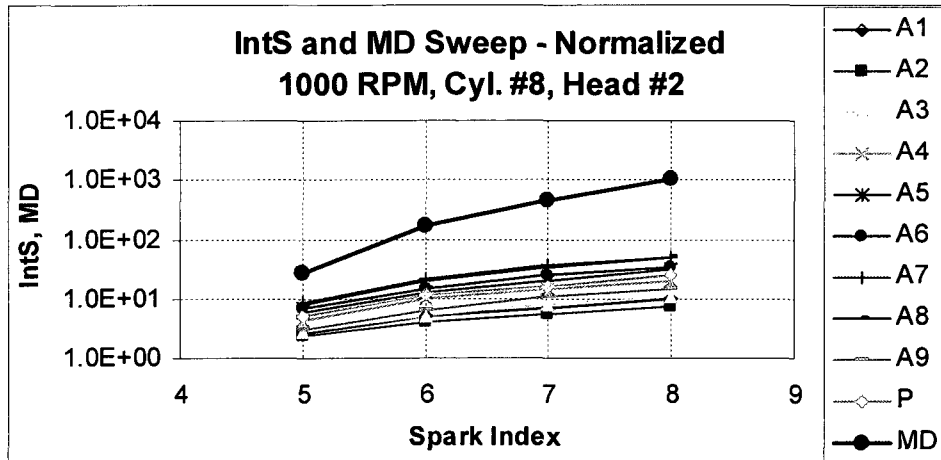


Figure C.5 v - MD / IntS Sweep (Normalized) - 1000 RPM, Cyl. #8, Head #2

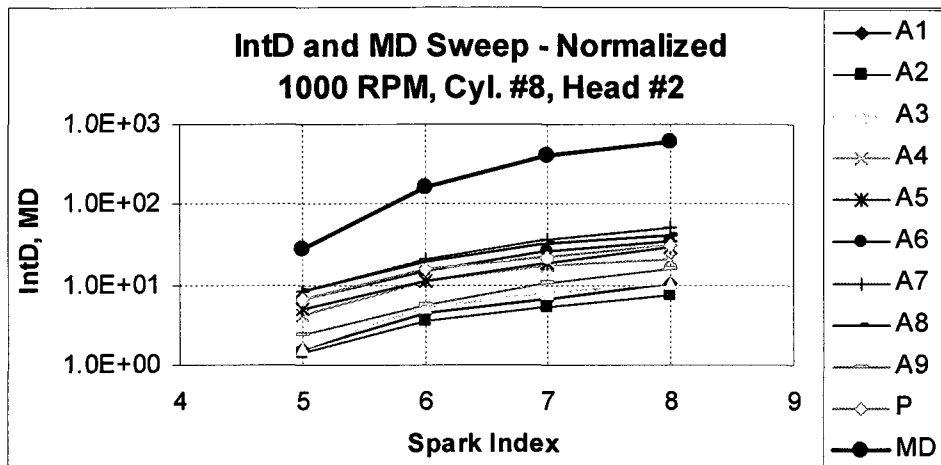


Figure C.5 w - MD / IntD Sweep (Normalized) - 1000 RPM, Cyl. #8, Head #2

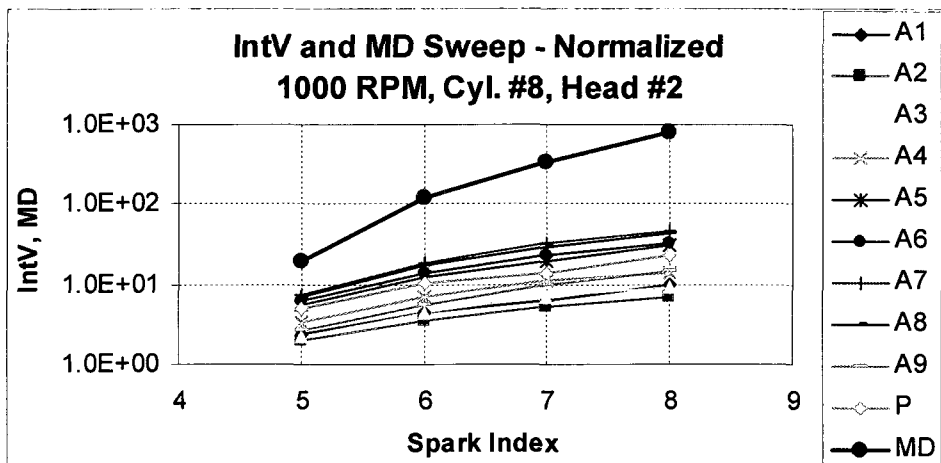


Figure C.5 x - MD / IntV Sweep (Normalized) - 1000 RPM, Cyl. #8, Head #2

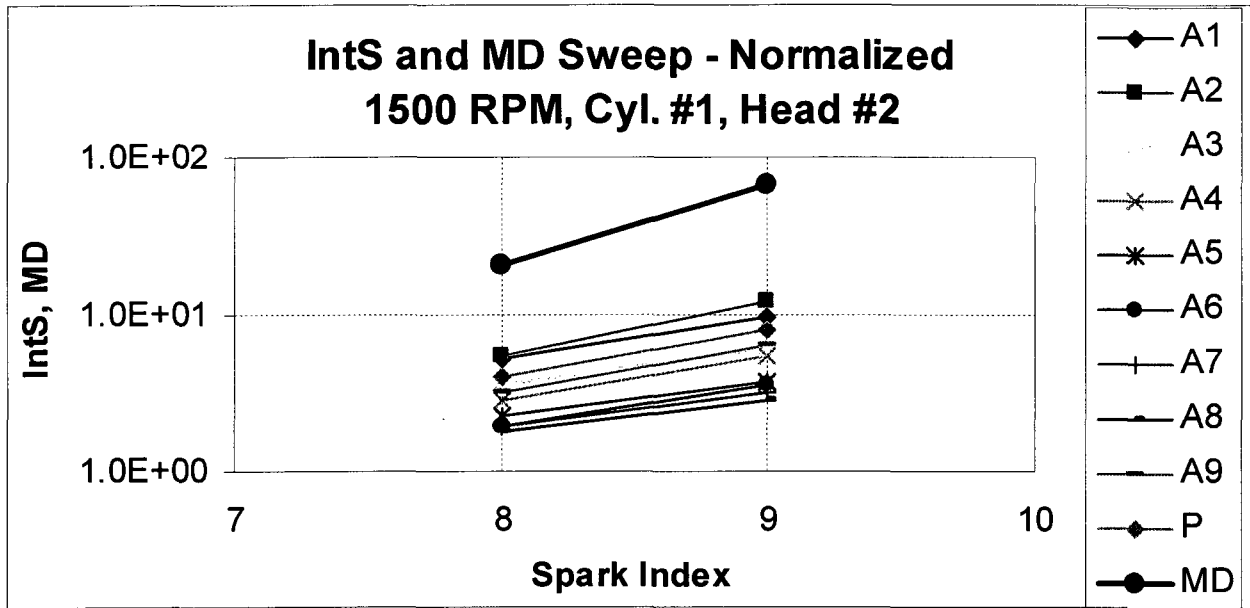


Figure C.6 a - MD / IntS Sweep (Normalized) - 1500 RPM, Cyl. #1, Head #2

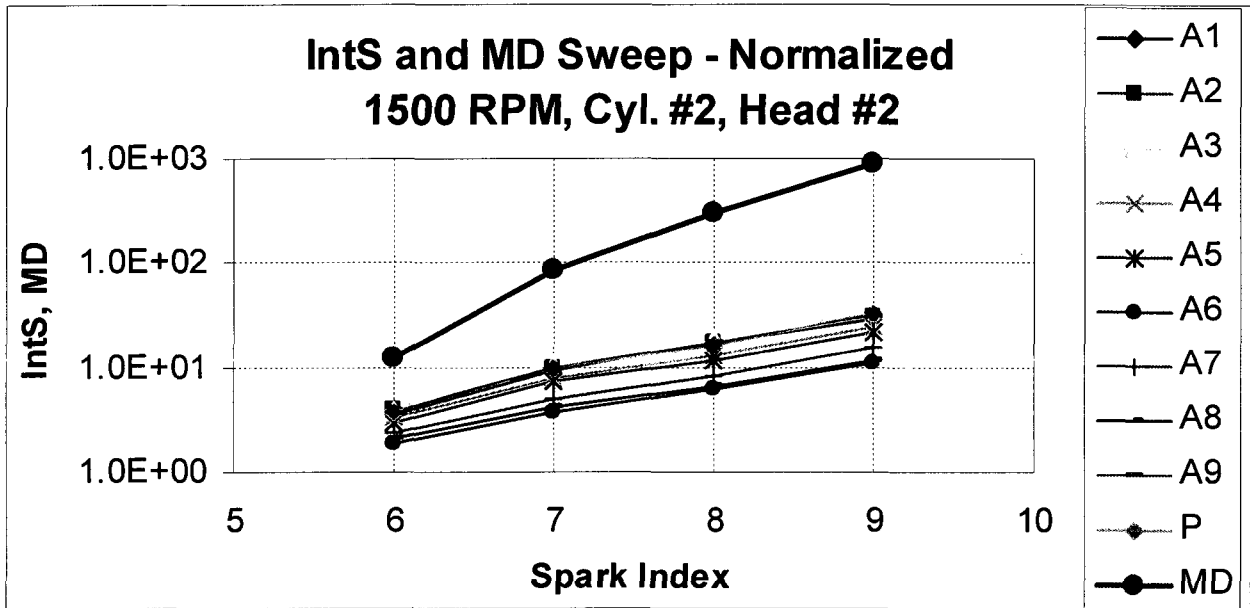


Figure C.6 b - MD / IntS Sweep (Normalized) - 1500 RPM, Cyl. #2, Head #2

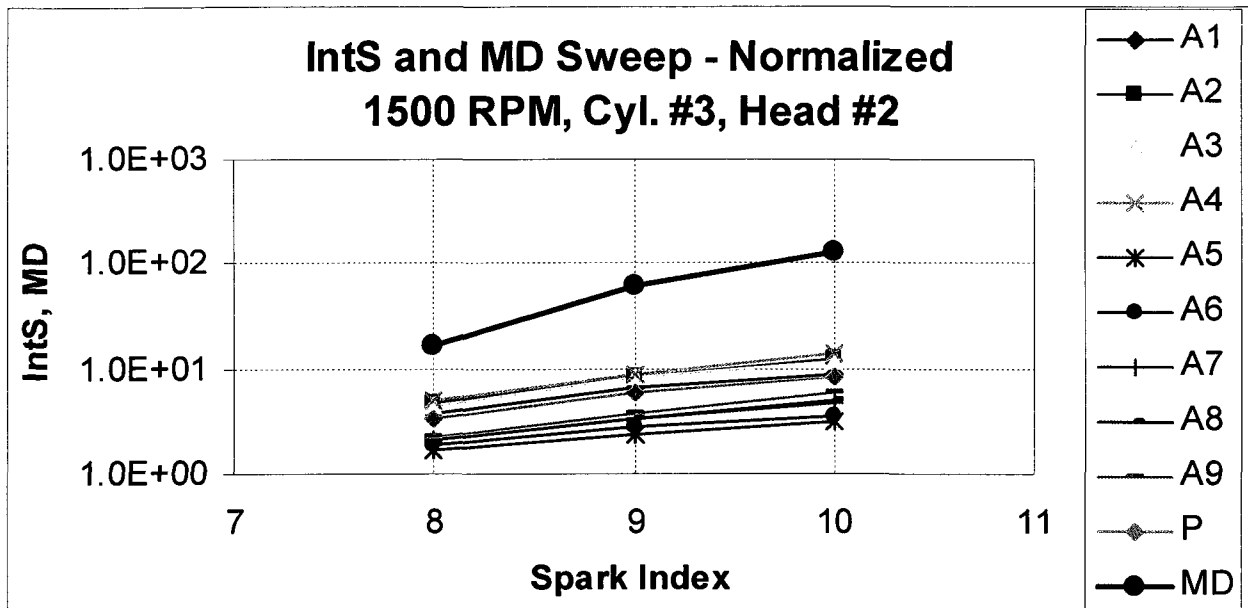


Figure C.6 c - MD / IntS Sweep (Normalized) - 1500 RPM, Cyl. #3, Head #2

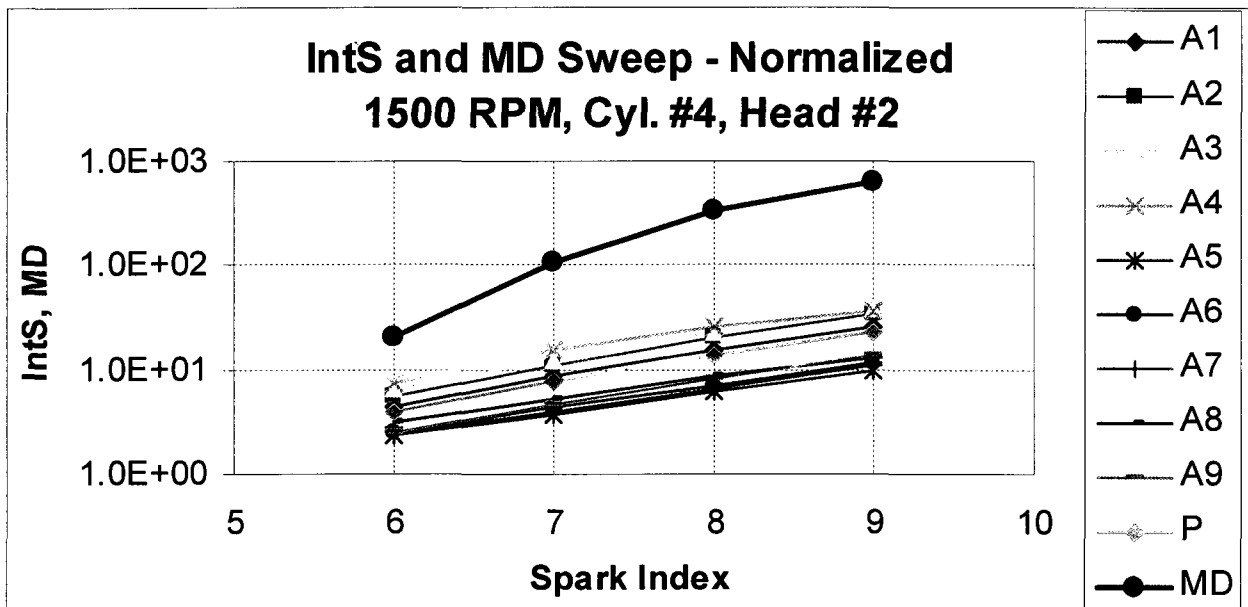


Figure C.6 d - MD / IntS Sweep (Normalized) - 1500 RPM, Cyl. #4, Head #2

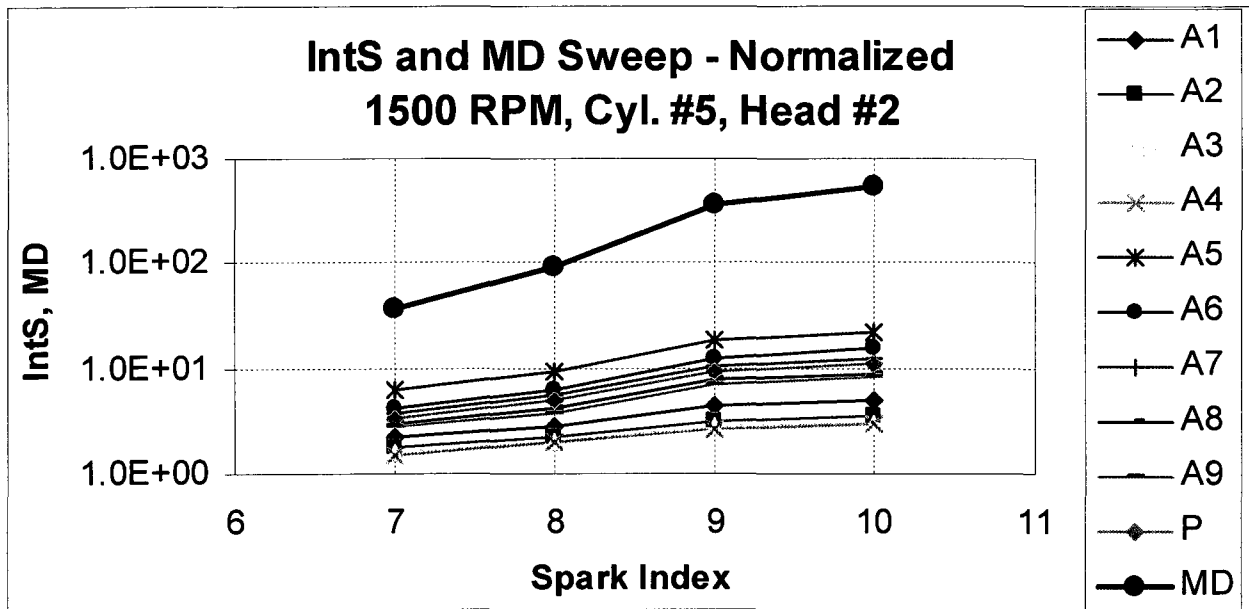


Figure C.6 e - MD / IntS Sweep (Normalized) - 1500 RPM, Cyl. #5, Head #2

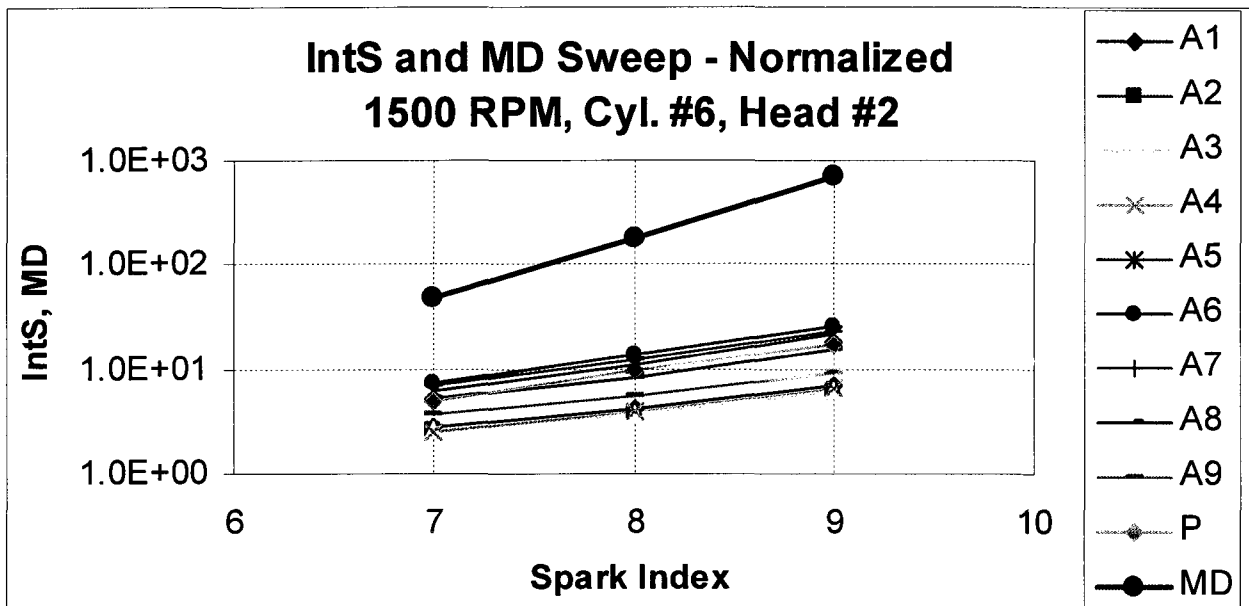


Figure C.6 f - MD / IntS Sweep (Normalized) - 1500 RPM, Cyl. #6, Head #2

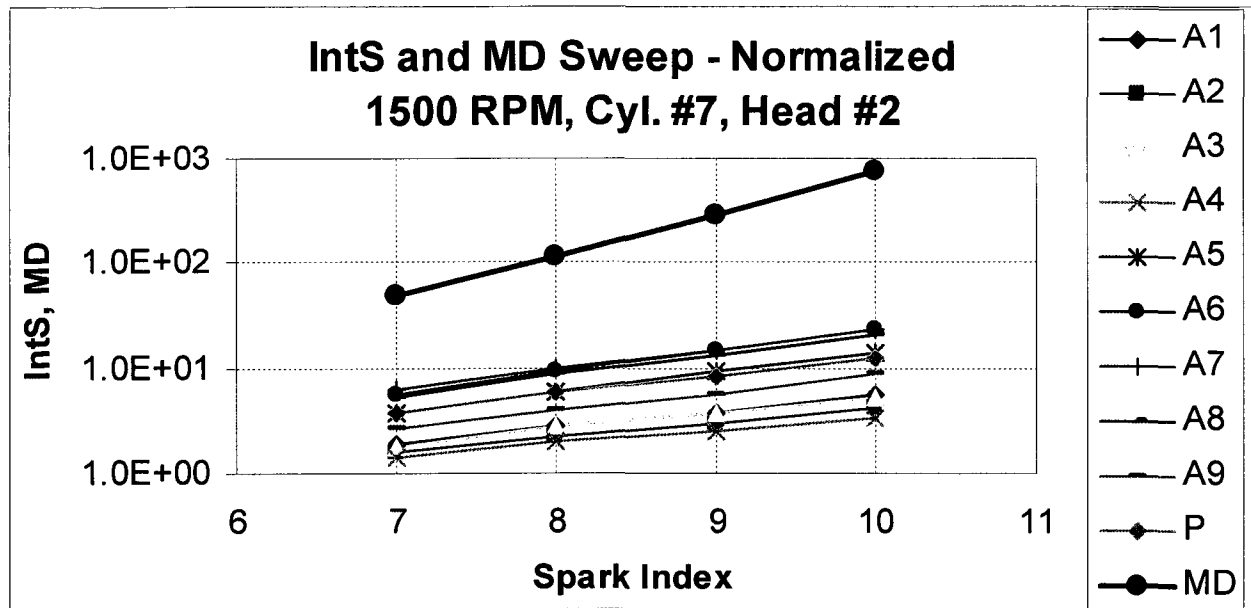


Figure C.6 g - MD / IntS Sweep (Normalized) - 1500 RPM, Cyl. #7, Head #2

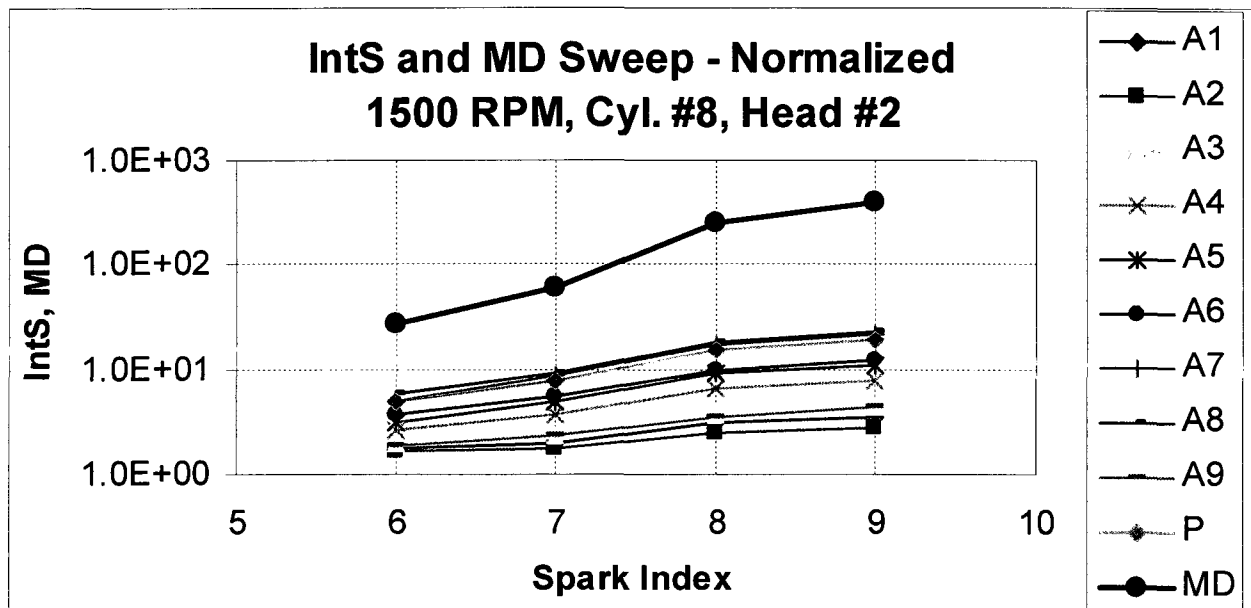


Figure C.6 h - MD / IntS Sweep (Normalized) - 1500 RPM, Cyl. #8, Head #2

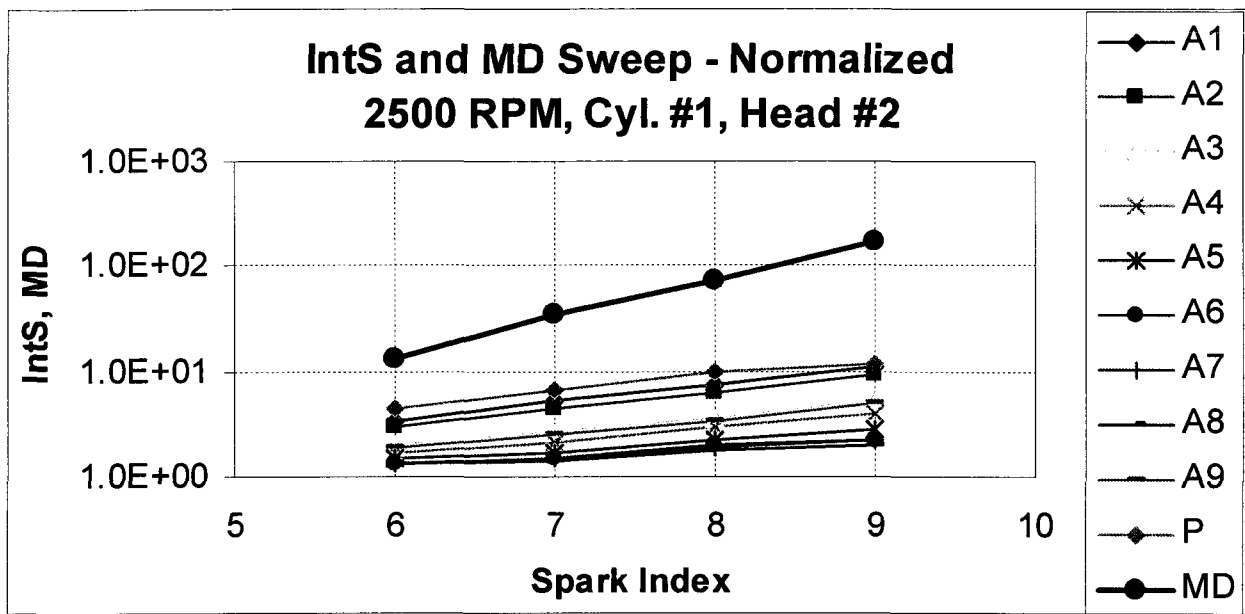


Figure C.6 i - MD / IntS Sweep (Normalized) - 2500 RPM, Cyl. #1, Head #2

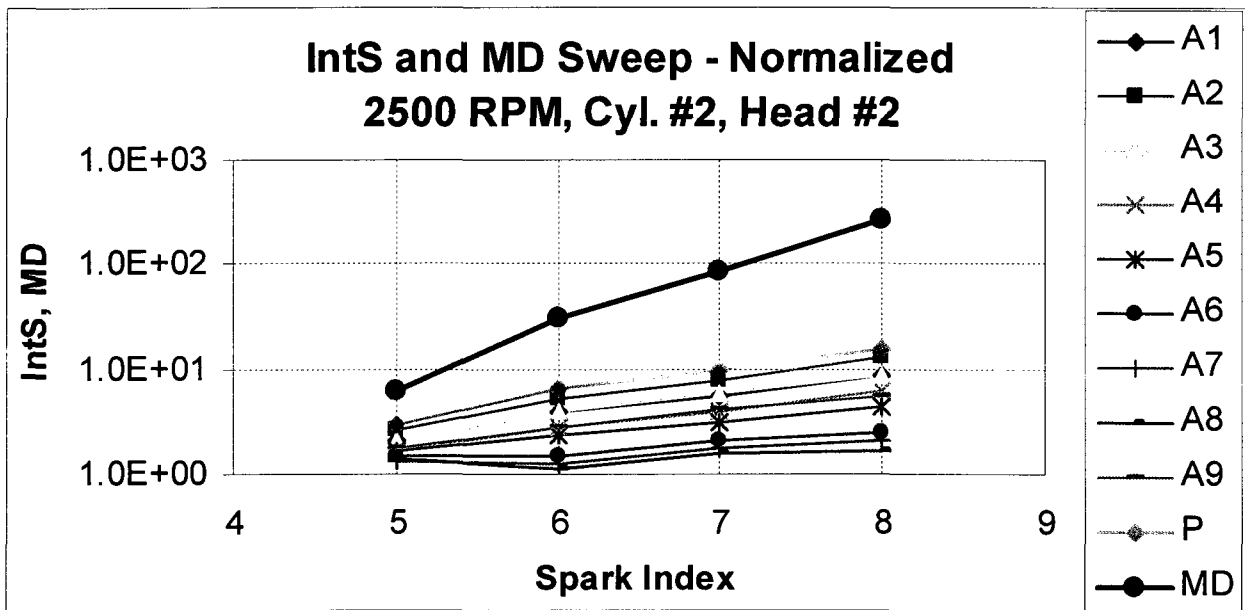


Figure C.6 j - MD / IntS Sweep (Normalized) - 2500 RPM, Cyl. #2, Head #2

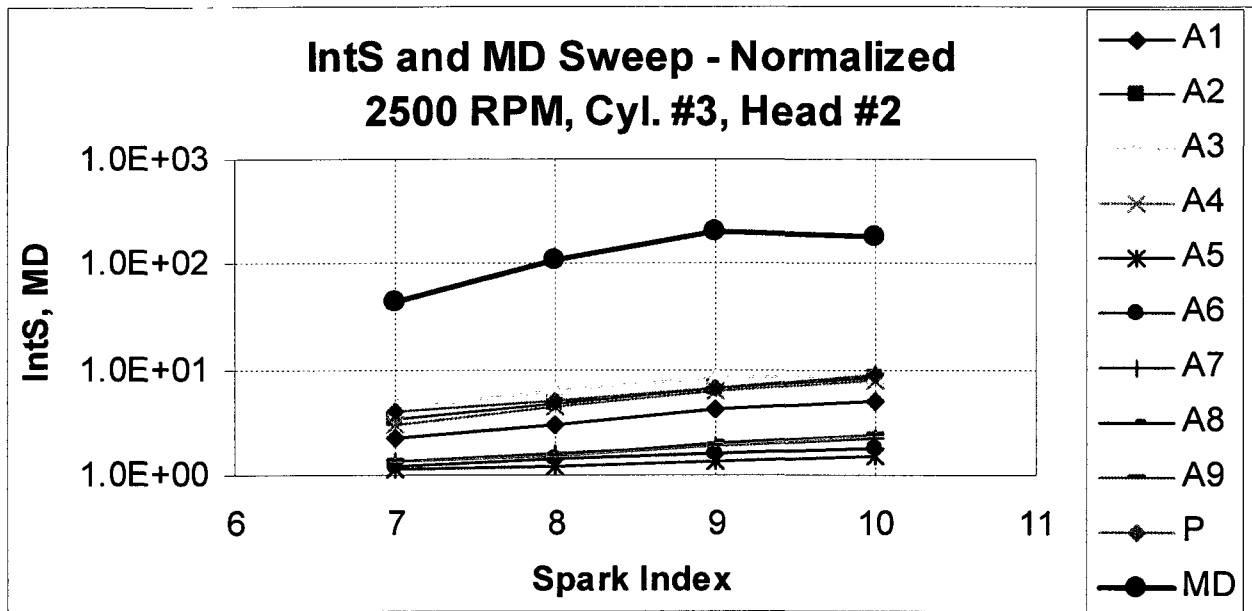


Figure C.6 k - MD / IntS Sweep (Normalized) - 2500 RPM, Cyl. #3, Head #2

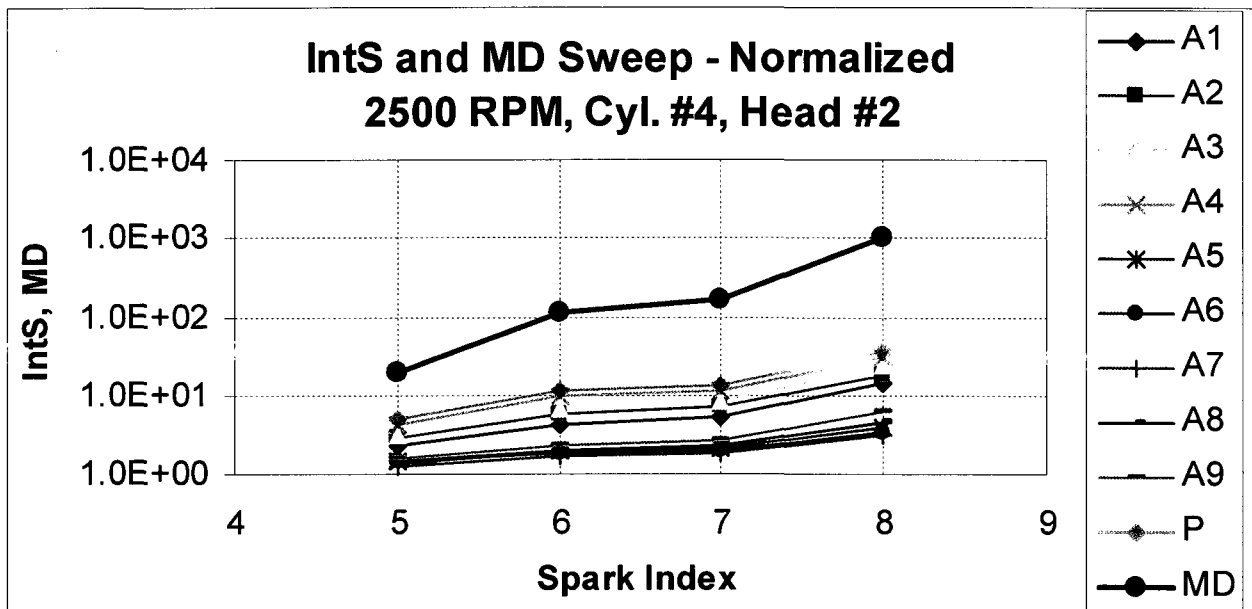


Figure C.6 l - MD / IntS Sweep (Normalized) - 2500 RPM, Cyl. #4, Head #2

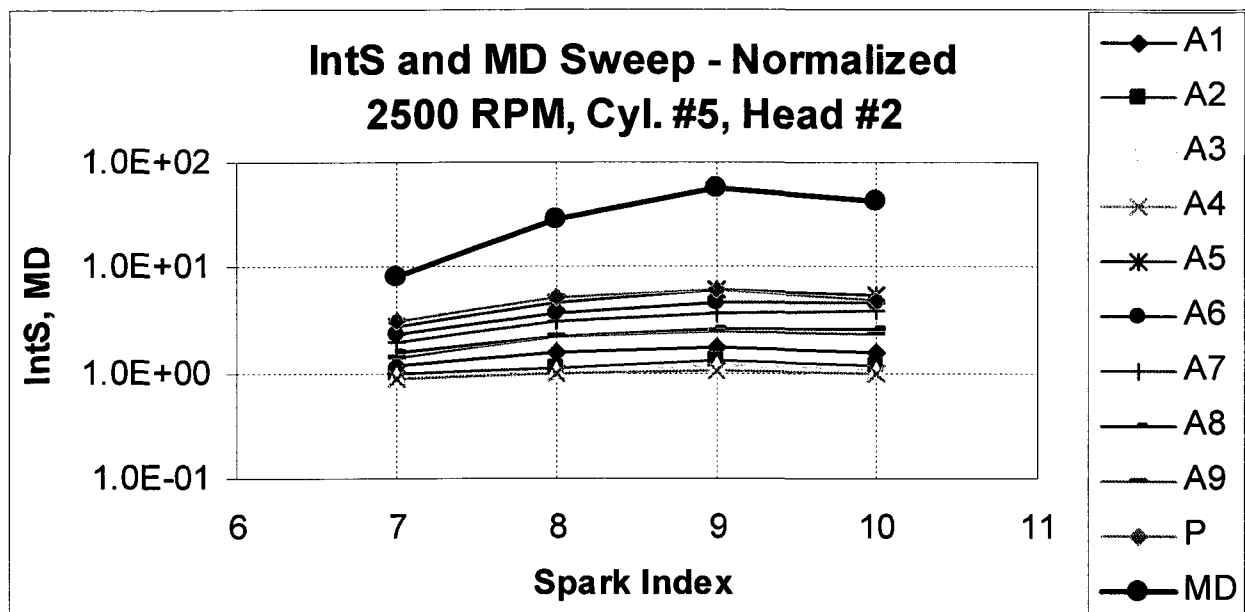


Figure C.6 m - MD / IntS Sweep (Normalized) - 2500 RPM, Cyl. #5, Head #2

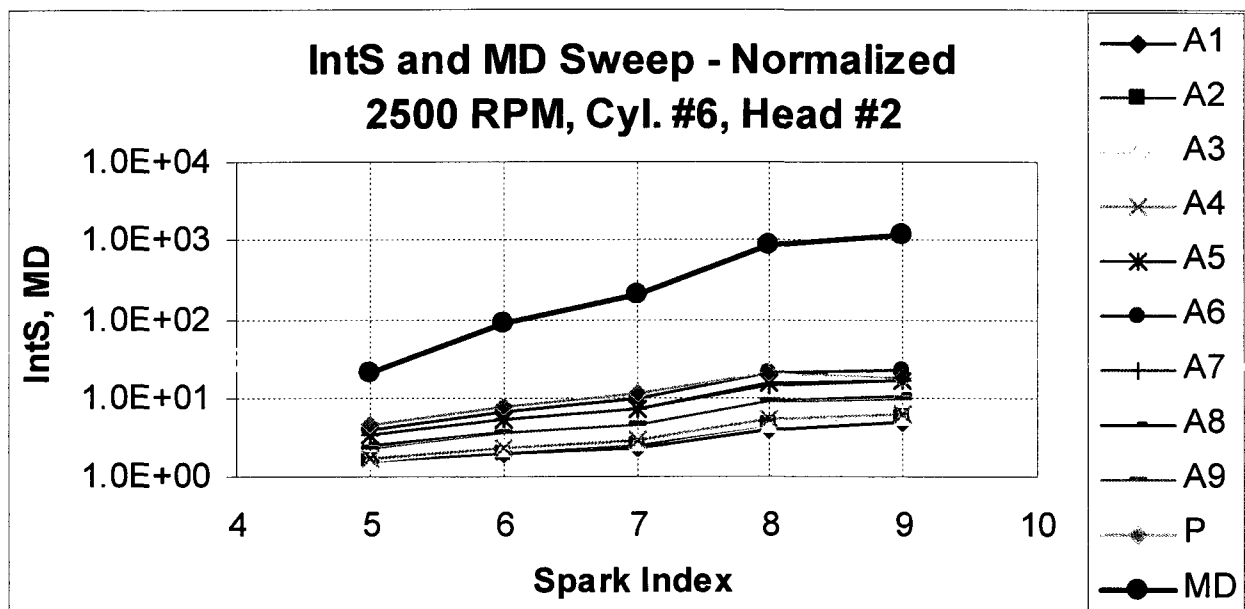


Figure C.6 n - MD / IntS Sweep (Normalized) - 2500 RPM, Cyl. #6, Head #2

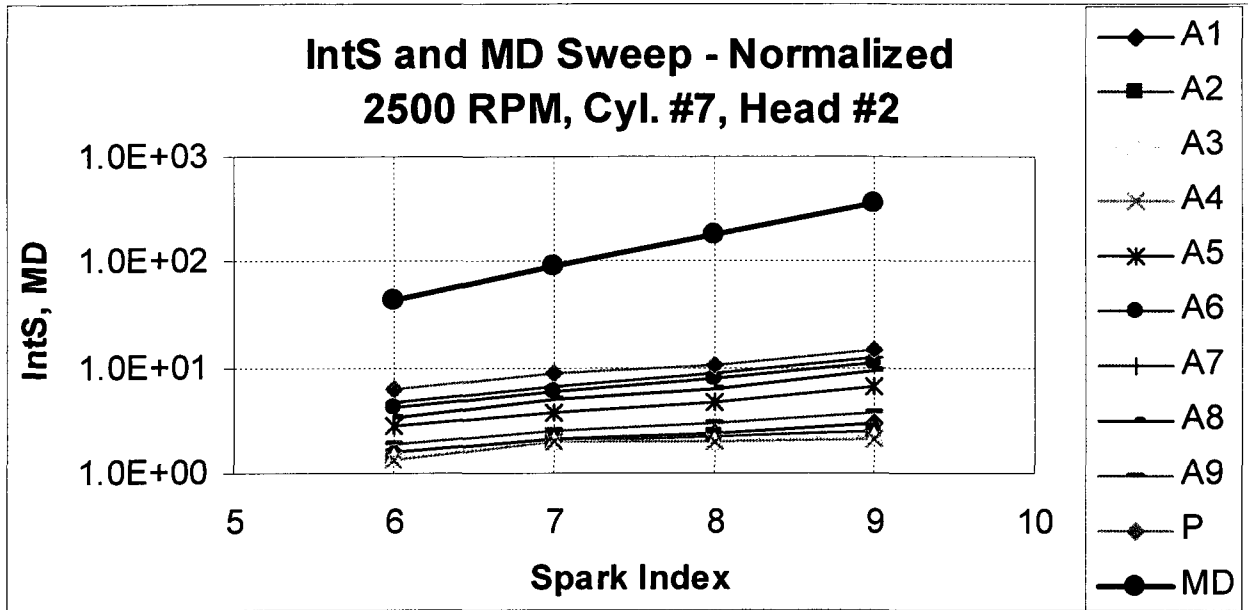


Figure C.6 o - MD / IntS Sweep (Normalized) - 2500 RPM, Cyl. #7, Head #2

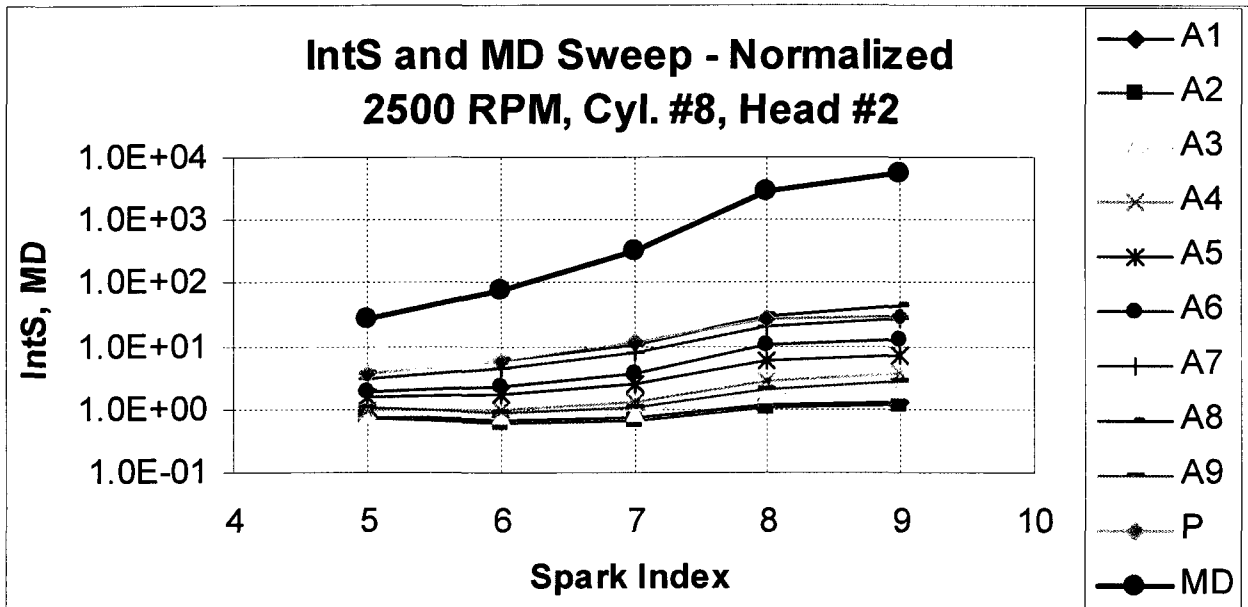


Figure C.6 p - MD / IntS Sweep (Normalized) - 2500 RPM, Cyl. #8, Head #2

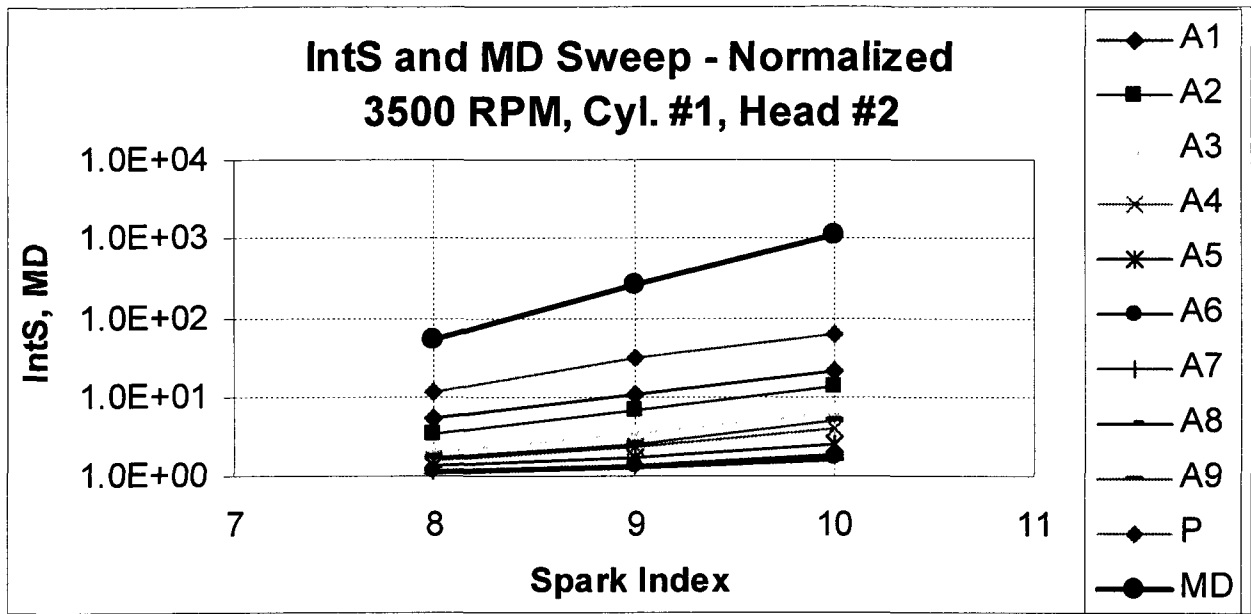


Figure C.6 q - MD / IntS Sweep (Normalized) - 3500 RPM, Cyl. #1, Head #2

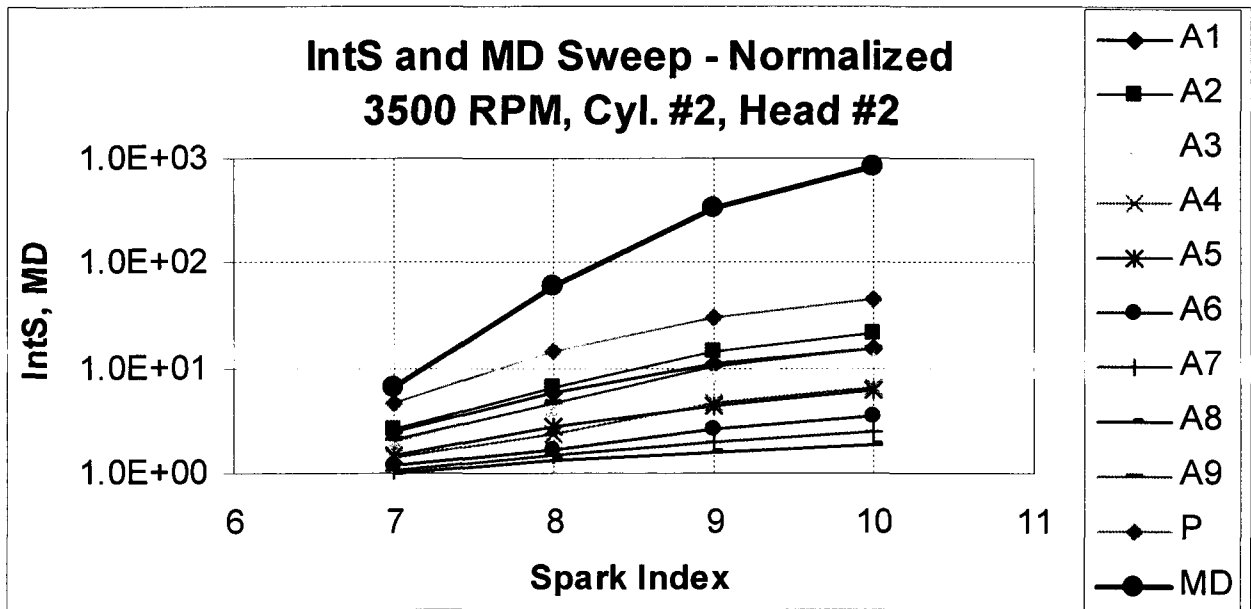


Figure C.6 r - MD / IntS Sweep (Normalized) - 3500 RPM, Cyl. #2, Head #2

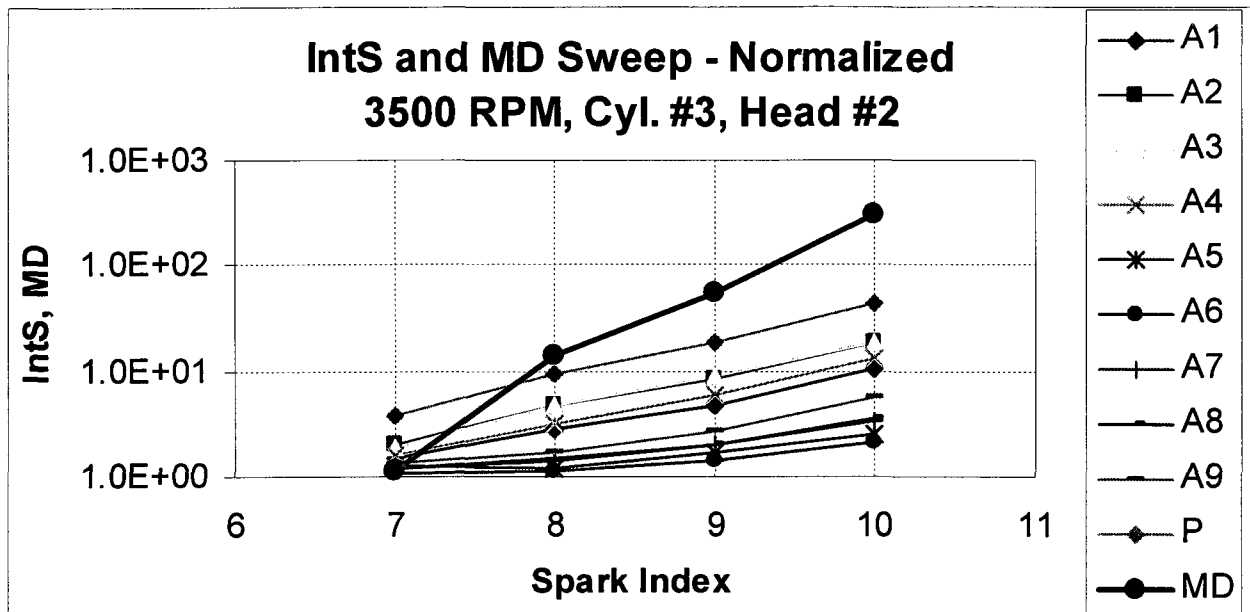


Figure C.6 s - MD / IntS Sweep (Normalized) - 3500 RPM, Cyl. #3, Head #2

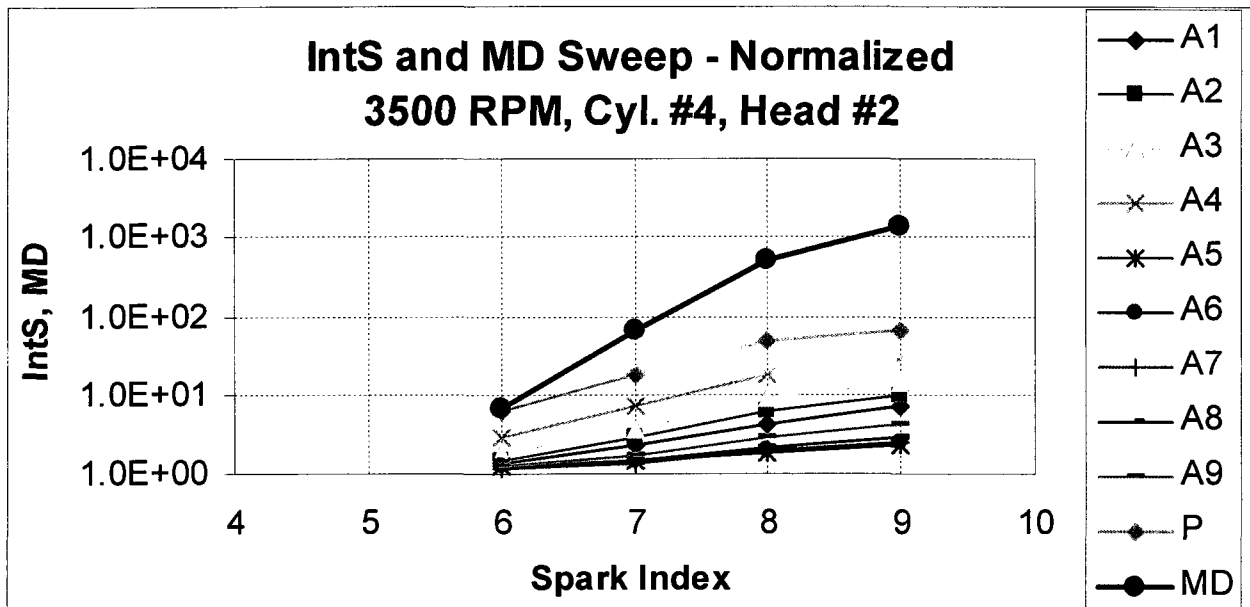


Figure C.6 t - MD / IntS Sweep (Normalized) - 3500 RPM, Cyl. #4, Head #2

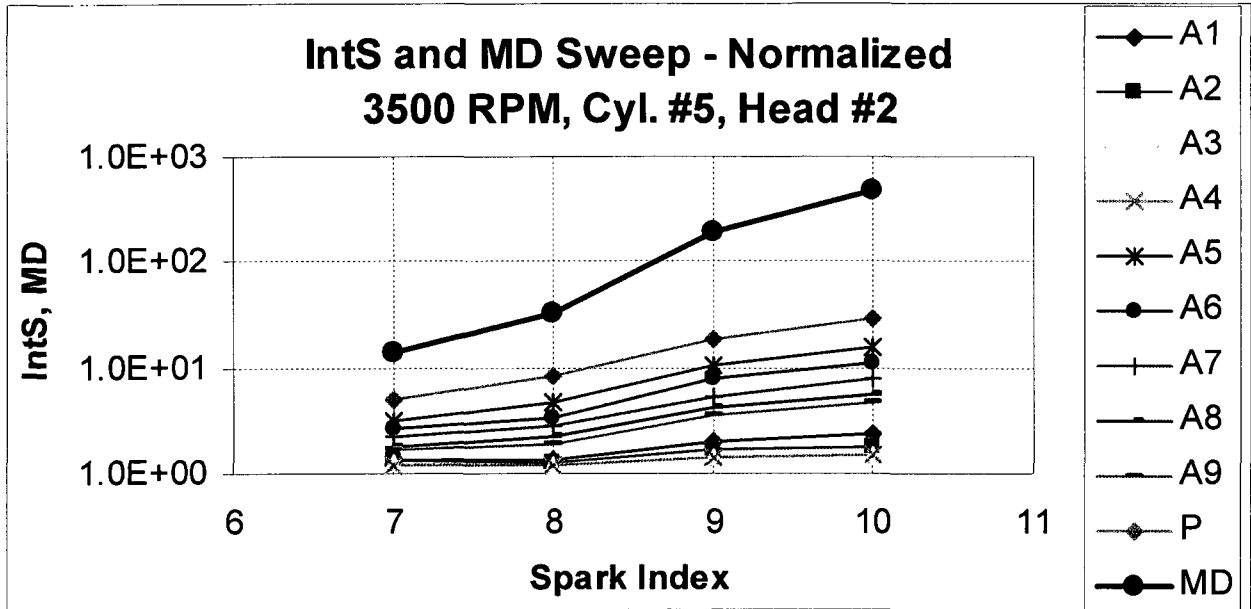


Figure C.6 u - MD / IntS Sweep (Normalized) - 3500 RPM, Cyl. #5, Head #2

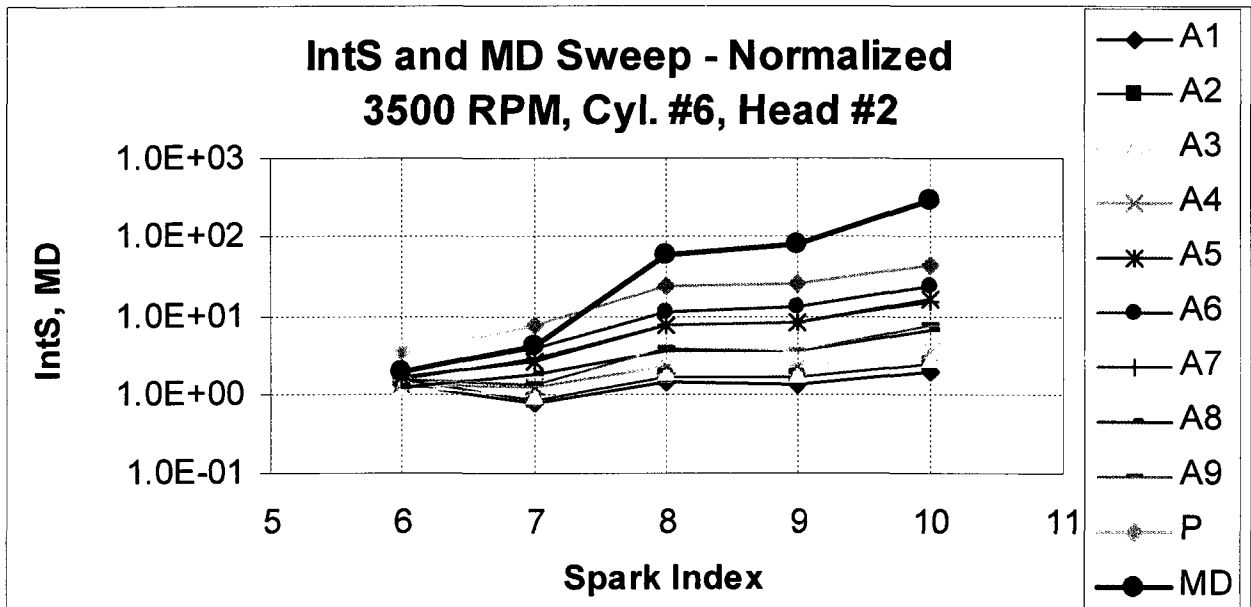


Figure C.6 v - MD / IntS Sweep (Normalized) - 3500 RPM, Cyl. #6, Head #2

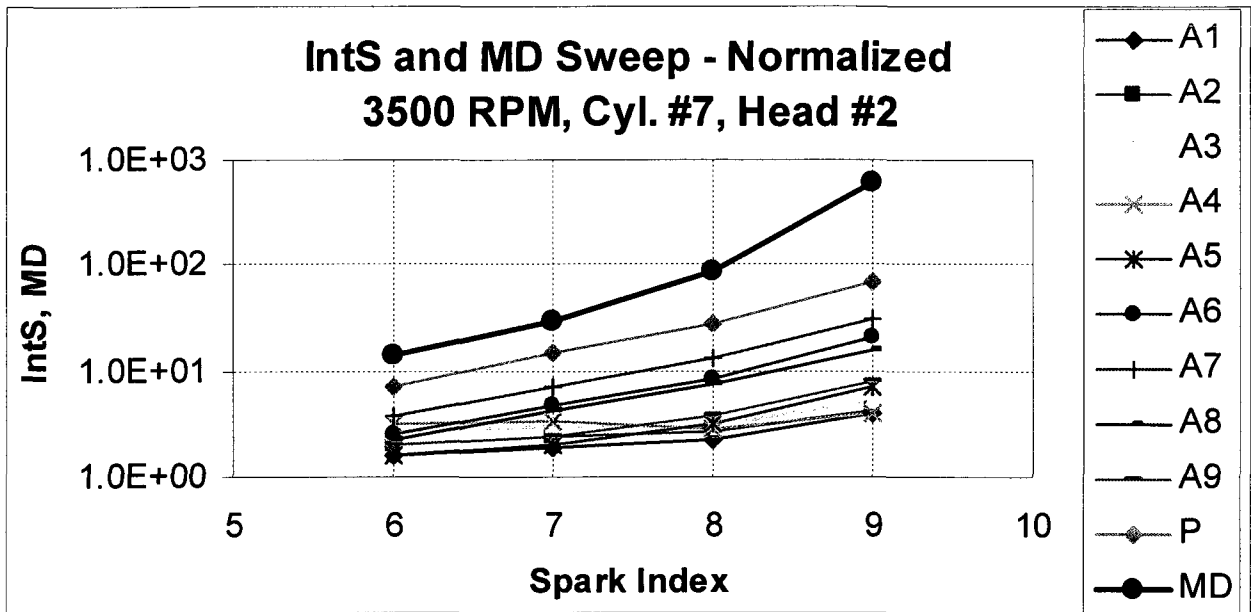


Figure C.6 w - MD / IntS Sweep (Normalized) - 3500 RPM, Cyl. #7, Head #2

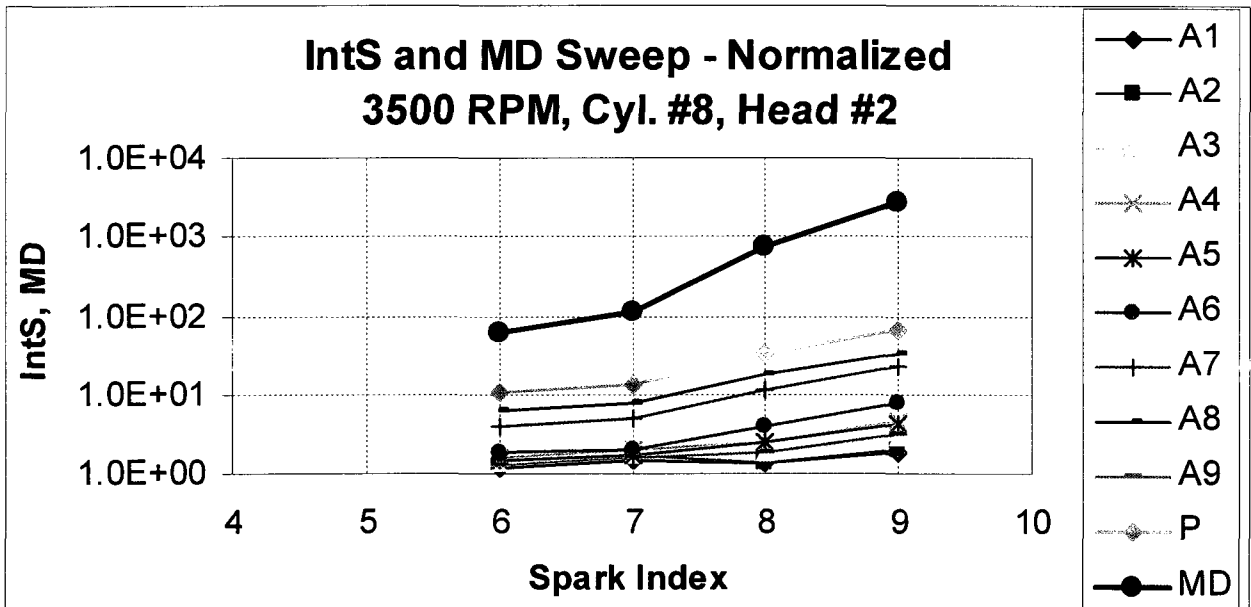


Figure C.6 x - MD / IntS Sweep (Normalized) - 3500 RPM, Cyl. #8, Head #2

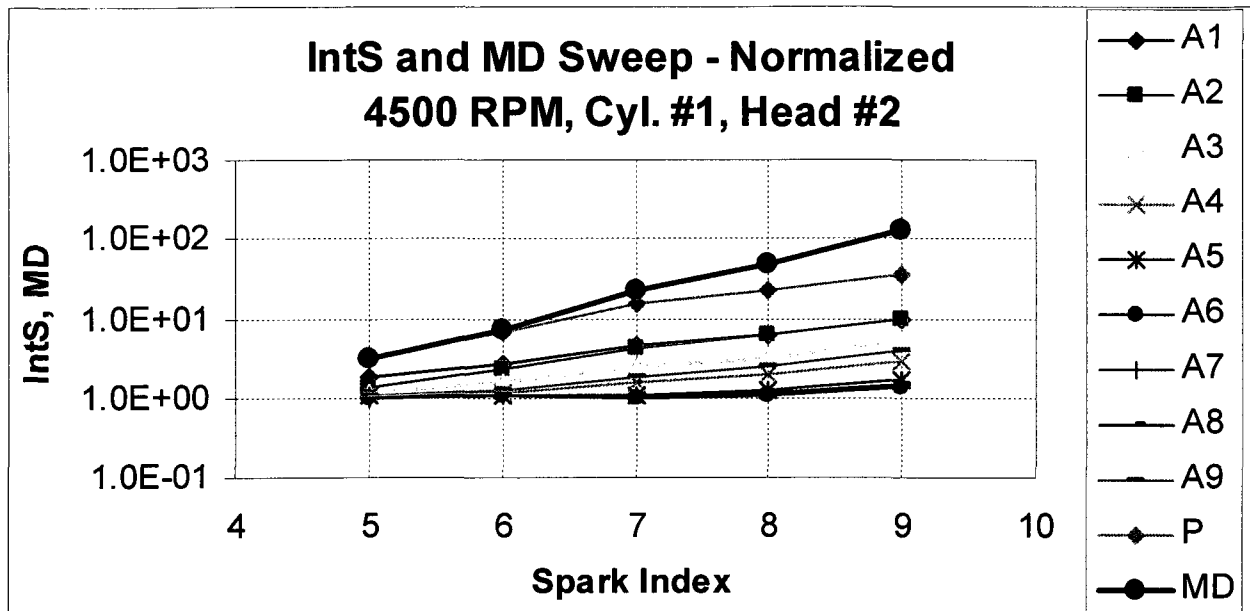


Figure C.6 y - MD / IntS Sweep (Normalized) - 4500 RPM, Cyl. #1, Head #2

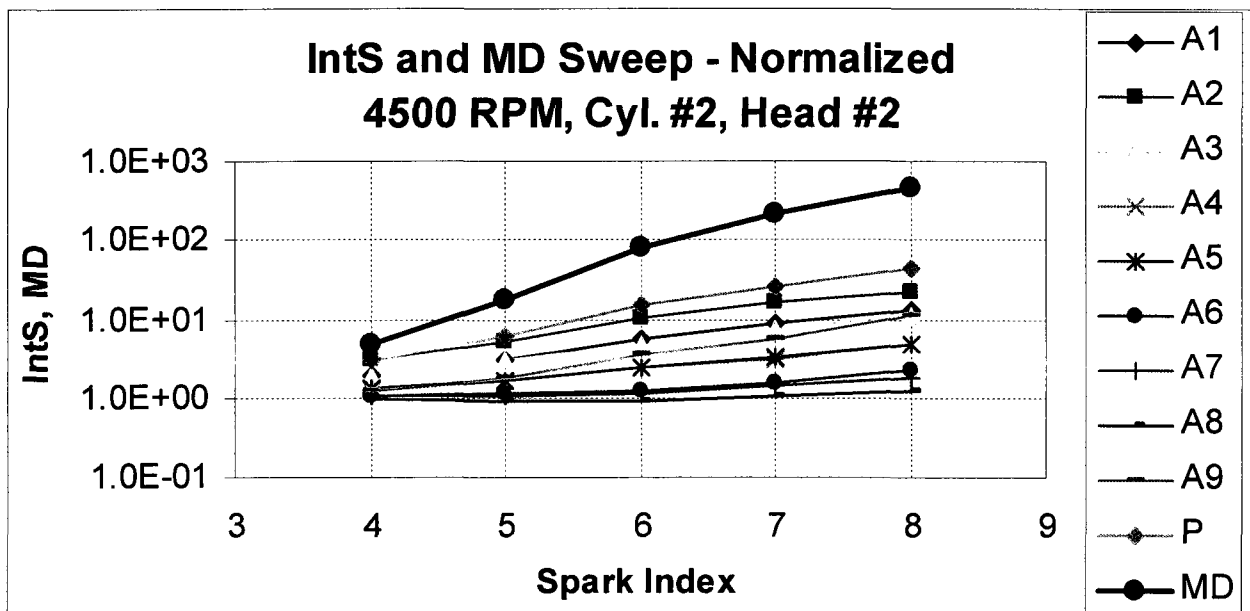


Figure C.6 z - MD / IntS Sweep (Normalized) - 4500 RPM, Cyl. #2, Head #2

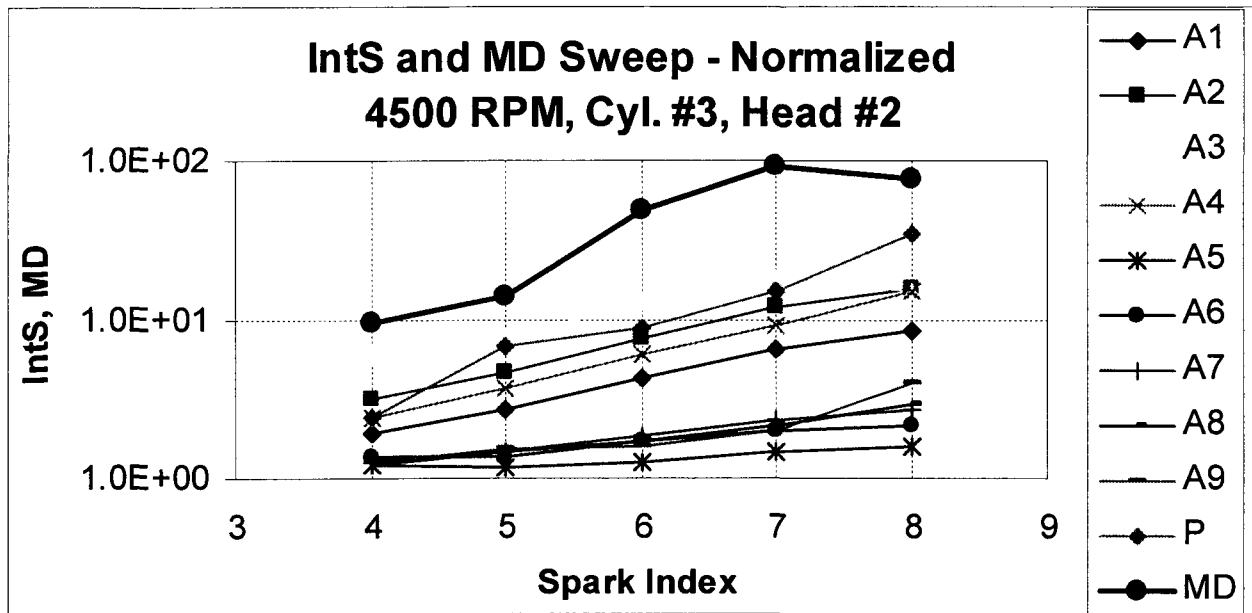


Figure C.6 aa - MD / IntS Sweep (Normalized) - 4500 RPM, Cyl. #3, Head #2

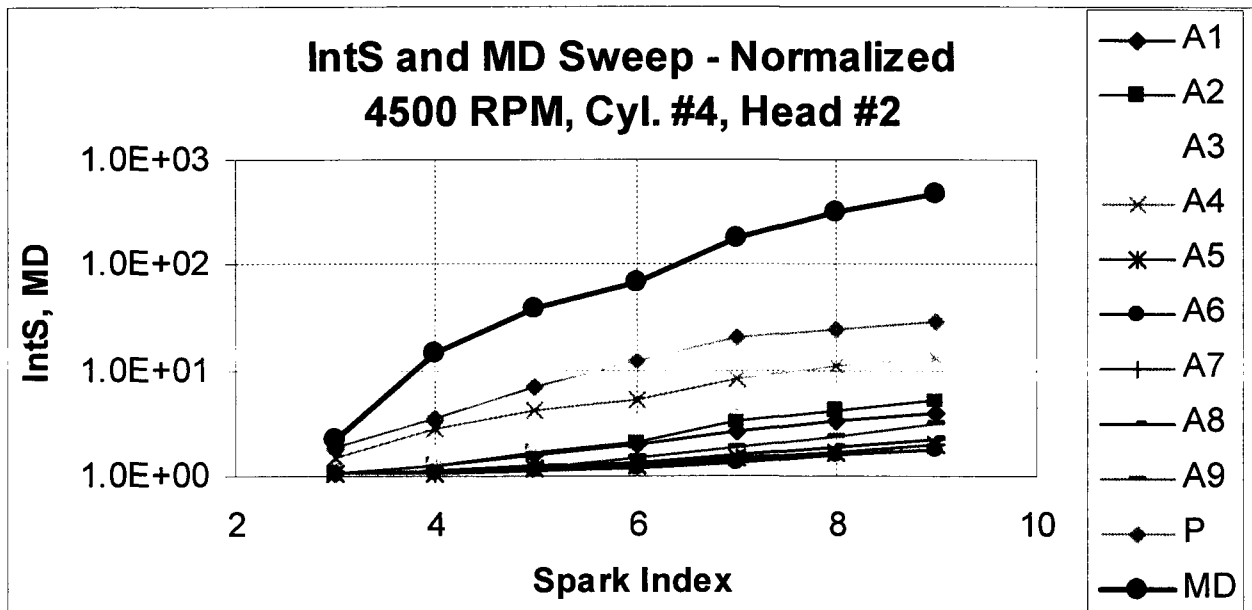


Figure C.6 bb - MD / IntS Sweep (Normalized) - 4500 RPM, Cyl. #4, Head #2

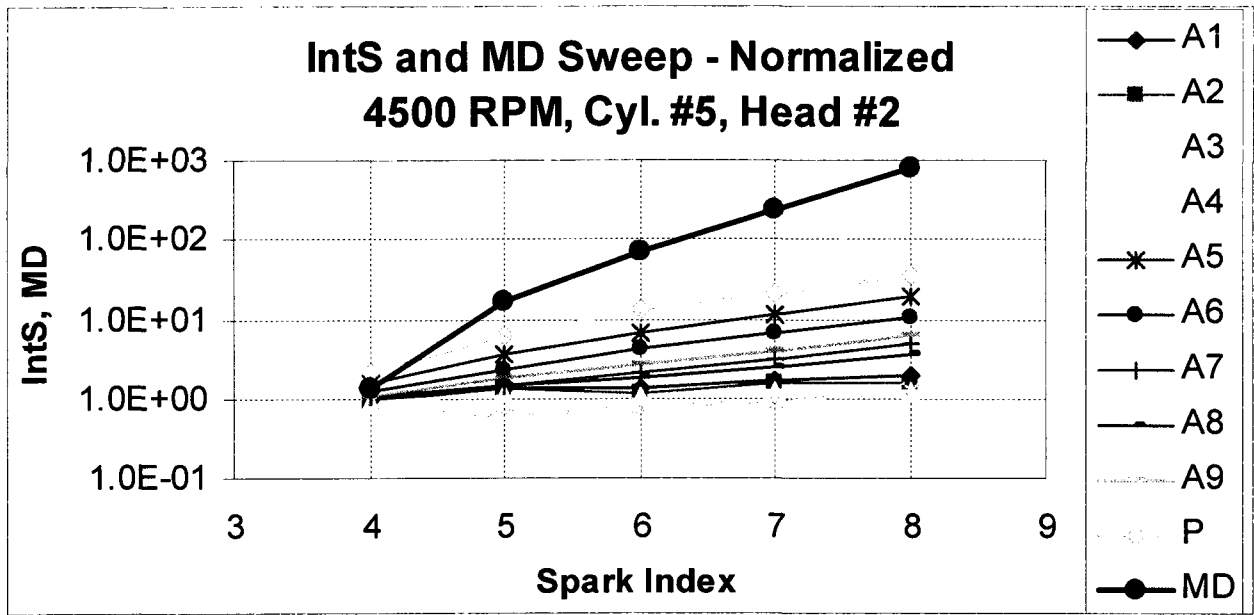


Figure C.6 cc - MD / IntS Sweep (Normalized) - 4500 RPM, Cyl. #5, Head #2

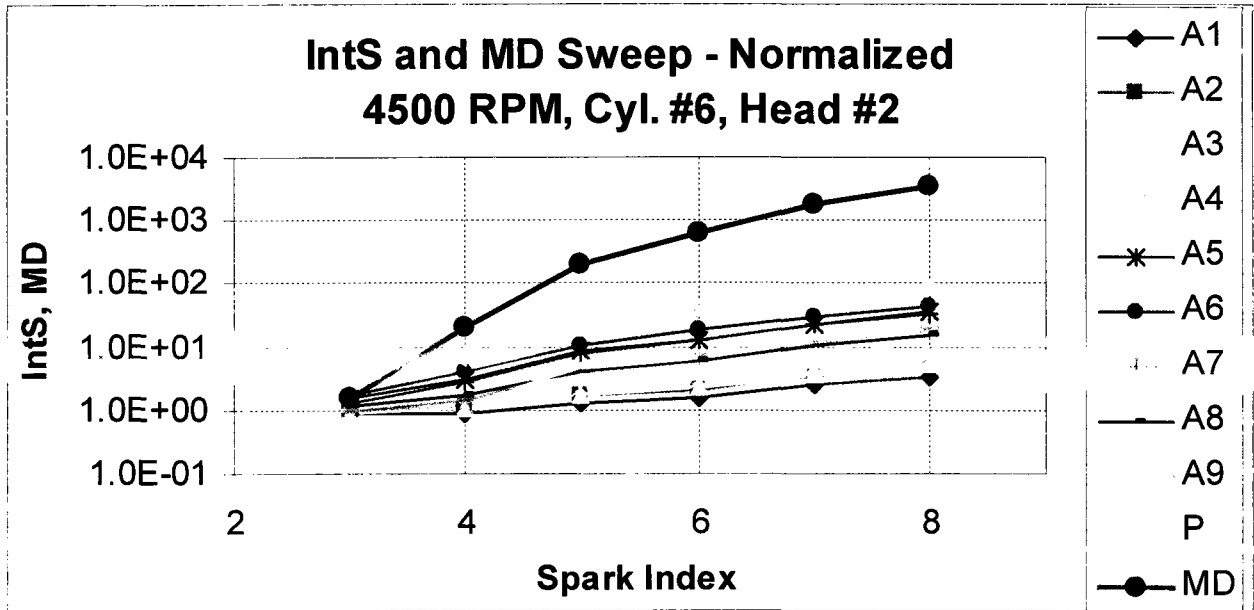


Figure C.6 dd - MD / IntS Sweep (Normalized) - 4500 RPM, Cyl. #6, Head #2

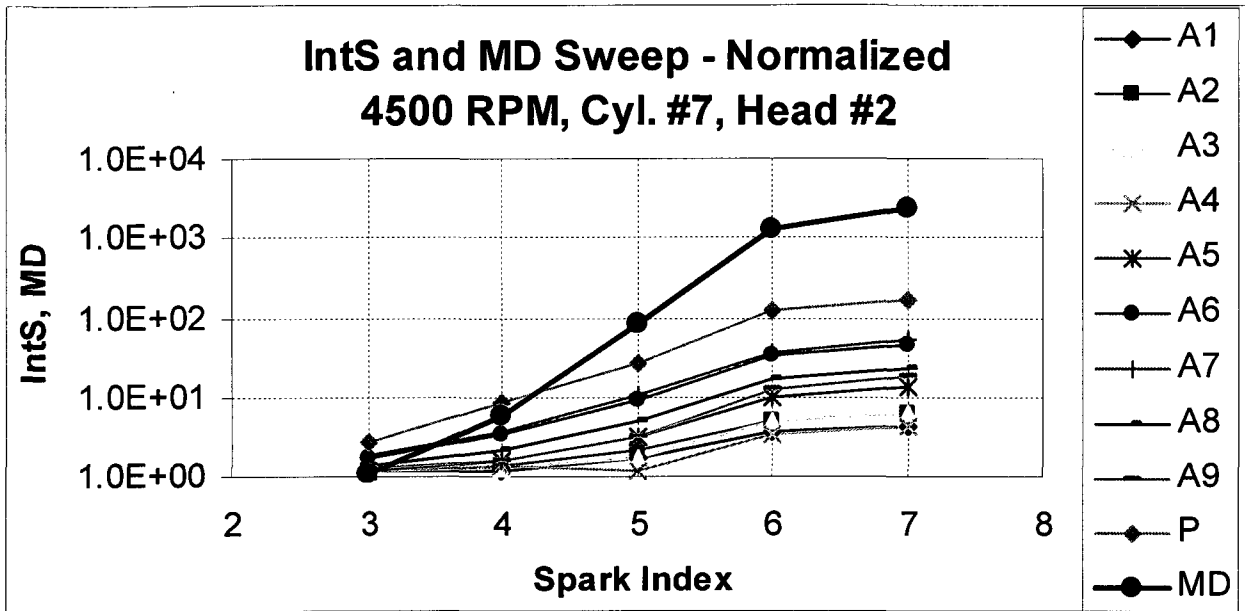


Figure C.6 ee - MD / IntS Sweep (Normalized) - 4500 RPM, Cyl. #7, Head #2

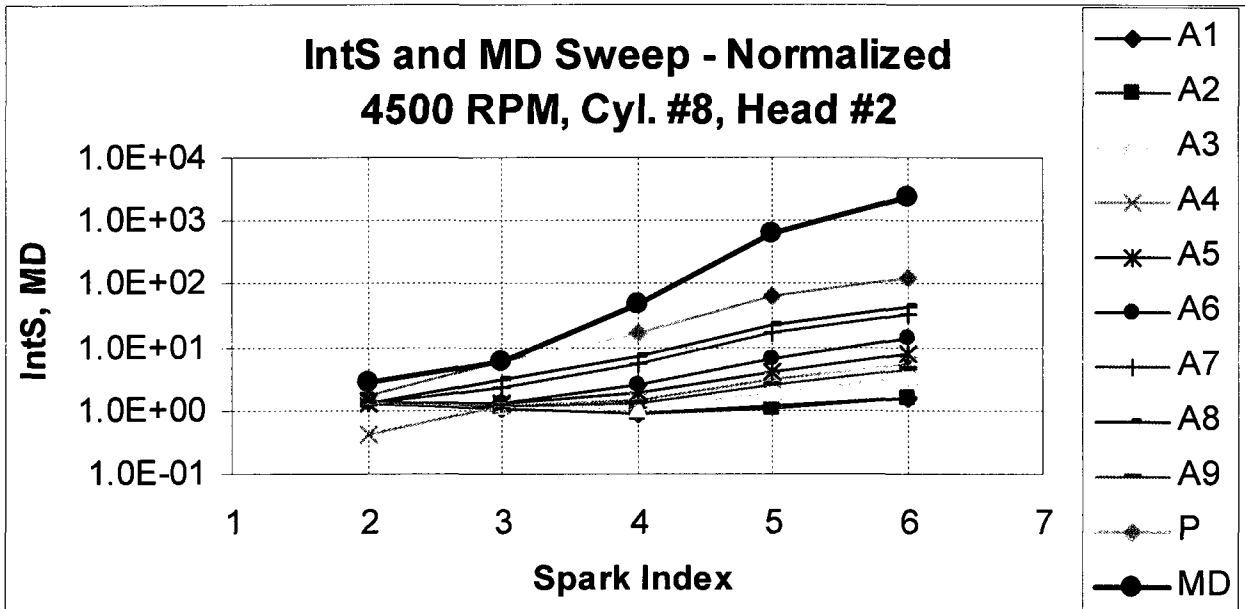


Figure C.6 ff - MD / IntS Sweep (Normalized) - 4500 RPM, Cyl. #8, Head #2

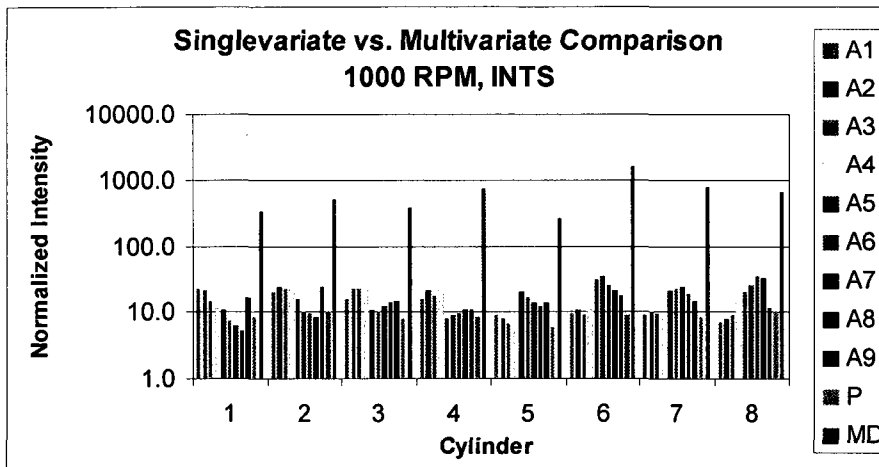


Figure C.7 a - Normalized Intensity - 1000 RPM, INTS

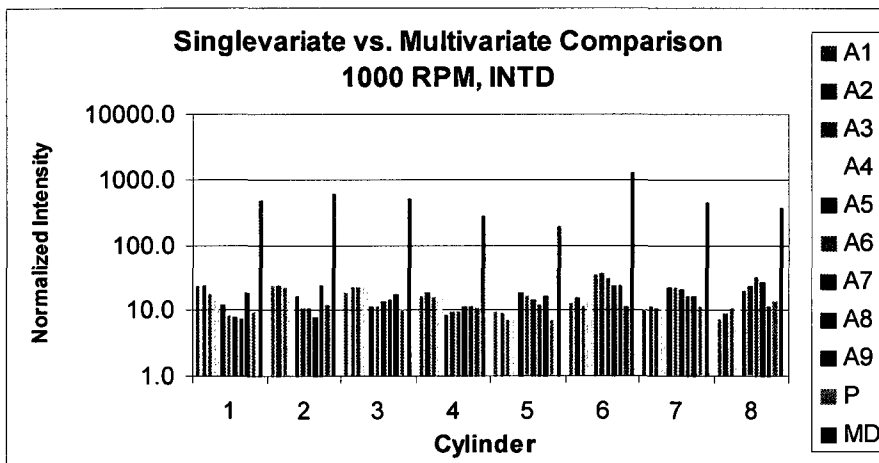


Figure C.7 b - Normalized Intensity - 1000 RPM, INTD

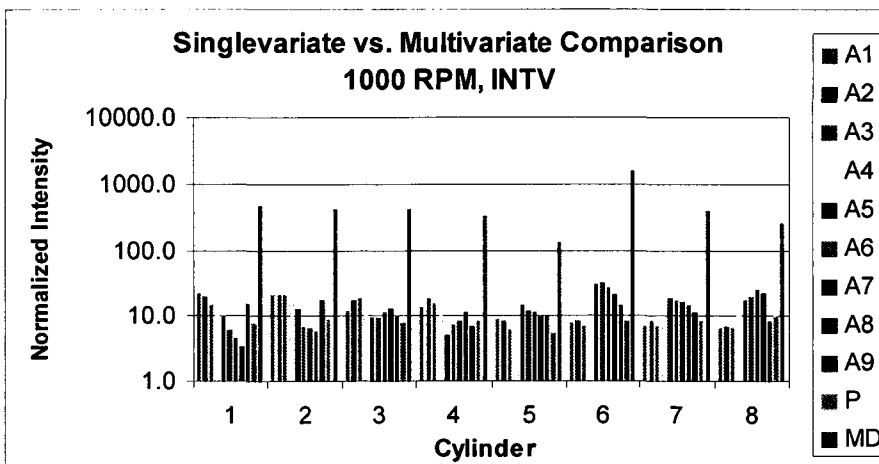


Figure C.7 c - Normalized Intensity - 1000 RPM, INTV

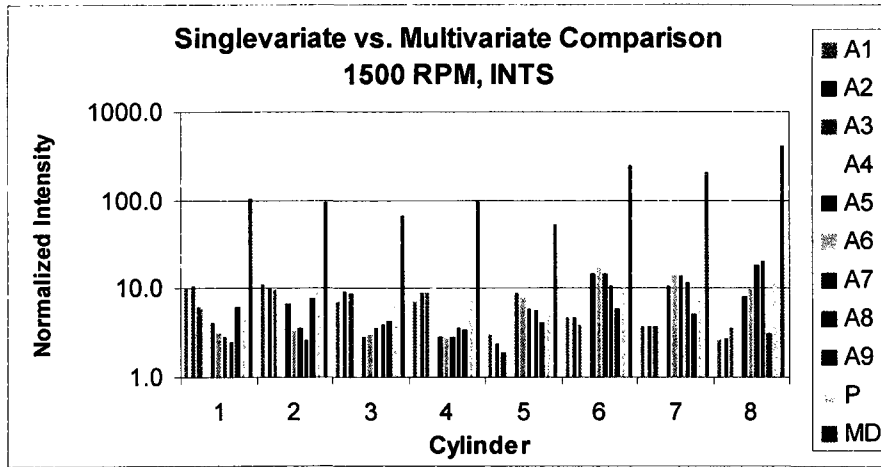


Figure C.7 d - Normalized Intensity - 1500 RPM, INTS

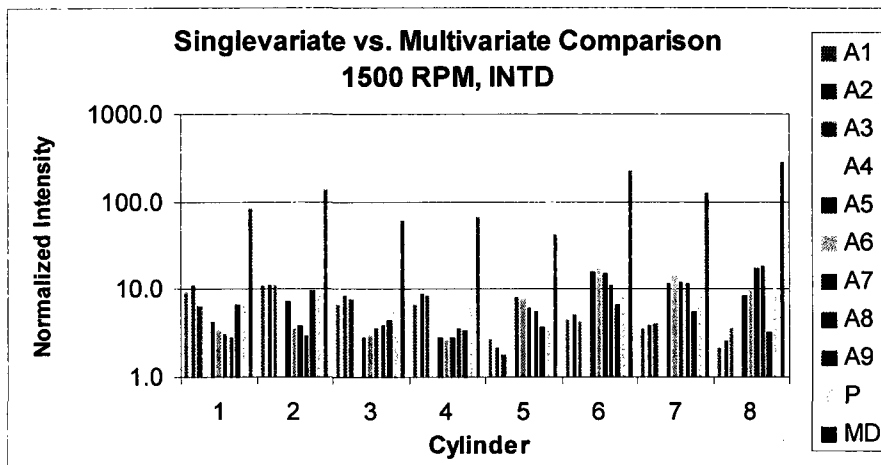


Figure C.7 e - Normalized Intensity - 1500 RPM, INTD

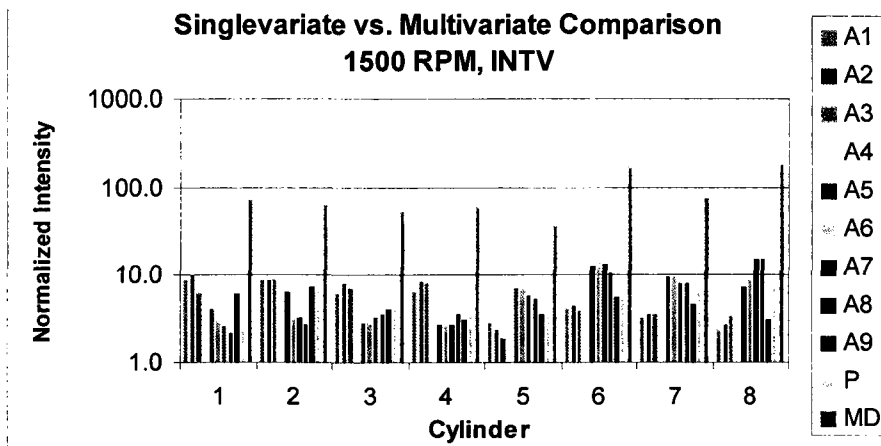


Figure C.7 f - Normalized Intensity - 1500 RPM, INTV

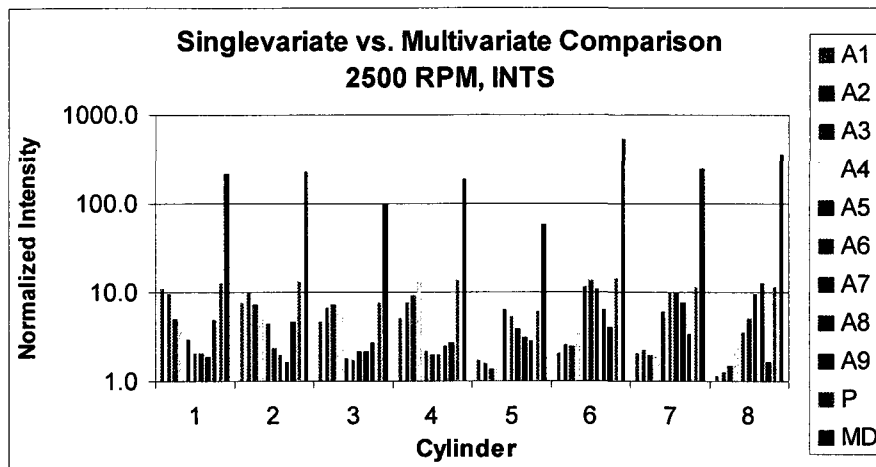


Figure C.7 g - Normalized Intensity - 2500 RPM, INTS

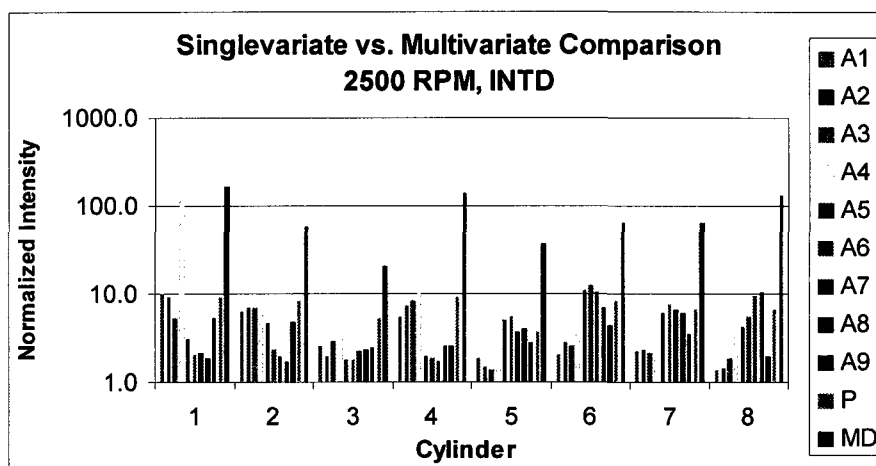


Figure C.7 h - Normalized Intensity - 2500 RPM, INTD

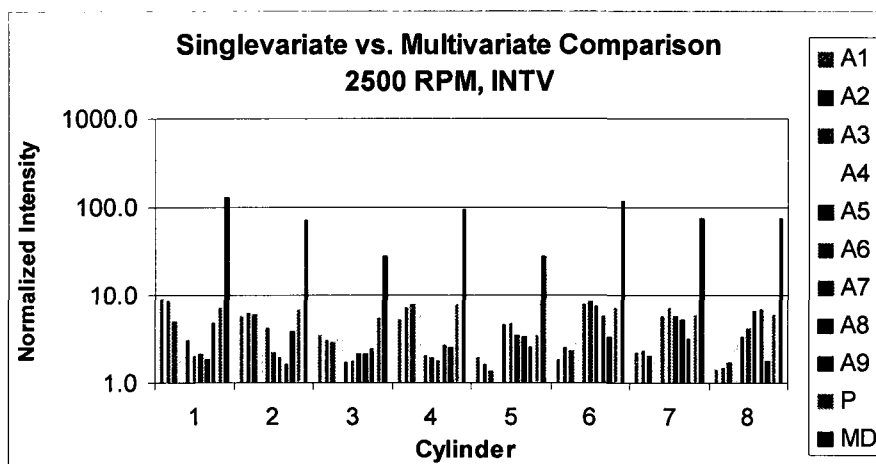


Figure C.7 i - Normalized Intensity - 2500 RPM, INTV

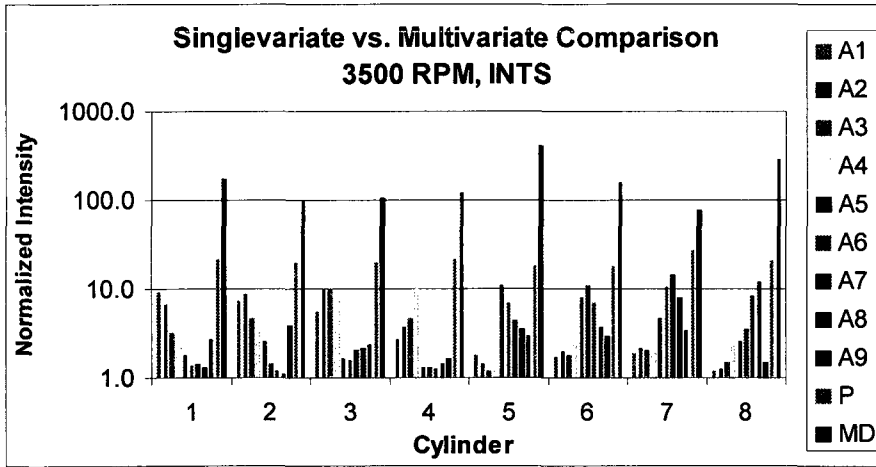


Figure C.7 j - Normalized Intensity - 3500 RPM, INTS

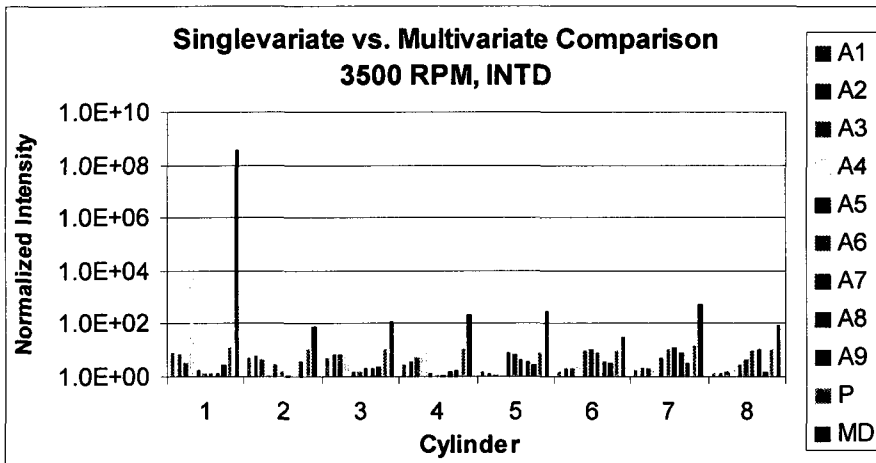


Figure C.7 k - Normalized Intensity - 3500 RPM, INTD

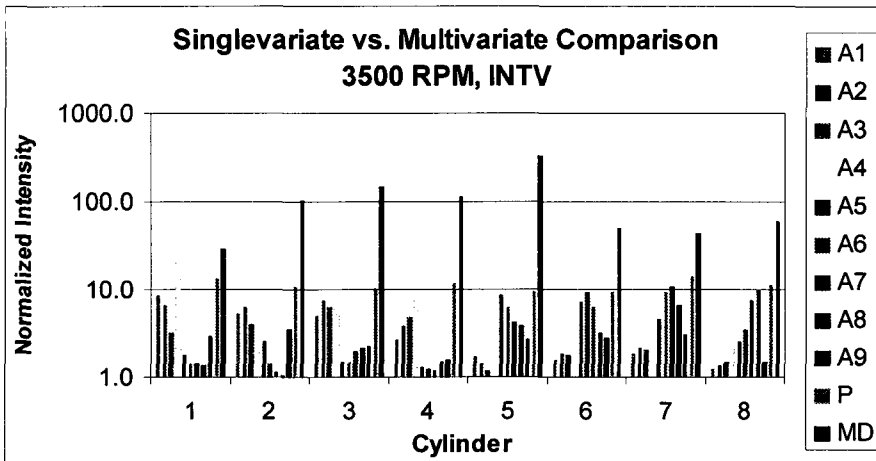


Figure C.7 l - Normalized Intensity - 3500 RPM, INTV

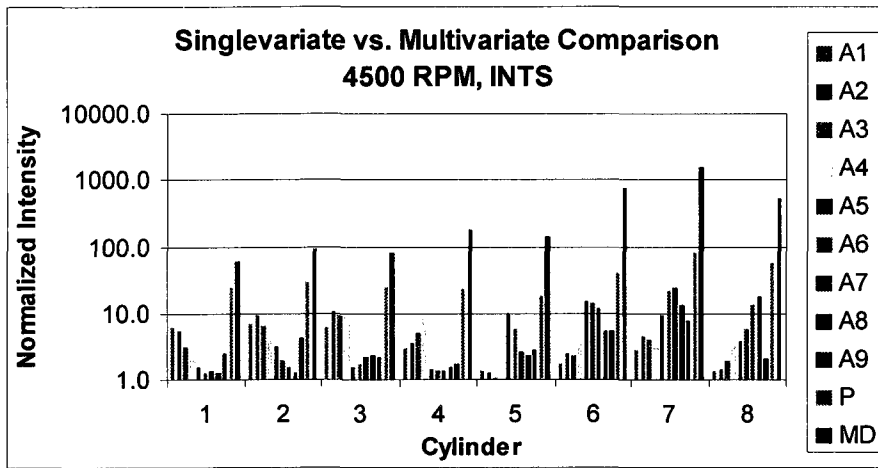


Figure C.7 m - Normalized Intensity - 4500 RPM, INTS

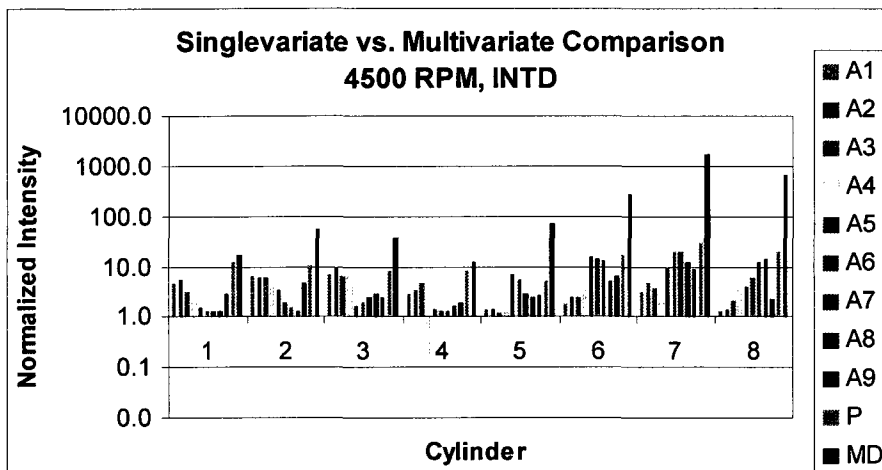


Figure C.7 n - Normalized Intensity - 4500 RPM, INTD

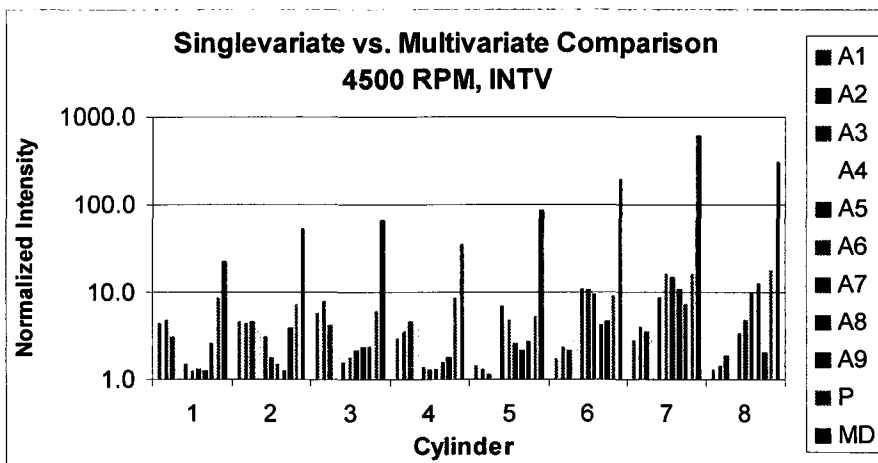


Figure C.7 o - Normalized Intensity - 4500 RPM, INTV

VITA AUCTORIS

Todd E. Tousignant was born on June 4, 1976 in Windsor, Ontario, Canada. He graduated from Walkerville Secondary School, Windsor, Ontario in 1995. He enrolled in Engineering at the University of Windsor, Windsor, Ontario later that year and received his Bachelor of Applied Science degree in mechanical engineering in the summer of 1999. Todd is currently a member of the Ford / University of Windsor, Powertrain Engineering Research and Development Group and a candidate in the Ph.D. program at the University of Windsor.